Reply to **RC1** 'Comments on NHESS 2018-62', by Raphael Paris

Section 1 main comments

COMMENT #1:
All section on the criteria used for identifying the tsunami units (lines 178-195) is not well-written and should be updated. Many recent references are missing (e.g. references on the 2011 Japan tsunami).
AUTHORS REPLY
This section is significantly revised. In order to clarify the text we have rewritten large sections of the paragraph (see underlined) and added four new references (Lionello et al., 2006; Morton et al., 2007; Costa et al., 2014; and Matsumoto et al., 2016) dedicated to the tsunami identification. The updated specific lines for the criteria are in 188-208. Among 16 newly added references (see underlined), 5 are related to the tsunami deposits following the 2004 Sumatra and 2011 Tohoku earhquakes.

COMMENT #2:
The vertical trends of grain size (and sorting), organic matter, and magnetic susceptibility are not enough described and should be discussed in more details.
AUTHORS REPLY
For this issue, we add more details on the grain size (and sorting) distribution, organic matter, and bulk mineralogy in the supplementary material including grain size and sorting analysis (Tables S1-S24, Figs.S4-S27) at lines 113 -116 & 233-246.

COMMENT #3:
Organization of the manuscript: Many sentences or paragraphs that appear in the results should move to the discussion (see my suggestions in the file attached). Section 6 could be the first section of the discussion. In general, this discussion should be better organized.
AUTHORS REPLY
As also requested by other reviewers, we moved several sentences and paragraphs to discussion section, and re-organized section 6 according to the annotated manuscripts (see underlined paragraphs).

COMMENT #4:
I would avoid using the term "tsunami" in the description of the cores (results). It's an interpretation that has to be argumented later in the discussion. Improving your introduction on the tsunami deposits (see my comment below) will help you better argumenting the tsunami interpretation.
AUTHORS REPLY
Except in discussion and conclusions, we have changed "tsunami deposits" in all manuscript and used instead "high energy sedimentary layers" until section 6.

COMMENT #5:

There is a clear inconsistency of the ages, depending on the type of sample (e.g. shells or charcoals) and degree of reworking of the sediments. When trying to explain these inconsistencies, you have underestimated the power of erosion and reworking of the sedimentary system by a large tsunami. Erosion of underlying soils and lagoon sediments by the tsunami might explain some ages older than expected, especially for the bioclasts (shells) that perhaps are remobilised by the tsunami from older formations (e.g. old marine terrace reworked by tsunami).

AUTHORS REPLY

In order to clarify the signification of the obtained ages, we have changed and added sentences with more explanations from line 564 to 588, also noting in particular the role of erosion during large earthquake tsunamis on the inconsistency of dated samples (line 579-580).

COMMENT #6:

In the conclusion, there is an attempt to correlate the characteristics of tsunami deposits with the location and magnitude of the earthquakes. It's extremely difficult to correlate the thickness of tsunami deposits with the proximity and/or magnitude of the seismic rupture. If you want to discuss this issue, it has to be developed and better justified.

AUTHORS REPLY

We agree with the reviewer comment and removed the lines 589 to 593. However, we leave an inference on the proximity of tsunami sources and tsunami layers (lines 617 – 624). In order to properly describe the spatial distribution of tsunami deposits (and perhaps infer their size), more investigated sites with more trenches and cores are indeed needed.

COMMENT #7:

Some comments on the tables and figures

a-Table 2a: It's hard to get how samples are ordered here. Re-order them by date and site by site? Table 2b: same remark as for table 2a + distinguish charcoals, bones and shells. 30 ages are presented in the table, but only 26 are shown on the cores.

b-Fig 4: add depth of samples, and modify Kafr (Kefr).

AUTHORS REPLY

The missed two ages are dates from test pits (not from cores) in the El Alamein site.

The dated samples of core 6/1sa1 and core 7/sa1 are missing in core figures; they are added with the missing others two ages in supplementary material (it will be 28 samples).

As requested, we have arranged the dates, and in Table 2a we use white background color for charcoal and grey for shell ages. For Table 2b we use white background color for charcoal, dark grey for bones, grey for shells, and light grey for roots ages (lines 910-945).

b-Fig 4: We have added depth of samples, and modified Kafr in Kefr.

COMMENT Fig 5: The symbol used for pointing tsunami events is not appropriate and is not mentioned in the legend. That would be nice to have distinct symbols for dated charcoals and dated shells (on all figures).

AUTHORS REPLY

Figure 4 is updated and for figure 5 a, we use arrows instead of hand to point the high energy sedimentary layers with distinct the symbols for dated charcoal and dated shells.

COMMENT #8:
The manuscript needs proofreading. There are several mistakes and misspellings and the work will benefit from the input of a English native speaker. There are parts that are just to wordy and redundant.

AUTHORS REPLY
The proofreading of manuscript for English syntax and grammar has been done.

Section 2: Comments of reviewers in the text changes in manuscript and the authors changes in text:

No.	Lines edit	Pervious manuscript	Reserved manuscript	New edit lines	Comments
1	82	nearby coastline	omitted	83	C: What do you mean with nearby? if it's generated from the Nile Delta, it's really proximal. R: We removed the expression nearby coastline
2	100	geochemical analysis	textural, geochemical analysis	112	
3	120	west	western	134	
4	116	(born 325 -330, died c. 391 – 400	omitted	-	C: omit R : done
5	127-128	Abu-El Fida (1907) reported in 1329 that the Alexandria city and Nile delta were flooded	Abu-El Fida (1907) reported that the Alexandria city and Nile delta were flooded in 1329	139-140	
6	136	wave	waves	147	
7	136	quays	docks	147	
8	138	felt shaking	shaking felt	149	
9	152	of	for	162	
10	153-159			165	C: Any bibliographic reference? R: we added Sayed 2013 which is PhD thesis
11	164	weathered	eroded	175	

12	166-167			172-173	C: move this sentence to beginning of the paragraph R: it is moved
13	174-176			185-187	C: Uncorrect sentence. Please rephrase. R: it was rephrased see line 185-187
14	181	with	of	192	
15	181	that include	such as	192	
16	184	erosion of lagoon deposits	erosion of lagoon and soil deposits	196	
17	185-195			188-208	C: All this section on the criteria used for identifying the tsunami units is not well-written and should be updated. Many recent references are missing. R: updated with new references (188-208)
18	193			557-563	C: The low peaks of MS obszeerved by Font et al. (2010) are in contradiction with the peaks of heavy minerals and the high values of MS obtained in your study. See my remark at line 437. It would be nice to discuss this issue. R: We discuss this part in lines 557-563
19	207	used methods	Methods used	220	
20	208	The trench size is ~2 x 1	The trench size is typically ~2 x 1	221	
21	209	and	that	222	
22	210			223	C: what kind of core ? R: conventional

					corning
23	210-212			223-224	C: Rephrase? R: done
24	222		, and	236	
25	220-221		( )	240	C :add two brackets ? R:done
26	225			237-239	C: This sentence is not useful. This kind of information could appear in the figure caption only. R: We rearranged the paragraphs again and I add some details of grain size and put it in useful sequence.
27	227	are	was	247	
28	229	coherency	coherence	249	
29	238	Description of trenches and cores sedimentary layers	Description of exposed trenches and cores penetrated with C14 dating of sedimentary layers	258	C: It's not only descriptive R: We add C14 dating in the title
20	246	are 20 to 40 meters distance	are 40 to 154 meters distance from shoreline	266-267	C: revise English R: We corrected this lines
21	254 - 257			553-555	C: moved to Discussion? R: moved with rephrased
22	268-270			553-556	C: move to Discussion? R: moved
23	278-288	The Oxcal dating simulation provides the 137 – 422 AD bracket of the white sandy layer unit that may be correlated with the tsunami deposits of the 21 July 365 earthquake (Fig. 4).			C: move to Disscusion or section 6 R: We removed it because repeated in section 6 in lines 508-511

24	281-288			519-528	C: discussion or section 6? R: We moved it to section 6
25	313-317	We interpret this layer as of tsunami origin and although its stratigraphy is located close to the surface, the mixed and reworked sedimentation explains the obtained old age 13985- 14415 BC (Table 2b). The second sample is a rodent bone at 50 cm depth and provides 403-603 AD calibrated age that postdate a catastrophic layer made of white sandy layer with broken shells. This catastrophic layer may correlate well with the 365 AD major earthquake of the eastern Mediterranean (313-317).	omitted		C: move to Discussion R: omitted because it is repeated in the section 6 in 504-510
26	97	Paleotsuanmi	high energy sedimentary	109	Comment in line 320 C:It has to be clear if you already consider that the units are tsunami units at this stage of the paper. Sometimes you write "conspicious layer" instead of tsunami. Be coherent. I would avoid using the term "tsunami" in the descirption of the cores. It's an interpretation. R: We change here all tsunami layers to high energy
	235	tsunami	high energy sedimentary	255	
	261	tsunami	high energy sedimentary	278	
	298	tsunami	high energy sedimentary	306	
	307	tsunami	high energy sedimentary	316	
	320	tsunami	high energy sedimentary	324	
	320	tsunami	omit	325	
	327	tsunami	high energy sedimentary	332	

	329	tsunami	high energy sedimentary	334	sedimentary layers
	333	tsunami	high energy sedimentary	338	
	333, 337	tsunami	omit	340,344	
	341	tsunami	high energy sedimentary	348	
	344	tsunami	high energy sedimentary	352	
	345	tsunami	omit	353	
	346	tsunami	omit	355	
	350	tsunami	high energy sedimentary	358	
	355	tsunami	high energy sedimentary	363	
	357	tsunami	high energy sedimentary	365	
	359	tsunami	high energy sedimentary	367	
	359	tsunami	omit	367	
	361	tsunami	omit	369	
	363	tsunami	omit	371	
	369	tsunami	high energy sedimentary	377	
	370	tsunami	high energy sedimentary	378	
	372	transport of tsunamis	omit	380	
	374	tsunami	high energy sedimentary	382	
	375, 378, 379	tsunami	omit	382, 386,387	
	383	tsunami	high energy sedimentary	391	
	384	tsunami	high energy sedimentary	392	
	385	tsunami	omit	393	

389	tsunami	omit	397
392	tsunami	high energy sedimentary	400
393	tsunami	omit	401
397	tsunami	omit	405
401	tsunami	high energy sedimentary	409
402	tsunami	high energy sedimentary	411
405	tsunami	high energy sedimentary	412
406	tsunami	omit	413
410	tsunami	omit	417
414	tsunami	high energy sedimentary	420
415	tsunami	high energy sedimentary	422
418	tsunami	high energy sedimentary	425
419	tsunami	omit	426
423	tsunami	omit	430
429	tsunami	high energy sedimentary	436
434	tsunami	high energy sedimentary	440
435	tsunami	high energy sedimentary	441
443	tsunami	high energy sedimentary	450
454	tsunami	omit	461
460	tsunami	high energy sedimentary	467

27	394	ahigh	a high	402	
28	399	bad	poor	407	
29	401	that	and	409	
30	402	gives	gives a	409	
31	403-404				C: Interpretation R: omitted due to it was repeated in lines 584-586.
32	410-411			417-419	C: Rephrase? R: the sentence was rephrased in lines 417-419
34	416-417		Omit		C: move to section 6 or Discussion R: it was repeated in discussions, we removed it.
35	424	bad	poor	431	
36	432-433		omit	439	C: omitted these lines R: omitted
37	440			557-563	C: Interesting and quite usual for a tsunami deposit, but in contradiction with Font et al. (2010) R: We discuss this point in 557-563
38	445	and	Omit		
39	460-464			498-503	C: move to section 6 R: Moved
40	476		It might correspond to Santorini eruption tsunami.	577	C: It's interesting. Any idea about the source? R: it is may compared with Santorini ~1400 BC tsunami
41	479				C:This could be the first section of the discussion R: We leave this structure because relevant here and consistent with the aim of topic.
42	489	All these signatures with only three layers in the ~ 2	The high energy sedimentary	479-481	C: I don't understand this sentence.

		m thick sedimentary units indicate that this layer suggests tsunami deposits rather than storm.	characteristics with four layers in the ~ 2 m thick sedimentary units indicate that these layers are tsunami deposits rather than storm		R: We rewrote again as we meant here the frequency of four layers in 2 m thick sediment.
43	496		also	487	
44	498	Coarse brown and horizontal lamination	laminated coarse brown sand	489	
45	500	The pebbles also are	Pebbles are found	491	
46	506				C: What is loading structure? R: We have changed it with loadcast sedimentary figure.
47	505	Organic content greater than 5 mark	organic content greater than 5 % of dry weight	496	C: 5 what? unit? R: weight percent of dry sample
48	506	Folk 1968	omit		C : omit ?
49	509	Low energy marine	Low energy lagoon and marine	505	
50	521	X,y,z correlate	X,y,z might correlate	517	
51	538		Morton et al., 2007	544	C: references? R: We add Morton et al.,2007
52	540		This a probable large tsunami.	546	C: at two sites , It's indeed convincing and indicates a regional-scale event, so probably a really large tsunami. R: yes , we add this comment
53	545	Bimodal distribution			C: explanation of bimodal distribution ? R: We mean a

					mixture of fine and coarse grain size of sediments, the bimodal sediment distribution is common features of tsunami induced depositions depend on relations of fine to coarse particles and degree of erosion.
54	557-580		omit		C: avoid reputations ? R: removed
55	581		omit		C: idem, repeating. Try to organise better the discussion. R: removed
56	589-593				C: It's difficult to correlate the thickness of tusnami deposits with the proximity and/or magnitude of the seismic rupture. If you want to discuss this issue, it has to be develop and better justified. R: We agree with paragraphs comment. We removed these lines 589 to 593. To describe this well, We will need more cores and that will be in the frame of future perspectives.

Paleotsunami deposits along the coast of Egypt correlate with historical earthquake records of eastern Mediterranean

A. Salama, (1, 2, *), M. Meghraoui (1**), M. El Gabry (2, *),

S. Maouche (3, *), H. M. Hussein (2, *), and I. Korrat (4)

[1.] EOST-IPGS - CNRS - UMR 7516, Strasbourg, France
[2.] NRIAG, 11421 Helwan, Egypt
[3.] CRAAG, Bouzareah, Algeria
[4.] Mansoura University, Mansoura, Egypt

* Also at *North Africa Group for Earthquake and Tsunami Studies (NAGET), Ne t40/OEA ICTP, Italy*

**Corresponding author*

Submitted to Natural Hazards and *and Earth System Sciences* (*NHESS*)

Revised version June 2018

Abstract.

We study the sedimentary record of past tsunamis along the coastal area west of Alexandria (NW Egypt) taking into account the occurrence of major historical earthquakes in the eastern Mediterranean. The two selected sites at Kefr Saber (~32-km west of Marsa-Matrouh city) and ~10 km northwest of El Alamein village are coastal lagoons protected by 2 to 20-m-high dunes parallel to the shoreline. Field data were collected by: 1) Coastal geomorphology along estuaries, wedge-protected and dune-protected lagoons, and 2) identification of paleotsunamis deposits and their spatial distribution using five trenches (1.5-m-depth) at Kefr Saber and twelve cores (1 to 2.5-m-depth) at El Alamein. Detailed logging of sedimentary sections were analysed using X rays, grain size and sorting, total organic and inorganic matter, bulk mineralogy, magnetic susceptibility and radiocarbon dating necessary for the identification of past tsunamis records. Generally of low energy, the stratigraphic succession made of coastal lagoon and alluvial deposits includes intercalated high-energy deposits made of mixed fine and coarse sand with broken shells, interpreted as catastrophic layers correlated with tsunami deposits. Although the radiocarbon dating of 46 samples consist in mixed old (> 13000 year BP) and young (< 5500 year BP), dated charcoal and shells in sedimentary units allow the correlation with the 24 June 1870 (Mw 7.5), 8 August 1303 (Mw ~8) and 21 July 365 (Mw 8 – 8.5) large tsunamigenic earthquakes that caused inundations in Alexandria and northern Egyptian shoreline. Our results point out the size and recurrence of past tsunamis and the potential for tsunami hazard over the Egyptian coastline and the eastern Mediterranean regions.

Key words: paleotsunami, coring, trenching, coastal geomorphology, northern Egypt

1. Introduction:

Egypt has a well-documented historical catalogue of earthquakes and tsunamis recorded in ancient texts and manuscripts. Original documents and archives from past civilizations are considered as the principal sources of macroseismic data for major historical earthquakes and tsunamis (Poirier and Taher, 1980; Maamoun et al., 1984; Ambraseys et al., 1994, 2009; Guidoboni et al., 1994, 2005; Soloviev et al. 2000, Tinti et al., 2001). The catalogue of Ambraseys et al., 2009 reports that coastal cities of northern Egypt have experienced repeated tsunamis inundations with severe damage in the past. While historical earthquakes and tsunamis are well documented, it appears that there is a lack of holistic investigations for tsunami deposits along the Mediterranean coastlines. The geomorphology along the Mediterranean coastline of northern Egypt with low-level topography (Hassouba, 1995), dunes and lagoons constitutes an ideal natural environment for the geological record of past tsunamis.

The Eastern Mediterranean region experienced major earthquakes (with Mw > 7.5) mainly along the Hellenic subduction zone due to the convergence between the Eurasian and African plates (Fig. 1; Ambraseys et al., 1994, Taymaz et al., 2004). Major historical tsunamis in the eastern Mediterranean region that affected northern Egypt are triggered by large earthquakes (Papadopoulos et al., 2014) but the possibility of landslide tsunami associated with local earthquakes may also exist (El-Sayed et al., 2004; Tinti et al., 2005). Yalciner et al. (2014) estimated from modelling that up to 500 km^3 landslide volume, with wave height ranging from 0.4 to 4 m, may have taken place offshore the Nile Delta. Coastal landslides may generate giant tsunamis as the Storrega event that hit Norway and the North Atlantic Ocean in ~6100 BC (Bondevik et al., 2012).

85   Tsunami research of the past 20 years has led to the discovery of coastal tsunami

86   sedimentary records dating back to thousands of years. Among the early studies, the evidence

87   of more than 6 soil levels buried below tsunami deposits 87 in the past 7000 years were found

88   at Puget Sound coastline of Washington state (Atwater, 1987). Costa et al., 2014, studied the

89   sedimentological records and related microtexture and heavey mineral assemblage for three

90   events in Portugal in AD 1755, Scotland in 8200 calendar year BP and in Indonesia associated

91   with the 2004 Sumatra earthquake. Sawai (2001) and Nanayama et al. (2003) recognized

92   major tsunamis due to extensive coastal inundation along the eastern coast of Hokkaido

93   (northern Japan); the repeated sand sheet layers several kilometres inland evidenced a 500-

94   year tsunami cycle in the period between 2000 and 7000 years BP. Following the 2004

95   Sumatra earthquake (Mw 9.1) and beside the coral reef uplift and subsidence (Meltzner et al;

96   2009), Malik et al. (2015) identified in trenches three historical tsunamis during the past 1000

97   years along the coast of South Andaman Island (India). Lario et al. (2011) document five

98   tsunami events in the Gulf of Cadiz (Spain) generated by strong earthquakes in the last 7000

99   years, previous to 1755 AD Lisbon earthquake tsunami. In the Mediterranean, De Martini et

100   al. (2012) identified two tsunami deposits during the first millennium BC and another one in

101   650-770 AD and estimated 385 year average recurrence interval for strong tsunamis along the

102   eastern coast of Sicily (Italy). Minoura et al. (2000) described tsunami deposits with volcanic

103   ashes along the coast in Crete (Greece) that correlate with Thera (Santorini) eruption in late

104   Minoan time (1600–1300 B.C.). Papadopoulos et al. (2012) documented three paleotsunami

105   layers attributed to the 1303, 1481 and 1741 historically documented tsunamis in Dalaman

106   (SW Turkey). Using tested methodology as granulometry, XRD, XRF and FT-IR, Tyuleneva

107   et al. (2017) identified two sedimentary events offshore Casearea (Israel) that may correlate

108   with landslide tsunamis in AD 749 and in 5.7 ka BP (Chalcolithic cultural period).

109 In this paper, we investigate the high energy sedimentay deposits in the northern coast

110 of Egypt and their correlation with the historical tsunami catalogue of the Eastern

111 Mediterranean. Using coastal geomorphology with trenching and coring, we examine the

112 geological evidence of tsunami deposits using textural, geochemical analysis, magnetic

113 susceptibility and radiocarbon dating to identify the tsunamis records. We have analysed 120

114 samples weighted 25 grams from core tubes every 15 cm for the geochemical analysis

115 including grain size, bulk mineralogy and totally organic and inorganic matter. The magnetic

116 susceptibility was measured every 3 cm in cores. The Bayesian simulation (Oxcal 4.2; Bronk-

117 Ramsey, 2009) is applied to the radiocarbon results and stratigraphic succession of coastal

118 deposits in order to generate a precise paleochronology of tsunami events.

120 **2. Major historical tsunamis of the Mediterranean coast of Egypt**

121 The tsunami catalogue of Egypt cites the work of Ambraseys (2005) that report

122 several large historical tsunamigenic earthquakes with severe damage in the eastern

123 Mediterranean regions (Table 1). Among these events, the tsunamis of 21 July 365, 8 August

124 1303 and 24 June 1870 inundated the harbour of Alexandria city as well as the Mediterranean

125 coast of Egypt.

126 Early in the morning of 21 July 365, an earthquake with estimated magnitude ~Mw 8-

127 8.5 located offshore West of Crete generated a major tsunami that affected the eastern

128 Mediterranean coastal regions (Ambraseys et al., 1994). The Roman historian Ammianus

129 Marcellinus (Guidoboni et al., 1994) reported sudden shaking with occurrence of a "gigantic"

130 wave toward the Mediterranean coastal areas. The tsunami wave generated great damage to

131 the Alexandria harbour and city. The ships were drowning up to house roofs due to the effect

132 of tsunami waves. As modelled by Hamouda (2009), the estimated wave height of this

133 tsunami was larger than 8 m in Alexandria. The seismic source of this earthquake is located in

western Crete, according to archeological and historical damage distribution, combined with coastal uplift measurements and modelling (Fig. 1; Guidoboni et al., 1994; Stiros, 2001; Shaw et al., 2008 and Ambraseys, 2009).

On 8 August 1303 a major earthquake with magnitude ~Mw 8 located between Crete and Rhodes islands (Fig.1) generated a tsunami that greatly damaged the coastal cities of the eastern Mediterranean (Ambraseys, 2009, Papadopoulos et al. 2014). Abu-El Fida (1907) reported that the Alexandria city and Nile delta were flooded in 1329 and many houses were damaged in Cairo and northern Egypt. In Alexandria, part of the city walls collapsed, the famous lighthouse was destroyed and some ships were torn apart and (or?) carried up inland due to the tsunami waves (Abu-El Fida, 1907).

On 24 June 1870, a large earthquake affected many places of the eastern Mediterranean region and was felt in Alexandria at around 18 h with no damage in the city but with slight damage in Cairo (Ambraseys, 2009). In Alexandria coastline and Nile Delta, the sea waves flooded the docks of ports and inland fields (Coumbary, 1870). The epicentre location of this earthquake at eastern edge of Crete is inferred from damage in Heraklion and related shaking felt around the east Mediterranean (Fig. 1; Schmidt, J.F., 1879; Jusseret and Sintubin, 2017).

The AD 365 and AD 1303 were classified as very large earthquakes (with Mw ≥ 8; Stiros et al., 2001; Shaw et al., 2008; Hamouda, 2006, 2009) that generated major tsunamis with basin-wide impacts, while the 1870 earthquake was of a lower magnitude (Mw ~7 – 7.5; Ben Menahem et al., 1991; Soloviev, 2000). Several studies of the 21 July 365 and 8 August 1303 historical earthquakes with tsunami waves report inundation in Alexandria and coastlines of northern Egypt, and therefore with the potential of tsunami records in the sedimentary deposits. There have been some debates on the 1870 event location, size and the possibility of tsunami waves, but several authors (Soloviev et al., 2000; Ben Menahem et al.,

159   1979; Salamon et al., 2007; Papadopoulos et al., 2010; and Maramai et al., 2014) support the

160   tsunami generation by 1870 earthquake.

162   **3. Coastal geomorphology and site selection for paleotsunami records**

163   The northwest Mediterranean coast of Egypt forms the northern extremity of the

164   Marmarica plateau which is a Miocene homoclinal limestone that extends west of Alexandria

165   for about 500 km (Sayed, 2013), acting as a major catchment area feeding the drainage system

166   (Fig. 1). The plateau runs from the Qattara Depression southward to the piedmont plain

167   northward with various elevations reaching ~100 m at Marsa Matrouh escarpment. The

168   geomorphological landform of the study area is characterized by a 60-m-high northern plateau

169   that includes ridges, sand dunes, lagoons, and rocky plains within a 20-km-wide strip along

170   the coastline (Fig. 1). The rocky Pleistocene limestone ridges include a veneer of carbonate

171   sand that are mostly composed of oolitic grains (Frihy et al., 2010).

172   The beach-dune ridge is developed along the receding Quaternary shorelines and

173   embayment of the Mediterranean Sea (Hassouba, 1995). Coastal dune-ridges protect inner

174   lagoons from the sea and constitute outstanding landform features at several locations parallel

175   to the shoreline (Figs 2). When the sand dunes are removed they leave rocky headland

176   outcrops (Abbas et al., 2008). The 2 to 20-m-high coastal beach-dune ridges mainly

177   composed of oolitic and biogenic calcareous sand separates coastal lagoons and *sabkhas* (salt

178   lake) from the sea. The lagoons with flat depressions separated from the sea by the coastal

179   dunes (with different heights and sometimes with seawater outlets) are likely sites for the

180   record of past tsunami deposits.

181   The accumulation of large boulders (Shah-Hosseini et al., 2016) near the selected sites

182   is considered as a possible witness of past tsunami events. However, the boulders along the

183   coastlines may either results from storms (Hall et al. 2006; Spiske et al. 2008) or tsunami

184   waves (Goff et al. 2006; 2009; Morhange et al. 2006). The imbricated surface observed in the

185   large boulders near our investigated sites directed towards south direction. These boulders

186   appear to be displaced by strong waves from the Mediterranean, and they are very similar to

187   the tsunami boulders studied along the Algerian coastline (Maouche et al. 2009).

188   The discrimination between storm and tsunami deposits is a challenge in the

189   Mediterranean regions (Maouche et al., 2009; Marriner et al., 2017). However, in comparison

190   with the high frequency of storm events and possible related deposits (Lionello et al., 2006),

191   the tsunami stratigraphic record is less recurrent (according to Tinti et al., 2001; Morton et al.,

192   2007) and often presents a specific sedimentary signature of mixed deposits such as : 1) The

193   basal contact of tsunami layer is extremely sharp with loadcast sedimentary structures where

194   layers contain organic rich mud and vegetation (Matsumoto et al., 2008; Switzer and Jones

195   2008); 2) the presence of rip up clasts that also suggest considerable erosion of lagoon and

196   soil deposits usually associated with tsunami deposits (Szczuciński et al 2006); 3) as shown

197   by the effect of 2011 Tohoku-oki earthquake tsunami in Hasunuma site and by the 2004

198   Sumatra earthquake tsunami in Thailand (Matsumoto et al., 2016), tsunami deposits show

199   general tendancy of thinning landward; 4) concentration of heavy minerals assemblages in

200   total sediments decreases in upward in the tsunami layer (Costa et al., 2014); 5) The low peak

201   value of magnetic susceptibility linked to the amount of sand originated from the littoral

202   dunes and reworked mixed sediments from tsunami waves (Font et al., 2010); 6) the large

203   number of mixed broken bivalve shells and gastropods occupy vertical and horizontal

204   stratigraphic positions due to high wave current (Donato et al., 2008); 7) the tsunami deposits

205   tendency of being poorly sorted, with bimodal grain particle size as compared with the storm

206   grain size which tends to be unimodal (Paris et al., 2007); 8) the saltwater inundation during

207   tsunami event indicated by chemical analysis and used as evidence of paleotsunami waves

208   (Chagué et al., 2011).

209   The local geomorphological and topographic settings contribute to the site selection

210   for paleotsunami investigations. Our site selection for trenching and coring took into account

211   the accessibility to dry lagoons (during summer season) in areas with no urbanization or

212   artificially reworked soil. Suitable sites for trenching and coring are located in areas protected

213   from the sea by the rather low (~2-m-high) sand dune topography that allows tsunami waves

214   and related material to deposit into the lagoon. Two ~200 km apart sites of seasonal dry

215   lagoons have met the selection criteria for paleotsunami investigation (Figs. 1 and 2): 1) Kefr

216   Saber located at ~32-km west of Marsa-Matrouh city, and 2) El Alamein site at ~10 km

217   northwest of El Alamein city and ~150 km west of Alexandria. Five trenches were dug at

218   Kefr Saber (Fig 2a), and 12 cores were performed at the El Alamein site (Fig 2b).

220   **4. Methods for paleotsunami investigations**

221   The trench size is typically ~2 x 1 meter with ~1.5-m-depth depending on the water

222   table reach; all trench walls exposed fine-grained sedimentary layers that were logged in

223   details. The conventional cores are arranged to be distributed in the lagoon area from

224   depression to the outlet of sea water in order to observe the thickness variations of high

225   energy sedimentary layers. The maximum core depth reached ~2.6 m.

226   The core tubes were split in half lengthwise, photographed using both normal and

227   ultra-violet lightning accompanied by detail description of textures and sedimentary

228   structures. An X-ray scanning was performed immediately after core opening and all cores

229   were sent to the laboratory of the National Institute of Geophysics and Astronomy (NRIAG,

230   Cairo) for sampling and further analysis. The magnetic susceptibility measurements were

231   operated along cores and samples were collected for radiocarbon dating, physical, chemical

232   and organic matter analyses.

233   The magnetic susceptibility was measured for cores every 3 cm at the NRIAG Rock

234   Magnetism laboratory then corrected against air by using Bartington compatible software.

235   120 samples were collected from cores every 15 cm for geochemical analysis with weighted

236   25 gram, and then analysed for a) grain size analysis (the procedures include separating the

237   weighed samples through a series of sieves (or screens) from 0.75 to 1000 microns. Statistics

238   of the grain-size distribution were calculated using Folk and Ward (1957) to obtain mean

239   grain-size and sorting of the sediments along the cores (see supplementary material, Tables S13 –

240   S24 and Figs.S16-S27); b) bulk minerology (X-ray diffraction using a Philips PW 1730

241   measurement). The intensity of the most intense diffraction peak of each mineral (see

242   supplementary material, Tables S1-12 and Figs.S4-S15) was measured and the identification of

243   crystalline substance and crystalline phases in a specimen is achieved by comparing the

244   specimen diffraction spectrum with spectra of known crystalline substances (according to the

245   International Centre for Diffraction Data - ICDD); c) The total organic and inorganic

246   measurements were carried out at the laboratory of Central Metallurgical Research &

247   Development Institute (CMRDI at Eltebbin, Egypt).

248   Three laboratories (Poznan laboratory in Poland, CIRAM in France and Beta

249   Analytical laboratory in USA) did the radiocarbon AMS dating of samples in order to ensure

250   quality of results (see Tables 2 a and b). The collected samples are made of charcoal, bones,

251   gastropods, shells and organic matter. The radiocarbon dating results of samples are

252   subsequently corrected using a recent calibration curve (Reimer et al., 2013) and the Oxcal

253   software (Bronk-Ramsay, 2009) for the probability density function with 2σ uncertainty for

254   each dated sample. In addition, from a succession of calibrated dates, a Bayesian analysis

255   provides the simulated age in probability density function of a catastrophic event. The

256   simulated age allows the correlation between the high energy sedimentary deposits, the

257   related isotopic chronology and the historical tsunami events in catalogues.

5. Description of sedimentary layers in trenches and cores with C14 dating results

The selected sites revealed a succession of sedimentary units typical of lagoon deposits with fine strata made of a mix of fine gravel, sand, silt and clay (Salama, 2017). At both Kefr Saber and El Alamein sites, trenches and cores present comparable soft sediment content and stratigraphy. The variation of sediments content in the different cores is due to the distance from the shore and to the core location in the lagoons with regard to dunes heights. A detailed description of the trenches and cores at both Kefr Saber and El Alamein sites is presented here below:

5. 1. Kefr Saber site: Trenches P1, P2, P3 and P4 are 40 to 154 meters distance from shoreline, have quite similar sedimentary succession with fine-grained mostly alluvial deposits made of sandy-silty layers with mixed coarse and white fine sand that contains broken shells of marine origin (Fig. 3 and trench logs in supplemental material S1). A conspicuous layer of white mixed sand, gravel and broken shells with variable 2 to 15 cm thicknesses is found at 25 – 55 cm below surface in P1, P2, P3; its thickness decreases landward to 1 cm in P4 (see supplemental material S1 a, b, c, d, e). Trench P5 which is close to the dunes and shoreline shows a succession of coarse and fine sand, and 30 to 40 cm thick mixed with pebbles which, as observed in other trenches, are fining inland.

The mixed radiocarbon dating of samples in trenches is an issue at Kefr Saber. Two charcoal samples collected in Trench P1 at 35 cm and 53 cm depth yield modern age (younger than 1650 AD) and 39000-38250 BC, respectively. In Trench P3, two other charcoal samples collected at 73 cm and 100 cm below surface and both below the high energy sedimentary layer labelled 1 (Fig. S1-b) indicate 50 - 70 AD and 5300-5070 BC, respectively (see also Table 2a). In Trench P4, four charcoal samples collected at 15 cm, 25 cm, 40 cm and 61 cm depth reveal modern ages (younger than 1650 AD). A fifth charcoal sample recovered at 60 cm below surface provides 17200- 15900 BC. In Trench P5, four charcoal samples are

collected with the uppermost sample located at 12 cm depth is dated at 360-50 BC, the second

sample at 17 cm depth show 30- 180 AD, the third, and fourth charcoal samples found at 33

cm and 37 cm depth are dated at 350 - 1050 BC and 2400-4000BC, respectively. The mixing

of old (older than 7000 years BP) and relatively young ages (younger than 2000 years BP)

points to reworked of former deposits and redeposit on a lagoon.

Results: Although the sedimentary deposits in trenches at Kefr Saber indicate mixed

and reworked sedimentation, the well identified coarse and fine white sand layer with broken

shells of marine origin located between 25 and 55 cm depth in all trenches P1 to P4 suggests

a single homogeneous sedimentary unit of relatively young age deposited in the lagoon.

Considering the deposits of neighboring trenches at Kefr Saber, and their relative sedimentary

chronology of units deposited in the same lagoon as comparable, and taking into the possible

reworked deposits that may include older ages, we selected the radiocarbon dates younger

than 2000 year BP that bracket the white sandy layer unit (i.e., samples TSU P5 S4 and S5,

TSU P3 S1 and S3 that predate the unit, and sample TSU P3 S2 that postdates the unit).

**5. 2. El Alamein site*:* The 12 cores extend between 1 m and 2.6 m depth and except,

for cores 1 and 9 which are shown in Figures 5 a and b, the detailed stratigraphic logs and

related measurements are presented in the supplemental material S2. In a previous

reconnaissance field investigation, a coarse and fine white sand layer was identified at ~ 30

cm below surface in a test pit. Two charcoal samples El Al sa1 and El Al sa2 collected at 25

cm and 56 cm depth give 1680-1908 AD and 1661-1931 AD ages, respectively. The

description of cores is as following:

Core 1: This core is located at ~166 m from the shoreline (Fig. 2 b), east of the study area

behind the sand dunes and near the outlet of the seawater. The core depth reached a depth of

~2.14 m and the stratigraphic section includes 3 high energy sedimentary layers recognized as

following (Fig. 5 a section 1 and its continuation at depth in Fig. S2-1):

The first layer located at ~12.5 cm depth, ~34.5 thick, is made of brown clay fine grained sediments, poorly sorted, with low peak in magnetic susceptibility, rich in organic matter, and X-ray image reflects clear lamination. The second layer which is located at ~70 cm depth has ~5 cm thickness, characterized by highly broken shells fragments with the very poor sorting of sediments granulometry. The third layer at ~75 cm depth is ~22 cm thick, made of pale yellow sand with poor sorting of sediments size, and a high peak in magnetic susceptibility. The chemical analysis shows the presence of gypsum and minor goethite, and X-ray scanning shows some turbiditic current structures with rip clasts, cross bedding and laminations. A fourth high energy sedimentary layer is identified at 158 cm (see Fig. S2-1; section 2). It is characterized by pale brown silty clay, with broken shell fragments and extremely poor sorting, and with a high peak of magnetic susceptibility at the base of the layer.

Two samples were collected for radiocarbon dating from core 1. The first and uppermost sample is a charcoal fragment at 40 cm below surface located within a layer of catastrophic mixed sedimentary unit characterized by poor sorting, highly broken shell fragments and the low peak value of magnetic susceptibility.

Core 2: As shown in (Fig.S2-2), the core 2 is ~90 cm deep, located at ~264 m from the shoreline (Fig. 2 b). Two penetrated high energy sedimentary layers are identified. The first layer is a ~12 cm thick brown clay sediments, at ~13 cm depth, mixed with gravel and sand. The layer is rich in organic matter (> 1), with a small peak of magnetic susceptibility and where the geochemical analysis shows a minor component of goethite. The second layer at ~50 cm depth is ~15 cm thick, made of mixed yellow sand with silty-clay pockets, broken shells fragments, poor sorting and with low peak magnetic susceptibility. It is rich in organic matter comparing to the other layer, and the geochemical analysis shows minor amounts of halite.

332   Several samples were collected below and above the high energy sedimentary layers

333   but, unfortunately, their content did not deliver enough carbon for dating. The two shells

334   (gastropod) samples collected at 75 cm and 77 cm depth (well below the lowermost high

335   energy sedimentary layer, Fig.S2-2) have calibrated dates 32971-34681 and 34362-36931 BC,

336   respectively (Table 2b). These obtained ages may well be due to a mixed and/or reworked

337   sedimentation.

338   **Core 3:** This core located at 270 m from the shoreline, has revealed three high energy

339   sedimentary layers near the outlet (lowland between high dunes) that allow tsunami wave

340   inundation (Fig. 2b and Fig. S2 – 3). The first layer is at ~25 cm depth and corresponds to a

341   26 cm thick pale brown clay characterized by broken shells fragments and sediments rich in

342   organic matter. The second layer at ~70 cm depth is 17.5 cm thick characterized by white

343   sand laminated at the top with a low peak of magnetic susceptibility, and with high organic

344   matter > 2 % of dry weight. The third layer at 106 cm below surface is 32 cm thick,

345   characterized by yellow sand with minor illite and broken shells fragments.

346   Two shell samples were collected for dating at 37 cm and 45 cm depth and have

347   calibrated dates 43618 BC and 34218-37224 BC respectively (Fig.S2-3 and Table 2b). These

348   two samples are located within the stratigraphic high energy sedimentary layer 2 and may

349   correspond to reworked sediments due to the high energy sedimentation during the

350   catastrophic event.

351   **Core 4:** The core is located at 435 m from the shoreline and shows sedimentary units where

352   we identify two high energy sedimentary layers with low magnetic susceptibility (Fig. S2 - 4).

353   The first layer is the white sand at ~12.5 cm depth 7 cm thick with poorly sorted sediments,

354   broken shells fragments with organic matter > 2 % of dry weight of total sediment fraction.

355   The second layer is pale yellow sand at ~102 to 130 cm depth, characterized by broken shell

356   fragments in a yellow sand with a minor amount of illite and gypsum.

357   One shell sample collected for dating at 37 cm depth provides a calibrated date at

358   32887-34447 BC (Table 2b). This sample located in the stratigraphic high energy sedimentary

359   layer 1 apparently results from high energy reworked sedimentation during the catastrophic

360   event (Fig. S2-4).

361   **Core 5:** The core is the southernmost in the El Alamein site, located at 490 m distance from

362   the shoreline (Fig. 2 b; Fig. S2 - 5). The core reaches a depth of 73 cm and the sedimentary

363   succession does not show any possible catastrophic sedimentary layer of high energy

364   sedimentary origin. According to its content, core 5 may show the limit of inundation area

365   with respect to at least the first and second high energy sedimentary layers.

366   **Core 6:** This core is located south of the sand dunes at 320 m from the shoreline (Fig. 2 b). It

367   is characterized by three high energy sedimentary layers (Fig. S2 - 6). The first layer is a ~24

368   cm thick pale yellow sand with broken shells fragments (between 5 and 26 cm depth) and

369   poorly sorted sediments rich in organic matter (larger than 2.5). The second layer is ~18.5 cm

370   thick at 50 - 75 cm depth characterized by yellow sand with mixed gastropods and bivalves,

371   and a high value of magnetic susceptibility at the base of the layer. The third layer at 130 cm

372   depth is ~20 cm thick, rich in organic matter, characterized by white sand mixed with gravel

373   and pebble and bioclasts.

374   Three samples were collected for dating in core 6. The first sample is a gastropod shell

375   at ~45 cm depth and shows 35002-37441 BC calibrated dates. The second and third samples

376   are coral fragments at ~60 cm and ~80 cm depth that gave 42776-69225 BC and modern

377   (younger than 1650AD) calibrated ages. The first sample is above the high energy

378   sedimentary layer 2 while the second sample was within the stratigraphic high energy

379   sedimentary layer 2 (Fig S2-7). These samples may result from mixed sedimentation and

380   reworking due to high current waves.

381   **Core 7:** This core was located at 273 m from the shoreline (Fig. 2 b). It is characterized by

382   sedimentary units that may include three high energy sedimentary layers within 120 cm core

383   depth (Fig. S2 - 7). The first layer is a 6 cm thick brown sand with broken shell fragments at

384   ~14 cm depth and a considerable amount of cement gypsum with a minor amount of Illite and

385   goethite. It is rich with organic matter (> 2) of a swampy environment and the noticeable peak

386   of magnetic susceptibility. The second layer at 50 cm depth is 20 cm thick, characterized by

387   laminated pale brown clay mixed with gravel and pebbles at the bottom. The third layer is 15

388   cm thick at 115 cm depth characterized by white sand, poor sorting sediments with a minor

389   amount of pyrite.

390   A single sample of shell fragment collected at 17 cm depth for radiocarbon dating

391   within high energy sedimentary layer 1 provides an age 293-1113 BC.

392   **Core 8:** This core is located at 214 m from the shoreline (Fig. 2 b). Three high energy

393   sedimentary layers are recognized (Fig.S2 - 8). The first layer is a 16 cm thick pale yellow

394   silty clay at ~14 cm depth, rich in organic matter, with minor amount of goethite and bioclasts

395   rich. The second layer is a 22 cm thick at ~52 cm depth, of pale yellow silty-clay with broken

396   shells, characterized by a high peak of magnetic susceptibility and rich inorganic matter

397   (>2.5). The third layer is 9 cm thick at ~128 cm depth, characterized by pale yellow sand with

398   broken shell fragments and poorly sorted angular gravel sized clasts. No samples were

399   suitable for dating in this core.

400   **Core 9:** The core is located at 130 m from the shoreline. Three high energy sedimentary

401   layers are recognized (Fig. 5 b; Fig. S2 - 9). The first layer is white sand at ~16 cm depth and

402   13 cm thick with a high content of organic matter and rip up clasts that appear in X-ray

403   scanning characterized by highly broken shell fragments and rich in organic matter. The

404   second layer at 67 cm depth is 22 cm thick characterized by white sand, with a peak of

405   magnetic susceptibility, high content of organic matter larger than 5. The third layer at 139 cm

406 depth is 14 cm thick characterized by broken shell fragments and white sand with highly

407 angular sediments that reflect the poor granulometric sorting.

408   Two samples were collected for dating in core 9. The first sample is a gastropod shell

409 located at 24 cm depth within the high energy sedimentary layer 1 and gives a 1052-1888 BC

410 calibrated age. The second sample at 55 cm depth is a bivalve (lamellibranch) located above

411 the high energy sedimentary layer 2 dated at 40521-43169 BC calibrated age.

412 **Core 10:** The core is located at 245 m from the shoreline (Fig. 2 b). Three high energy

413 sedimentary layers are recognized (Fig. S2 - 10). The first layer is 9 cm thick brown silty clay,

414 at ~19 cm depth with broken shells fragments, rich in organic matter (> 4) and high peak of

415 magnetic susceptibility; rip up clasts and laminations appear in X-ray scanning. The second

416 layer 38 cm thick brown sand at 48 cm depth with broken fragments of shells, peak of

417 magnetic susceptibility and high organic matter (> 1.5) at the bottom of the layer. The third

418 layer is 28 cm thick pale yellow sand at 101 cm depth. It is characterized by rich organic

419 matter and poor sorting sediments.

420   Two samples were collected for dating in core 10. The first sample located in the high

421 energy sedimentary layer 1 is a shell fragment at 24 cm depth that gives 2623-3521 BC

422 calibrated age. The second sample located in the high energy sedimentary layer 2 is a rodent

423 bone at 70 cm below surface with estimate age of 41256-46581 BC calibrated age (see also

424 Table 2b).

425 **Core 11:** The core is located at 151 m from the shoreline (Fig. 2 b). Three high energy

426 sedimentary layers are recognized (Fig.S2 - 11). The first layer is 10 cm thick white sand with

427 broken shell fragments at ~19 cm depth; the layer also shows high magnetic susceptibility,

428 rich organic matter (> 4) with a high percent of gypsum (>50%). The second layer is 9 cm

429 thick white sand at 76 cm depth, with broken shell fragments, a high peak of magnetic

430 susceptibility and organic matter larger than 1.5. The third layer is 21 cm thick grey silty sand,

431 with broken shell fragments at 107 cm depth; poor sorting, high organic rich matter and a

432 minor amount of Illite and gypsum.

433   Eight samples were collected for dating in core 11. The sedimentary units at 112 - 175

434 cm depth (core bottom) and related succession of ages between 3943 BC and 2475 BC (from

435 shell gastropods and a charcoal fragment; see Table 2 b), may indicate a consistent dating of

436 the high energy sedimentary layer 3. However, the first sample (gastropod shell) at ~20 cm

437 depth that gives 3638-4328 BC, the second sample (broken shell) at 62 cm depth with an age

438 at 17869 - 18741 BC, and the 33294 – 36120 BC and 2619 – 3386 BC out of sequence dating

439 (Table 2 b).

440 **Core 12:** The core is located at 127 m from the shoreline (Fig 2 b). Four high energy

441 sedimentary layers are recognized in section 1 and one high energy sedimentary layer in

442 section 2 (Fig. S2 – 12 a, b). The first layer is ~7.5-cm-thick at ~19-cm-depth and is made of

443 poorly sorted white sandy deposits, and highly broken gastropods and lamellibranch fossils.

444 The layer is characterized by high value of organic matter and low peak magnetic

445 susceptibility. The second layer is ~13-cm-thick white sandy deposits intercalated with coarse

446 brown sand at ~32.5-cm-depth, characterized by horizontal lamination, poor sorting

447 sediments, rich in organic matter and high peak of magnetic susceptibility. The third layer is

448 ~25-cm-thick grey sandy clay at 89-cm-depth, with laminations at the bottom of deposits,

449 vertically aligned gastropods, broken shells fragments, rich in total organic matter and a low

450 peak of magnetic susceptibility. A fourth high energy sedimentary layer of medium to fine

451 pale yellow sand, with broken shells fragments, is identified in section 2 (Fig. S2 – 12 b) at

452 151 cm depth. It is characterized by poor sorting, low peak of magnetic susceptibility, a large

453 amount of organic matter (> 5.5) and high amount of gypsum.

454   Five samples were collected for dating in core 12. In core section 1, the first sample is

455 a gastropod found at 44 cm depth that gives an age of 3367-3366 BC. The second sample is a

456   shell found at 108 cm depth and shows an age of 3097-3950 BC (Table 2 b). The third sample

457   is a gastropod found at 114 cm depth dated at 3331-4050 BC. The fourth and fifth samples in

458   core section 2,sample are gastropod shells found at 117 cm and 135 cm depth with calibrated

459   age 39560- 40811 BC and 3365-4071 BC, respectively (Table 2 b). The fourth sample is off

460   sequence with respect to the other samples and may result from sediment transport and

461   reworking due to high energy waves. The other samples are in sequence from 4071 to 2457

462   BC age, comparable to the sedimentary succession of core 11.

463   ***Results:*** The sedimentary deposits in the El Alamein lagoon also result from

464   intercalated high-energy marine deposits into low energy marine and alluvial deposits with

465   reworked sedimentation. A first observation in almost all cores is the existence of the white

466   sand layer with broken shells of marine origin located ~ 10 cm to 170 cm depth in El Alamein

467   site, and the identified three to four high energy sedimentary layers.

468

469   **6. Summary of results from trenching and coring**

470   The cores and trenches in both Kefr Saber and El Alamein sites expose three main

471   layers characterized by fine and coarse sand mixed with bioclasts. We assume that indicate

472   the occurrence of high energy and catastrophic sedimentary deposits in the coastal lagoon

473   environment (Figs. 2 a, b, and c, and Fig. 3). Although the two studied sites are ~200 km

474   apart, a white sandy layer with broken shells is found in all trenches (see Fig. 3 and

475   supplemental material S1 a, b, c, d, e) and cores (except for core 5, see Figs. 5 a and b, and

476   supplemental material in Fig. S2 – 1 to 12). The recurrent white sandy deposits in trenches

477   and cores are well visible as coarse sand units mixed with gravel and broken shells that

478   become finer-grained and thinner landward (see trench P4, Fig. 3) or disappear when distant

479   from the shore (core 5, Fig. S2 –5). The high energy sedimentary characteristics with four

480 layers in the ~ 2 m thick sedimentary units suggest that these layers are tsunami deposits

481 rather than storm.

482   In most cores (Figures. 5 a and b, and supplemental material Fig. S2 – (1 - 12), the

483 first tsunami layer is ~7.5-cm-thick at ~19 cm-depth and is made of poorly sorted white sandy

484 deposits with broken gastropods and lamellibranch (shell) fossils. This layer is characterized

485 by bi-modal grain size distribution with high value of organic matter and low peak of

486 magnetic susceptibility with a rich content in carbonates and quartz. Goethite and pyrite

487 heavy minerals were found in the cores at the base of layer 1, which also contains rip up clasts

488 from underlying sediments. The second layer is ~13-cm-thick at ~32.5-cm-depth

489 characterized by white sandy deposits intercalated with laminated coarse brown sand, very

490 poor sorting of sediments, rich in organic matter and with a low peak of magnetic

491 susceptibility. Pebbles are found at the base of this layer which reflects a loadcast sedimentary

492 structure. A considerable amount of heavy minerals like goethite and pyrite can be found in

493 this layer. The third layer is ~25-cm-thick at ~89-cm-depth is made of grey sandy clay, with a

494 high peak of magnetic susceptibility, laminations at the bottom of deposits, vertically aligned

495 gastropods, broken shell fragments, and rich in total organic matter. In all three layers, the

496 poorly sorted sediments and organic content are greater than 5 % of dry weight in the high

497 energy deposits and tsunami records. These characteristics at the El Alamein site lead us to

498 interpret the three sedimentary layers as tsunami deposits. The tsunami layers and their

499 catastrophic content are identified in photography and X-rays, magnetic susceptibility,

500 organic/mineral content and by the existence of mixed coarse and fine sand with broken

501 marine shells. A main difficulty, however, is the age determination of the tsunami layers due

502 to the mixed radiocarbon dates that can be ranged in old and young ages, between 50000 year

503 BP - 13430 year BP, and 5065 year BP - 125 year BP, respectively, in all cores .

In a synthesis of all dated units in trenches and cores in Figures 4 and 6, the sedimentary succession of low energy lagoon and marine and alluvial deposits intercalated with high-energy deposits provides evidence for the identification of four tsunami deposits at Kefr Saber and El Alamein sites. In the case of Kefr Saber trenches, the dating of charcoal fragments allows to bracket of a tsunami event with a simulated age between AD 137 and AD 422, which includes the AD 365 western Crete earthquake (Figs. 4 and Table 2 a). The dating of sedimentary units at the El Alamein site turned out to be more complex due to highly reworked sedimentation and significant mix of old (> 13000 year BP) and young ages (< 5500 year BP; Table 2 b). Using the latter ages, the radiocarbon dating (including the Oxcal Bayesian analysis) of shells, bone and charcoals fragments at El Alamein site (Fig. 6) results in a sequence of ages that allow to bracket of an event W between 1434 BC and 1126 BC, and event X between AD 48 and AD 715, and event Y between AD 1168 and AD 1689, and an event Z between AD 1805 and AD 1935 (Figure 6). The three most recent simulated dates of tsunami events X, Y and Z might correlate with the seismogenic tsunamis of AD 365, AD 1303 and AD 1870 reported in catalogues (Table 1).

In the north of the trench sites at Kefr Saber, the dating of shells Dendropoma (worm snails) of common species Dendropoma petraeum and Vermetus triquetrus of a sample collected in a large boulder Long: 26° 55.154 and Lat.: 31° 26.385 provide a radiocarbon calibrated date of 940-1446 AD. The dating of Dendropoma collected in a boulder often marks the catastrophic coastal environmental change with displaced large boulders from an intertidal to shoreline position due to a tsunami event. The Dendropoma sample age at Kefr Saber may correlate with the 8 August 1303 earthquake and tsunami event that dragged large boulders on the shoreline in agreement with the results of Shah-Hosseini et al. (2016). However, we could not identify the 1303 event in the trenches dug in the nearby lagoon at Kefr Saber.

529

530   **Discussions and Conclusions**

531   The identification of high energy sedimentary layers considered as tsunami deposits

532   within the stratigraphic layers and results of radiocarbon dating allow us to identify four

533   tsunami events (Figs. 4 and 5). The historical seismicity catalogue of the Eastern

534   Mediterranean reported two significant tsunamigenic seismic events of the Hellenic

535   subduction zone that affected the Mediterranean coast of Egypt: 1) The 21 July 365

536   earthquake (Mw 8.3 – 8.5; Stiros and Drakos, 2006; Shaw et al., 2008), 2) the 8 August 1303

537   earthquake (Mw 7.8 – 8.0; Abu Al Fida, 1907; Ambraseys, 2009). A third tsunami event is

538   also reported during the 24 June 1870 earthquake (Mw 7 - 7.5), but despite some debates on

539   its occurrence, the inundation of the Alexandria harbour leaves no alternative on the tsunami

540   waves on the Egyptian coastline (see section 2).

541   In our study, the distinction of tsunami sedimentary records from storm deposits is

542   based on: 1) The record of the small number (3 to 4) layers while storm deposits controlled by

543   seasonal climatic catastrophic events should have been more frequent (Lionello et al., 2006;

544   Morton et al., 2007). 2) The existence of white sand sheet layers with broken shells at two

545   sites (Kefer Saber and El Alamein) located ~200 km apart, bearing comparable age, structure

546   and texture. This is a probable large tsunami. 3) The existence of organic rich clasts in sand

547   sheets of some cores which indicates a catastrophic event with sufficient energy to break and

548   erode the coastal barrier made of the shoreline rocky headlands, organic sediments and coastal

549   dunes before reaching the lagoons. 4) The bimodal distribution of the grain size of sandy

550   sedimentary units that include a large proportion of broken shell comparable to that of

551   tsunami deposits (Scheffers and Kelletat, 2003). 5) The correlation between the simulated

552   ages of tsunami layers from the radiocarbon dating and the large historical tsunamigenic

553   earthquakes of the eastern Mediterraan (Figs. 4 and 6). 6) The high energy fining inland

554   sedimentary sequence observed in trenches and cores which is related to tsunami deposits

555   rather than storm deposits. 7) The consistent depth of tsunami layers in cores of the El

556   Alamein site (Fig. 7).

557   The magnetic susceptibility measurements along the cores are normally having low

558   peak value (values near surrounded the zero value). It reflects a tsunami layer because it

559   contains more carbonates and quartz than the underlying sediments. This rule are not coincide

560   all the cores due to presence of 0.91 -14.9 % of goethite and 1.3 - 21.02 % of pyrite iron

561   oxides minerals. The value of the peak increase slightly above the zero value and reach 20-

562   100 X 10^{-6} of magnetic susceptibility and this increase happen usually on the bottom of the

563   tsunami layer.

564   As the sedimentary units in the 1 m to 2.6 m depth cores result from young deposition

565   processes with high-energy marine units intercalated into low energy marine and alluvial

566   deposits, we consider the radiocarbon dating older than 13430 year BP as a result of

567   reworking of older rocks. Considering that the succession of 2.6 m uppermost deposits and

568   related stratigraphic chronology are comparable in all cores in the El Alamein lagoon, we

569   select the radiocarbon dates younger than 5500 year BP as representative of the recent

570   sedimentary units that include tsunami layers. Using the radiocarbon dating of samples and

571   related selected young ages, the sedimentary sequence of catastrophic layers and their ages

572   obtained from the Bayesian simulation (Oxcal 4.2; Bronk-Ramsey, 2009) allow a correlation

573   with the AD 365, AD 1303 and AD 1870 tsunamigenic earthquakes of the east Mediterranean

574   Sea (Fig. 6). Hence, the dating of the three high energy sedimentary layers deposited along

575   the Egyptian coastline at Kefr Saber and El Alamein sites correlate with the historically

576   recorded seismogenic tsunamis of the Hellenic subduction zone. In addition, a fourth tsunami

577   layer can be identified between 1126 BC and 1434 BC.

The lagoon sedimentary environment is a natural site of mixed and reworked marine and continental deposits, with a significant erosion during major tsunamis that may explain the mixed radiocarbon dates (Tables 2 a and b). The mixing of old (older than 7000 years BP) and relatively young ages (younger than 2000 years BP) points to reworked of former deposits and redeposit on a lagoon environment. The apparently incoherent dating may result from: 1) The different type of samples used in radiocarbon dating as charcoal, shell, bone and root (see Tables 2 a and b), and uncertainties that also result from different species of mollusks, and/or the reservoir effect; 2) the old events as a result of eroded or transported deposits of previous tsunami or storm waves, which is difficult to evaluate since we found that the stratigraphic record of these high-energy events is probably incomplete or underestimated (Tables 2 a and b where among 30 samples 12 dated samples are > 30 ka).

Indeed, by considering the mixed sedimentation of reworked deposits intercalated with new units, our selection of samples younger than 2000 year BP at Kefr Saber, and younger than 5500 year BP at El Alamein allowed us to distinguish between old and new isotopic dating and infer a consistent chronology of tsunami deposits. For instance at the El Alamein lagoon, the clear separation between old (50000 year BP to13430 year BP) and young (5065 year BP - 125 year BP) radiocarbon dating, with no intermediate dates of sedimentation, confirms the different origin and processes of deposition. The radiocarbon dating indicates that the white sand and coarse mixed layers represent deposits that may result from tsunami events in 365, 1303 and 1870 (see Table 1). The first two events correlate with large earthquakes with Mw≥8 with well documented tsunami waves in the historical sources. The existence of the 365 tsunami seems to be widely recorded through widespread massive turbidities of the eastern Mediterranean region (Stanley and Bernasconi 2006; Polonia et al., 2016). The four recognized catastrophic layers in trenches and cores have physical and chemical characteristics that correlate with high energy environmental conditions of tsunami

603   deposits. The four low magnetic susceptibility peaks of the four deposits also correlate with

604   the high content of organic carbon matter and carbonates.

605   The record of past tsunami deposits along the Egyptian Mediterranean coastline is

606   favored by the low topography and platform geomorphology. The coastal environment with

607   similar lagoons and dunes with large areas with relatively flat morphology allowed the

608   deposits of catastrophic marine deposits intercalated within alluvial deposits. The lagoon

609   shapes elongated along the shoreline at Kefr Saber and El Alamein sites explain the similarity

610   between the sedimentary units and the tsunami deposits. The correlation between the core

611   deposits at El Alamein and trench deposits at Kefr Saber is marked by the dating of tsunami

612   deposits and the correspondence one of them with the AD 365 earthquake. The succession of

613   sudden high-energy deposits with low energy and slow sedimentation may include reworked

614   units that imply a disorder in the chronological succession. Although the results of dated

615   shells may be suspicious (due to the unclosed mineralogical system), their reliability is tested

616   with the comparison of nearby radiocarbon dating.

617   The size of past tsunamis can be compared with the thickness of catastrophic

618   sedimentary units in trenches at Kefr Saber and core units of the El Alamein site. It appears

619   that the tsunami deposits of the AD 365 tsunamigenic earthquake are thicker at Kefr Saber

620   site than at the El Alamein site. In contrast, the thickness of sedimentary layers of the AD

621   1303 and AD 1870 are thicker at the El Alamein site. These results on the identification of

622   past tsunamis and their repetition along the coastlines in Egypt and North Africa are decisive

623   for the tsunami wave propagation and hazard models in the East Mediterranean Sea (Salama,

624   2017).

625

626

627

Acknowledgments

We are grateful to Prof. Hatem Odah and NRIAG administration, and staff for their keen efforts and help during the development of this work. We are grateful to the North African Group for Earthquake and Tsunami studies (NAGET) and Drs. Assia Harbi, Adel Samy, Hany Hassen, Mohamed Maklad, Mohamed Sayed for support and discussions. We are grateful to the "*Centre d'Etudes Alexandrine*" for the lending of the COBRA instrument for coring. We address our special thanks to the Egyptian Armed Forces for issuing permissions and their support during field work. This research programme is conducted with the funding support of the ASTARTE EC project (Assessment, Strategy And Risk Reduction for Tsunamis in Europe - FP7-ENV2013 6.4-3, Grant 603839), the French-Egyptian IMHOTEP project, and the Academy of Scientific Research and Technology of Egypt.

Supplementary data

Supplementary data associated with this manuscript are:
- Figures S1 a, b,c, d and e of five trench logs of Kefr Saber site (trench P4 as Fig. 3).
- Figure S2 – 1 (section 2) to 10 of core descriptions of El Alamein site (cores 1 and 9 as Figs a and b).

References

Abbas, M.S., El-Morsy, M.H., Shahba, M.A. and Moursy, F.I.,: Ecological studies in coastal sand dune rangelands in the North-West of Egypt, Meeting of the Sub-network on Mediterranean Forage Resources of the FAO-CIHEAM Inter-regional Cooperative Research and Development Network on Pastures and Fodder Crops, Spai: , 389–393, 2008.

Abu al-Fida Ismail Ibn Hamwi (born 1273 – died 1331). : The Concise History of Humanity or Chronicles (in Arabic **'Tarikhu 'al-Mukhtasar fi Akhbar al-Bashar' in 1329**). Al-Husayniyah Press, Cairo, 2 volumes , 1112 p., 1907.

Ambraseys, N.N., Melville, C.P. and Adam, R.D.: The seismicity of Egypt, Arabia and Red Sea: A Historical Review, Cambridge University Press, 181 p., 1994.

Ambraseys, N.N., Melville, C.P. and Adams, R.D.: The seismicity of Egypt, Arabia and the Red Sea: a historical review. Cambridge University Press, 181p., 2005

Ambraseys, N.: Earthquakes in the Mediterranean and Middle East: A Multidisciplinary Study of Seismicity up to 1900, Cambridge University Press, 947 p., 2009.

Atwater, B.: Evidence for great holocene earthquakes along the outer coast of Washington state, Science, 236, 942 – 944, 1987.

Bondevik, S., S.K. Stormo, and G. Skjerdal.: Green mosses date the Storegga tsunami to the chilliest decades of the 8.2 ka cold event. Quaternary Science Reviews 45, 1–6, 2012

Ben Menahem, A.: Earthquake catalogue for the Middle East (92 B.C. to 1980 A.D.) Bollettino di Geofisica Teorica ed Applicata, 2I, 245-310, 1979.

Ben Menahem, A.: Four thousand years of seismicity along the Dead Sea rift, Journal of Geophysical Research, 96, 195–216, 1991.

Bronk Ramsey, C.: Bayesian analysis of Radiocarbon, Radiocarbon, 51(1), 337–360, 2009.

Bronk Ramsey, C., & Lee S.: Recent and Planned Developments of the Program OxCal, Radiocarbon, 55(2-3), 720-730, 2013.

Coumbary, A. : Sur le tremblement de terre du 24 juin 1870, Nouvelles Météorologiques Paris, 3, 200-201, 1870.

Chagué-Goff, C., Schneider, J.-L., Goff, J.R., Dominey-Howes, D., Strotz, L.: Expanding the proxy toolkit to help identify past events — lessons from the 2004 Indian Ocean Tsunami and the 2009 South Pacific Tsunami, Earth-Science Reviews, 107, 107–122, 2011

Costa, P.J.M., Andrade, C. Freire, Freitas, M.C., Oliveira, M.A., Cascalho, J., Application of microtextural and heavey mineral analysis in the study of onshore tsunami deposits – examples from Portugal, Scotland and Indonesia, Comunicações Geológicas, III, 1439-1443, 2014.

CMT catalogue: Centroid Moment Tensor catalogue of Harvard, http://www.seismology.harvard.edusearch.html.

De Martini, P.M., Barbano, M.S., Pantosti, D., Smedile, A., Pirrotta, C., Del Carlo, P., and Pinzi, S.: Geological evidence for paleotsunamis along eastern Sicily (Italy): An overview: Natural Hazards and Earth System Sciences, 12 (8), 2569–2580, 2012.

Donato, S.V., E.G. Reinhardt, J.I.Boyce, R. Rothaus & T. Vosmer.: Identifying tsunami deposits using bivalve shell taphonomy, Geology, 36 (3), 199-202, 2008.

691   El-Sayed, A., Korrat, I., and Hussein, H. M.: Seismicity and seismic hazard in Alexandria
692   (Egypt) and its surroundings, Pure and Applied Geophysics, 161, 1003–1019, 2004.

693   Folk RL, Ward WC. : Brazos River bar: a study in the significance of grain size parameters.
694   Journal of Sedimentary Petrology 27: 3–26, 1957.

695   Font, E., C. Nascimento, Baptista M.A. & Silva P.F.: Identification of tsunami induced
696   deposits using numerical modelling and rock magnetism techniques: A study case of the
697   1755 Lisbon tsunami in Algarve, Portugal, Physics of the Earth and Planets Interiors,
698   182, 187–198, 2010

699   Frihy , O.E., Deabes, E. a., and El Gindy, A. a.: Wave Climate and Nearshore Processes on
700   the Mediterranean Coast of Egypt: Journal of Coastal Research, 261, 103–112 , 2010.

701   Fokaefs, A., and G. A. Papadopoulos.: Tsunami hazard in the Eastern Mediterranean: strong
702   earthquakes and tsunamis in Cyprus and the Levantine Sea, Natural Hazards, 40 (3), 503–
703   526, 2007.

704   Galanopoulos, A.G.: The seismic sea-wave of 9 Iouliou 1956, Praktika Academy Athens, 32,
705   90–101, 1957.

706   Goff J, Dudley WC, de Maintenon MJ, Cain G, Coney JP.: The largest local tsunami in 20th
707   century Hawaii, Marine Geology 226, 65–79, 2006

708   Goff, J.R., Lane, E., Arnold, J.: The tsunami geomorphology of coastal dunes, Natural
709   Hazards Earth System Sciences, 9 (3), 847–854, 2009.

710   Guidoboni, E., Comastri, A. and Traina G.: Catalogue of Ancient Earthquakes in the
711   Mediterranean area up to the 10th century, INGV-SGA, Bologna, 504 p., 1994.

712   Guidoboni, E., and A. Comastri : Catalogue of earthquakes and tsunamis in the Mediterranean
713   area from the 11th to the 15th century, INGV-SGA, Bologna, 1037 p., 2005.

714   Hassouba, A.B.H.: Quaternary Sediments from the Coastal Plain of Northwestern Egypt
715   (from Alexandria to Elomayid), Carbonates and Evaporites, 10 (1), 8–44, 1995.

716   Hall AM, Hansom JD, Williams DM, Jarvis J.: Distribution, geomorphology and lithofacies
717   of cliff- top storm deposits: examples from the high-energy coasts of Scotland and
718   Ireland. Marine Geology, 232, 131–155, 2006.

719   Hamouda, A.Z.: Numerical computations of 1303 tsunamigenic propagation towards
720   Alexandria, Egyptian coast, Journal African Earth Science, 44, 37-44, 2006.

721   Hamouda, A.Z.: A reanalysis of the AD 365 tsunami impact along the Egyptian
722   Mediterranean coast, Acta Geophysica, 58 (4), 687–704, 2009.

723 Jusseret, S. and Sintubin, M., Minoan Earthquakes: Breaking the Myth through
724   Interdisciplinarity, Studies in Archaeological Sciences, Leuven University Press, 440 pp.,
725   2017.

726 Lario, J., Zazo, C., Goy, J.L., Silva, P.G., Bardaji, T., Cabero, A., Dabrio, C.J., Holocene
727   palaeotsunami catalogue of SW Iberia. Quaternary International 242, 196–200, 2011.

728 Lionello, P., J. Bhend, A. Buzzi, P.M. Della-Marta, S.O. Krichak, A. JansÃ, P. Maheras, A.
729   Sanna, I.F. Trigo, and R. Trigo, Chapter 6 in Cyclones in the Mediterranean region:
730   Climatology and effects on the environment", Elsevier, 4, 325-372, 2006.

731 Maamoun, M., Megahed, A. and Allam, A.: Seismicity of Egypt, NRIAG Bulletin, IV (B),
732   109–160, 1984.

733 Maramai, A., Brizuela, B., Graziani, L. : The Euro- Mediterranean tsunami catalogue. Annals
734   of Geophysics, 57 (4), 1-26, 2014.

735 Marriner, N., Kaniewski, D., Morhange, C., Flaux, C., Giaime, M., Vacchi, M., and Goff, J.:
736   Tsunamis in the geological record, making waves with a cautionary tale from the
737   Mediterranean, Science Advances, 1-12, 2017.

738 Malik, J.N., Banerjee, C., Khan, A., Johnson, F.C., Shishikura, M., Satake, K., and Singhvi,
739   A.K.: Stratigraphic evidence for earthquakes and tsunamis on the west coast of South
740   Andaman Island, India during the past 1000years, Tectonophysics, 661, 49–65, 2015.

741 Matsumoto, D., H. Naruse, S. Fujino, A.Surphawajruksakul, T., Jarupongsakul, N., Sakakura
742   & M. Murayama: Truncated flame structures within a deposit of the Indian Ocean
743   Tsunami: evidence of syn-sedimentary deformation, Sedimentology, 55, .1559-1570,
744   2008.

745 Matsumoto, D., Sawai, Y., Tanigawa, K., Fujuwara, O., Namegaya, Y., Shishikura, M.,
746   Kagohara, K., Kimura, H., Tsunami deposit associated with the 2011 Tohoku-oki tsunami
747   in the Hasunuma site of the Kujukuri coastal plain, Japan, Island Arc, 25, 269-385, 2016.

748 Maouche, S., Morhange, C. and Meghraoui, M.: Large boulder accumulation on the Algerian
749   coast evidence tsunami events in the western Mediterranean, Marine Geology, 262 (1),
750   96-104, 2009.

751 Meltzner, A.J., K. Sieh, H.-W. Chiang, C.-C. Shen, B.W. Suwargadi, D.H. Natawidjaja, B.E.
752   Philibosian, R.W. Briggs, and J. Galetzka, Coral evidence for earthquake recurrence and
753   an A.D. 1390-1455 cluster at the south end of the 2004 Aceh-Andaman rupture, *J.
754   Geophys. Res.***115**, B10402, doi:10.1029/2010JB007499, (2010).

755 Minoura, K., Imamura, F., Kuran, U., Nakamura, T., Papadopoulos, G. A., Takahashi, T.,
756   Yalciner, A. C.: Discovery of Minoan tsunami deposits. *Geology* 28(1):59–62. 2000.

757 Morhange, C., Marriner, N., Pirazzoli, P.A.: Evidence of Late-Holocene tsunami events from

758   Lebanon, Z. Geomorphology, 46, 81–95, 2006.

759 Morton, R, A., Gelfenbaum, G. and Jaffe, B. E., Physical criteria for distinguishing sandy

760   tsunami and storm deposits using modern examples,

761   Sedimentary Geology, 200, 3, 184-207, 2007.

762 Nanayama, F., Satake, K., Furukawa, R., Shimokawa, K., Atwater, B.F., Shigeno, K., and

763   Yamaki, S.: Unusually large earthquakes inferred from tsunami deposits along the Kuril

764   trench, Nature, 424 (6949), 660–663, 2003.

765 Paris, R., F., Lavigne, P.,Wassmer, and J.,Sartohadi : Coastal sedimentation associated with

766   the December 26, 2004 tsunami in Lhok Nga, West Banda Aceh (Sumatra, Indonesia).

767   Marine Geology, 238, 93–106, 2007.

768 Papadopoulos, G.A., E. Daskalaki, A. Fokaefs and N. Giraleas.: Tsunami hazard in the

769   Eastern Mediterranean Sea: strong earthquakes and tsunamis in the West Hellenic Arc

770   and Trench System, Journal Earthquake and Tsunami, 4 (3), 145-179, 2010.

771 Papadopoulos, G.A., Minoura, K., Imamura, F., Kuran, U., Yalçiner, A., Fokaefs, A.,

772   Takahashi, T., Strong earthquakes and tsunamis in the East Hellenic arc. Research in

773   Geophysics 2 (e12), 90–99. http://dx.doi.org/10.4081/rg.2012.e12. 2012.

774 Papadopoulos, G. A., Gràcia, E., Urgeles, R., Sallares, V., De Martini, P. M., Pantosti, D.,

775   González, M., Yalciner, A. C., Mascle, J., Sakellariou, D., et al.: Historical and pre-

776   historical tsunamis in the Mediterranean and its connected seas: Geological signatures,

777   generation mechanisms and coastal impacts, Marine Geology, 354, 81–109, 2014.

778 Polonia, A., Vaiani, S.C., de Lange, G.J.: Did the A.D. 365 Crete earthquake/tsunami trigger

779   synchronous giant turbidity currents in the Mediterranean Sea?, Geology, 44, 191-194,

780   2016.

781 Poirier, J. P. and Taher, M.A.: Historical Seismicity in the near and Middle East, North

782   Africa, and Spain from Arabic Documents (VIIth- XVIIIth Century). Bulletin Society

783   Seismology American, 70 (6), 2185–2201, 1980.

784 Reimer PJ, Bard E, Bayliss A, Beck JW, Blackwell PG, Bronk Ramsey C, Buck CE, Edwards

785   RL, Friedrich M, Grootes PM, Guilderson TP, Haflidason H, Hajdas I, Hatté C, Heaton

786   TJ, Hogg AG, Hughen KA, Kaiser KF, Kromer B, Manning SW, Reimer RW, Richards

787   DA, Scott EM, Southon JR, Turney CSM, van der Plicht J.: Selection an treatment of

788   data for radiocarbon calibration: an update to the International Calibration (IntCal)

789   criteria, Radiocarbon, 55 (4), 1869-1887, 2013.

790 Salama, A.: Active tectonics and Paleo-tsunami recordsof the Northern Coast of Egypt, Ph.D
791   thesis dissertation, University of Strasbourg, 429 pp., 2017.

792 Sayed, A.: Evaluation of the land resources for agriculture development. Case study : EL
793   Hammam canal and its extension, NW coast of Egypt, Ph.D thesis dissertation, university
794   of Hamburg, 241pp., 2013.

795 Salamon, A., Rockwell, T., Ward, S. N., Guidoboni, E. & Comastri, A.: Tsunami hazard
796   evaluation of the Eastern Mediterranean: Historical analysis and selected
797   modeling, Bulletin of the Seismological Society America, 97, 705–724, 2007.

798 Sawai, Y. Episodic emergence in the past 3000 years at the Akkeshi estuary, Hokkaido,
799   northern Japan. *Quat. Res.* **56,** 231-241 (2001).

800 Schmidt, J.F.: Studien ueber Erdbeben. 1-136, 316-360, Leipzig, 1879.

801 Scheffers, A. & Kelletat, D. (2003): Sedimentologic and Geomorphologic Tsunami Imprints
802   Worldwide – a Review. Earth Science Reviews, 63, 1-2, 83-92.

803 Shah-Hosseini, M., Saleem, A., Mahmoud, A. and Morhange, C.: Coastal boulder deposits
804   attesting to large wave impacts on the Mediterranean coast of Egypt, Natural Hazards, 83
805   (2), 849-865, 2016.

806 Shaw, B., Ambraseys, N. N., England, P.C., Floyd, M., Gorman, G.J., Higham, T.F.G.,
807   Jackson, J., Nocquet, J-M., Pain, C. C., and Piggott, M. D.: Eastern Mediterranean
808   tectonics and tsunami hazard inferred from the AD 365 earthquake, Nature Geoscience, 1
809   (April), 268–276, 2008.

810 Soloviev, S.L., Solovieva, O.N., Go, C.N., Kim, K.S., and Shchetnikov, N.A.: Tsunamis in
811   the Mediterranean Sea 2000 B.C.-2000 A.D., Advances in Natural and. Technological
812   Hazards Research, Kluwer Academic Publishers, Dordrecht,. Netherlands, 13, 237 p.,
813   2000.

814 Stanley, J.D. – Bernasconi, M.P.: Holocene depositional patterns and evolution in
815   Alexandria's eastern harbor, Egypt, Journal of Coastal Research, 22 (2), 283-297, 2006.

816 Stiros, S. C.: The AD 365 Crete Earthquake and Possible Seismic Clustering During the
817   Fourth to Sixth Centuries AD in the Eastern Mediterranean: A Review of Historical and
818   Archaeological Data, Journal of Structural Geology, 23, 545–562, 2001.

819 Stiros, S., and Drakos, A.: A fault model for the tsunami-associated magnitude >8.5 Eastern
820   Mediterranean, AD 365 earthquake, Zeitschriftfür Geomorphologie, 146, 125–137,
821   2006.

822   Spiske M, Bo ̈cz Z, Bahlburg H.: The role of porosity in discriminating between tsunami and
823   hurricane emplacement of boulders—a case study from the Lesser Antilles, southern
824   Caribbean, Earth Planet Science Letters, 268, 384–396, 2008.

825   Switzer, A. D. and Jones, B.G.: Large scale washover sedimentation in a freshwater lagoon
826   from the southeast Australian coast: sea level change, tsunami or exceptionally large
827   storm?, The Holocene, 18 (5), 787-803, 2008.

828   Szczucinski, W., N. Chaimanee, P. Niedzielski, G. Rachlewicz, D. Saisuttichai, T. Tepsuwan,
829   S.Lorene& J. Siepak : Environmental and geological impacts of the 26 December 2004
830   Tsunami in coastal zone of Thailand- Overveiw of short and long term effects. In:
831   Polish Journal of Environmental studies, 15 (5), 793-810, 2006.

832   Taymaz, T., Westaway, R., and Reilinger, R.: Active faulting and crustal deformation in the
833   Eastern Mediterranean region, Tectonophysics, 391, 1–9, 2004.

834   Tinti, S., Maramai, A. and Graziani, L. (2001a). "A New Version of the European Tsunami Catalogue:
835   Updating and Revision", Natural Hazards and Earth System Sciences, 1, 255-262, 2001.

836   Tinti, S., Manucci, A., Pagnoni, G., Armigliato, A., and Zaniboni, F.: The 30 December 2002
837   landslide-induced tsunamis in Stromboli: sequence of the events reconstructed from the
838   eyewitness accounts, Natural Hazards and Earth System Science, 5 (6), 763–775, 2005.

839   Tyuleneva, N., Braun, Y., Katz, T., Suchkov, I., Tchernov, B.N.G.: A new chalcolithic-era
840   tsunami event identified in the offshore sedimentary record of Jisr al-Zarka (Israel) ,
841   Marine Geology (article in press), 1-12, 2017.

842   Tuttle, M.P., Ruffman, A., Anderson, T., and Jeter, H.: Distinguishing tsunami from storm
843   deposits in eastern North America: the 1929 Grand Banks tsunami versus the 1991
844   Halloween storm, Seismological Research letters, 75, 117-31, 2004.

845   Yalciner, A., Zaytsev, A., Aytore, B., Insel, I., Heidarzadeh, M., Kian, R., and Imamura, F.: A
846   Possible Submarine Landslide and Associated Tsunami at the Northwest Nile Delta,
847   Mediterranean Sea: Oceanography, 27, (2), 68–75, 2014.

848

Table captions

Table 1: Major earthquakes of the eastern Mediterranean with tsunami wave records in northern Egypt. Estimated magnitudes are given in Mw when calculated and in M when estimated.

Table 2 a: Radiocarbon dating samples and calibrated ages at Kefr Saber site using OxCal v4.2.4 (Bronk-Ramsey, 2013).

Table 2 b: Radiocarbon dating samples and calibrated ages in El Alamein site using OxCal v4.2.4 (Bronk-Ramsey, 2013)

Figure captions

Figure1: Seismicity (instrumental with M> 5.5) and main tectonic framework of the east Mediterranean regions. Black boxes indicate the paleoseismic sites of Kefr Saber and El Alamein east of the Nile delta. The major historical earthquakes (blue box) of AD 365 (Mw 8 − 8.5), AD 1303 (Mw ~8) and AD 1870 (Mw > 7 − 7.5) are located along the Hellenic subduction zone according to Guidoboni et al. (1994), Stiros (2001); Ambraseys (2009); Papadopoilos et al. (2014) and Jusseret and Sintubin (2017). Focal mechanisms are CMT-Harvard.

Figure 2: Location of trenches and core sites at (a) Kafr Saber, (b) El Alamein (see also Figure 1), and (c) Dune ridge and a lagoon south of the Mediterranean Sea as a selected site for coring and trenching at EL Alamein site.

874

875   Figure 3: a) Trench ponorama at Kefr Saber, and (b) description of sedimentary layers of

876   trench P 4 with carbon dating sampling (yellow flags); the horizontal ruler indicates 20 cm

877   scale.

878

879   Figure 4: Radiocarbon dating calibrated with probability density function (pdf) using Oxcal

880   version 4.2 (Bronk-Ramsey, 2009) and chronology of sedimentary layers and tsunami record

881   of trenches at Kefr Saber. The dating characteristics are in Table 2 a. The Bayesian dating

882   simulation of the white sandy unit in Fig. 3 b can be correlated with the 365 AD tsunami

883   event.

884

885   Figure 5: a) Core 1 log description with X-ray scanning, lithology log, magnetic

886   susceptibility, mean grain size, sediment sorting, total organic and inorganic matter and bulk

887   mineralogy. The arrows show the high values of each measurement that may correlate with

888   tsunami deposits.

889   b) Core 9 log description with X-ray scanning, lithology log, magnetic susceptibility, mean

890   grain size, sediment sorting, total organic and inorganic matter and bulk mineralogy. The

891   arrows show the high values of each measurement that may correlate with tsunami deposits.

892   (Similar illustrations of cores 2 to 12 are in supplemental materials).

893

894   Figure 6: Radiocarbon dating calibrated with probability density function (pdf) using Oxcal

895   version 4.2 (Bronk-Ramsey, 2009) and chronology of sedimentary layers with dated tsunami

896   records at El Alamein. The dating characteristics are in Table 2 b. Black pdfs refer to the

897   dated samples and red pdfs are simulated dating of the four tsunami records. Three

898 sedimentary records are correlated with the historical earthquake and tsunami catalogue of the

899 eastern Mediterranean (See also Table 1).

900

901 Figure 7: Depth distribution of tsunami layers in cores at the El Alamein site (see also core

902 locations in Fig. 2 b). The depth correlation of paleotsunami layers indicates the consistent

903 succession of deposits in the lagoon. Deposits of layers 1, 2 and 3 are related with tsunami

904 events 1870 AD, 1303 AD and 365 AD of the East Mediterranean Sea (see also Fig. 6 and

905 Table 1). Layer 4 corresponds to tsunami event 1491 – 1951 BC and is not reported in

906 tsunami catalogues.

907

908

909

910

911

912
913   TABLES
914
915
916   Table 1: Major earthquakes of the eastern Mediterranean with tsunami wave records in
917   northern Egypt. Estimated magnitudes are given in Mw when calculated and in M when
918   estimated.
919
920

Date	Epicentre	Estimated Magnitude	Comment	Reference
21 July 365	Western Crete	8.3 – 8.5 (M_w)	Tsunami northern Egypt	Stiros and Drakos, 2006; Shaw et al., 2008, Hamouda 2009
18 Jan. 746	Dead Sea Fault	7.5 (M)	Tsunami eastern Medit.	Ambraseys, 1962
881 - 882	Palestine	?	Tsunami in Alexandria & Palestine	Galanopoulos A., 1957
4 Jan. 1033	Jordan Valley Fault	7.4 (M)	Tsunami northern Egypt	Ambraseys, 1962
18 Jan. 1068	Northern Lebanon	6.9 (M)	Waves in Lebanon Until northern Egypt	Ambraseys, 1962, Soloviev et al., 2000
8 Aug. 1303	Karpathos & Rhodos islands	8 (M)	>8-m-high wave in Alexandria	Abu al-Fida1329, Ambraseys 2009, Hamouda 2006
24 June 1870	Hellenic Arc	M_L 7.2	Inundation in Alexandria harbour	Ben-Menahem, 1979, Soloviev et al., 2000

921
922
923
924
925
926

Table 2 a: Radiocarbon dating samples and calibrated age at KefrSaber site using OxCal v4.2.4 (Bronk-Ramsey, 2013). White background color is for charcoal and grey for shell ages

No.	Sample name	Laboratory Name	Type of samples	Depth (m)	Date BP	Calibrated. date
1	TSU P4 S2	CIRAM	Charcoal	61	Modern	-
2	TSU P4 S3	CIRAM	Charcoal	40	Modern	-
3	TSU P4 S4	CIRAM	Charcoal	15	Modern	-
4	TSU P1 S07B	Poznan	Charcoal	35	110.14±0.3	Modern
5	TSU P4 S6	Poznan	Charcoal	25	101.42 ± 0.68	1700 – 1920 AD
6	TSU P3 S2	Poznan	Charcoal	72	1075 ± 30 BP	890 – 1020 AD
7	KSB2S2	Poznan	Dendropoma	Boulder	890 ± 30 BP	940 - 1446 AD
8	TSU P5S3	Poznan	Charcoal	17	2060 ± 35 BP	180 – 30 AD
9	TSU P3S2	CIRAM	Charcoal	73	2000 BP	50-70 AD
10	TSU P5S1	Poznan	Charcoal	12	2145 ± 30 BP	360 – 50BC
11	TSU P5S4	Poznan	Charcoal	33	2590 ± 140 BP	1050 – 350 BC
12	TSU P5S2	Poznan	Charcoal	37	4560 ± 300 BP	4000 – 2400 BC
13	TSU P3S3	CIRAM	Charcoal	100	6240 BP	5300 – 5070 BC
14	TSU P4 S5	Poznan	Charcoal	60	15490 ± 70 BP	17200 – 15900 BC
15	TSU P1 S09B	CIRAM	Charcoal	53	40560 BP	39000-38250 BC

- CIRAM Lab. science for art cultural heritage ,archeology department http://www.ciram-art.com/en/archaeology.html
- Poznan Lab. Poznan Radiocarbon Laboratory, Poland, email: c.fourteen@radiocarbon.pl http://radiocarbon.pl/index.php?lang=en.
- Beta Analytic radiocarbon dating, Miami, Florida, USA http://www.radiocarbon.com/, e-mail: lab@radiocarbon.com

Table 2 b: Radiocarbon dating samples and calibrated date in El Alamein site using OxCal v4.2.4 (Bronk-Ramsey, 2013). Underlined dark grey color is for bone, grey for shell, light grey for root and white for charcoal samples.

No.	Sample name	Laboratory Name	Type of samples	Depth (m)	Date BP	Calibrated date (2σ)
a	AL1 S1 (test pit)	CIRAM	charcoal	25	130±20	1680-1908 AD
b	AL1 S2 (test pit)	CIRAM	charcoal	56	190±20	1661-1931 AD
1	core 6/2 sa1	Poznan	charcoal	80	125±30	<1620 AD
2	core 1/1sa2	Poznan	Bone	50	1540±60	403-634 AD
3	core 7/1sa1	Poznan	shell	17	3000±30	293-1113 BC
4	core 9/1sa1	Poznan	gastropod	24	3320±30	1052-1888 BC
5	core10/1sa3	Poznan	shells	20	4515 ±30	2623-3521 BC

6	core11/2sa1	Beta analytic	roots	139	4810±30	2666 - 2817 BC
7	core11/2Sa4	Poznan	gastropod +shell	116	4500±35	2619-3386 BC
9	core11/2sa6	Poznan	gastropod	126	4405±35	2477-3368 BC
10	core 11 2_5	Poznan	gastropod	121	4360±40	2457-3366 BC
11	core 12/2sa1	Beta analytic	gastropod	108	4885±35	3097-3950 BC
12	core 12/2sa2	Poznan	gastropod	114	5000±35	3331-4050 BC
12	core 12/1 sa1	Poznan	gastropod	44	5065±30	3367-4072 BC
13	core 12/2sa4	Beta analytic	roots	135	5060±30	3365-4071 BC
14	core 11/1sa1	Beta analytic	gastropod	20	5230±30	3638-4328 BC
15	core 11-2	Beta analytic	charcoal	180	5020±30	3710-3943 BC
16	core 1/1sa1	Poznan	charcoal	40	13430±60	13985-14415 BC
17	core 11/2sa2	Beta analytic	shell	62	16900±60	17869-18741 BC
18	core2/1sa6	Poznan	gastropods	75	32000±360	32971-34681 BC
19	core 4/1sa1	Poznan	shell	28	31840±350	32887-34447BC
20	core11/2 sa11	Beta analytic	shells	152	32500±500	33294-36120 BC
21	core2/1sa4	Poznan	gastropods	77	35500±500	34362-36931 BC
22	core 3/1sa1	Poznan	shell	45	33500±600	34218- 37224 BC
23	core 6/1 sa6	Poznan	gastropod	45	34000±400	35002-37441 BC
24	core 12/2 sa3	Beta analytic	broken shell	117	37940±420	39560 -40811 BC
25	core 9/1sa5	Poznan	bivalve	55	40000±800	40521-43169 BC
26	core 10/1sa2	Poznan	bone	70	42000±1300	41256-46581 BC
27	core 3/1sa2	Poznan	bivalve	37	45000±2000	43618 BC
28	core 6/1sa9	Poznan	coral	60	50000±4000	42776-69225 BC

943

944 ▪ CIRAM Lab. science for art cultural heritage ,archeology department http://www.ciram-
945 art.com/en/archaeology.html
946 ▪ Poznan Lab. Poznan Radiocarbon Laboratory, Poland, email: c.fourteen@radiocarbon.pl
947 http://radiocarbon.pl/index.php?lang=en.
948 ▪ Beta Analytic radiocarbon dating, Miami, Florida, USA http://www.radiocarbon.com/, e-mail:
949 lab@radiocarbon.com

950

951

952

953

954

955

956

957   Figure 1
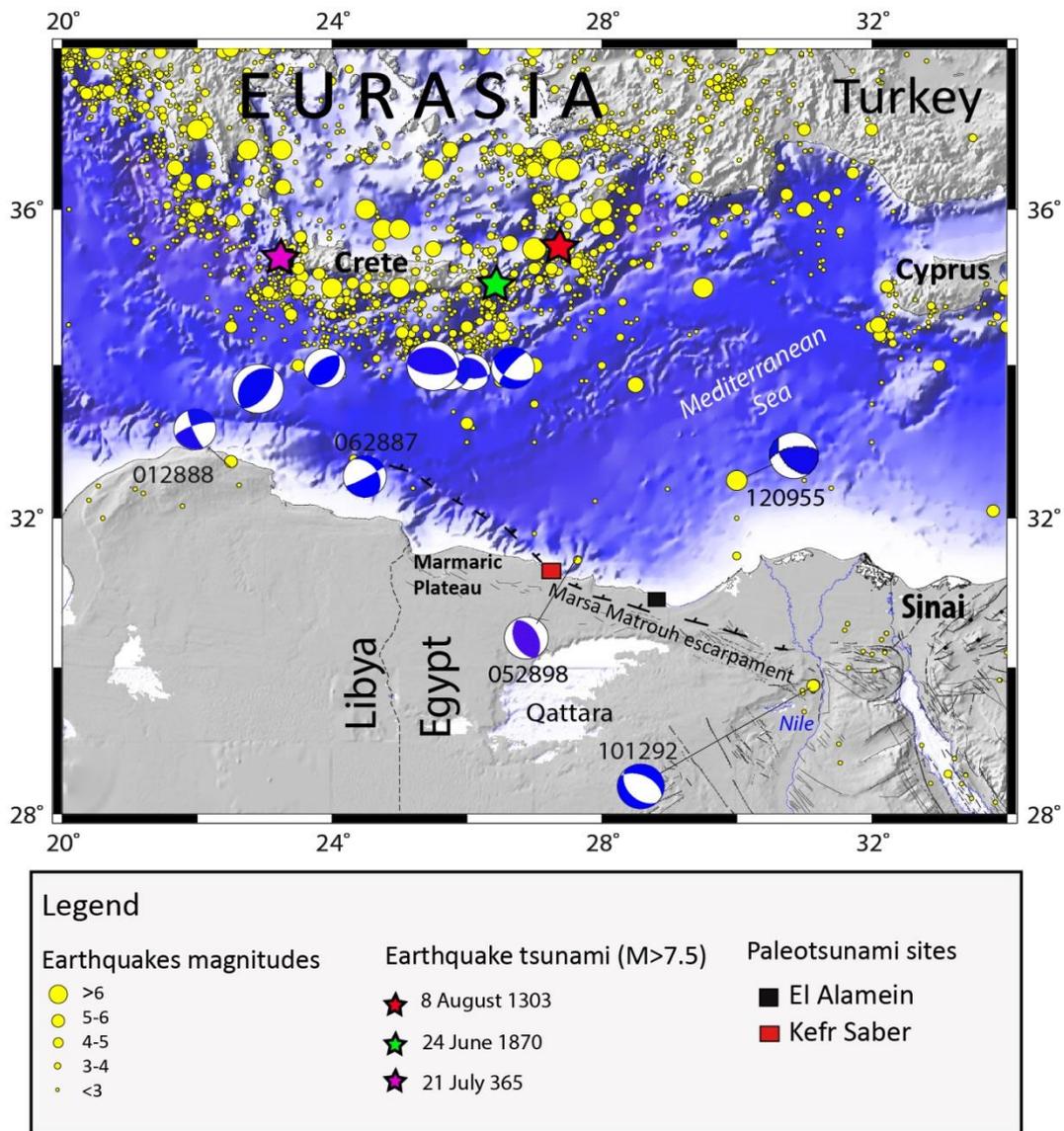
958

959

960

961

962

963

964

965

966

967   Figure 2
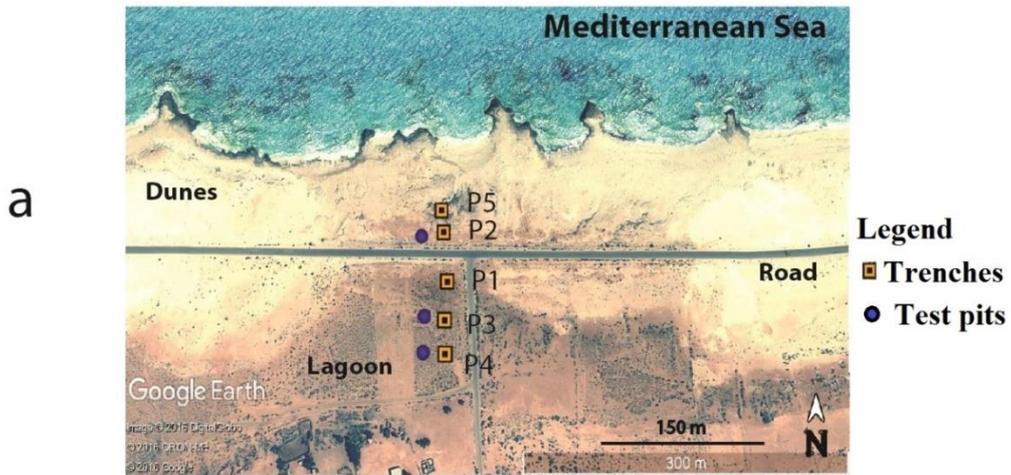
Kefr Saber

EL Alamein

968

969

970

971

972   Figure 3
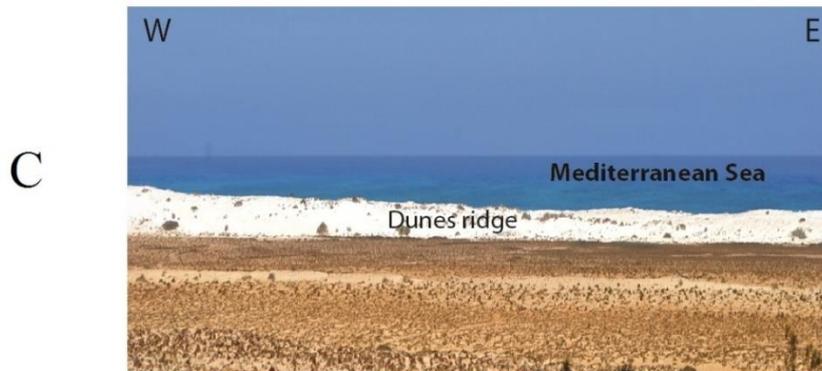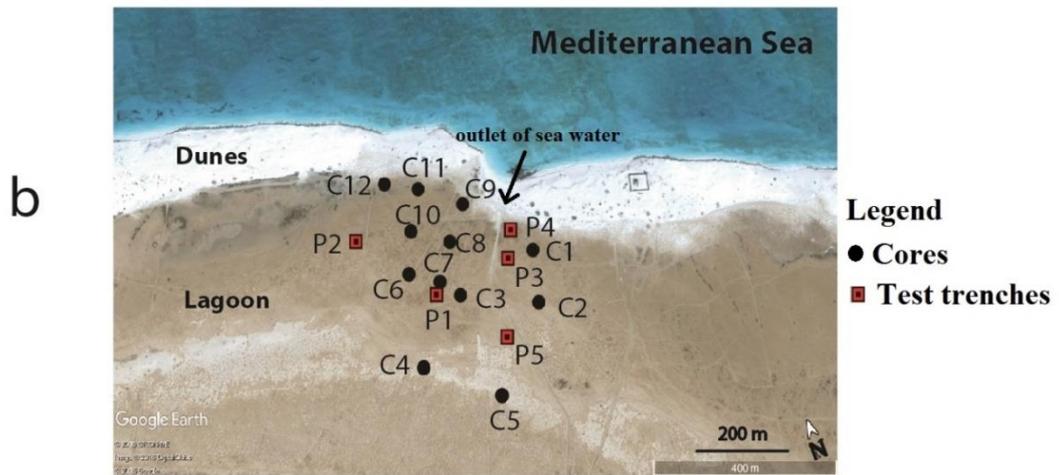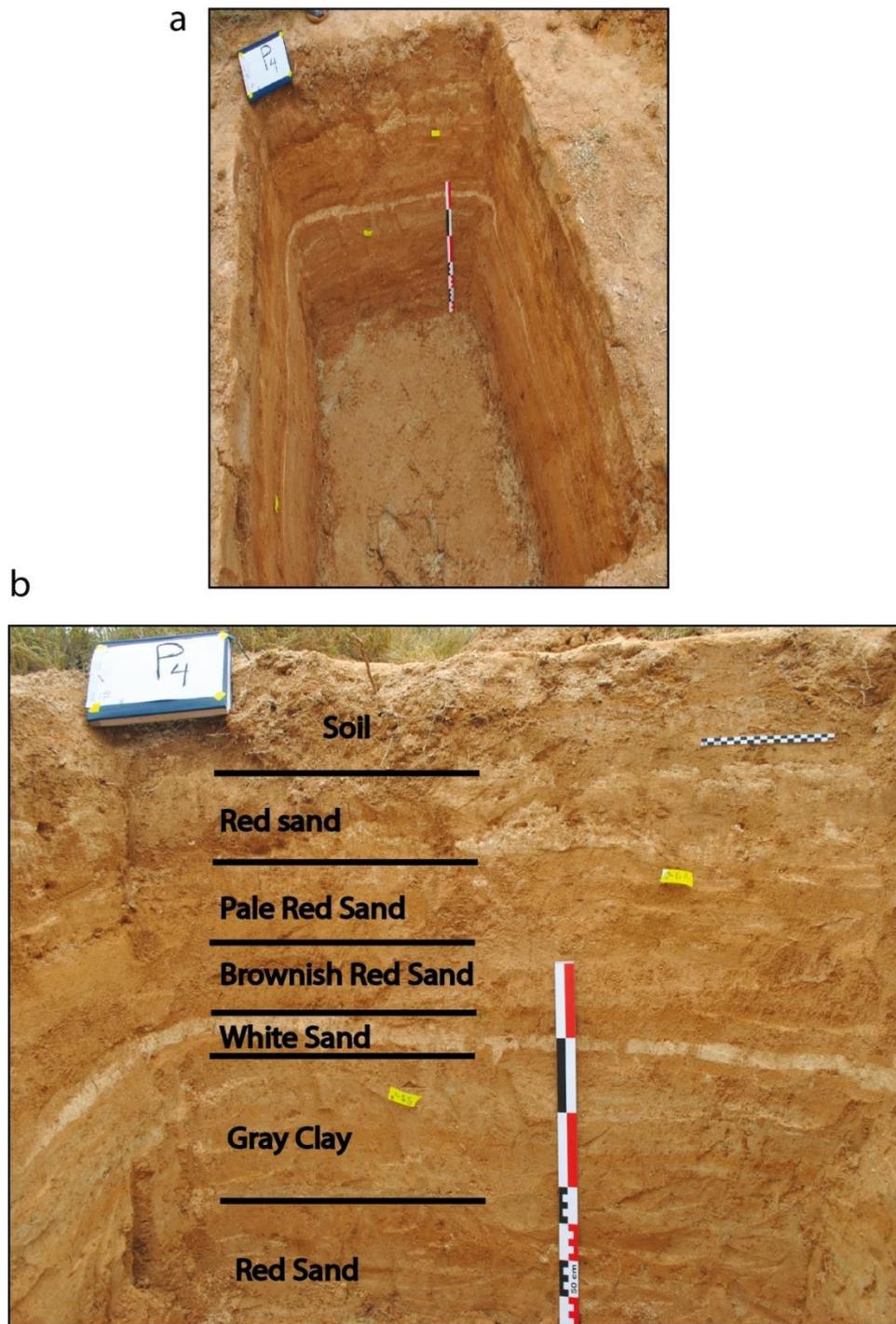
973

974
975
976

977

978

979

980   Figure 4
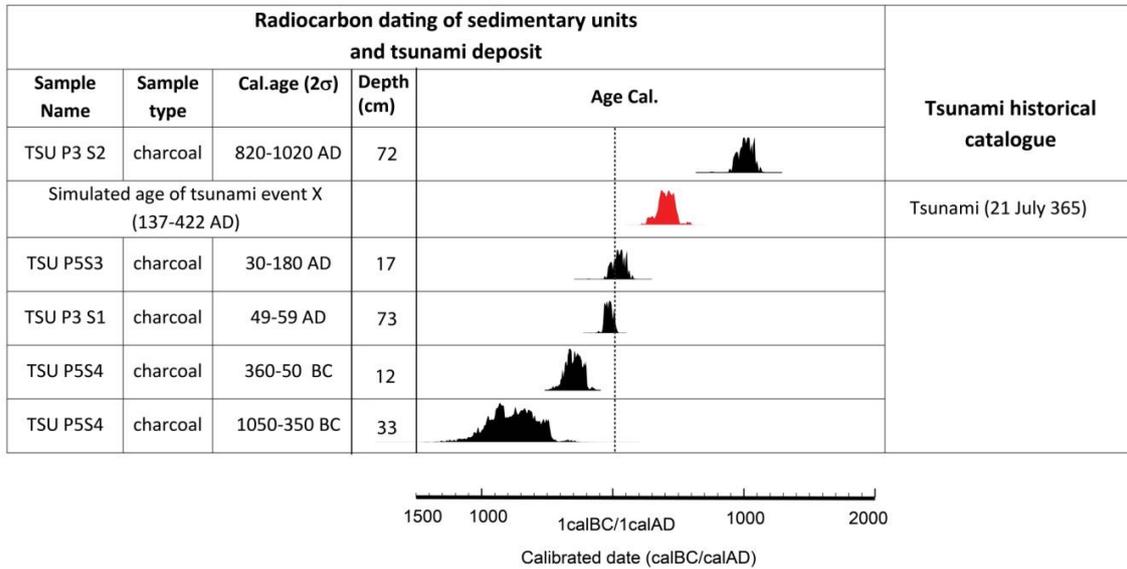
981

982   **See main comment #29** from C. J. Dabrio Gonzalez and author edit in this figure

983   **See main comment #7 b-** from R. Paris and author edit in this figure

984   Figure 5 a
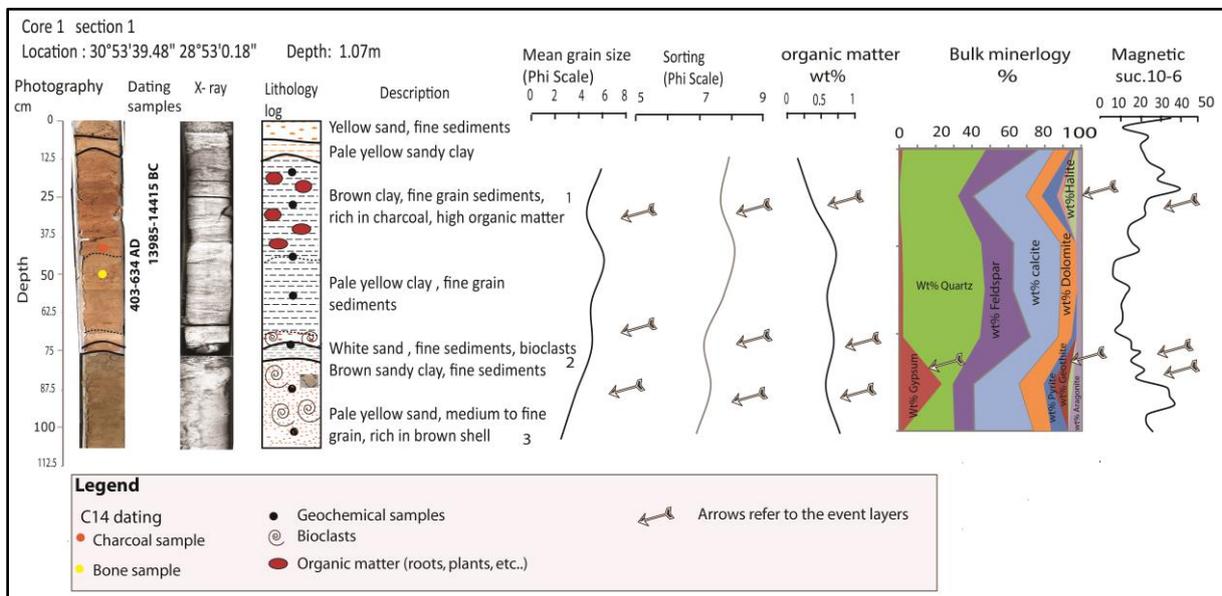
985

986

987

988

989   Figure 5 b

990

991

992   Figure 6

993

994
995

Supplementary Material

to the submitted manuscript Nat. Hazards Earth Syst. Sci. Discuss.,
https://doi.org/10.5194/nhess-2018-62

Methodology

1. Grain size

Grain-size statistical parameters and graphic representations are given in φ units. Converting from microns to mm (as 1 micron = 10^{-3} mm) to Phi units using the following equation: -

$$\varphi = - \log_2 (d) \quad \text{where d is grain diameter in millimetres}$$

The calculated grain size analyses distribution parameters have been calculated following Folk and Ward (1957) to determine to mean grain size, sorting. The most useful parameters of grain-size analysis for this study are the mean grain size and sorting. This following equations of calculate mean size, sorting according to Folk (1968).

1. "Mean" - is the average grain-size. Several formulas are used in calculating the mean. The most inclusive graphically derived value is that given by Folk (1968),
According to equations:

$$Mz = \frac{\varphi 16 + \varphi 50 + \varphi 84}{3}$$

Where 16, 50, and 84 represent the size at 16, 50, and 84 percent of the sample by weight.

2. Sorting is a method of measuring the grain-size variation of a sample by encompassing the largest parts of the size distribution as measured from a cumulative curve.
Folk (1968) introduced the "inclusive graphic standard deviation", that is calculated as follows:=

$$\sigma = \frac{_\varphi 84 - _\varphi 16}{4} + \frac{_\varphi 95 - _\varphi 5}{6.6}$$

where 84, 16, 95, and 5 represent the phi values at 84, 16, 95, and 5 percentiles.

The classification scale for sorting:

<0.350: very well sorted;

0.35-0.500: well sorted;

0.5-0.710: moderately well sorted;

0.71-1.00: moderately sorted;

1.00-2.00: poorly sorted;

2.00-4.00: very poorly sorted;

> 4.00: extremely poorly sorted.

2. **Bulk minerology and x-ray diffraction**

According to (Pecharsky et al., 2009), X-ray diffraction (XRD analysis) is a very useful tool for the identification of bulk mineral phases in powder specimens in the form of powder thin-film samples. The key for identifying materials by this method is their unique crystalline structure.The XRD instrument was called an X-ray diffractometer.

In cooperation with the Central Metallurgical Research Center Laboratory, Cairo, the collected samples were mounted in X-ray specimen holder on glass slides. The powder specimens were stuck on a glass slide using double-sided tape or Vaseline. The machine is equipped with a Philips PW 1730 X-ray diffractometer to measure the samples in the studied area under target Fe, filter Mn, KV 30, Ma 20, with speed 1 degree.

The data were analyzed in a semi-quantitative way following Cook et al. (1975). The intensity of the most intense diffraction peak of each mineral was measured and the identification of crystalline substance and crystalline phases in a specimen is achieved by comparing the specimen diffraction spectrum with spectra of known crystalline substances (Table 1). X-ray diffraction data from a known substance (called fingerprint) are recorded as a powder diffraction file (PDF).

Most PDFs were obtained with Cu*Kα* radiation Standard diffraction published by the International Centre for Diffraction Data (ICDD) and summarized in Table 1, and they are updated and expanded from time to time.

Table 1: Diffraction standard main peak identify minerals according to (ICDD)

Minerals	Principal diffraction peak (Å)
Gypsum (CaSo4.2H2O	7.56
Quartz	3.34
Calcite	2.92
Dolomite (CaMg(Co3)2	2.89
Feldspar (Albite)	3.1875
Feldspar (Orthoclase)	3.3193
Aragonite	3.3985
Halite	2.81
Goethite	4.19
Pyrite (FeS)	2.7090
Illite	10
Montmorillonite	15

3. Regional wave regime during storms

In the Mediterranean, the tropical to subtropical cyclones storms are frequent seasonal events, with ~100 recorded tropical like storms between 1947 and 2011. From tide stations recorded in front of Alexandria, the maximum wave height surge is 43 cm between 1971-2004 (Hamed et al., 1988), the maximum wave height surge is 76.9 cm between 1996-2000 (Hussein et al., 2010).

References

Cook, H. E., Johnson, P. D., Matti, J. C. & Zemmels, I., Methods of sample preparation and x-ray diffraction data analysis, x-ray mineralogy laboratory. In: Kaneps, A. G. (Ed.), Initial reports of the DSDP 28, Washington DC, p.997-1007, 1975

Folk, R.L.: Petrology of sedimentary rocks, 170 pp, Hemphill's Book Store, in Austin, Texas), 1968

Folk RL, Ward WC. : Brazos River bar: a study in the significance of grain size parameters. Journal of Sedimentary Petrology 27: 3–26, 1957.

Hamed, A.A. and El Gindy, A.A., Storm surge generation by winter cyclones at Alexandria, Egypt, International Hydrographic Review, Monaco, LXV(l), January 1988.

Hussein, M.M.A., Moursy, Z.A., and Tayel, M.F., General Pattern of Alexandria Western Harbor Sea Level Changes, JKAU: Mar. Sci., Vol. 21, No. 2, pp: 47-61, 2010. DOI : 10.4197/Mar. 21-2.4

Pecharsky, V.K. and P.Y. Zavalij.:Fundamentals of Powder Diffraction and Structural Characterization of Materials. 2009: Springer US., pp.713, 2009
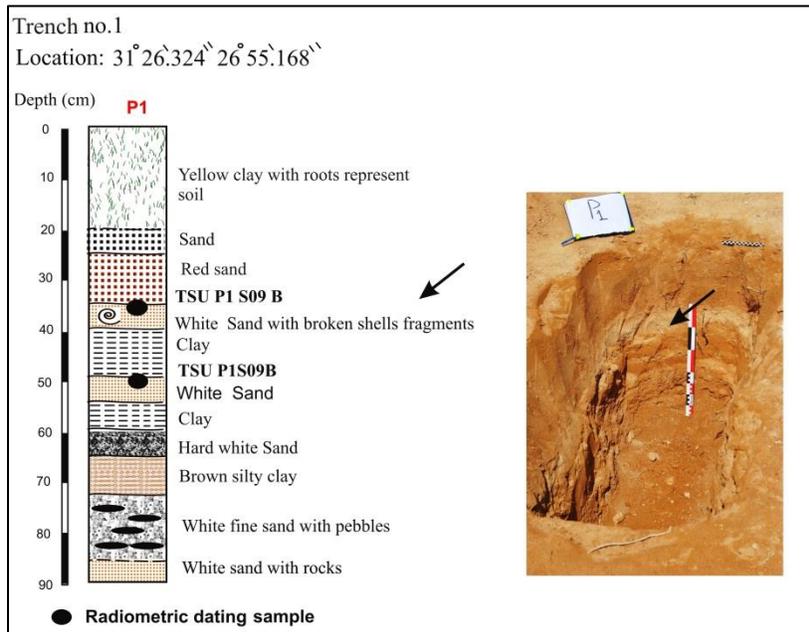
Figure S1 a: Description of Trench no.1 with black arrow refers to white coarse sand high energy sedimentary layer rich in reworked fossils
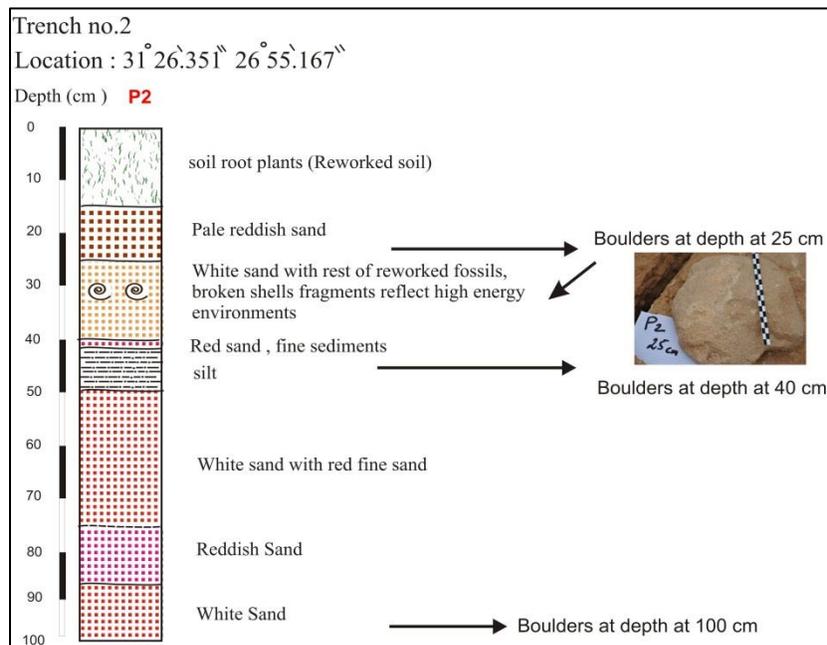
Figure S1 b: Description of Trench no.2 with black arrow refers to white coarse sand high energy sedimentary layer rich in reworked fossils
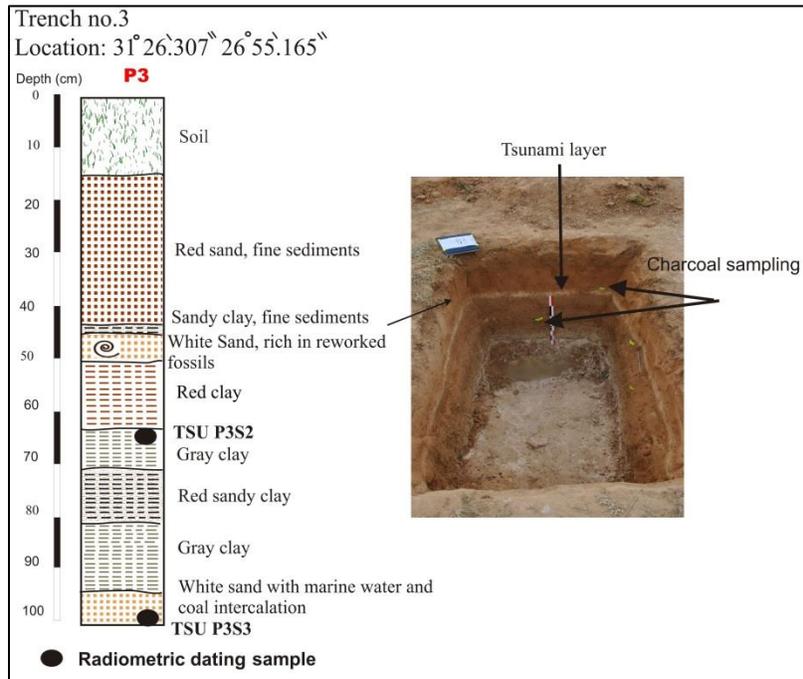
Figure S1 c: Description of Trench no.3 with black arrow refers to white coarse sand high energy sedimentary layer rich in reworked fossils.
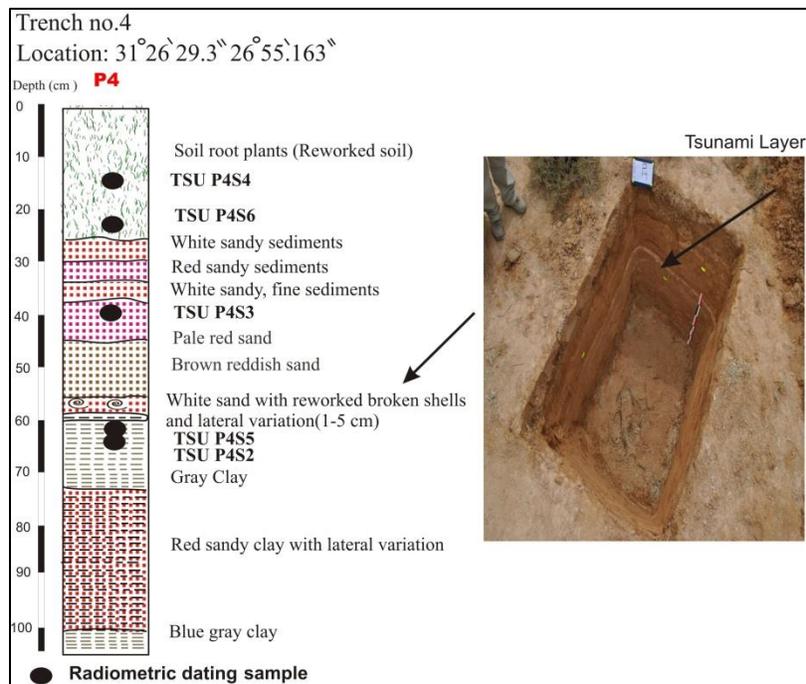
Figure S1 d: Description of Trench no.4 with black arrow refers to white coarse sand high energy sedimentary layer rich in reworked fossils.
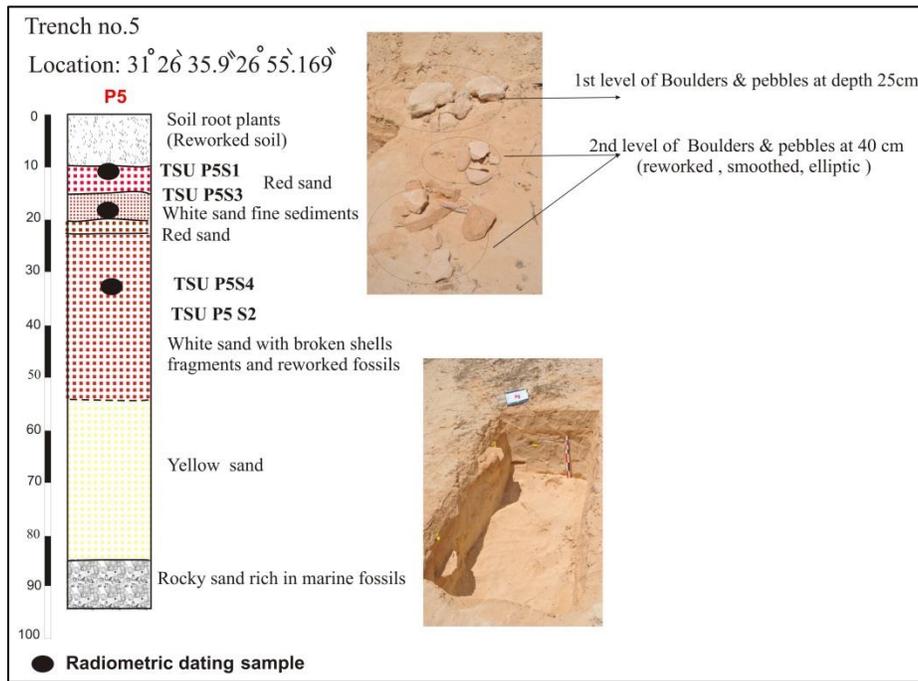
Figure S1 e : Description of Trench no.5
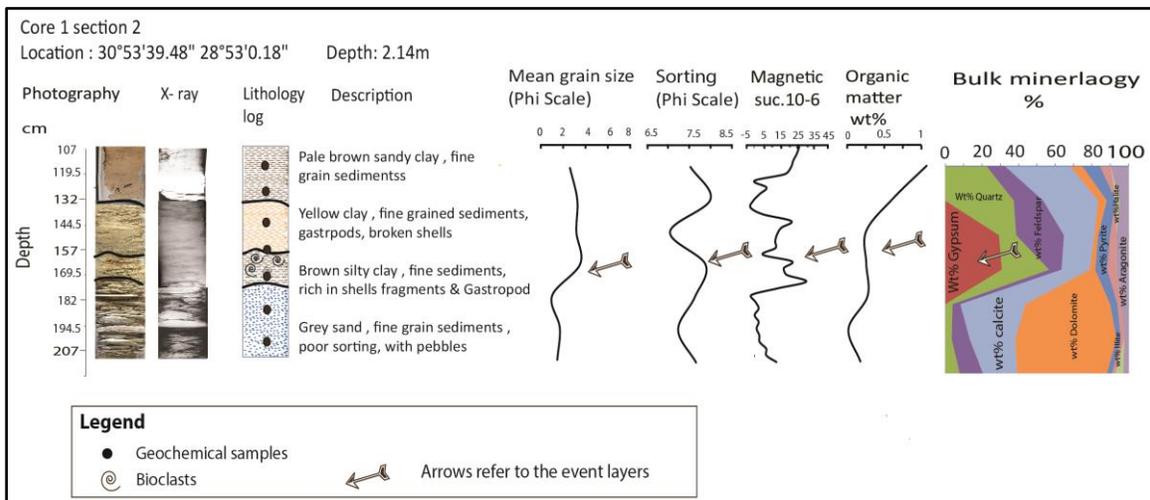
Figure S2 – 1: Description of core no.1 section 2 with photography, x-ray scanning, detail description of lithology, mean grain size, sorting, total organic and inorganic matter and bulk mineralogy. The fourth layer (see pointed arrows) of high energy deposits with coarse sand and mixed clay and organic matter. This layer characterized by low value at top to high value at bottom of magnetic susceptibility in the bottom due to presence of pyrite and also, high organic matter content are interpreted as deposits of high energy sedimentary origin.
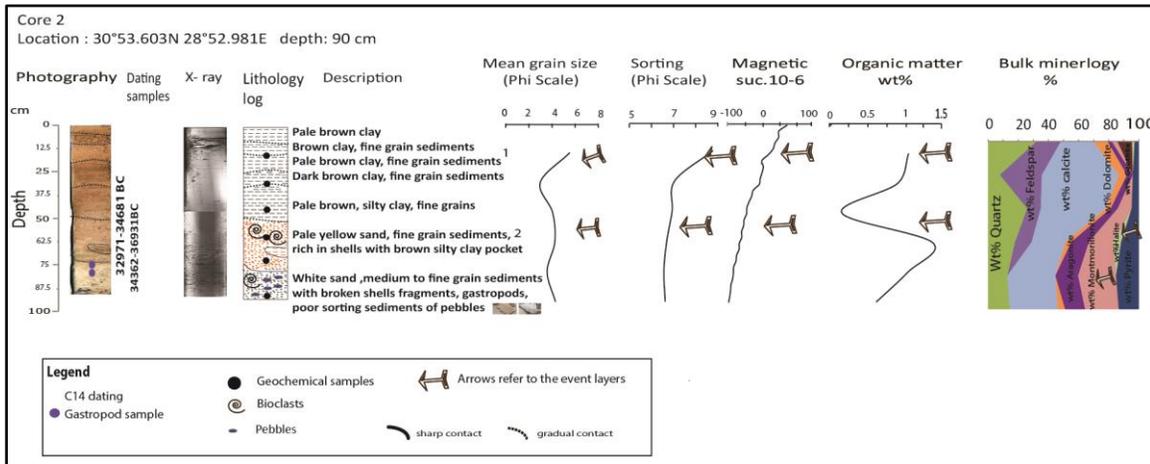
Figure S2 -2 : Description of core no.2 with photography, x-ray scanning, detail description of lithology, mean grain size, sorting, total organic and inorganic matter and bulk mineralogy. The core is at s ~90 cm deep located south of core 1 at ~264 m from the shoreline. It reveals 2 main layers (see numbers and pointed arrows) of high energy deposits with coarse sand and mixed clay and organic matter. The layers with low values of magnetic susceptibility (especially for 1 and 2) and organic matter are interpreted as deposits of high energy sedimentary origin.
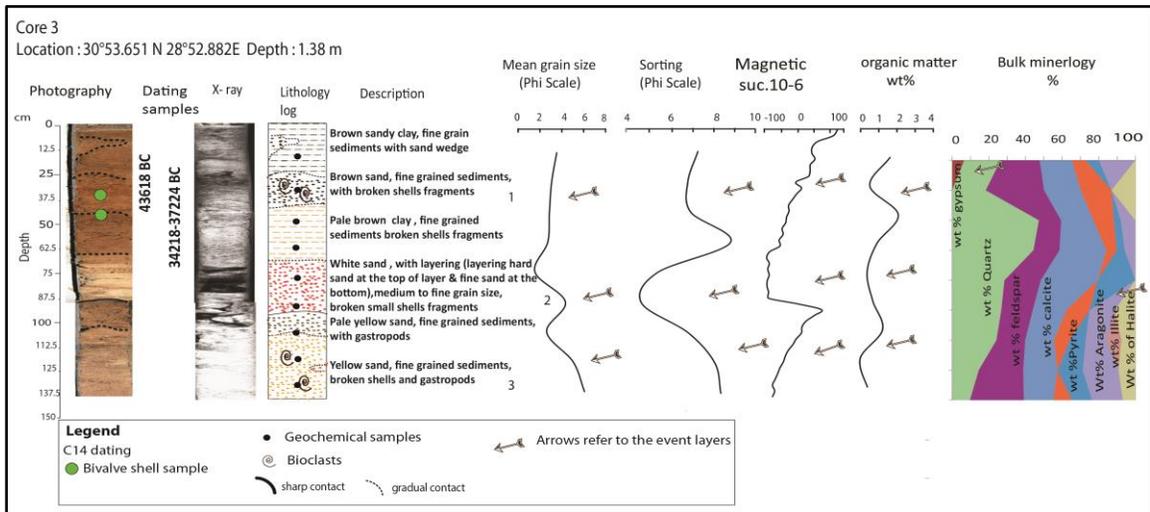
Figure S2 -3: Description of core no.3 with photography, x-ray scanning, detail description of lithology, mean grain size, sorting, total organic and inorganic matter and bulk mineralogy. The core is at located at 270 m far from the shoreline and the outlet of seawater. It reveals 3 main layers (see numbers and pointed arrows) of high energy deposits with coarse sand and mixed clay and organic matter. The layers with low values of magnetic susceptibility (especially for 1 and 2 and 3) while high value at the bottom of layer 2 and with laminations at 2 and high organic matter content are interpreted as deposits of high energy sedimentary origin.
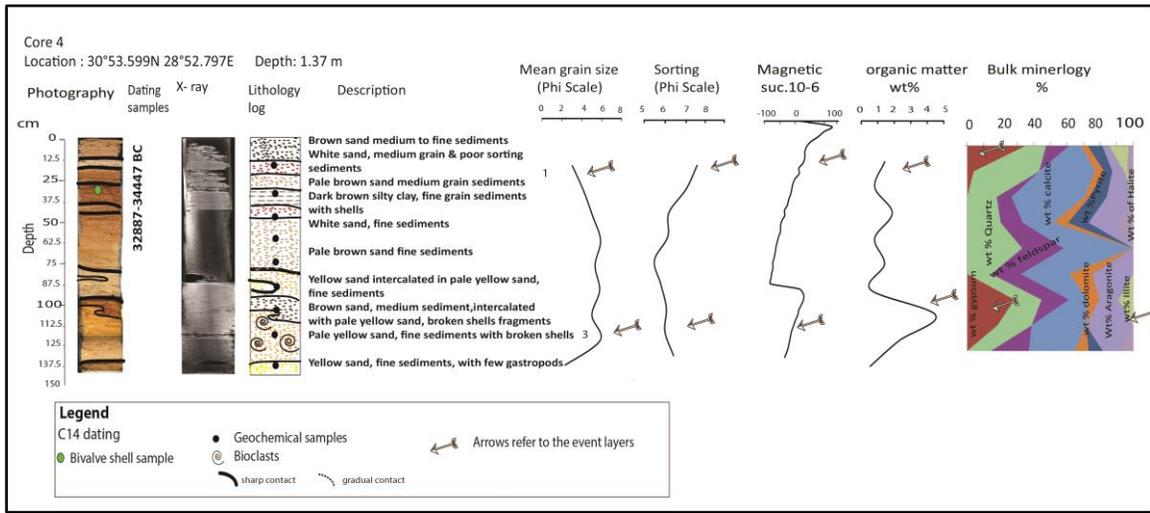
Figure S2 - 4: Description of core no.4 with photography, x-ray scanning, detail description of lithology, mean grain size, sorting, total organic and inorganic matter and bulk mineralogy. The core is at 435 m from the shoreline 166 m from the shoreline. It reveals 2 main layers (see numbers and pointed arrows) of high energy deposits with coarse sand and mixed clay and organic matter. The layers with low values of magnetic susceptibility (especially for 1 and 3) and high content organic matter are interpreted as deposits of high energy sedimentary origin.
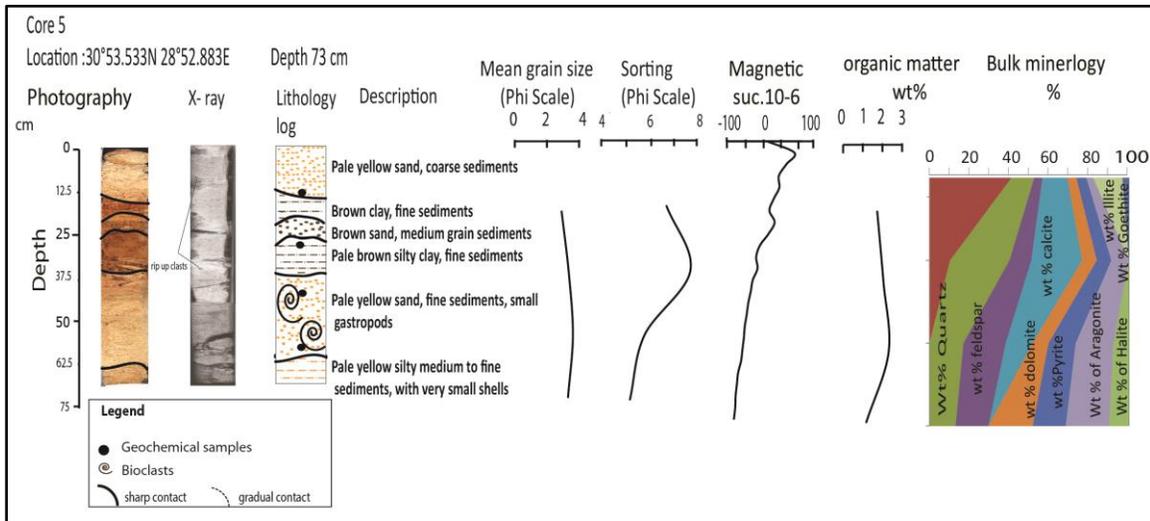
Figure S2 - 5: Description of core no.5 with photography, x-ray scanning, detail description of lithology, mean grain size, sorting, total organic and inorganic matter and bulk mineralogy. The core is at 490 m distance from the shoreline and the sedimentary succession does not show any possible sedimentary catastrophic layer of high energy sedimentary origin.
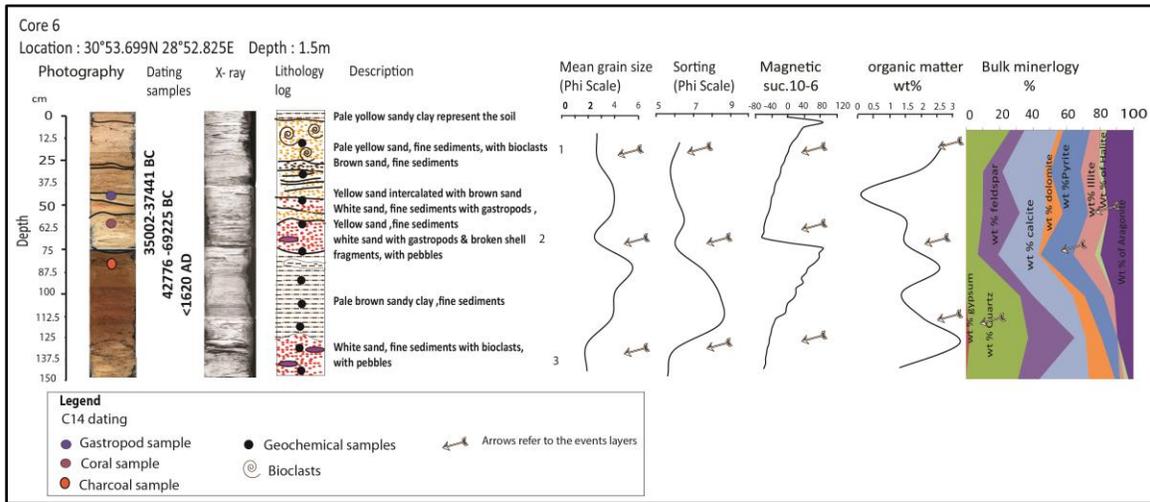
Figure S2 - 6 : Description of core no.6 with photography, x-ray scanning, detail description of lithology, mean grain size, sorting, total organic and inorganic matter and bulk mineralogy. The core is at 320 m from the shoreline and reveals 3 main layers (see numbers and pointed arrows) of high energy deposits with coarse sand and mixed clay and organic matter. The layers with low values of magnetic susceptibility and high organic matter content are interpreted as deposits of high energy sedimentary origin.
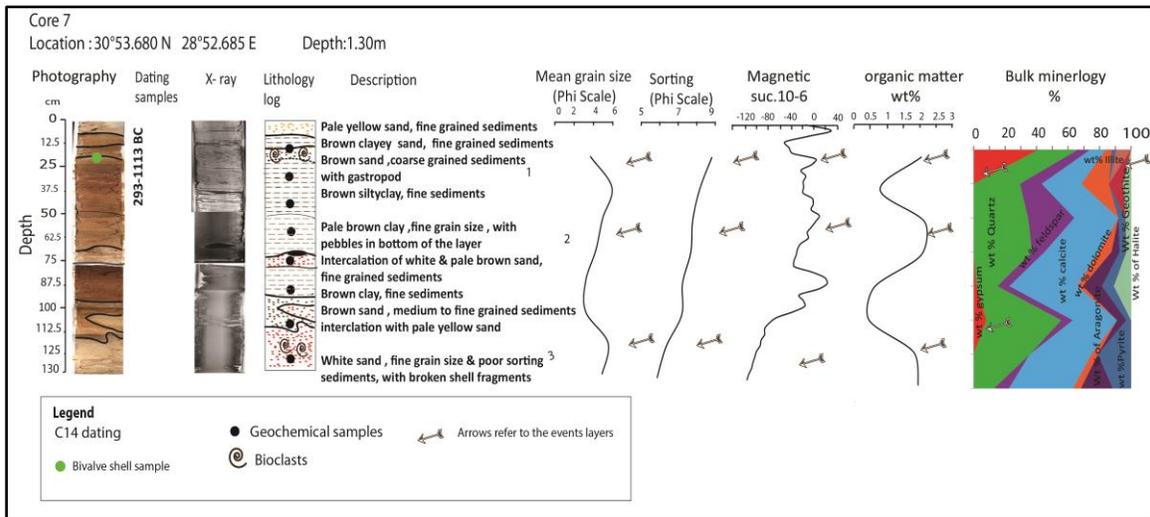
Figure S2 - 7 : Description of core no.7 with photography, x-ray scanning, detail description of lithology, mean grain size, sorting, total organic and inorganic matter and bulk mineralogy. The core is at 273 m from the shoreline and reveals 3 main layers (see numbers and pointed arrows) of high energy deposits with coarse sand and mixed clay and organic matter. The layers with low values of magnetic susceptibility (especially for 1 and 2) and high organic matter content are interpreted as deposits of high energy sedimentary origin.
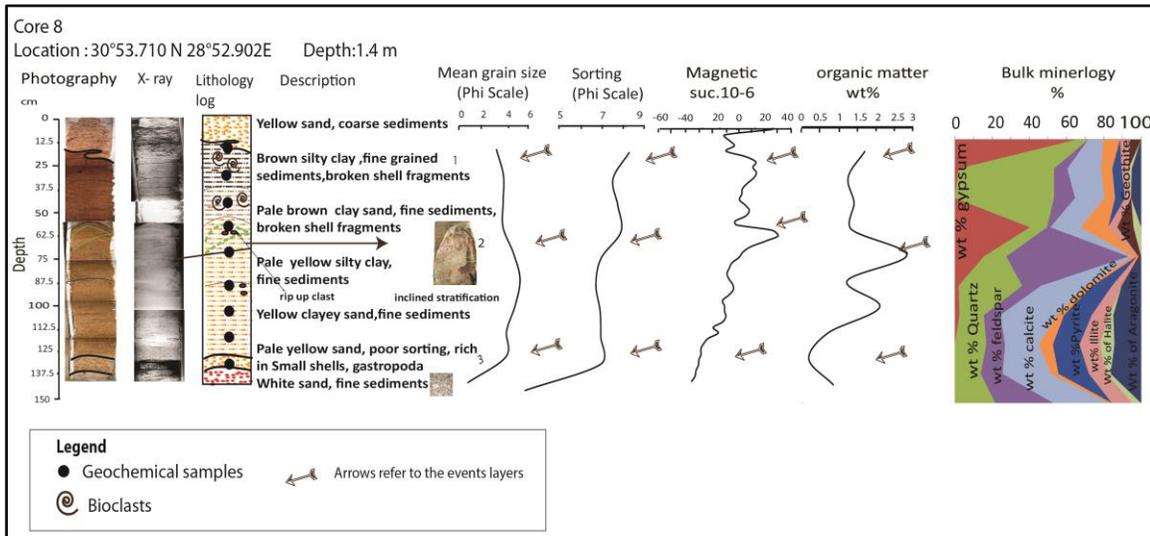
Figure S2 - 8 : Description of core no.8 with photography, x-ray scanning, detail description of lithology, mean grain size, sorting, total organic and inorganic matter and bulk mineralogy. The core is at 214 m from the shoreline and reveals 3 main layers (see numbers and pointed arrows) of high energy deposits with coarse sand and mixed clay and organic matter. The layers with high values of magnetic susceptibility (especially for 2) and organic matter are interpreted as deposits of high energy sedimentary origin.
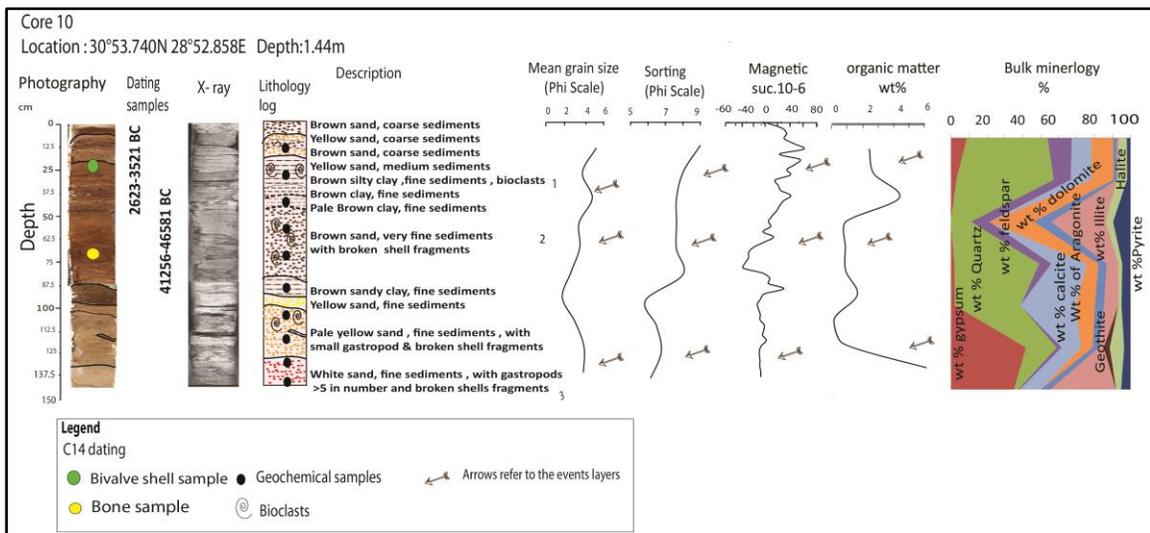
Figure S2 - 9: Description of core no.10 with photography, x-ray scanning, detail description of lithology, mean grain size, sorting, total organic and inorganic matter and bulk mineralogy. The core is at 245 m from the shoreline and reveals 3 main layers (see numbers and pointed arrows) of high energy deposits with coarse sand and mixed clay and organic matter. The layers with high values of magnetic susceptibility (especially for 1) and high organic matter content are interpreted as deposits of high energy sedimentary origin.
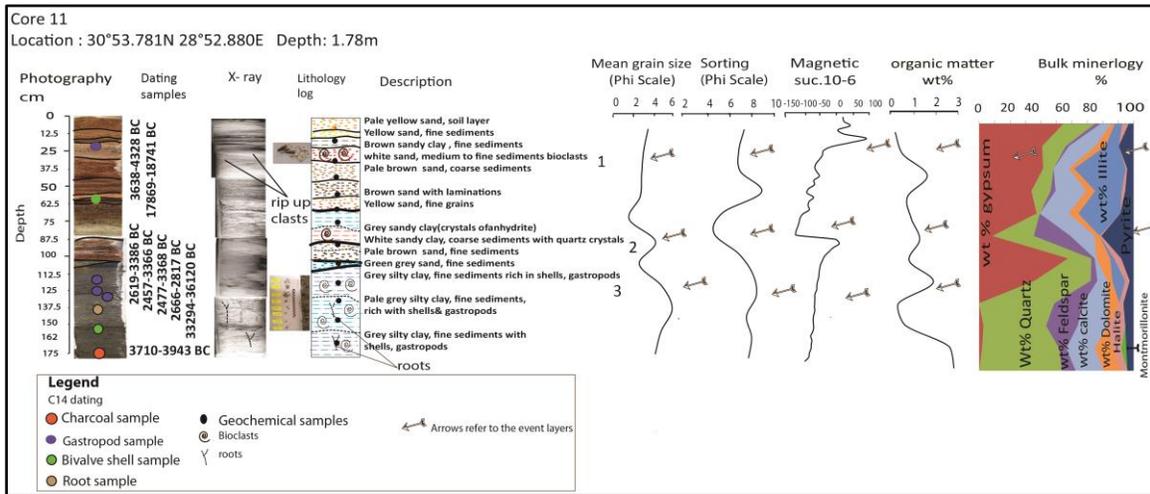
Figure S2 – 10 : Description of core no.11 with photography, x-ray scanning, detail description of lithology, mean grain size, sorting, total organic and inorganic matter and bulk mineralogy. The core is at 151 m from the shoreline and reveals 3 main layers (see numbers and pointed hands) of high energy deposits with coarse sand and mixed clay and organic matter. The layers with high values of magnetic susceptibility (especially for 1 and, base of layer 2) and high organic matter content are interpreted as deposits of high energy sedimentary origin
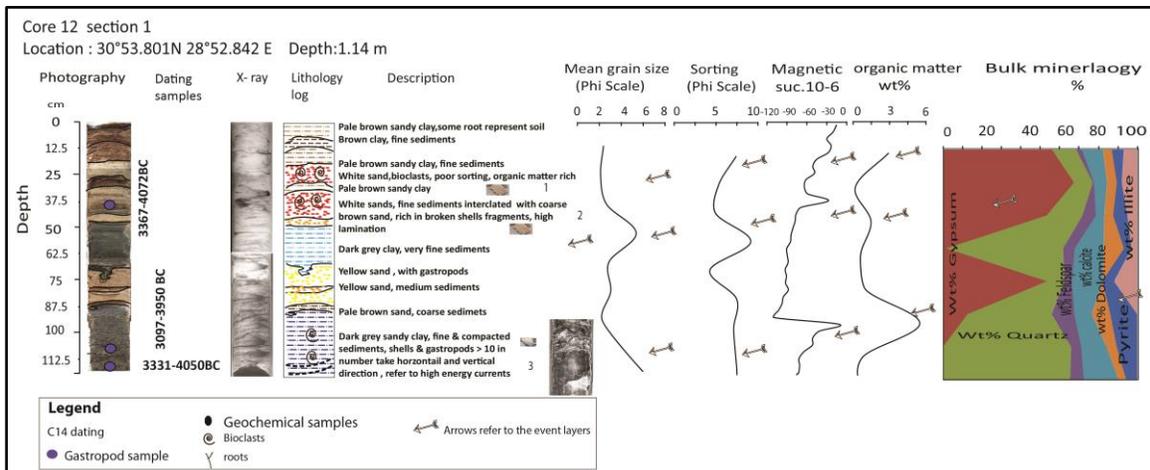
Figure S2 – 11a : Description of core no.12 section 1 with photography, x-ray scanning, detail description of lithology, mean grain size, sorting, total organic and inorganic matter and bulk mineralogy. The core is at 151 m from the shoreline and reveals 3 main layers (see numbers and pointed hands) of high energy deposits with coarse sand and mixed clay and organic matter. The layers with low values of magnetic susceptibility (especially for 1 and, 2 and 3) and organic matter are interpreted as deposits of high energy sedimentary origin.
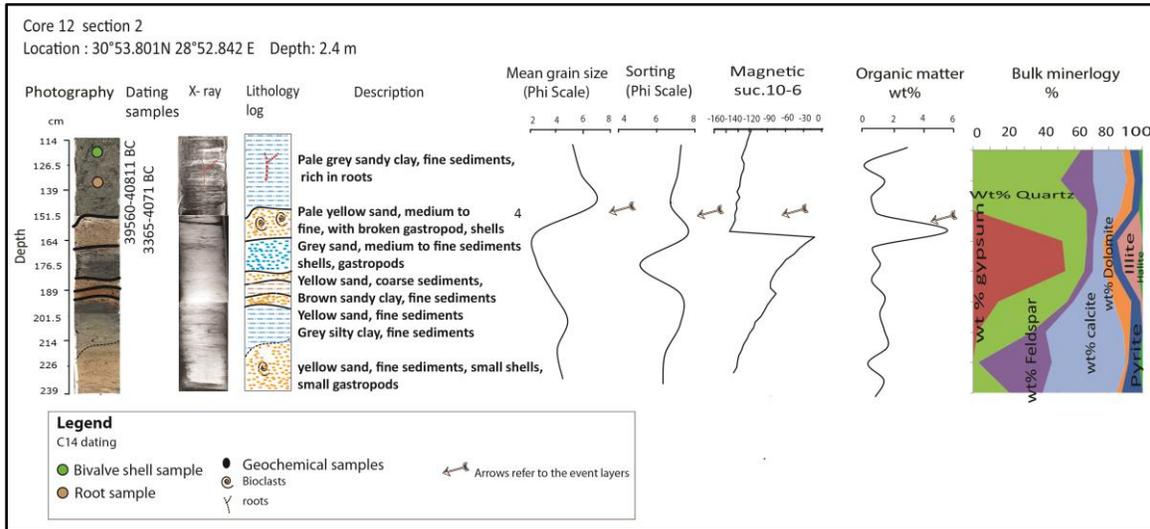
Figure S2 – 11 b : Description of core no.12 section 2 with photography, x-ray scanning, detail description of lithology, mean grain size, sorting, total organic and inorganic matter and bulk mineralogy. The fourth layer (see numbers and pointed hands) of high energy deposits with coarse sand and mixed clay and organic matter. The layers with low values of magnetic susceptibility and high organic matter content are interpreted as deposits of tsunami origin
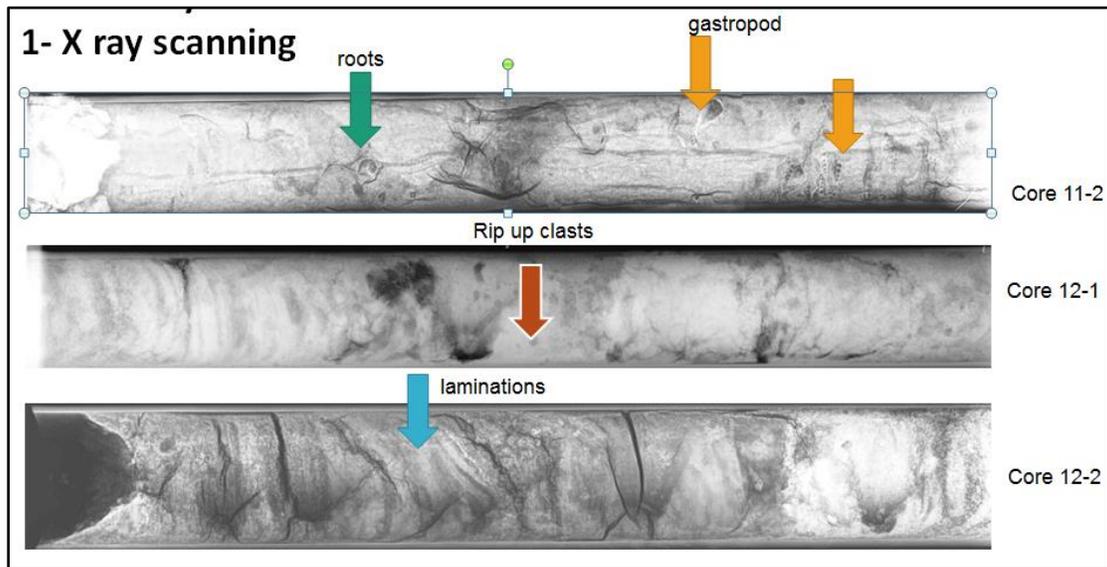
Figure S3 Turibitic features found in some core in El Alamein site by X ray scanning (rip up clasts, laminations and some gastropods before open the cores)

Bulk mineralogy semi quantitative data

2Theta	d (A)	Height	Area	FWHM	Identified mineral	WT%
17	**6.54906**	14.1	24.2	0.1959	Gypsum	1.767138739
25.207	4.43635	10.4	17.9	0.2284	-	0
26.2	4.27096	80.4	224.4	0.2609	-	
26.878	**4.16509**	7.3	20.4	0.2648	Goethite	0.914901617
29.135	3.84871	7.3	20.4	0.2668	-	
30.344	3.69869	64.1	174.5	0.2688	-	
31.308	3.5876	17.6	47.9	0.3164	-	
31.725	3.54154	15.6	42.3	0.3401	-	
32.31	**3.47908**	13.5	36.7	0.352	Aragonite	1.691941346
33.633	**3.34596**	336.5	1545.2	0.3639	Quartz	42.17320466
34.65	**3.25063**	130	597.2	0.3755	Feldspar (orthoclase)	16.29276852
35.152	**3.20569**	145.5	668.2	0.3813	Albite	18.23536784
37.221	**3.03326**	65.9	338.3	0.3872	Calcite	8.259180348
39.075	**2.89461**	62.2	304.3	0.3949	dolomite	7.795463091
40.166	**2.81908**	12.5	60.9	0.3591	Halite	1.566612357
42.422	**2.67551**	10.4	50.8	0.3412	Pyrite	1.303421481
45.598	2.49811	17.6	86.1	0.3323	-	
46.356	2.45949	46.7	181.3	0.3233	-	
47.353	2.41057	9.4	36.4	0.312	-	
48.189	2.37119	9.4	36.4	0.3063	-	
50.147	2.28426	50.2	165.7	0.3006	-	
Total		797.9				

Table S1-1 X ray diffraction data of core 1 sample no.1
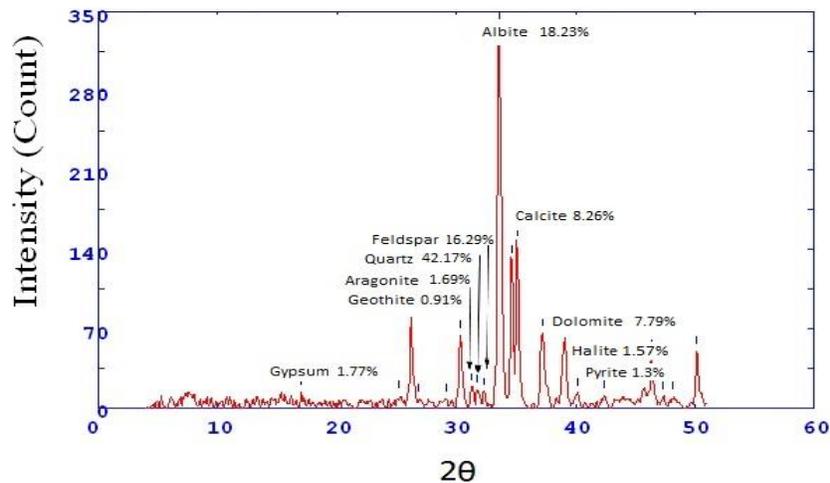
Fig.S4-1 X ray diffractogram of core 1 sample no.1

2Theta	d (A)	Height	Area	FWHM	Identified mineral	WT%
11.008	**10.09211**	13.1	74.7	0.3574	Illite	3.116821318
24.681	4.52938	12.6	51.4	0.3356	-	0
26.207	4.26987	30.8	97.7	0.2652	-	
27.931	4.0111	7.6	24.3	0.2974	-	
29.077	3.85612	21.4	90.1	0.3297	-	
30.351	**3.69791**	10.6	44.6	0.2948	Aragonite	2.522008089
33.57	**3.35211**	154.2	353.1	0.26	Quartz	36.68807994
34.523	**3.26222**	24.6	56.2	0.3908	Feldspar (orthoclase)	5.85296217
35.108	**3.2096**	14.4	33	0.4562	Albite	3.426124197
37.22	**3.03336**	139.9	945.6	0.5217	Calcite	33.28574828
39.053	**2.89614**	40	215.2	0.4159	dolomite	9.517011658
40.031	**2.82818**	11.9	63.9	0.3186	Halite	9.517011658
41.875	**2.70891**	11.6	26.4	0.2213	Pyrite	2.759933381
45.7	2.49284	32.8	355.3	0.9235	-	
47.208	2.41755	15.3	165.4	0.5999	-	
Total		420.3				

Table S1-2 X ray diffraction data of core 1 sample no.2
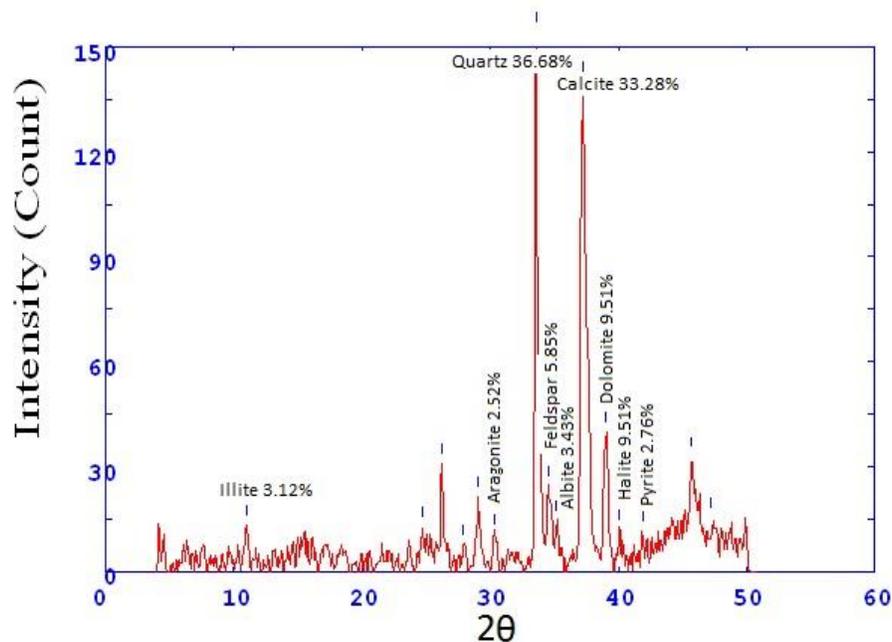
Fig.S4-2 X ray diffractogram of core 1 sample no.2

2Theta	d (A)	Height	Area	FWHM	Identified mineral	WT%
15.408	**7.22089**	12.4	89.9	0.5334	Gypsum	1.651571657
24.948	4.4817	10.4	75.3	0.3984	-	0
26.212	4.26897	70.9	212.5	0.2634	-	
29.054	3.85916	16.6	49.8	0.2498	-	
30.366	3.69605	32.8	82.5	0.2363	-	
31.326	**3.58558**	21.8	54.7	0.2368	Aragonite	2.903569526
33.592	**3.35**	325.3	699.6	0.2373	Quartz	43.32711774
34.646	**3.25106**	133.2	286.5	0.33	Feldspar (orthoclase)	17.74107619
37.218	**3.03354**	196.2	948.1	0.4227	Calcite	26.13212573
39.072	**2.8948**	61.9	261.7	0.3479	dolomite	8.244539158
45.633	2.49629	27.2	406.4	0.9975	-	
46.266	2.464	24.9	371.7	0.7214	-	0
48.712	2.34725	10.4	155.6	0.5833	-	
50.15	2.28412	43.5	242	0.4452	-	
51.246	2.23847	12.5	0	0	-	
52.207	2.20008	11.4	0	0	-	
Total		750				

Table S1-3 X ray diffraction data of core 1 sample no.3
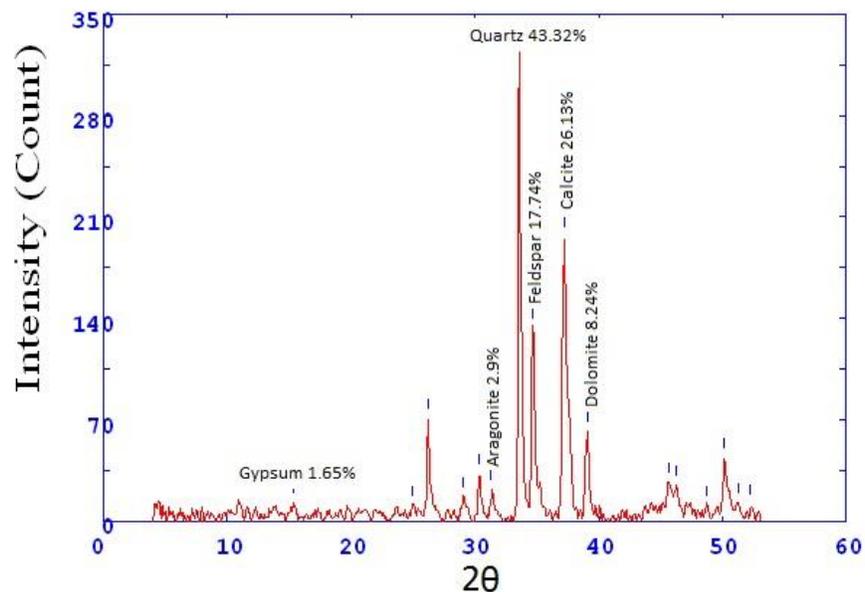
Fig.S4-3 X ray diffractogram of core 1 sample no.3

2Theta	d (A)	Height	Area	FWHM	Identified mineral	WT%
15.354	**7.24607**	15.8	72	0.4291	Gypsum	2.243362204
26.29	4.25668	39.8	142.2	0.3088	-	0
29.193	3.84117	24.4	87.4	0.2846	-	
30.473	3.68344	36.3	87.5	0.2604	-	
31.586	**3.55673**	16.6	40.1	0.2581	Aragonite	2.356950163
33.704	**3.33918**	315	700.4	0.2558	Quartz	44.72525912
34.749	**3.24171**	73.1	162.7	0.353	Feldspar (orthoclase)	10.37909982
35.347	**3.18855**	36.1	80.3	0.4016	Albite	5.12565668
37.347	**3.02339**	185.6	1102.9	0.4502	Calcite	26.35240664
39.207	**2.88523**	62.1	304.6	0.3948	dolomite	8.81726537
43.033	2.6393	16.8	38.6	0.2072	-	
45.94	2.48052	28	202.3	0.5829	-	
46.373	2.45864	21.5	155.5	0.536	-	
50.333	2.27634	37	263	0.4891	-	
51.415	2.23159	8.8	0	0	-	
Total		703.1				

Table S1-4 X ray diffraction data of core 1 sample no.4
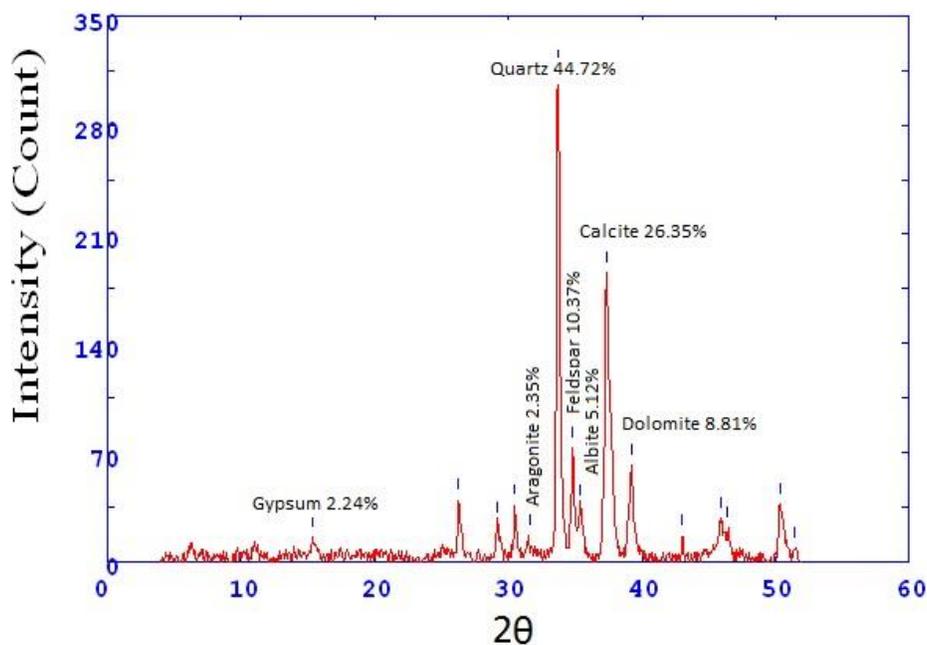
Fig.S4-4 X ray diffractogram of core 1 sample no.4

2Theta	d (A)	Height	Area	FWHM	Identified mineral	WT%
17.139	**6.49624**	16.5	47.7	0.2592	Gypsum	2.160534241
23.727	4.70878	8.4	24.2	0.2634	-	0
24.966	4.47848	11.5	33.2	0.2654	-	
26.259	4.26147	50.3	144.7	0.2675	-	
27.692	4.04493	9.4	27.2	0.2481	-	
29.097	3.85359	9.4	27.2	0.2288	-	
30.417	3.6901	60	63.5	0.1901	-	
31.328	**3.58535**	20.9	22.1	0.2439	Aragonite	2.736676706
33.633	**3.34595**	331.6	1301.9	0.2978	Quartz	43.42019117
34.798	**3.23728**	178.9	702.5	0.3642	Feldspar (orthoclase)	23.42542883
35.294	**3.19323**	37.5	147.3	0.3974	Albite	4.910305094
37.244	**3.03148**	122.2	626.1	0.4307	Calcite	16.00104753
39.1	**2.89278**	56.1	366.2	0.4861	dolomite	7.34581642
42	**2.70119**	21	89.7	0.3611	Pyrite	2.749770852
45.748	2.49039	27.2	218.7	0.6017	-	
46.365	2.45903	18.8	151.4	0.5858	-	
48.1	2.37531	13.6	100	0.57	-	
50.244	2.28014	30.8	93	0.3152	-	0
Total		763.7				

Table S1-5 X ray diffraction data of core 1 sample no.5
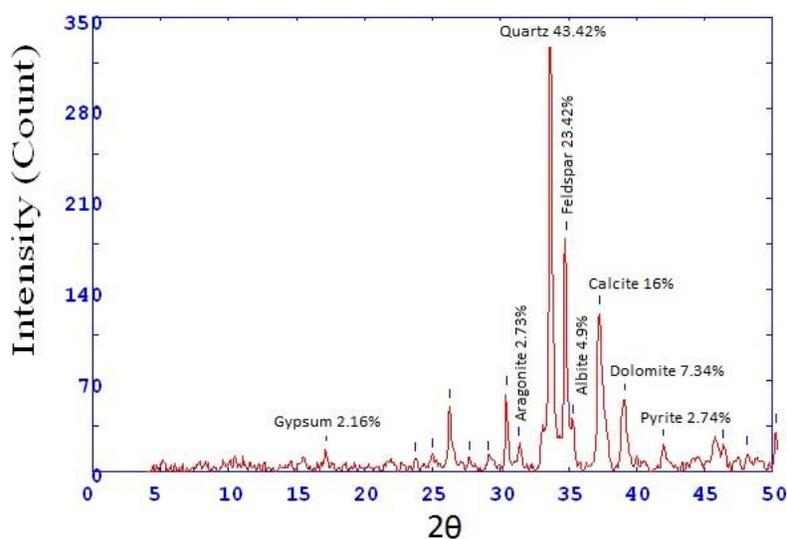
Fig.S4-5 X ray diffractogram of core 1 sample no.5

2Theta	d (A)	Height	Area	FWHM	Identified mineral	WT%
14.926	**7.4528**	140.2	268.1	0.2051	Gypsum	23.04404997
24.139	4.62956	9.8	18.7	0.2147	-	
25.181	4.44076	8.8	16.9	0.2243	-	0
25.877	4.32342	10.8	20.6	0.2435	-	
26.652	**4.19975**	58	176.9	0.2819	Goethite	9.533201841
29.9	3.75237	48.7	138.5	0.2685	-	
30.83	**3.64184**	30.2	85.9	0.2611	Aragonite	4.963839579
33.436	**3.3651**	36	102.5	0.2574	Quartz	5.917159763
34.005	3.31046	305.5	866.3	0.2537	-	
35.087	**3.21139**	39.9	113.2	0.3511	Feldspar (orthoclase)	6.558185404
35.696	**3.15841**	28.2	80.1	0.3998	Albite	4.635108481
37.661	**2.99911**	150.7	858	0.4485	Calcite	24.76988823
39.435	**2.86922**	79.8	607.4	0.4946	dolomite	13.11637081
40.388	**2.80423**	17.6	133.6	0.4097	Halite	2.892833662
42.3	**2.68291**	27.8	122.1	0.3247	Pyrite	4.569362262
46.2	2.46732	31.1	192	0.4667	-	
46.818	2.43654	21.4	132.4	0.3899	-	
Total		608.4				

Table S1-6 X ray diffraction data of core 1 sample no.6
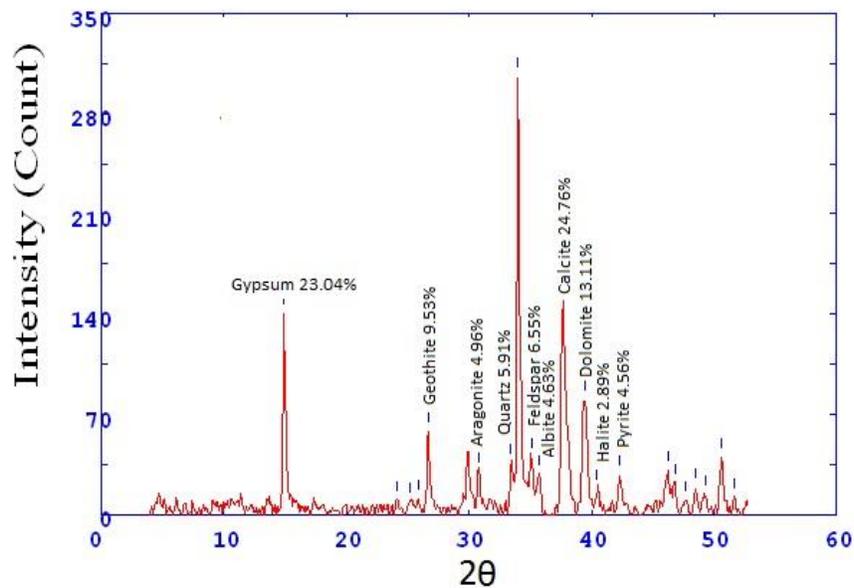
Fig.S4-6 X ray diffractogram of core 1 sample no.6

2Theta	d (A)	Height	Area	FWHM	Identified mineral	WT%
15.414	**7.21807**	11.4	94.4	0.8724	Gypsum	2.366618227
19.4	5.74515	8.2	94.4	0.8724	-	
21.267	5.24597	7.9	27.1	0.1957	-	
22.609	4.93835	8.8	22.9	0.148	-	
24.888	4.49223	10.4	27.2	0.2573	-	
26.255	4.26213	26.7	123.3	0.3665	-	
29.195	3.84093	19.3	85.8	0.3034	-	0
30.36	3.69679	9.4	41.6	0.2881	-	
33.055	**3.40278**	35.8	158.8	0.2805	Aragonite	7.432011625
33.631	**3.34617**	141.8	414.4	0.2729	Quartz	29.43740918
34.689	**3.24714**	30.1	87.9	0.3337	Feldspar (orthoclase)	6.248702512
35.424	**3.18185**	24.9	72.8	0.364	Albite	5.169192443
37.29	**3.02783**	165	698.5	0.3944	Calcite	34.25368487
39.134	**2.89041**	47.8	334.5	0.5099	dolomite	9.923188707
42.034	**2.69908**	24.9	136.3	0.4053	Pyrite	5.169192443
45.792	2.48812	42.1	253.4	0.4755	-	
Total		481.7				

Table S1-7 X ray diffraction data of core 1 sample no.7
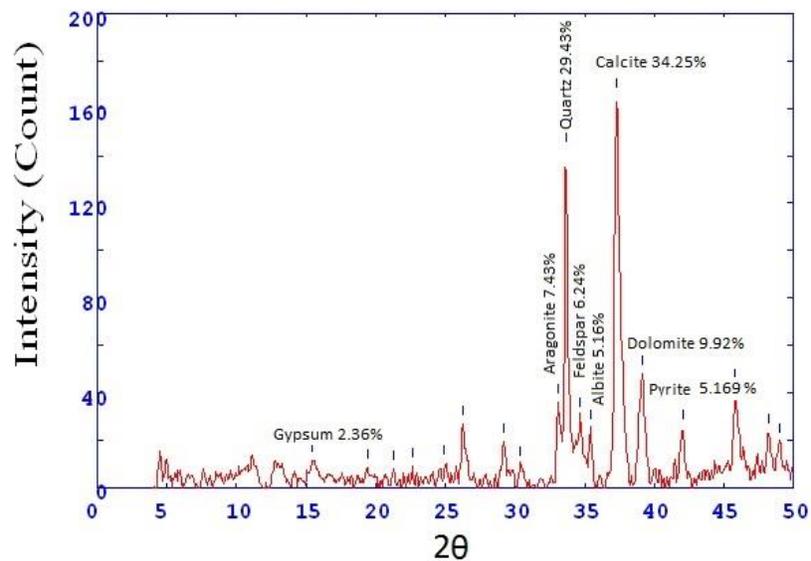
Fig.S4-7 X ray diffractogram of core 1 sample no.7

2Theta	d (A)	Height	Area	FWHM	Identified mineral	WT%
26.28	4.25817	25.9	106.1	0.3271	-	
29.132	3.84901	18.3	102	0.4633	-	
29.949	3.74633	12.9	71.7	0.3677	-	0
30.416	3.69012	12.9	71.7	0.3199	-	
33.126	**3.39576**	49.5	276.4	0.296	Aragonite	10.8220376
33.644	**3.34495**	109.6	390.4	0.2721	Quartz	23.96152164
34.527	**3.26188**	29.7	106	0.3281	Feldspar (orthoclase)	6.493222562
35.088	**3.21137**	21.6	76.9	0.356	Albite	4.722343682
37.262	**3.03002**	183	884.9	0.384	Calcite	40.00874508
39.011	**2.89913**	33.8	163.6	0.3723	dolomite	7.389593354
41.948	**2.70441**	30.2	129.8	0.3606	Pyrite	6.602536073
44.144	2.57606	10.1	40.9	0.3333	-	
45.789	2.48828	43.3	213.1	0.3939	-	
48.033	2.37842	20.3	107.9	0.4705	-	
48.821	2.34234	14.6	77.5	0.464	-	
Total	457.4					

Table S1-8 X ray diffraction data of core 1 sample no.8
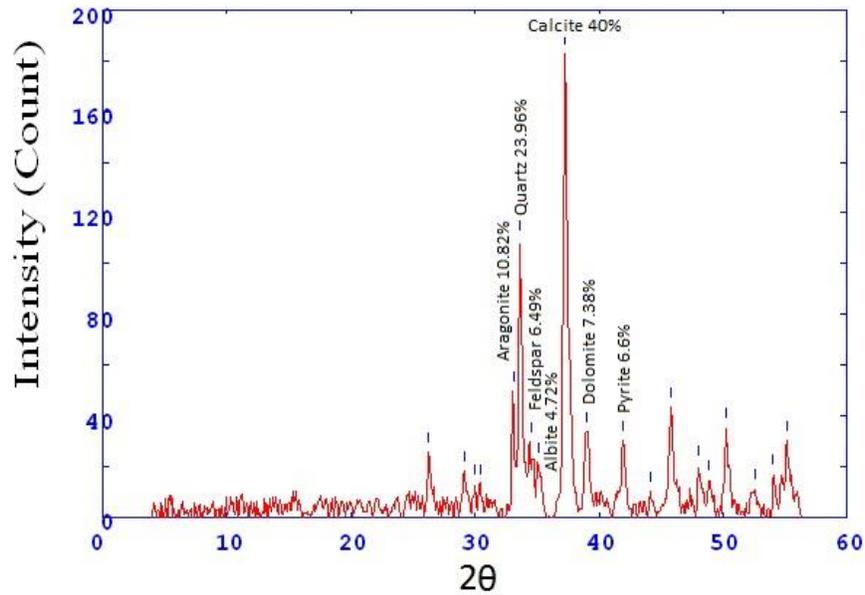
Fig.S4-8 X ray diffractogram of core 1 sample no.8

2Theta	d (A)	Height	Area	FWHM	Identified mineral	WT%
13.14	**8.46016**	20.7	66.9	0.2986	Illite	2.920428894
14.542	**7.64853**	147.8	273.4	0.2206	Gypsum	20.85214447
26.178	4.2745	31.5	90.1	0.2721	-	
28.299	3.95992	9	25.6	0.3067	-	
29.403	3.81438	32.2	122.1	0.3414	-	0
30.366	3.69609	23.1	146.9	0.4859	-	
31.9	3.52268	11.8	100.5	0.7569	-	
32.959	**3.41251**	26.8	227.2	0.5136	Aragonite	3.781038375
33.559	**3.35317**	205.7	585.9	0.2703	Quartz	29.02088036
34.543	**3.26045**	24	68.4	0.2693	Feldspar (orthoclase)	3.386004515
35.288	**3.19374**	64.2	184.6	0.2684	Albite	9.057562077
37.212	**3.03401**	165.2	979.9	0.4741	Calcite	23.30699774
39.087	**2.89373**	26.1	149.9	0.4795	dolomite	3.68227991
39.947	**2.83387**	11.2	64.3	0.5949	Halite	1.58013544
41.903	**2.70715**	17.1	157.3	0.7103	Pyrite	2.412528217
43.866	2.59161	9.6	70.6	0.5639	-	
45.737	2.49095	33.2	187.6	0.4583	-	
Total	708.8					

Table S1-9 X ray diffraction data of core 1 sample no.9
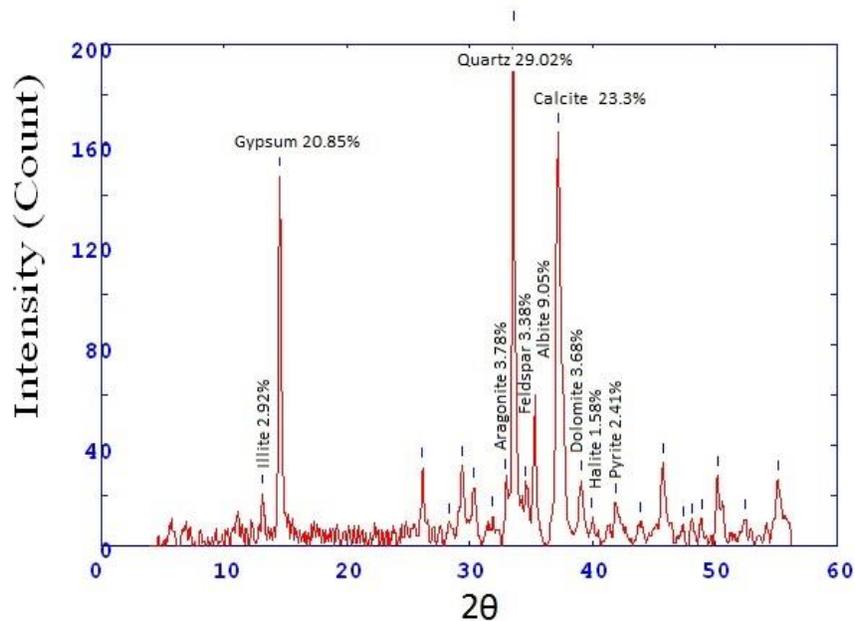
Fig.S4-9 X ray diffractogram of core 1 sample no.9

2Theta	d (A)	Height	Area	FWHM	Identified mineral	WT%
13.156	**8.45006**	23.1	60.7	0.2354	Illite	2.946052799
14.538	**7.65071**	238.4	465.5	0.2324	Gypsum	30.40428517
23.702	4.71352	10	52.5	0.4071	-	
26.2	4.271	35.7	193.4	0.4343	-	
29.422	3.812	43.7	129.9	0.3166	-	
30.363	3.69645	13.7	40.7	0.267	-	0
31.322	3.58594	24.6	54.1	0.2174	-	
32.876	**3.42085**	52.4	114.9	0.2426	Aragonite	6.682821069
33.59	**3.35019**	76.2	225.2	0.2678	Quartz	9.718148195
34.626	**3.25281**	212.3	418.3	0.2266	Feldspar (orthoclase)	27.07562811
37.218	**3.03355**	135.8	993.3	0.6056	Calcite	17.31921949
38.994	**2.9004**	16.7	135.2	0.5603	dolomite	2.129830379
41.867	**2.7094**	29.2	121.8	0.3559	Pyrite	3.724014794
45.747	2.49042	31.2	182.2	0.4542	-	
48.05	2.37766	17.6	56.4	0.2938	-	
48.85	2.34102	15.2	48.9	0.4407	-	
50.217	2.28129	25.1	191.3	0.5876	-	
Total	784.1					

Table S1-10 X ray diffraction data of core 1 sample no.10
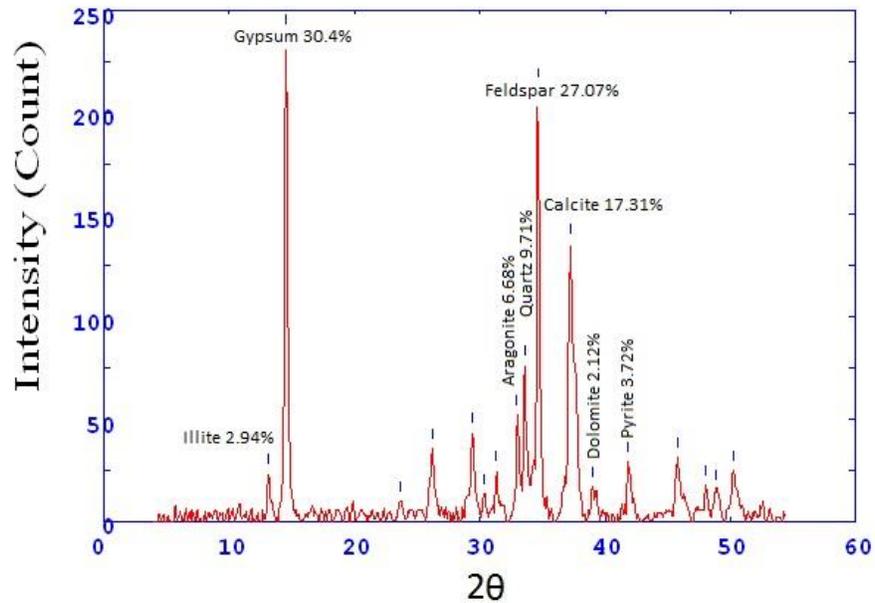
Fig.S4-10 X ray diffractogram of core 1 sample no.10

2Theta	d (A)	Height	Area	FWHM	Identified mineral	WT%
13.205	**8.41877**	22.2	530.9	0.2312	Illite	2.735000616
14.584	**7.62644**	260.8	530.9	0.2312	Gypsum	32.13009733
26.258	4.26164	25	103.6	0.3613	-	-
29.473	3.80552	57.8	122.5	0.2422	-	-
30.302	3.70367	19.7	41.8	0.2409	-	-
32.926	**3.41576**	55	116.6	0.2403	Aragonite	6.775902427
33.645	**3.34479**	218.1	468.5	0.2396	Quartz	26.86953308
34.45	**3.26898**	40.2	86.5	0.4538	Feldspar (orthoclase)	4.952568683
35.381	**3.1856**	16.5	35.4	0.5609	Albite	2.032770728
37.272	**3.02925**	130.5	1114.7	0.668	Calcite	16.07736849
38.936	**2.90455**	25.5	217.7	0.5544	dolomite	3.141554762
41.893	**2.7078**	42.9	244.3	0.4409	Pyrite	5.285203893
45.807	2.48735	34	256.5	0.5778	-	-
48.119	2.37443	25.2	112.3	0.3778	-	-
Total	811.7					

Table S1-11 X ray diffraction data of core 1 sample no.11
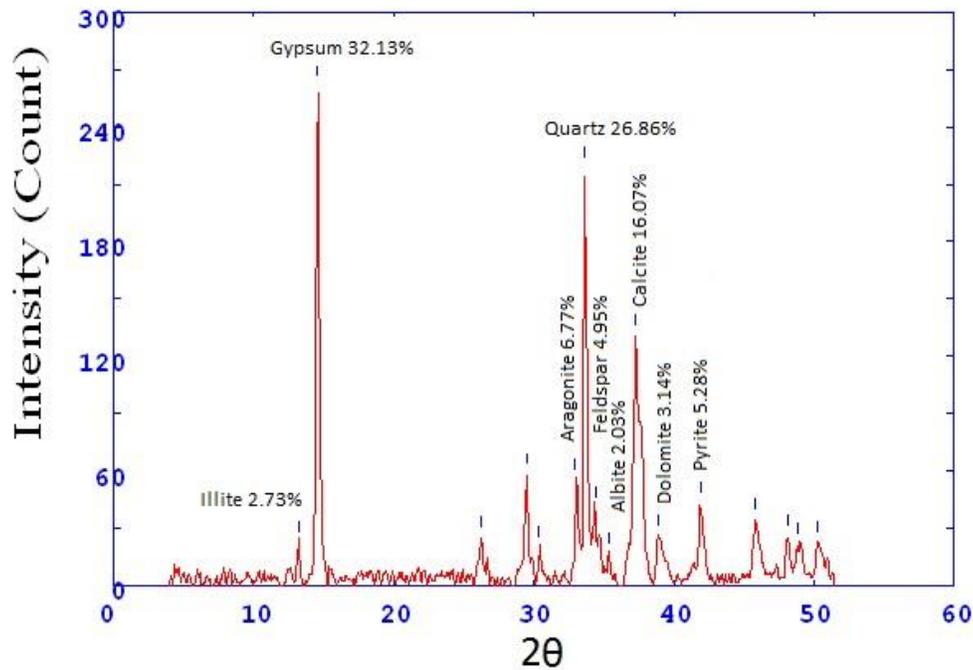
Fig.S4-11 X ray diffractogram of core 1 sample no.11

2Theta	d (A)	Height	Area	FWHM	Identified mineral	WT%
29.074	**3.85656**	27.6	79.1	0.283	Aragonite	3.998261625
33.634	**3.34594**	27.8	126.2	0.3931	Quartz	4.027234536
35.078	**3.21223**	29.9	97.3	0.3157	Feldspar (orthoclase)	4.331450094
37.244	**3.03147**	249.1	988.7	0.3364	Calcite	36.08575981
38.804	**2.91402**	323.7	1038.5	0.3192	dolomite	46.89265537
39.995	**2.83066**	17.6	56.4	0.3824	-	-
42.101	**2.695**	14.6	86.6	0.4457	pyrite	2.115022454
45.716	2.492	28.2	204.7	0.5439	-	-
47.068	2.42434	12.4	90.3	0.4881	-	-
50.233	2.28058	44.5	240.6	0.4322	-	-
52	2.20822	28	135.6	0.3539	-	-
55.133	2.09175	33.5	227.8	0.5053	-	-
Total	690.3					

Table S1-12 X ray diffraction data of core 1 sample no.12
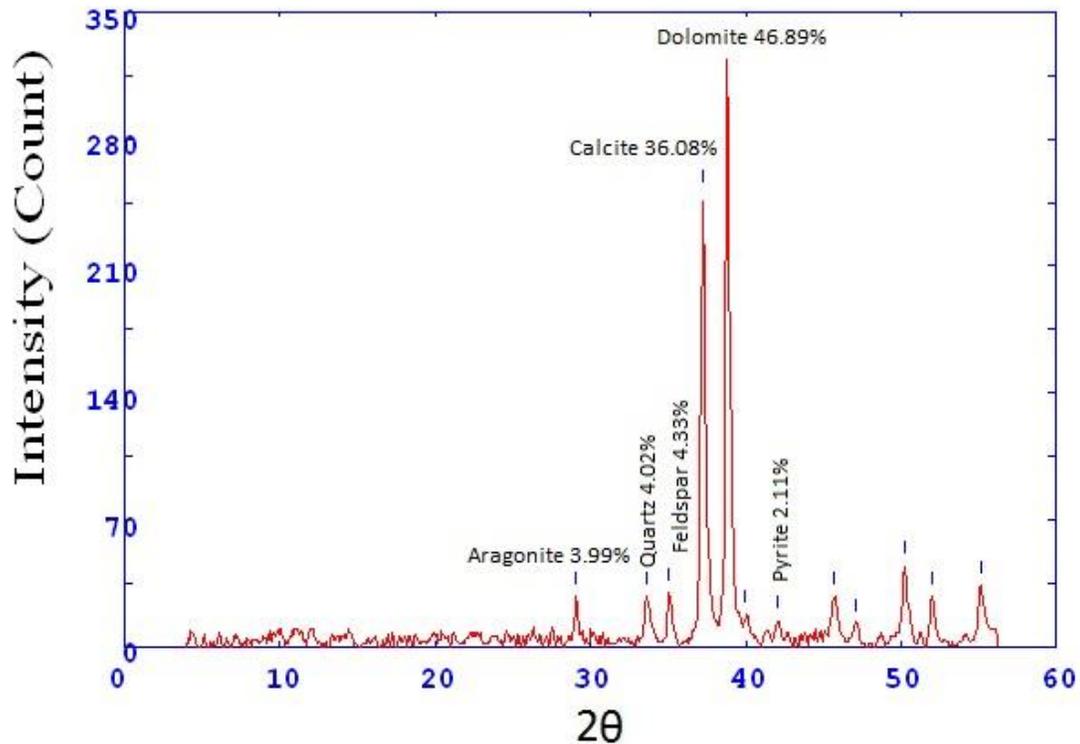
Fig.S4-12 X ray diffractogram of core 1 sample no.12

2Theta	d (A)	Height	Area	FWHM	Identified mineral	WT%
29.053	3.85937	19.5	87.4	0.3652	-	-
29.973	**3.74342**	13.9	62.4	0.3875	Aragonite	2.302849569
33.529	**3.35605**	21.5	97.3	0.4098	Quartz	3.561961564
35.011	**3.21819**	60.4	189.9	0.2922	Feldspar (orthoclase)	10.00662691
37.167	**3.03757**	154.5	744.2	0.3605	Calcite	25.59642147
38.833	**2.9119**	341.2	2226.2	0.4437	dolomite	56.52750166
42.017	**2.70017**	12.1	70.7	0.4667	Pyrite	2.004638834
44.284	2.56835	7.5	43.9	0.4824	-	-
45.674	2.4942	17.4	109.5	0.4981	-	-
47.074	2.42405	17.9	71.5	0.3496	-	-
50.09	2.28668	28	143.2	0.4343	-	-
51.989	2.20866	42.9	175.5	0.3811	-	-
Total	603.6					

Table S1-13 X ray diffraction data of core 1 sample no.13
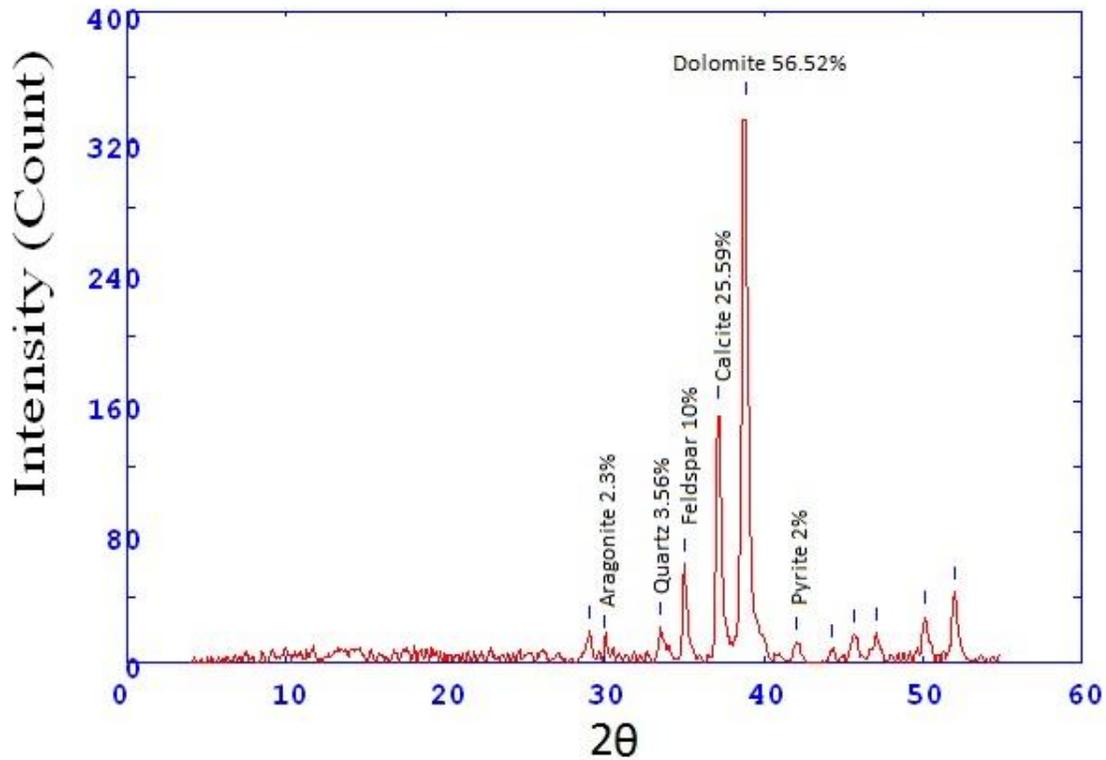
Fig.S4-13 X ray diffractogram of core 1 sample no.13

2Theta	d (A)	Height	Area	FWHM	Identified mineral	WT%
26.237	4.26512	11.8	78.4	0.4812	-	-
29.117	3.85107	20.1	95	0.4278	-	-
30.154	**3.72144**	19	89.9	0.3427	Aragonite	2.887537994
33.592	**3.34998**	53.2	150.4	0.2576	Quartz	8.085106383
35.07	**3.21298**	85.8	249.7	0.2744	Feldspar (orthoclase)	13.03951368
37.227	**3.03281**	125.7	508.3	0.3504	Calcite	19.10334347
38.759	**2.91728**	332.8	1345.4	0.4317	dolomite	50.5775076
40.027	**2.82847**	29.6	218.4	0.5131	Halite	4.498480243
42.201	**2.68892**	11.9	88.7	0.5155	Pyrite	1.808510638
45.652	2.49533	20.5	87.4	0.4439	-	-
47.168	2.41947	21.6	145.3	0.5547	-	-
50.167	2.28341	24.5	172.4	0.5065	-	-
52.025	2.20725	52.7	219.8	0.3621	-	-
Total	658					

Table S1-14 X ray diffraction data of core 1 sample no.14
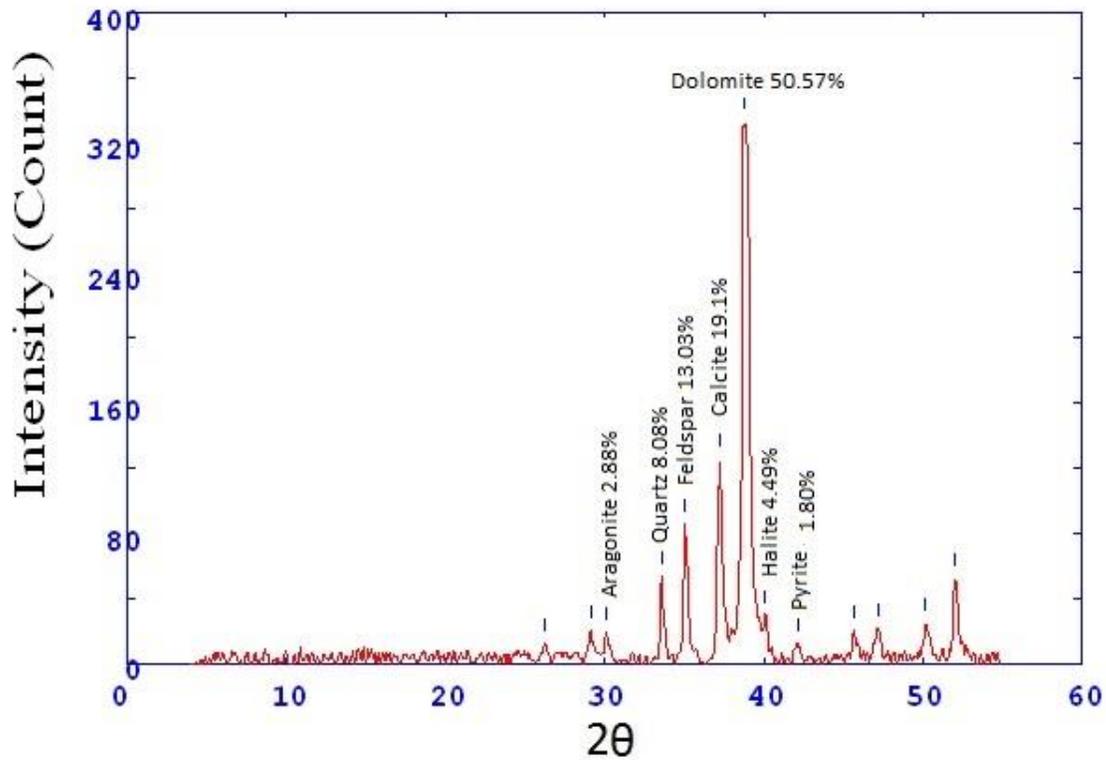
Fig.S4-14 X ray diffractogram of core 1 sample no.14

2Theta	d (A)	Height	Area	FWHM	Identified mineral	WT%
24.68	4.52958	22.1	20.9	0.1821	-	
26.422	4.23575	57.1	160.9	0.2629	Goethite	9.911473702
29.333	3.82326	15.7	44.1	0.2602	-	
30.548	3.67455	25.3	70.6	0.2574	-	
32.097	3.50156	13.8	38.7	0.2614	-	
33.146	3.39375	22.3	62.2	0.2634	Aragonite	3.870855754
33.782	3.33166	190.7	564.2	0.2654	Quartz	33.10189203
34.576	3.25743	19.9	58.7	0.2672	Feldspar (orthoclase)	3.454261413
35.434	3.18101	76.1	238.1	0.269	Feldspar (Albite)	13.20951224
37.425	3.01733	126.8	498.7	0.334	Calcite	22.0100677
39.234	2.88335	56.6	358.6	0.4627	Dolomite	9.824683215
40.2	2.81681	10.2	64.9	0.4647	Halite	1.77052595
42.167	2.691	16.4	84	0.4667	Pyrite	2.846727999
45.824	2.48646	24.7	101.7	0.3456	-	
46.573	2.44863	33.9	134.5	0.3314	-	
48.26	2.3679	10	26.3	0.244	-	
50.434	2.2721	30.8	130.5	0.3732	-	
52.635	2.18346	13.1	105.2	0.5804	-	
54.212	2.12453	13.2	106.7	0.468	-	
55.333	2.08478	21	82.7	0.3556	-	
Total	576.1					

Table S2-1 X ray diffraction data of core 2 sample no.1
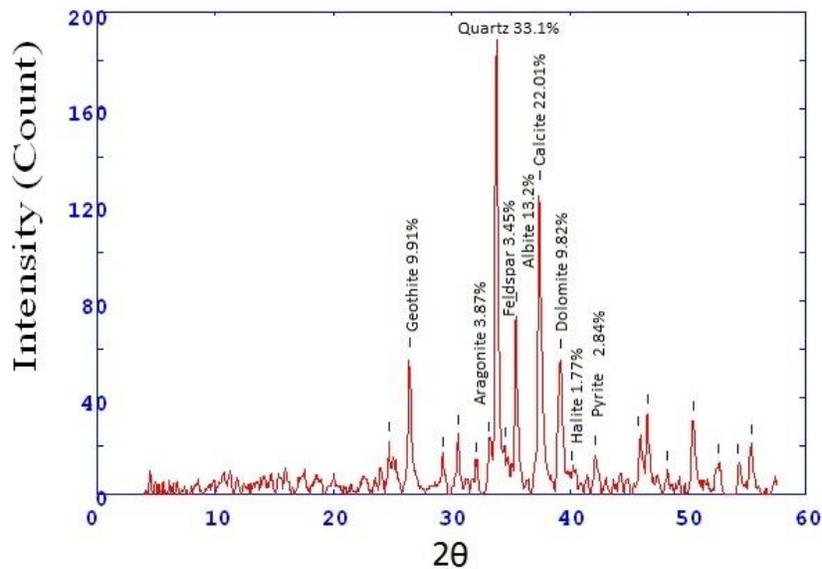
Fig.S5-1 X ray diffractogram of core 2 sample no.1

2Theta	d (A)	Height	Area	FWHM	Identified mineral	WT%
5.947	**18.65992**	228.2	179	0.1295	Mont.	38.16053512
29.701	3.77699	20.5	100	0.4178	-	
33.605	**3.34866**	30.4	147.9	0.3617	Quartz	5.08361204
34.224	**3.28991**	88	326	0.3055	Feldspar (orthoclase)	14.71571906
35.02	**3.21734**	19.1	70.8	0.3124	Albite	3.193979933
37.863	**2.98371**	196.8	758.3	0.3193	Calcite	32.909699
39.619	**2.8564**	20.5	79	0.3379	Dolomite	3.428093645
40.769	2.77913	9.9	38.3	0.3472	-	-
42.6	**2.66488**	15	70	0.3565	Pyrite	2.508361204
46.392	2.45768	34.1	173.3	0.44	-	-
47.844	2.38727	11.3	57.7	0.3613	-	-
48.673	2.34901	14	42.7	0.2825	-	-
50.811	2.25634	34.1	168	0.4058	-	-
Total	598					

Table S2-2 X ray diffraction data of core 2 sample no.2
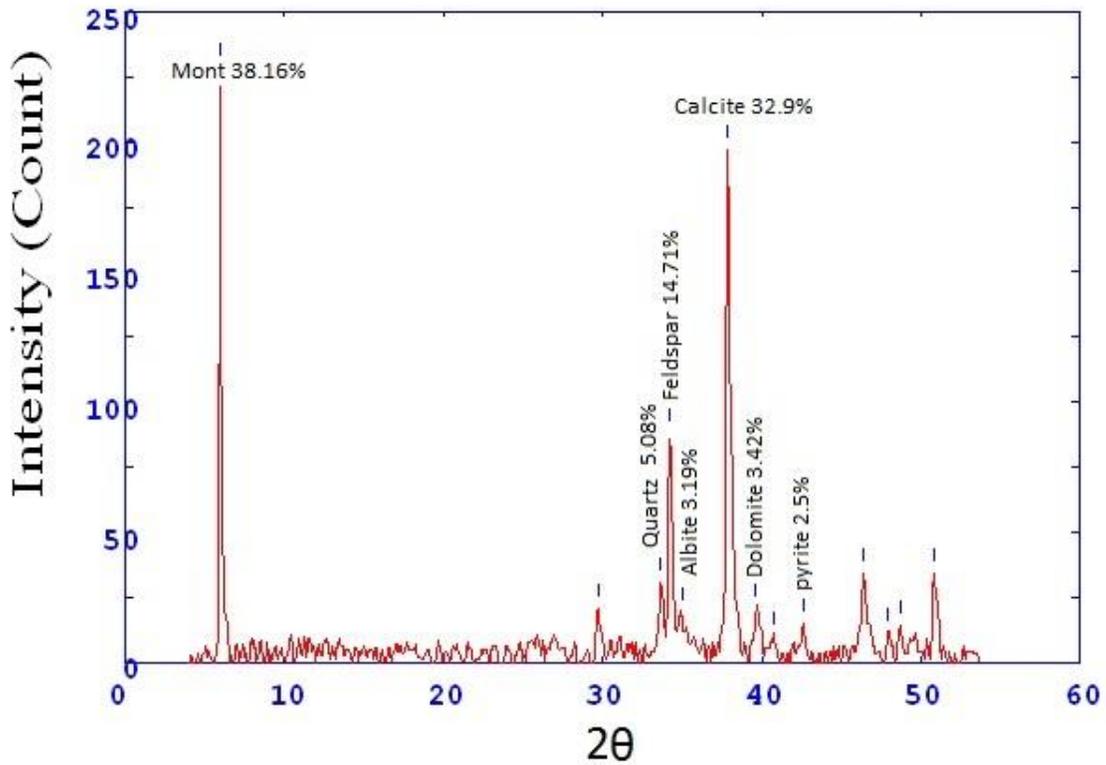
Fig.S5-2 X ray diffractogram of core 2 sample no.2

2Theta	d (A)	Height	Area	FWHM	Identified mineral	WT%
26.26	4.26137	36.7	102.7	0.2462	-	0
29.156	3.84603	19.6	62	0.317	-	
33.048	**3.4035**	34	107.6	0.2939	Aragonite	9.366391185
33.643	**3.34505**	96	290.4	0.2708	Quartz	26.44628099
34.531	**3.26148**	33	99.8	0.3013	Feldspar (Orthoclase)	9.090909091
37.263	**3.03002**	159.3	610.4	0.3318	Calcite	43.88429752
38.783	**2.9155**	11.7	44.8	0.3253	Dolomite	3.223140496
40.069	**2.82563**	11.7	44.8	0.3221	Halite	3.223140496
41.954	**2.70401**	17.3	53.7	0.3189	Pyrite	4.76584022
45.75	2.49027	28.5	183.4	0.4474	-	
48.052	2.37752	16.3	96.4	0.473	-	
48.969	2.33571	14.7	86.9	0.4218	-	
50.234	2.28056	29.1	125.5	0.3706	-	
55.217	2.08884	24.6	121.7	0.3801	-	
58.578	1.97873	24.7	129.5	0.3952	-	
Total	363					

Table S2-3 X ray diffraction data of core 2 sample no.3
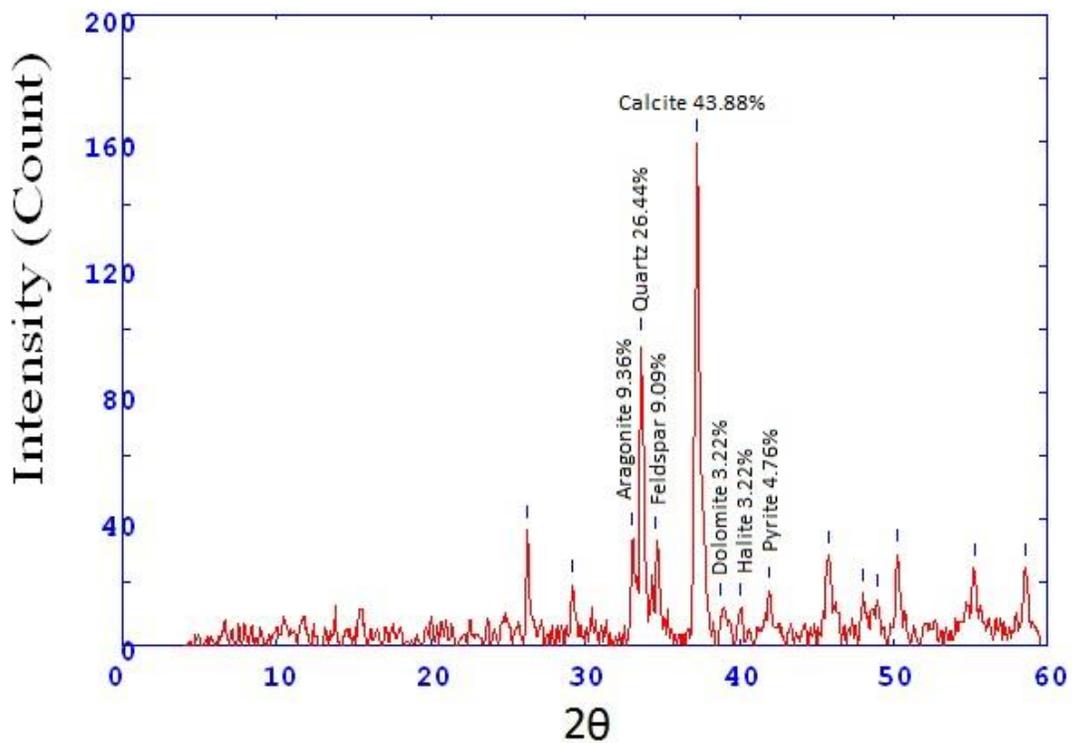
Fig.S5-3 X ray diffractogram of core 2 sample no.3

2Theta	d (A)	Height	Area	FWHM	Identified mineral	WT%
32.758	**3.43282**	64.4	214.7	0.2766	Aragonite	18.14084507
33.525	**3.35641**	72.1	214.7	0.2766	Quartz	20.30985915
34.202	**3.29199**	37.4	111.2	0.4672	Feldspar (orthoclase)	10.53521127
35.104	**3.20995**	6.9	20.6	0.5625	Feldspar (Albite)	1.943661972
37.194	**3.03538**	90.3	833.3	0.6578	Calcite	25.43661972
38.803	**2.91412**	15.3	140.7	0.458	Dolomite	4.309859155
40.019	**2.829**	21.5	68.2	0.2583	Halite	6.056338028
41.825	**2.71197**	47.1	148.9	0.2876	Pyrite	13.26760563
45.678	2.494	34.8	176.7	0.3911	-	
47.013	2.42703	11.8	59.9	0.3525	-	
47.967	2.38153	26.6	105.7	0.3139	-	
48.727	2.34659	22.2	88.1	0.5884	-	
50.7	2.26094	14.3	183.7	0.8628	-	
52.5	2.18866	7.1	69.6	0.6444	-	
54.05	2.13044	6.1	23.1	0.1167	-	
Total	355					

Table S2-4 X ray diffraction data of core 2 sample no.4
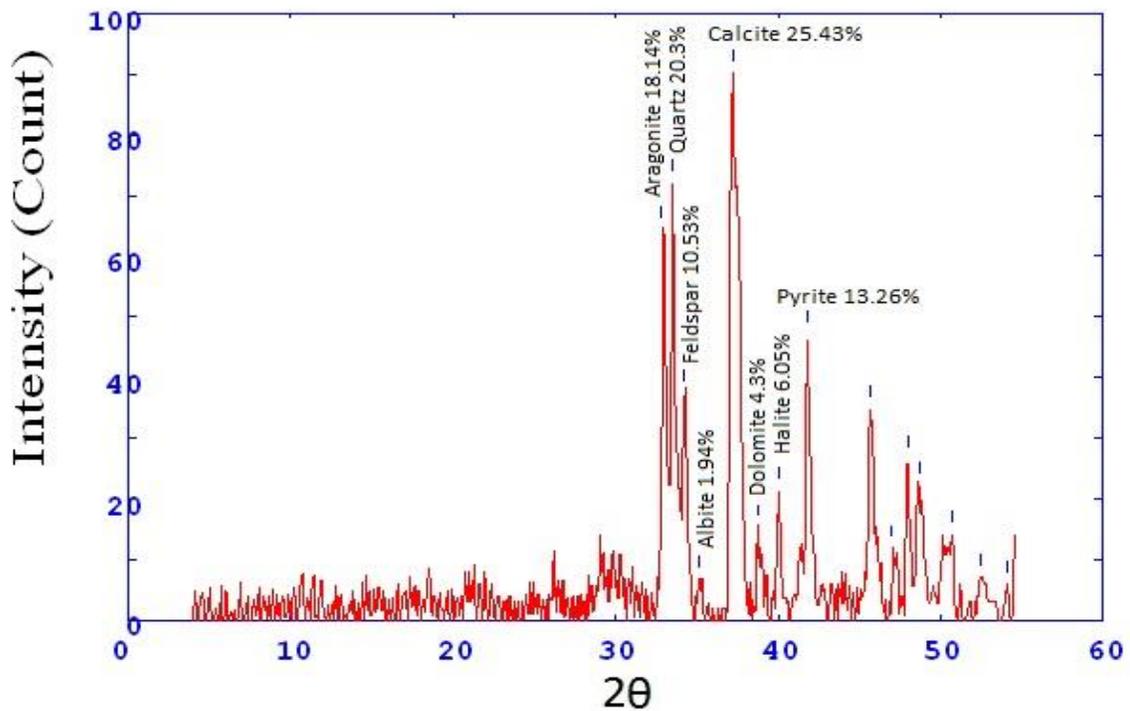
Fig.S5-4 X ray diffractogram of core 2 sample no.4

2Theta	d (A)	Height	Area	FWHM	Identified mineral	WT%
32.945	**3.41386**	70.7	212.3	0.3078	Aragonite	29.60636516
34.155	**3.29636**	36	108	0.4836	Quartz	15.07537688
37.24	**3.03179**	89.7	762.8	0.6595	Calcite	37.56281407
41.806	**2.71316**	42.4	130.2	0.2969	Pyrite	17.75544389
45.687	2.49353	39.6	161.1	0.3731	-	-
47.283	2.41394	10.2	41.6	0.3524	-	-
47.989	2.38048	29.5	121.1	0.3316	-	-
48.924	2.33771	24.4	100	0.6495	-	-
50.5	2.26933	18.2	236.4	0.9674	-	-
52.115	2.20369	9.6	236.4	0.9674	-	-
Total	238.8					

Table S2-5 X ray diffraction data of core 2 sample no.5
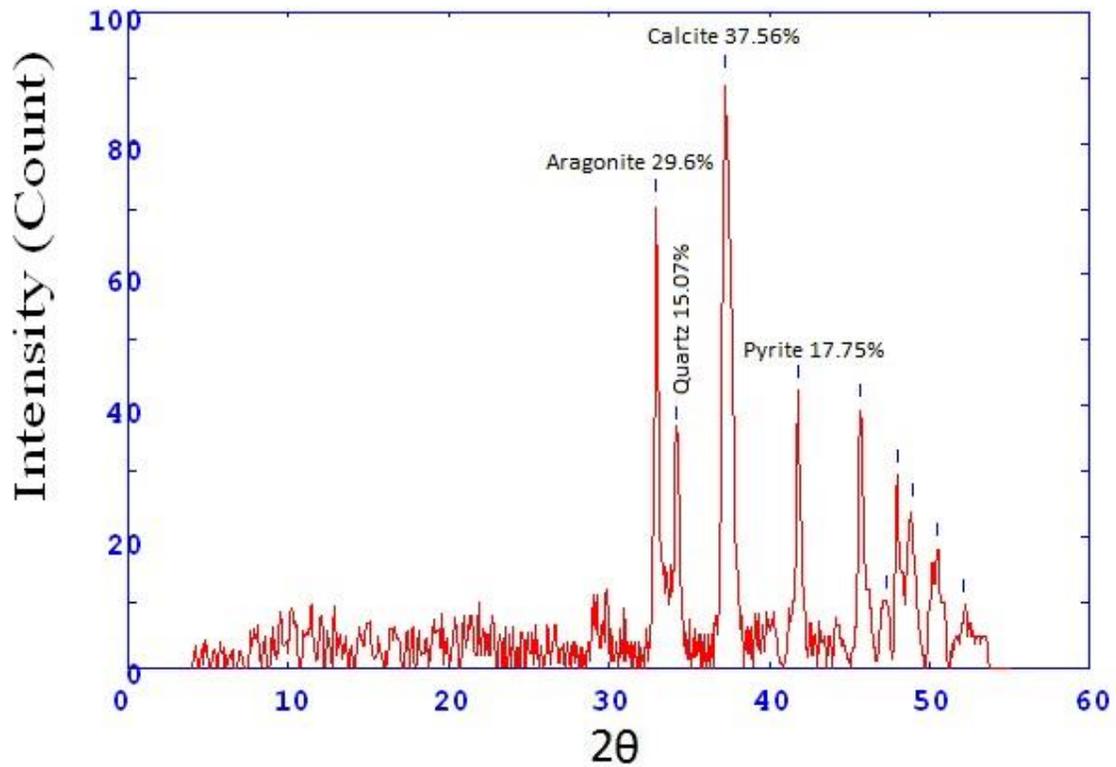
Fig.S5-5 X ray diffractogram of core 2 sample no.5

2Theta	d (A)	Height	Area	FWHM	Identified mineral	WT%
33.091	**3.39922**	83	337.1	0.3292	Aragonite	25.76039727
34.32	**3.28098**	53.7	218.4	0.4602	Quartz	16.66666667
37.385	**3.02047**	118.2	881.1	0.5912	Calcite	36.68528864
40.148	**2.8203**	18.1	134.5	0.4844	Dolomite	5.617628802
41.967	**2.70322**	49.2	188.8	0.3775	Pyrite	15.27001862
45.85	2.48512	49.3	247.7	0.4326	-	-
47.347	2.41084	18.1	86.9	0.9047	-	-
47.947	2.38242	36.1	12.3	0.1731	-	-
48.976	2.33538	27.4	19.8	0.2418	-	-
50.347	2.27575	18.8	143.6	0.9735	-	-
Total		322.2				

Table S2-6 X ray diffraction data of core 2 sample no.6
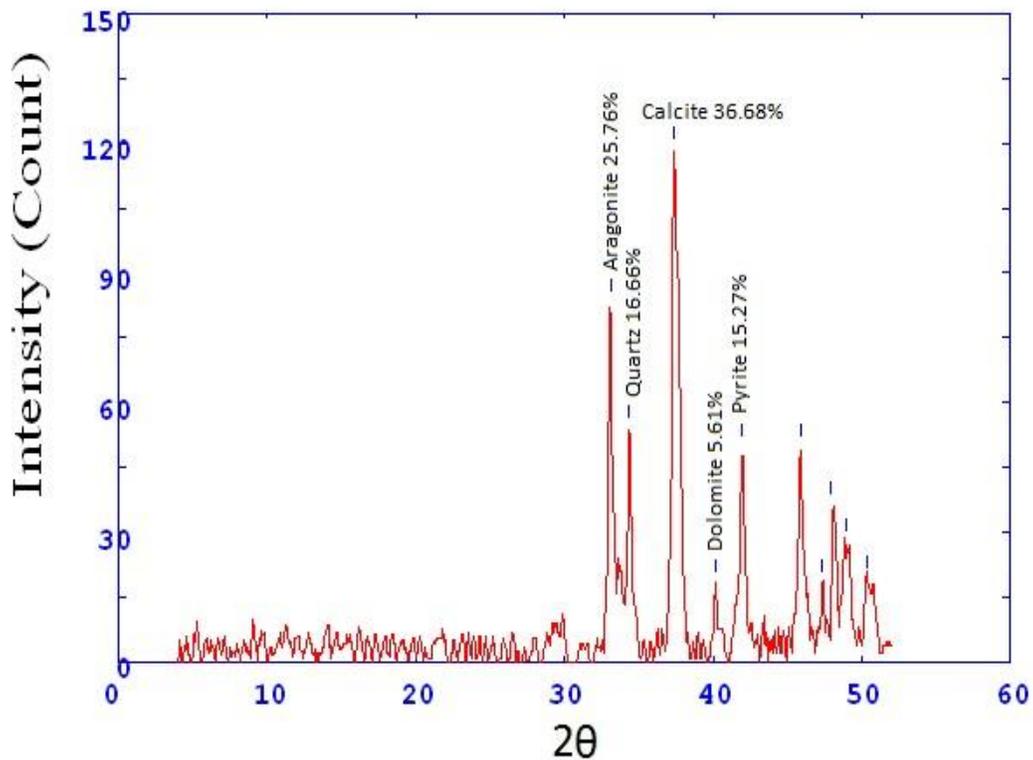
Fig.S5-6 X ray diffractogram of core 2 sample no.6

2Theta	d (A)	Height	Area	FWHM	Identified mineral	WT%
22.341	**4.9968**	12.4	258.9	0.2482	Gypsum	2.094948
23.509	4.75172	14.5	258.9	0.2482	-	
24.829	4.50278	94.1	258.9	0.2482	-	
28.783	3.89478	64.6	181	0.271	-	
32.033	3.50837	330.8	1764.2	0.374	-	
33.023	**3.40606**	37.1	198	0.3264	Aragonite	6.267951
33.66	**3.34336**	77.9	231.4	0.2789	Quartz	28.34788937
35.6	**3.16659**	39.7	118.8	0.3052	feldspar	6.707214
37.467	**3.01407**	61	358	0.4212	calcite	22.19796215
38.531	**2.93391**	33	193.7	0.4404	dolomite	12.00873362
42.3	**2.68291**	13.7	99.5	0.4596	pyrite	2.31458
44.767	2.54206	36	148.3	0.3118	-	
48.583	2.35309	30.2	170.8	0.4067	-	
Total		274.8				

Table S3-1 X ray diffraction data of core 3 sample no.1
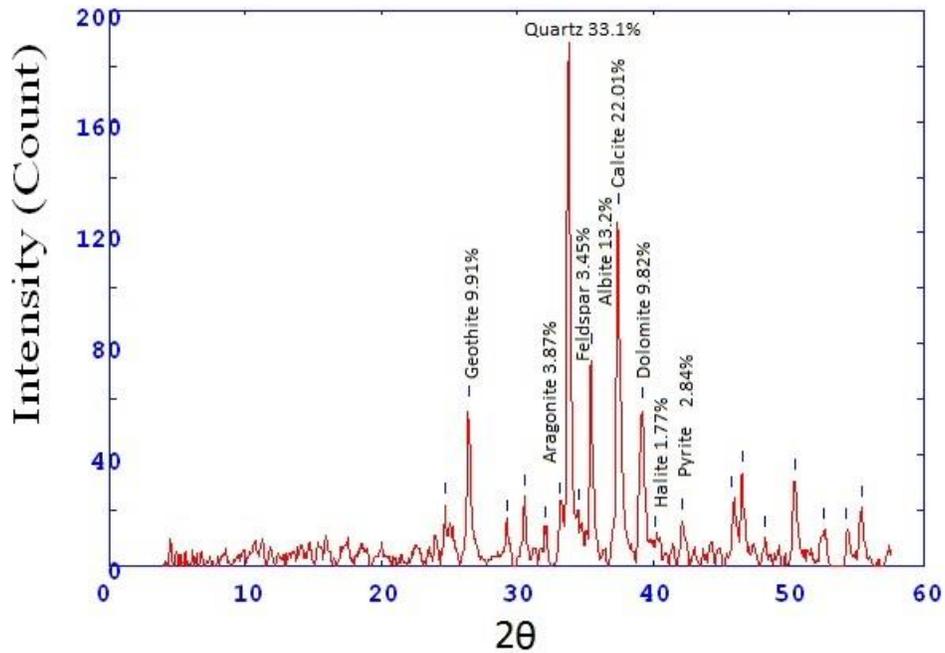
Fig.S6-1 X ray diffractogram of core 3 sample no.1

2Theta	d (A)	Height	Area	FWHM	Identified mineral	WT%
25.081	4.45827	90.2	16182.7	0	-	0
33.583	**3.3508**	124.5	12597.3	5	Quartz	18.34659593
34.578	**3.25722**	87.4	8843.6	3.0111	feldspar	12.87945771
35.216	**3.20007**	128.8	9830.7	1.0222	feldspar (Albite)	18.98025346
37.171	**3.03721**	136.4	2165.3	1.099	calcite	20.10020631
39.05	**2.89637**	113.5	17280	1.099	Dolomite	16.72561155
40.033	**2.82807**	88	13402.9	1.099	Halite	12.96787504
45.633	2.49629	79.4	15474.7	1.099	-	
47.193	2.4183	74.1	14450.9	1.099	-	
50.133	2.28483	79	10121.3	1.099	-	
Total		678.6				

Table S3-2 X ray diffraction data of core 3 sample no.2
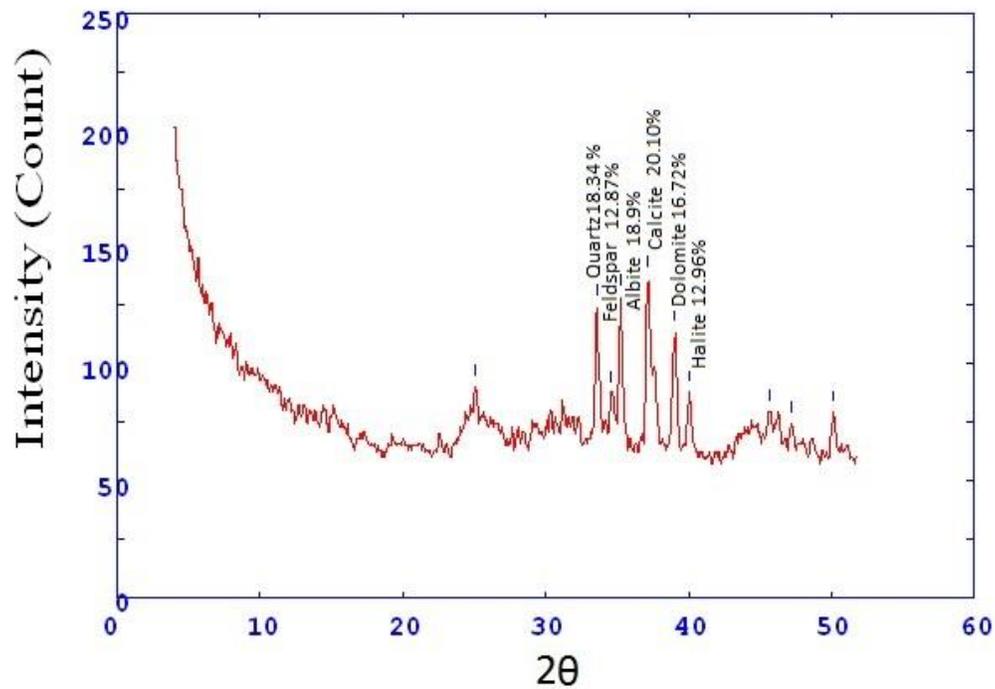
Fig.S6-2 X ray diffractogram of core 3 sample no.2

2Theta	d (A)	Height	Area	FWHM	Identified mineral	WT%
26.237	4.2651	65	141.3	0.2437	-	
30.395	3.69263	29.9	108.1	0.3231	-	0
33.176	**3.39079**	45.9	165.9	0.2885	Aragonite	7.9302
33.613	**3.34793**	274.1	777.9	0.2538	Quartz	47.3566
34.653	**3.2504**	44.2	125.5	0.3469	Feldspar	7.636489
35.348	**3.18846**	26	73.9	0.3934	Albite	4.492053
37.224	**3.03308**	102.1	512.8	0.44	Calcite	17.63994
39.054	**2.89611**	64.6	339.7	0.4255	Dolomite	11.16102
41.917	**2.7063**	21.9	73.7	0.3108	Pyrite	3.78369
45.767	2.48941	26.5	179.3	0.4574	-	
46.471	2.45374	20.8	141	0.3504	-	
48.133	2.37377	19	42.3	0.2433	-	
48.904	2.33862	12.2	27.2	0.3083	-	
50.215	2.28135	25.3	98.7	0.3733	-	
52.367	2.19384	16.3	71	0.3667	-	
Total		578.8				

Table S3-3 X ray diffraction data of core 3 sample no.3
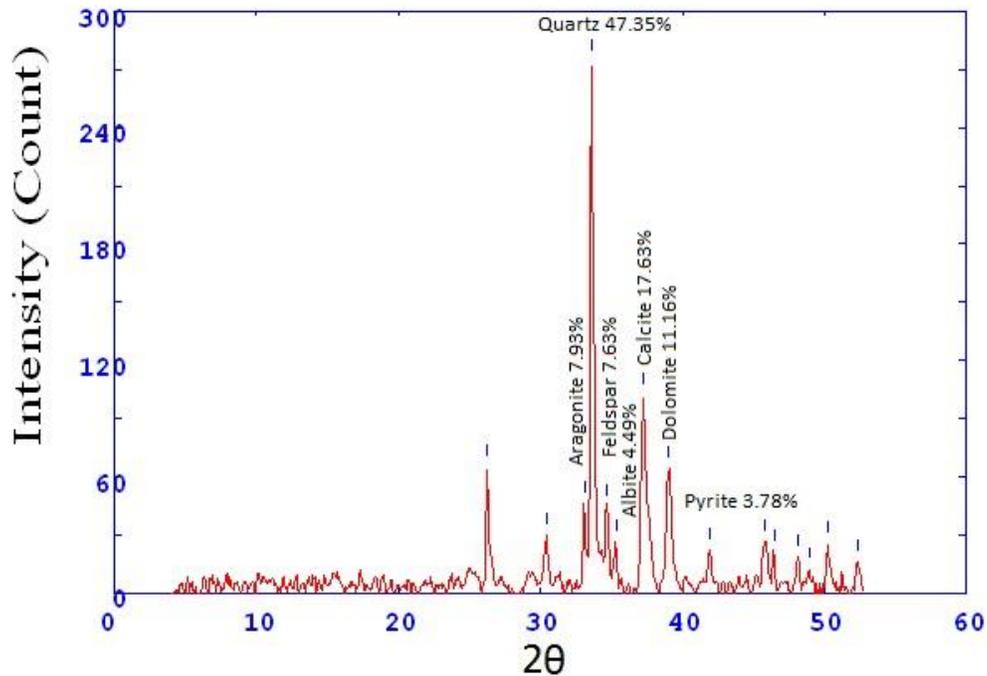
Fig.S6-3 X ray diffractogram of core 3 sample no.3

2Theta	d (A)	Height	Area	FWHM	Identified mineral	WT%
26.276	4.25876	45.2	143.5	0.3076	-	0
29.196	3.84075	15.3	48.5	0.2681	-	
30.421	3.68953	27	60.8	0.2286	-	
32.966	**3.41179**	34.5	77.6	0.2435	Aragonite	5.772126
33.631	**3.3462**	265.4	565.4	0.2583	Quartz	44.40355
34.671	**3.24878**	40.9	87.1	0.3559	Feldspar (orthoclase)	6.842898
35.299	**3.19275**	44.1	93.9	0.4047	Feldspar (Albite)	7.378283
37.264	**3.02987**	153	933.6	0.4535	calcite	25.59813
38.978	**2.90148**	33.7	205.4	0.3847	dolomite	5.63828
41.984	**2.7022**	26.1	114.5	0.3159	pyrite	4.366739
45.75	2.49027	32.5	212.1	0.4647	-	
48.022	2.37893	18.2	65.7	0.3456	-	
50.202	2.28189	35.6	182.6	0.4741	-	
52.621	2.18399	14	85.6	0.4748	-	
54.073	2.1296	16.9	115.4	0.4089	-	
Total		597.7				

Table S3-4 X ray diffraction data of core 3 sample no.4
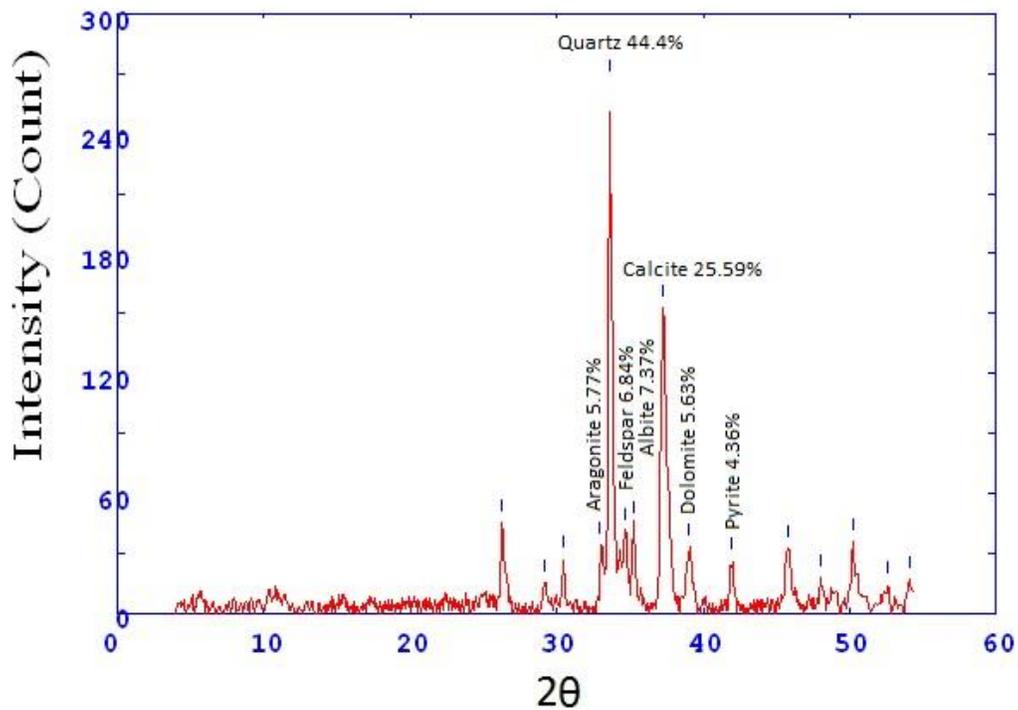
Fig.S6-4 X ray diffractogram of core 3 sample no.4

2Theta	d (A)	Height	Area	FWHM	Identified mineral	WT%
29.34	3.82237	62	12618.7	0	-	0
33.077	**3.40061**	135.4	1153.3	0.5883	Aragonite	28.57143
34.271	**3.2855**	93.9	799.3	0.7727	Feldspar (orthoclase)	19.81431
37.638	**3.00084**	147.2	2238.7	0.9571	calcite	31.06141
41.962	**2.70351**	97.4	2053.3	1.6	Pyrite	20.55286
45.833	2.48598	88.5	7870.7	2.4	-	
47.2	2.41793	55.7	4952.3	2.4	-	
48.133	2.37377	77	12202.7	2.4	-	
48.993	2.3346	74.1	11749.6	2.4	-	
50.315	2.27713	64.9	10287.2	2.4	-	
52.433	2.19125	55.1	11308	2.4	-	
54.681	2.1077	68.2	8512	2.4	-	
Total		473.9				

Table S3-5 X ray diffraction data of core 3 sample no.5
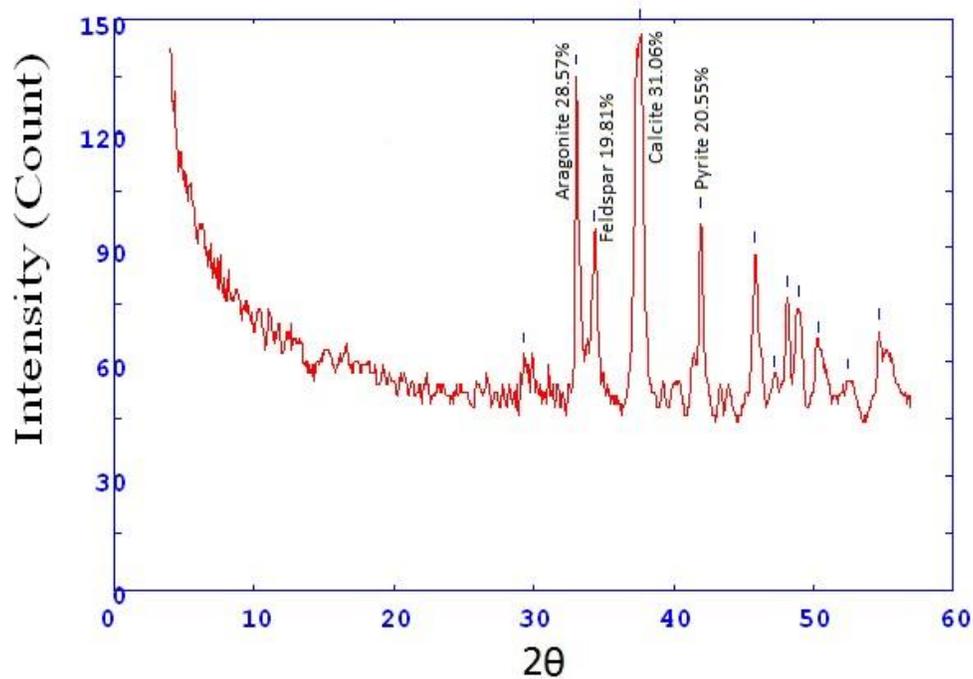
Fig.S6-5 X ray diffractogram of core 3 sample no.5

2Theta	d (A)	Height	Area	FWHM	Identified mineral	WT%
14.55	**7.64437**	132	1633.3	0.9556	Gypsum	12.18387
23.8	4.69447	63	12718.7	0.9556	-	
26.259	4.26147	110.1	1826.7	1.3333	-	
28.283	3.96212	58.1	963.7	1.3333	-	
29.425	3.81158	70.3	1165.4	1.3333	-	
30.395	3.69263	74	15790.7	1.3333	-	
33.013	**3.40701**	115.7	24685.7	0.858	Aragonite	10.67934
33.609	**3.34829**	223.7	1048	0.3827	Quartz	20.64796
34.563	**3.25862**	143.2	671.2	0.6589	Feldspar (orthoclase)	13.21765
35.297	**3.19295**	117.6	551.2	0.7971	Albite	10.85472
37.278	**3.02882**	154.2	2156	0.9352	calcite	14.23297
39.1	**2.89281**	104.3	14274.7	6.8	dolomite	9.6271
40.027	**2.82849**	92.7	12688.9	6.8	Halite	8.556397
41.25	2.7481	65.1	8920.1	6.8	-	
41.927	**2.7057**	82	14721.3	6.8	-	
45.756	2.48998	84.7	11344	6.8	-	
47.285	2.41385	61.3	8213.8	6.8	-	
48.019	2.37909	70.3	9414.5	6.8	-	
48.748	2.34561	71.3	7760	6.8	-	
Total		1083.4				

Table S3-6 X ray diffraction data of core 3 sample no.6
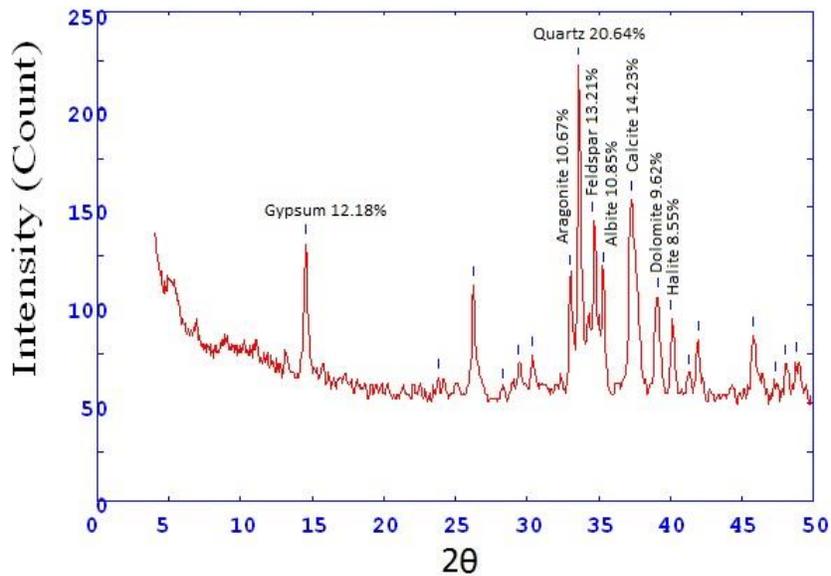
Fig.S6-6 X ray diffractogram of core 3 sample no.6

2Theta	d (A)	Height	Area	FWHM	Identified mineral	WT%
13.166	**8.44383**	79.8	1217.3	0.6667	Illite	7.123092029
14.522	**7.65891**	140.5	1217.3	0.6667	Gypsum	12.54128358
26.186	4.27326	73.2	12713.3	0.6667	-	
29.429	3.81109	72.6	12608.9	0.6667	-	
30.288	3.70546	76.8	15068	0.6667	-	
33.012	**3.40712**	111.5	21874.5	0.5117	Aragonite	9.952691243
33.56	**3.35302**	237	1069.3	0.3567	Quartz	21.15504776
34.574	**3.25758**	154	694.7	0.6307	Feldspar (othoclase)	13.74631795
37.278	**3.02882**	154.1	2069.3	0.9048	Calcite	13.75524413
38.984	**2.90106**	84.1	1129	0.9048	dolomite	7.50691779
40.087	**2.82442**	74	993.6	0.9048	Halite	6.605373561
41.9	**2.70735**	85.3	14253.3	0.9048	pyrite	7.614031956
44.313	2.56673	58.9	9842.8	0.9048	-	
45.8	2.48769	84	12822.7	0.9048	-	
47.345	2.41094	61	9316.6	0.9048	-	
48.1	2.37531	74.5	12541.3	0.9048	-	
48.816	2.34258	66.1	11123.1	0.9048	-	
50.286	2.27836	65.4	11001.8	0.9048	-	
52.333	2.19514	59	9957.3	0.9048	-	
Total		1120.3				

Table S3-7 X ray diffraction data of core 3 sample no.7
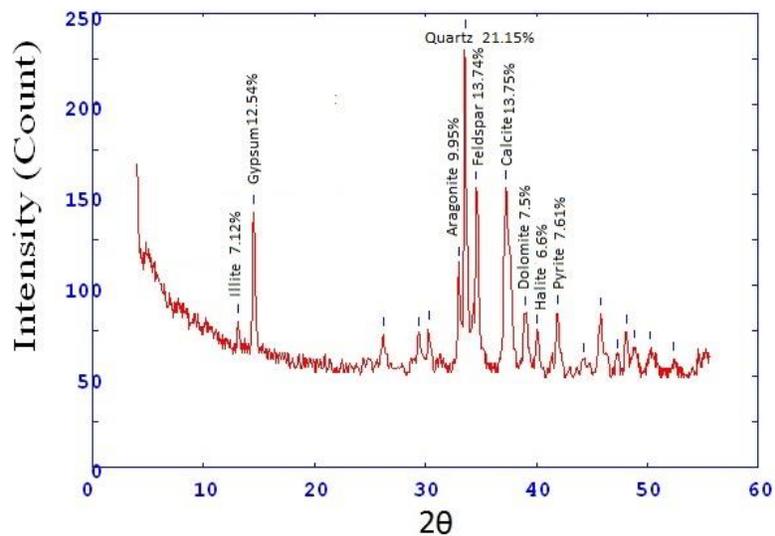
Fig.S6-7 X ray diffractogram of core 3 sample no.7

2Theta	d (A)	Height	Area	FWHM	Identified mineral	WT%
26.447	4.23183	63.2	11172	0	-	
29.952	3.74602	59.3	12373.3	0	-	0
33.179	**3.39041**	132.2	1036	0.563	Aragonite	19.53598
33.856	**3.32457**	98.4	771	0.8111	Quartz	14.54116
34.45	**3.26893**	94.3	738.9	0.9352	Feldspar (orthoclase)	13.93527
35.129	**3.20768**	70.1	549.4	0.9972	Albite	10.3591
37.518	**3.01011**	126.3	2124	1.0593	calcite	18.66411
40.2	**2.8168**	62	12397.3	1.0593	Halite	9.16211
42.013	**2.70037**	93.4	2062.7	1.7222	pyrite	13.80228
45.919	2.48159	82.2	11818.7	1.7222	-	
47.352	2.41065	57.8	8316.8	1.7222	-	
48.147	2.37315	82.4	9737.3	1.7222	-	
48.964	2.33591	72.2	0	0	-	
50.407	2.27323	61.1	0	0	-	
Total		676.7				

Table S3-8 X ray diffraction data of core 3 sample no.8
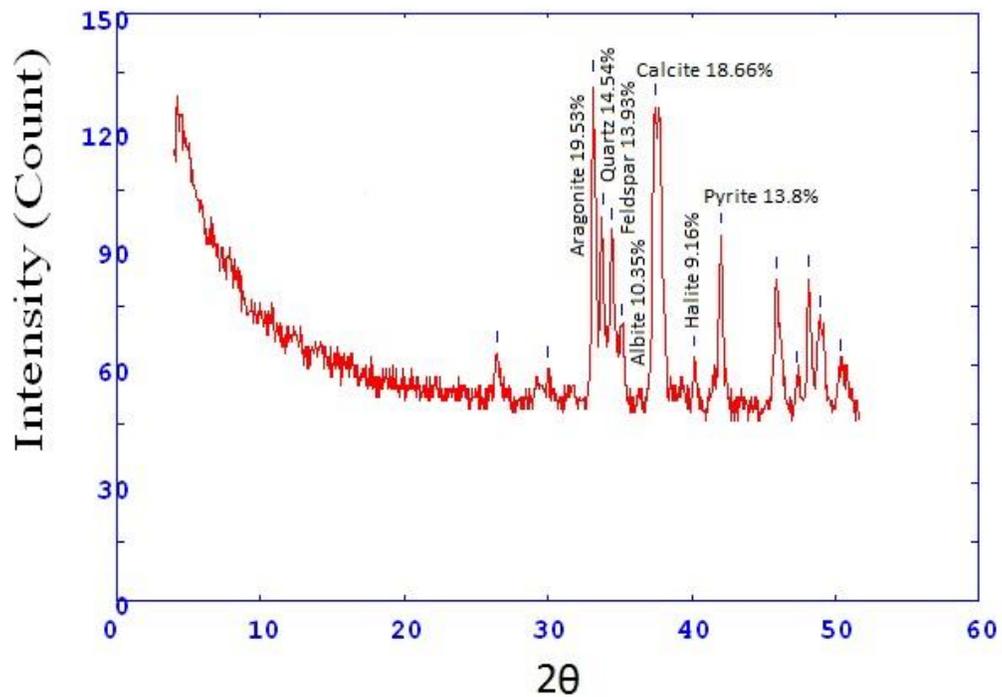
Fig.S6-8 X ray diffractogram of core 3 sample no.8

2Theta	d (A)	Height	Area	FWHM	Identified mineral	WT%
29.776	3.76761	63.4	13272	0	-	0
32.924	**3.41594**	140.3	1076	0.5172	Aragonite	17.68785
33.446	**3.36411**	81	621.4	1.5387	Quartz	10.2118
34.15	**3.29679**	93.4	716.4	2.0495	-	
34.747	**3.24188**	110.6	4132	2.5603	feldspar (orthoclase)	13.94352
37.525	**3.00962**	135.2	2118.7	0.9769	calcite	17.04488
38.812	**2.91343**	84.1	1318.3	0.9769	dolomite	10.60262
39.956	**2.83331**	56.8	889.9	0.9769	Halite	7.160867
41.773	**2.71519**	91.8	13505.3	0.9769	pyrite	11.57337
45.633	2.49629	87.9	12505.3	0.9769	-	
46.993	2.42799	60.9	8666.3	0.9769	-	
47.882	2.38549	82.3	12152	0.9769	-	
48.752	2.34545	68.6	10136.1	0.9769	-	
50.592	2.26548	62.1	9442.7	0.9769	-	
52.253	2.19826	62.2	7386.7	0.9769	-	
Total		793.2				

Table S3-9 X ray diffraction data of core 3 sample no.9
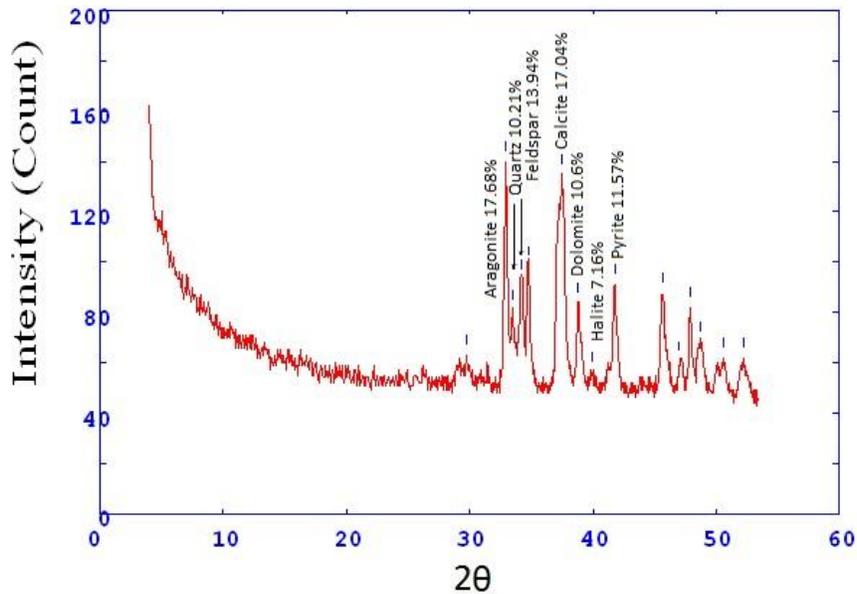
Fig.S6-9 X ray diffractogram of core 3 sample no.9

2Theta	d (A)	Height	Area	FWHM	Identified mineral	WT%
12.995	**8.55463**	108.2	2074.4	0.421	Illite	11.9969
14.5	**7.6705**	329.4	2074.4	0.421	Gypsum	36.5229
23.339	4.78594	11.8	86.1	0.5672	-	
25.977	4.30701	53.8	284.7	0.3977	-	
26.474	**4.22749**	24.6	130.1	0.3204	Goethite	
29.273	3.83091	219.3	603.1	0.2431	-	0
31.24	3.59516	12.6	35.8	0.2209	-	
32.723	**3.43638**	37.8	107.2	0.2347	Aragonite	4.191152
33.409	**3.36782**	113.4	315.8	0.2485	Quartz	12.57346
34.419	**3.27179**	75.6	210.4	0.518	feldspar (orthoclase)	8.382304
36.383	**3.10069**	54.2	150.8	0.6528	Albite	6.009535
36.983	**3.05207**	68.8	695.9	0.7875	calcite	7.62834
39.114	**2.89185**	34.3	134.3	0.3403	dolomite	3.803082
39.865	**2.83952**	27.6	108.1	0.4911	halite	3.060206
41.957	**2.70385**	28	221.2	0.6419	Pyrite	9.080829
44.596	2.5513	10.3	81.1	0.5279	-	
45.519	2.50222	21.6	114	0.4139	-	
47.078	2.42386	11.7	11.4	0.1928	Gypsum	
48.534	2.35536	14.9	95.4	0.4807	Gypsum	
49.875	2.29589	17.6	79.7	0.3828	Gypsum	
51.464	2.22963	13.6	42.5	0.2822	feldspar (orthoclase)	
Total		901.9				

Table S4-1 X ray diffraction data of core 4 sample no.1
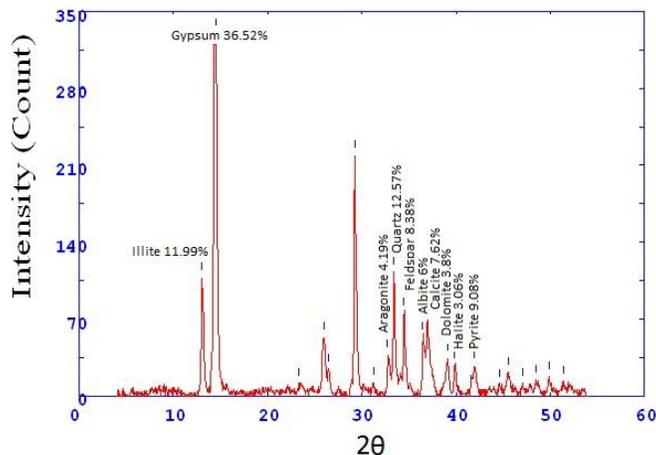
Fig.S7-1 X ray diffractogram of core 4 sample no.1

2Theta	d (A)	Height	Area	FWHM	Identified mineral	WT%
13.631	**8.1568**	8.6	47.9	0.2271	Illite	1.565344
14.954	**7.43883**	18.4	47.9	0.2271	Gypsum	3.349108
26.664	**4.198**	81.9	231.4	0.259	Goethite	14.90717
29.492	3.80305	19.5	90.8	0.3681	-	
30.795	3.64586	23.6	49.8	0.2012	-	0
33.522	**3.35674**	33.6	70.8	0.2302	Aragonite	6.115763
34.025	**3.30859**	184.3	523.8	0.2591	Quartz	33.54569
37.685	**2.99726**	158	621.4	0.3496	calcite	28.75865
39.502	**2.86453**	25.1	141.7	0.3957	dolomite	4.56862
40.572	**2.79205**	16.5	93.3	0.3907	halite	3.003276
42.401	**2.67683**	23	122.1	0.3857	Pyrite	4.186385
46.233	2.46564	35.8	193.6	0.4203	Aragonite	
46.699	2.44242	16.5	89.4	0.3725	Gypsum	
48.478	2.35791	16	64.1	0.3247	Gypsum	
49.3	2.32096	11.4	45.8	0.3437	Gypsum	
50.654	2.26287	36.1	153.2	0.3627	Gypsum	
Total		549.4				

Table S4-2 X ray diffraction data of core 4 sample no.2
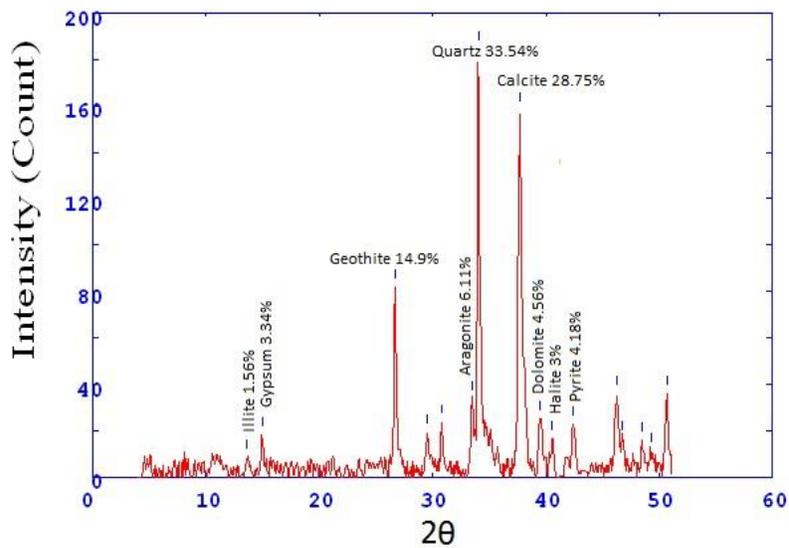
Fig.S7-2 X ray diffractogram of core 4 sample no.2

2Theta	d (A)	Height	Area	FWHM	Identified mineral	WT%
26.082	4.28994	13.5	65	0.3724	-	
29.071	3.85691	13.5	99.1	0.4811	-	0
32.807	**3.42778**	59.7	438	0.407	Aragonite	15.98394
33.471	**3.36169**	66.2	270.5	0.333	Quartz	17.72423
34.152	**3.2966**	33.8	137.9	0.4481	feldspar (orthoclase)	9.049531
37.144	**3.03938**	163.5	1182.2	0.5631	calcite	43.7751
38.943	**2.90403**	11.5	82.8	0.4291	dolomite	3.078983
41.726	**2.71812**	38.8	119.1	0.2951	Pyrite	10.38822
43.811	2.59471	8.6	34.8	0.2911	-	
45.541	2.50108	38.5	202.7	0.4232	-	
47.095	2.42301	14.6	76.6	0.3812	Aragonite	
47.811	2.38882	23.6	92.2	0.3392	Gypsum	
48.608	2.35197	18.2	71.2	0.4174	Gypsum	
49.938	2.29319	19.3	121.8	0.4956	gypsum	
Total		373.5				

Table S4-3 X ray diffraction data of core 4 sample no.3
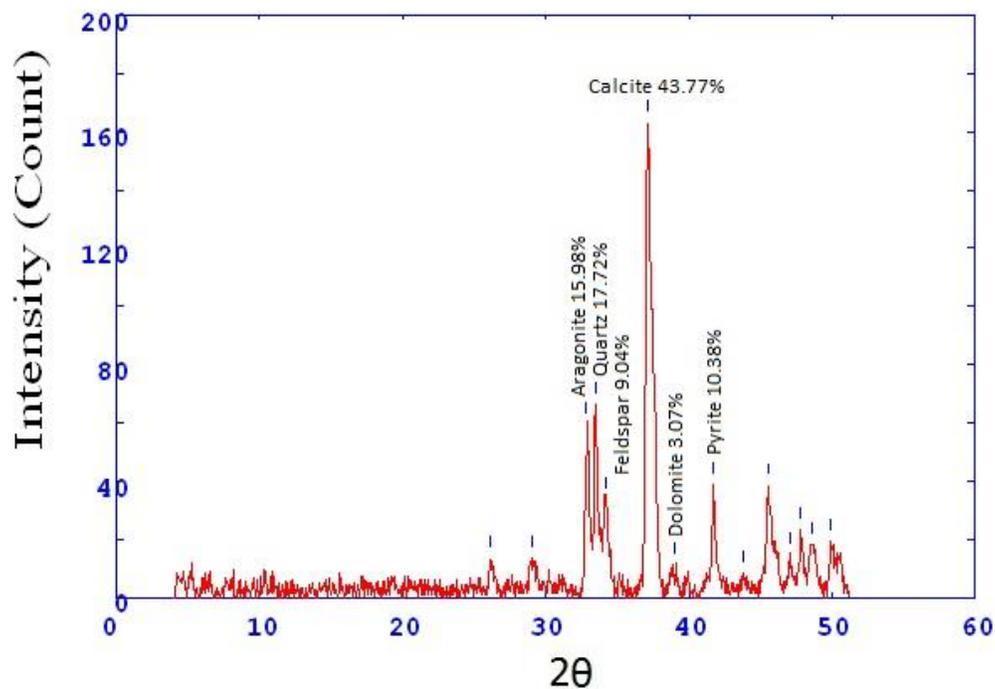
Fig.S7-3 X ray diffractogram of core 4 sample no.3

2Theta	d (A)	Height	Area	FWHM	Identified mineral	WT%
26.125	4.28301	60.1	12293.3	0	-	0
29	3.8662	63	13493.3	0	-	
32.864	**3.42203**	116.8	25010.1	0.3444	Aragonite	17.86752
33.469	**3.36194**	132	1182.7	0.6889	Quartz	20.19275
34.101	**3.30143**	87.2	781.3	0.8713	feldspar (orthoclase)	13.33945
37.427	**3.0172**	121.8	2036	1.0538	calcite	18.6324
38.71	**2.92083**	56.3	940.9	1.0538	dolomite	8.612513
39.933	**2.83483**	59	13505.3	1.0538	halite	9.025547
41.758	**2.71612**	80.6	13326.7	1.0538	Pyrite	12.32981
45.643	2.4958	74.4	12706.7	1.0538	Aragonite	
47.029	2.42625	55.9	9549.3	1.0538	Aragonite	
47.942	2.38269	76.1	12374.7	1.0538	-	
48.715	2.34712	68.9	11202.9	1.0538	-	
49.952	2.29261	64.1	10429	1.0538	-	
52.456	2.19038	59.1	12281.3	1.0538	Aragonite	
54.567	2.11178	59.3	12214.7	1.0538	-	
58.4	1.98422	88	2720	2.4667	-	
60.744	1.91456	61.4	1897.3	2.4667	-	
61.733	1.88682	77	11885.3	2.4667	-	
64.26	1.82013	68	9206.7	2.4667	-	
Total		653.7				

Table S4-4 X ray diffraction data of core 4 sample no.4
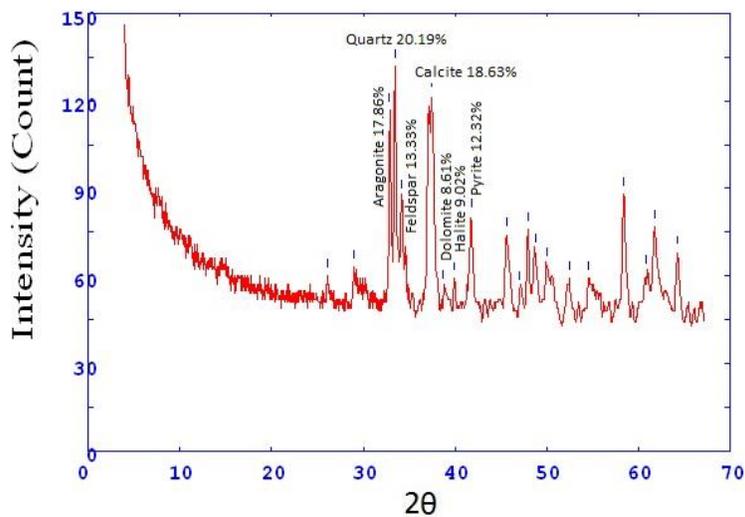
Fig.S7-4 X ray diffractogram of core 4 sample no.4

2Theta	d (A)	Height	Area	FWHM	Identified mineral	WT%
32.977	**3.41066**	62.8	694.7	0.7333	Aragonite	26.9066
34.255	**3.287**	47.5	525.3	0.7742	feldspar (orthoclase)	20.35133
37.589	**3.00465**	79.1	1041.3	0.815	calcite	33.89032
41.805	**2.71324**	44	942.7	1.4667	Pyrite	18.85176
45.667	2.49456	38	6237.3	1.4667	-	
48	2.37997	38	5693.3	1.4667	-	
48.826	2.34211	31.6	4729.1	1.4667	-	
50.667	2.26234	32	4450.7	1.4667	-	
Total		233.4				

Table S4-5 X ray diffraction data of core 4 sample no.5
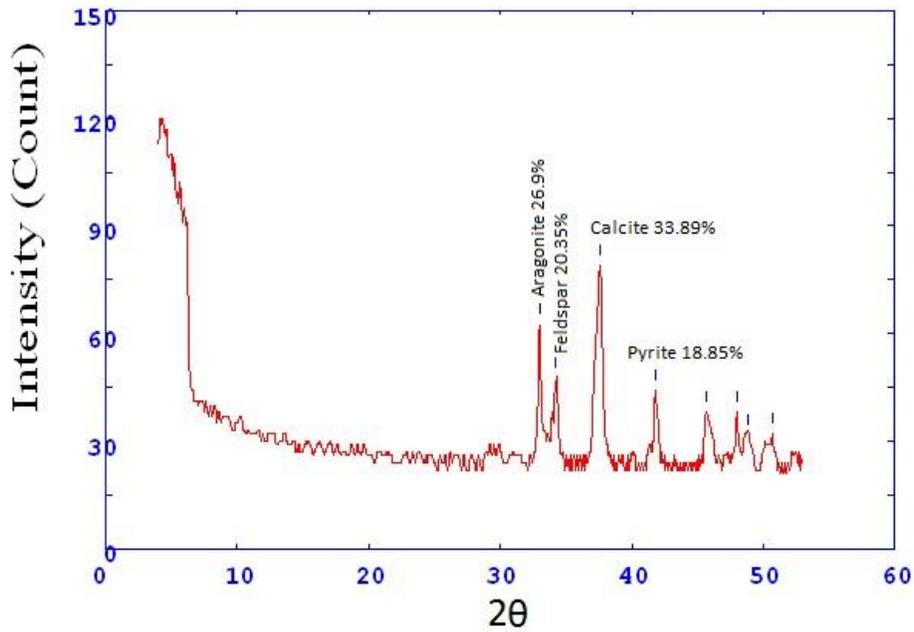
Fig.S7-5 X ray diffractogram of core 4 sample no.5

2Theta	d (A)	Height	Area	FWHM	Identified mineral	WT%
29.167	3.84459	60.4	12160	0	-	
29.826	3.76146	57.5	11584	0.9597	-	
30.889	3.63497	55.6	11191.6	1.4396	-	0
33	**3.40834**	113	2808	1.9194	Aragonite	20.71494
33.588	**3.35031**	66.8	1659.2	1.4523	Quartz	12.24565
34.325	**3.28055**	82.8	2058.6	1.2187	feldspar (orthoclase)	15.17874
37.567	**3.00636**	134.3	2150.7	0.9852	calcite	24.61962
40.033	**2.82804**	63	12472	0.9852	dolomite	11.54904
41.886	**2.70823**	85.6	12698.7	0.9852	Pyrite	15.69203
43.976	2.58545	50.7	7523.2	0.9852	-	
45.744	2.49055	77.1	10422.7	0.9852	-	
48.067	2.37686	71	7892	0.9852	-	
48.883	2.33954	68.7	0	0	Aragonite	
Total		545.5				

Table S4-6 X ray diffraction data of core 4 sample no.6
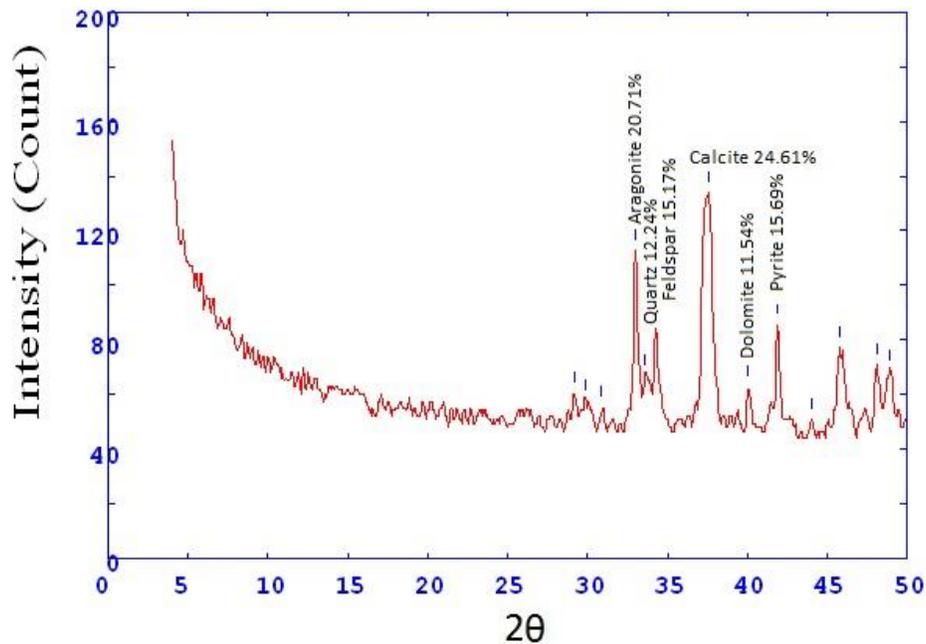
Fig.S7-6 X ray diffractogram of core 4 sample no.6

2Theta	d (A)	Height	Area	FWHM	Identified mineral	WT%
13.147	**8.4559**	79	1170.7	0.3364	Illite	8.072757
14.487	**7.67717**	254.9	1170.7	0.3364	Gypsum	26.04741
22.948	4.8662	62.3	12532	0.3364	-	
26.015	4.30078	74.3	12504	0.3364	-	
29.389	3.81615	79.1	13578.7	0.3364	-	
32.901	**3.41834**	103.4	17747.4	0.4219	Aragonite	10.56611
33.524	**3.3566**	146.4	1085.3	0.5074	Quartz	14.96015
34.11	**3.30055**	80.5	597.2	1.2093	feldspar (orthoclase)	8.226037
36.63	**3.08053**	66.8	495.4	1.5602	Albite	6.826078
37.338	**3.02411**	102	2962.7	1.9111	calcite	10.42305
39.149	**2.88932**	62.2	1807.4	1.9111	dolomite	6.356019
41.833	**2.71147**	83.4	13330.7	1.9111	Pyrite	8.522379
45.75	2.49026	77.1	12605.3	1.9111	Gypsum	
47.111	2.42224	59.2	9673.6	1.9111	Gypsum	
48	2.37997	71	12250.7	1.9111	Gypsum	
48.724	2.34673	63.8	11002	1.9111	Aragonite	
50.6	2.26513	60	12385.3	1.9111	Gypsum	
52.5	2.18866	55.1	12092	1.9111	dolomite	
54.569	2.11169	56.9	12481.3	1.9111	-	
55.433	2.08132	63.8	11328	1.9111	-	
58.5	1.98113	84.5	8129.3	1.9111	-	
Total		978.6				

Table S4-7 X ray diffraction data of core 4 sample no.7
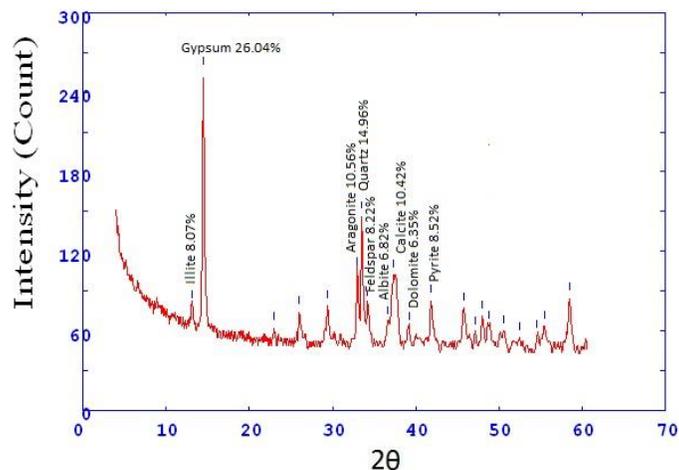
Fig.S7-7 X ray diffractogram of core 4 sample no.7

2Theta	d (A)	Height	Area	FWHM	Identified mineral	WT%
14.54	**7.6496**	73	13630.7	0	Gypsum	15.04844
26.221	4.26761	88.3	11534.7	0	Gypsum	
29.367	3.81897	60.6	12262.7	0	-	
29.803	3.76435	58.8	11903.2	0.9876	-	
30.864	3.6379	54	10929.2	1.4814	-	
33.027	**3.40563**	113.7	2874.7	1.9752	Aragonite	23.43847
34.136	**3.29812**	82.1	2075.9	1.4726	Quartz	16.92435
37.533	**3.00894**	131	1926.7	0.9699	calcite	27.00474
41.879	**2.70863**	85.3	12586.7	0.9699	Pyrite	17.584
45.817	2.48683	76.3	11912	0.9699	Gypsum	
47.136	2.42102	59.2	9256.1	0.9699	gypsum	
48.1	2.37531	70.3	11564	0.9699	gypsum	
48.817	2.34253	64.9	10677.9	0.9699	-	
50.585	2.26573	60.5	9951.3	0.9699	feldspar (orthoclase)	
52.519	2.18792	57.2	7060	0.9699	Aragonite	
Total		485.1				

Table S4-8 X ray diffraction data of core 4 sample no.8
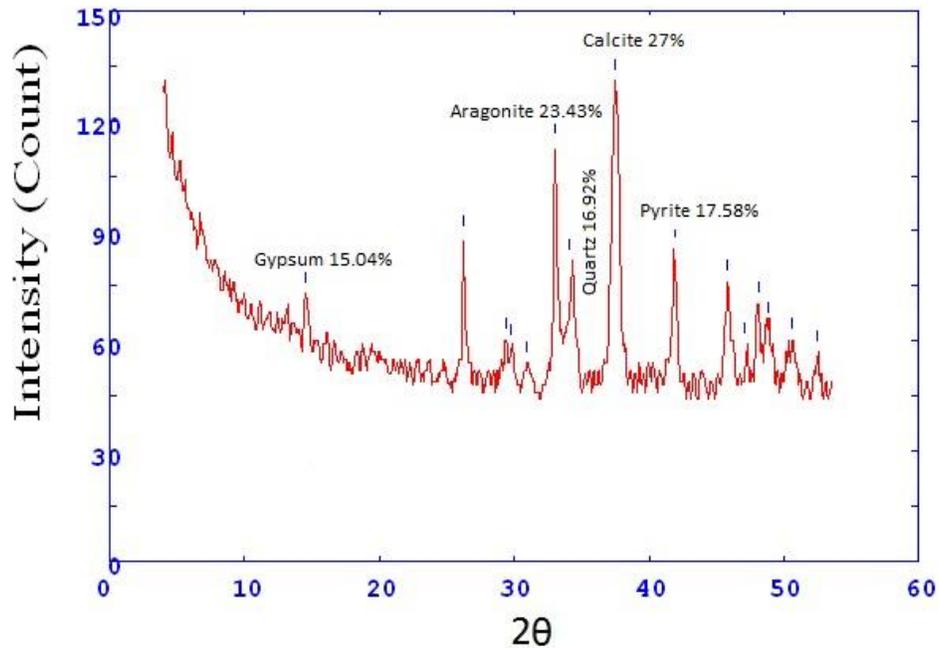
Fig.S7-8 X ray diffractogram of core 4 sample no.8

2Theta	d (A)	Height	Area	FWHM	Identified mineral	WT%
26.3	4.25501	59.3	11653.3	0	-	0
29.083	3.85536	68.3	12318.7	0	-	
32.97	**3.41133**	81.5	14711.3	1.1524	Aragonite	10.51613
33.619	**3.34739**	110.7	3404	2.3048	Quartz	14.28387
34.238	**3.28859**	71.9	2211.8	1.8904	feldspar (orthoclase)	9.277419
34.745	**3.24204**	105.5	3243.1	1.4761	Albite	13.6129
37.274	**3.02914**	215.2	1869.3	0.6474	calcite	27.76774
38.802	**2.91415**	63.7	553.5	0.6474	dolomite	8.219355
40.07	**2.82556**	59.6	517.8	0.6474	halite	7.690323
41.9	**2.70735**	66.9	13498.7	0.6474	Pyrite	8.632258
45.744	2.49055	82.1	11736	0.6474	-	
48.067	2.37686	59	9445.3	0.6474	-	
50.256	2.27963	70.1	7308	0.6474	Aragonite	
Total		775				

Table S4-9 X ray diffraction data of core 4 sample no.9
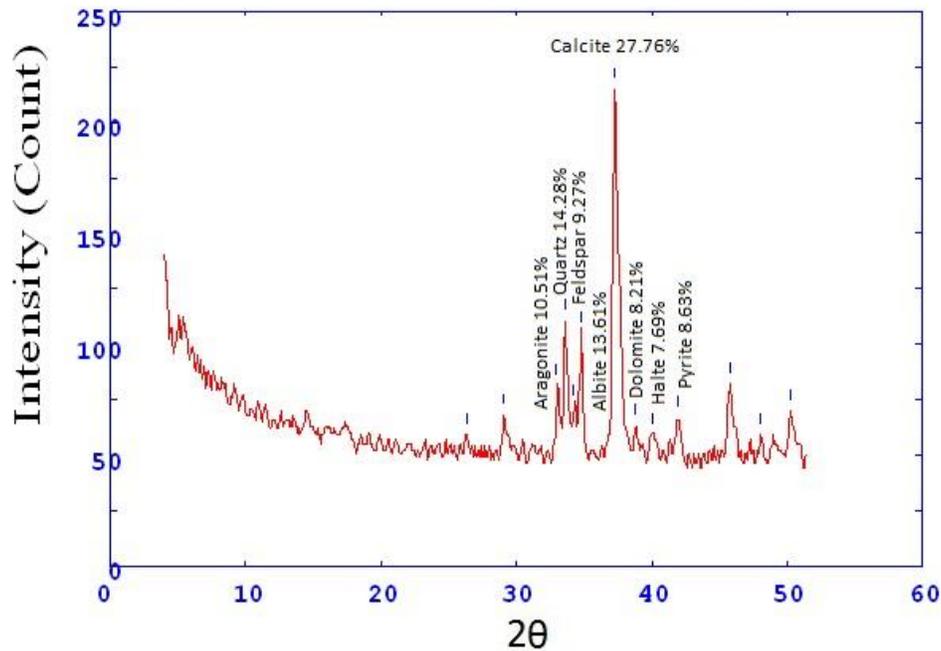
Fig.S7-9 X ray diffractogram of core 4 sample no.9

2Theta	d (A)	Height	Area	FWHM	Identified mineral	WT%
13.212	**8.41467**	116.7	2539.2	0.5017	Illite	24.15649
14.634	**7.60095**	328.4	2539.2	0.5017	Gypsum	67.97764
23.548	4.74408	13.7	41.4	0.2592	-	
26.08	4.29032	91.9	352.2	0.3322	-	
26.724	**4.18869**	25.7	98.3	0.2948	Goethite	5.31981
29.467	3.80626	223	629	0.2574	-	
30.417	3.69007	15.4	43.5	0.2616	-	
33.102	**3.39808**	27.7	78.1	0.2638	Aragonite	5.733803
33.6	**3.34918**	91.2	269.5	0.2659	Quartz	18.87808
34.445	**3.26939**	16.4	48.6	0.2844	feldspar (orthoclase)	3.394742
35.369	**3.18667**	16.4	48.6	0.303	Albite	3.394742
36.772	**3.06899**	99.6	394.8	0.3401	Calcite	20.61685
39.325	**2.87692**	35.9	235.8	0.5165	dolomite	7.431174
42.234	**2.68692**	39.8	188.3	0.385	Pyrite	8.23846
43.761	2.5975	9.3	44	0.383	-	
45.713	2.49215	18.2	77.3	0.381	gypsum	
48.1	2.37531	12.6	34.7	0.25	Gypsum	
Total		483.1				

Table S5-1 X ray diffraction data of core 5 sample no.1
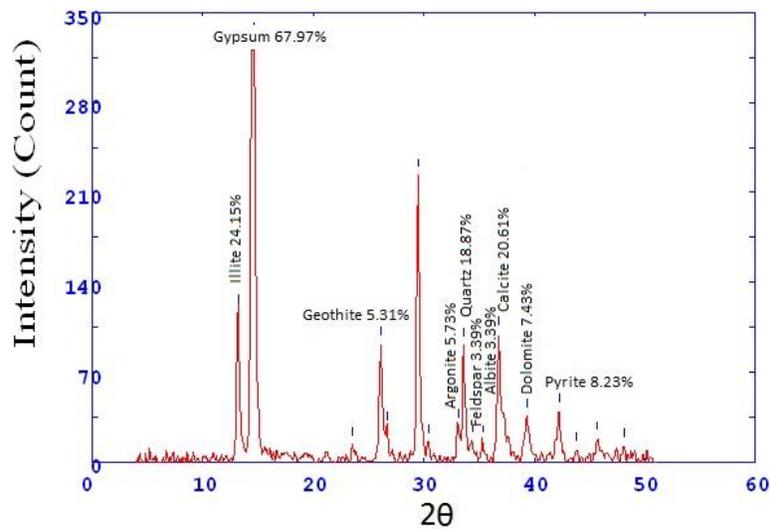
Fig.S8-1 X ray diffractogram of core 5 sample no.1

2Theta	d (A)	Height	Area	FWHM	Identified mineral	WT%
14.591	**7.62305**	53.5	113.8	0.2546	Gypsum	10.33217
25.082	4.45809	10.2	21.6	0.2793	-	0
26.258	4.26177	28	97.5	0.304	-	
29.228	3.83676	12.6	43.7	0.2963	-	
33.112	**3.39712**	45.4	157.7	0.2885	Aragonite	8.767864
33.644	**3.34493**	154.4	558.7	0.273	Quartz	29.81846
34.692	**3.24682**	41	148.5	0.3154	feldspar (orthoclase)	7.918115
35.352	**3.18815**	15.5	56	0.3365	Albite	2.993434
35.728	3.1556	9.2	33.3	0.3471	-	
37.261	**3.03017**	132.2	645.8	0.3577	Calcite	25.53109
39.101	**2.89276**	38.1	217.7	0.4269	dolomite	7.358053
41.982	**2.70227**	37.7	152.7	0.3288	Pyrite	7.280803
43.976	2.58542	7.3	29.5	0.3732	-	
45.848	2.48523	38.7	209.3	0.4176	Gypsum	
48.078	2.37636	20.6	228.5	0.7149	Gypsum	
48.915	2.33813	14.5	160.9	0.5387	Aragonite	
50.217	2.28127	29.9	134.3	0.3626	feldspar (orthoclase)	
52.435	2.19118	14.9	66.5	0.3097	dolomite	
55.167	2.09059	24.2	271.9	0.8289	-	
58.592	1.9783	32.7	156	0.3581	-	
Total		517.8				

Table S5-2 X ray diffraction data of core 5 sample no.2
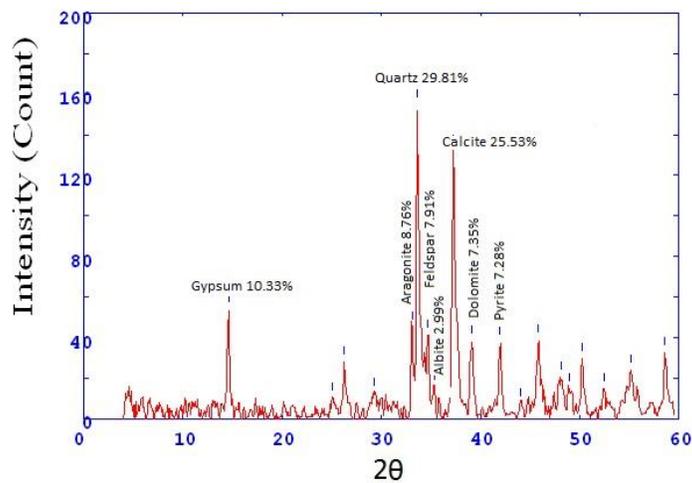
Fig.S8-2 X ray diffractogram of core 5 sample no.2

2Theta	d (A)	Height	Area	FWHM	Identified mineral	WT%
26.344	4.24796	65.2	11717.3	0	-	
29.414	3.81293	62.2	13189.3	0	-	0
29.96	3.74497	61.3	13007.8	0.4405	-	
30.631	3.6649	58.5	12421.6	1.1012	-	
33.156	**3.39279**	141.7	3205.3	1.7619	Aragonite	19.05082
33.732	**3.33647**	126.9	2871.5	1.5878	Quartz	17.06104
34.402	**3.27336**	98.9	2238.7	1.4137	feldspar (orthoclase)	13.29659
35.324	**3.19055**	58.9	1332.4	1.2396	Albite	7.918795
36.078	3.126	55.4	1254.3	1.1526	-	
37.336	**3.02431**	100	2262.1	1.1091	Calcite	13.44447
37.808	2.98789	131.1	2088	1.0656	-	
39.096	**2.89313**	59.6	949	1.6411	dolomite	8.012907
40.101	**2.82345**	56.5	899.5	1.785	Halite	7.596128
41.526	2.73064	61	971	1.9289	-	
42.013	**2.70042**	101.3	2741.3	2.2167	Pyrite	13.61925
45.919	2.48159	87.2	12380	2.2167	-	
47.393	2.40868	64.8	9198	2.2167	-	
48.156	2.37271	91.1	9693.3	2.2167	-	
48.901	2.33874	78.6	0	0	Aragonite	
50.242	2.28021	62.3	0	0	feldspar (orthoclase)	
Total		743.8				

Table S5-3 X ray diffraction data of core 5 sample no.3
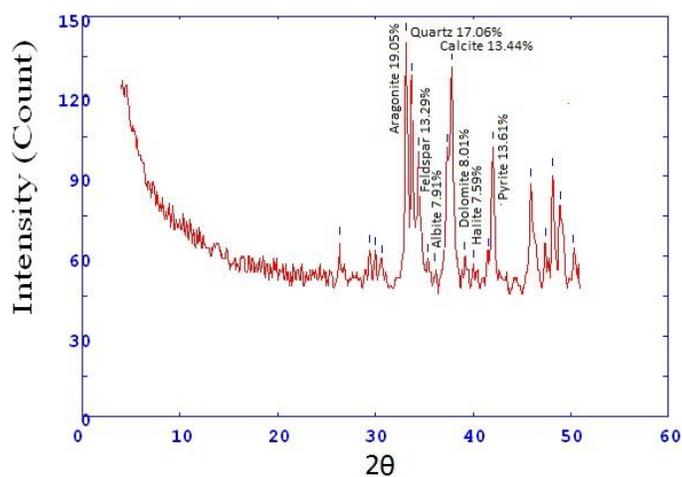
Fig.S8-3 X ray diffractogram of core 5 sample no.3

2Theta	d (A)	Height	Area	FWHM	Identified mineral	WT%
33.085	**3.39984**	126.8	1722.7	1.0667	Aragonite	21.80567
33.553	**3.35377**	76.4	1037.3	1.0883	Quartz	13.13844
34.238	**3.28857**	95.7	1299.7	1.11	feldspar (orthoclase)	16.45744
37.7	**2.99612**	129	2336	1.1533	dolomite	22.18401
40.1	**2.82353**	57.3	12921.3	1.1533	halite	9.853826
41.985	**2.70212**	96.3	1978.7	1.5333	Pyrite	16.56062
45.875	2.48384	90.1	9462.7	5.7	-	0
47.361	2.41017	57.4	6031.1	5.7	-	
48.133	2.37377	85	12134.7	5.7	-	
48.928	2.33751	72.4	10339.1	5.7	Aragonite	
50.299	2.27777	59.4	8481.9	5.7	feldspar (orthoclase)	
50.933	2.25128	62	12364	5.7	-	
52.258	2.19807	57.4	11455.1	5.7	dolomite	
54.742	2.10552	70.1	10548	5.7	-	
55.882	2.06595	59.8	8999	3.3056	-	
56.959	2.03005	57	8583.8	2.1083	-	
58.642	1.97675	99	1229.3	0.9111	-	
Total		581.6				

Table S5-4 X ray diffraction data of core 5 sample no.4
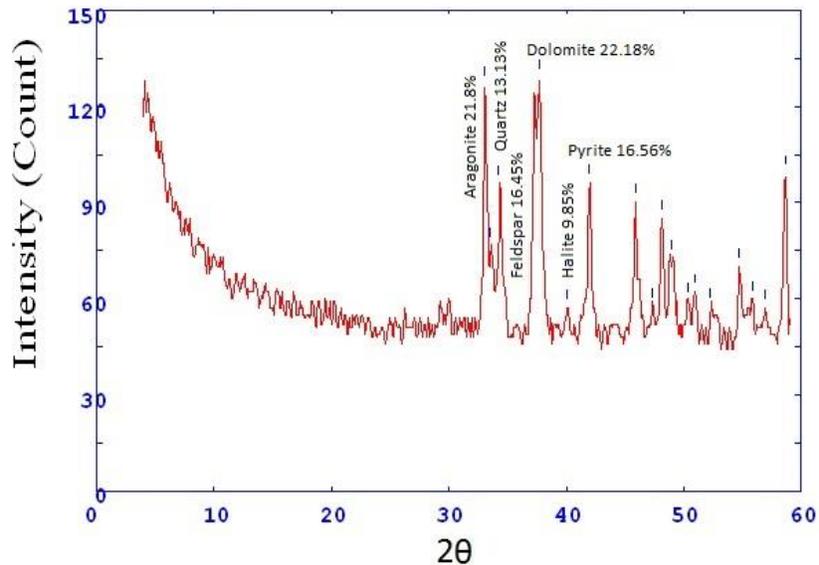
Fig.S8-4 X ray diffractogram of core 5 sample no.4

2Theta	d (A)	Height	Area	FWHM	Identified mineral	WT%
29.301	3.82728	10.3	32.1	0.1989	-	
30.415	3.69027	17.2	32.1	0.1989	-	0
33.11	**3.39737**	74.4	139	0.2336	Aragonite	18.81639
33.641	**3.34522**	122.5	359.2	0.2682	Quartz	30.98128
34.347	**3.27844**	40.5	118.7	0.5226	feldspar (orthoclase)	10.24279
37.707	**2.99559**	93.1	1131.2	0.7769	calcite	23.54578
38.917	**2.90588**	14.5	176.5	0.6549	dolomite	3.667172
40.194	**2.81719**	16.2	107.5	0.5329	halite	4.097117
41.488	2.73305	9.6	63.5	0.4416	-	
41.983	**2.70222**	34.2	139.8	0.3504	Pyrite	8.649469
44.233	2.57114	7.1	39.8	0.3775	-	
45.833	2.48599	36.8	266.8	0.6452	Quartz	
48.14	2.37344	27.6	90.3	0.3078	Pyrite	
49.009	2.33391	21.4	70.1	0.3765	Aragonite	
50.437	2.27198	15.7	51.3	0.4109	Pyrite	
52.466	2.18996	13.9	87.3	0.4453	dolomite	
55.833	2.06759	16.1	408.3	1.6143	-	
Total		395.4				

Table S6-1 X ray diffraction data of core 6 sample no.1
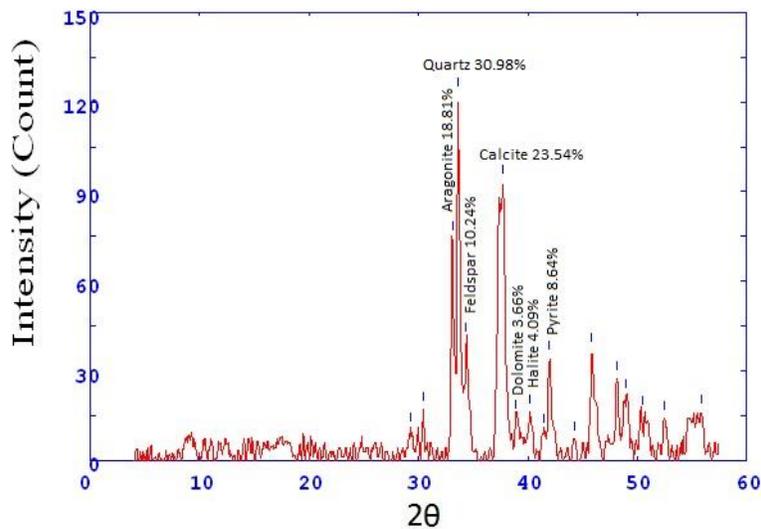
Fig.S9-1 X ray diffractogram of core 6 sample no.1

2Theta	d (A)	Height	Area	FWHM	Identified mineral	WT%
26.215	4.26852	16.7	46.9	0.2115	-	0
29.433	3.81058	13.6	78.4	0.4351	-	
33.044	**3.40397**	75.8	227.4	0.2787	Aragonite	22.27446
33.597	**3.34945**	42.4	127.2	0.4976	Quartz	12.45959
34.296	**3.28317**	43.1	129.2	0.607	feldspar (orthoclase)	12.6653
35.345	**3.18876**	5	15.1	0.6617	feldspar (Albite)	1.469292
36.131	3.1216	5	15.1	0.6891	-	
37.662	**2.99903**	104.9	1051.4	0.7164	Calcite	30.82574
38.839	**2.91146**	14	140.8	0.5365	dolomite	4.114017
39.975	**2.83198**	11.4	114	0.4465	halite	3.349985
41.9	**2.70735**	43.7	180.2	0.3565	Pyrite	12.84161
45.82	2.48666	36.4	318.5	0.6795	-	
47.14	2.42086	15.4	134.4	0.5137	Aragonite	
48.085	2.376	27.3	115.1	0.348	Aragonite	
48.8	2.3433	25.1	105.5	0.7028	feldspar	
50.5	2.26932	14.1	234.4	1.0575	Pyrite	
52.4	2.19254	16	138.7	0.644	dolomite	
Total		340.3				

Table S6-2 X ray diffraction data of core 6 sample no.2
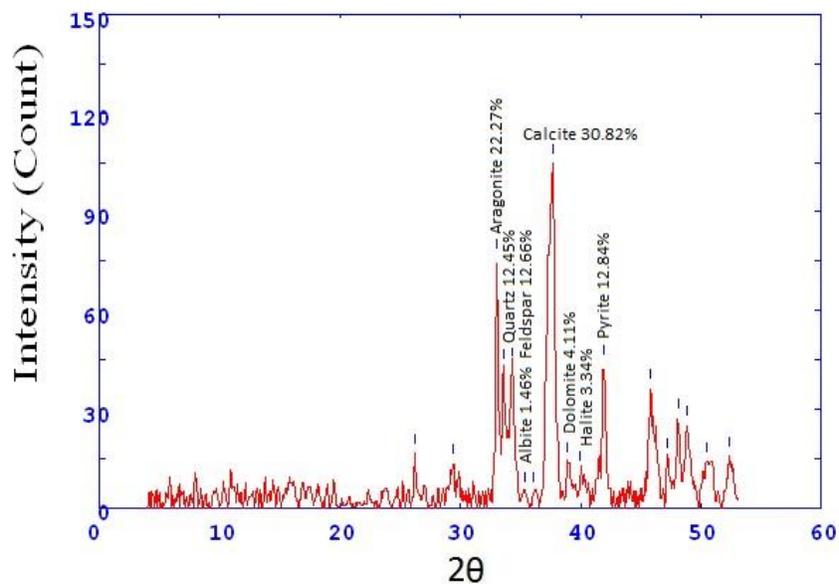
Fig.S9-2 X ray diffractogram of core 6 sample no.2

2Theta	d (A)	Height	Area	FWHM	Identified mineral	WT%
23.867	4.68155	51	9598.7	0	-	
26.267	4.26032	57	9589.3	0	-	0
29.367	3.81897	54.3	9978.7	0	-	
33.047	**3.40366**	82.7	4228	4.1333	Aragonite	17.69741
33.723	**3.33733**	54.7	2798.5	3.3569	Quartz	11.70554
34.352	**3.27801**	65.6	3352.7	2.5806	feldspar (orthoclase)	14.03809
35.071	**3.21287**	56.2	2873.4	1.8042	feldspar (Albite)	12.02654
36.239	3.11261	50	2558.9	1.416	-	
37.227	**3.03277**	89.3	4565.9	1.2219	Calcite	19.10978
37.627	3.00174	91.8	1522.7	1.0278	-	
38.486	2.93721	50.9	844.5	1.0278	-	
39.115	**2.89178**	52.7	873.7	1.0278	dolomite	11.27755
41.922	**2.70598**	66.1	10238.7	1.0278	Pyrite	14.14509
44	2.5841	51	9857.3	1.0278	-	
45.767	2.48941	65.6	9922.7	1.0278	-	
48.033	2.37841	59.3	9829.3	1.0278	Aragonite	
48.999	2.33433	56.8	9418.3	1.0278	-	
50.168	2.28337	55.6	9224	1.0278	Pyrite	
52.533	2.18737	52	6673.3	1.0278	dolomite	
54.1	2.1286	54.4	5157.3	1.0278	-	
Total		467.3				

Table S6-3 X ray diffraction data of core 6 sample no.3
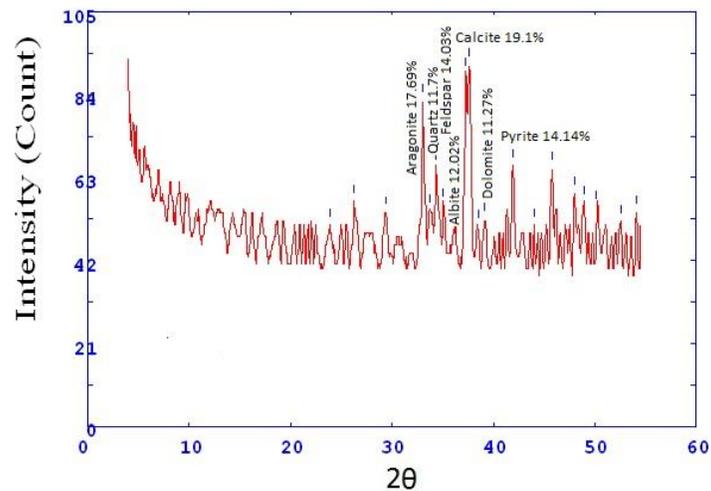
Fig.S9-3 X ray diffractogram of core 6 sample no.3

2Theta	d (A)	Height	Area	FWHM	Identified mineral	WT%
29.874	3.7555	13.3	11.9	0.1432	-	
33.009	**3.4074**	80.9	259.4	0.3146	Aragonite	24.47066
33.509	**3.35803**	28.8	92.4	0.5123	Quartz	8.711434
34.184	**3.29359**	50.3	161.3	0.6111	feldspar (orthoclase)	15.21476
37.54	**3.00843**	99.4	1046.7	0.71	Calcite	30.06655
39.396	**2.87193**	4.8	50.2	0.4886	dolomite	1.451906
40.074	**2.82528**	14.3	46	0.2672	halite	4.325469
41.423	2.73715	13.6	43.6	0.2843	-	
41.904	**2.70708**	52.1	164.8	0.3014	Pyrite	15.75923
45.75	2.49028	35.9	207.5	0.4446	Aragonite	
47.213	2.4173	15.5	89.8	0.4404	Aragonite	
48.034	2.37839	30.6	188.8	0.4362	Aragonite	
48.661	2.34957	25.6	158.1	0.8919	Aragonite	
50.109	2.28589	15.8	97.7	1.1198	feldspar	
50.784	2.25745	15.2	93.8	1.2337	Pyrite	
52.633	2.18353	11	210.9	1.3476	dolomite	
54.683	2.10762	19	137.1	0.4854	Aragonite	
55.61	2.07524	16.2	116.8	0.3883	-	
Total		330.6				

Table S6-4 X ray diffraction data of core 6 sample no.4
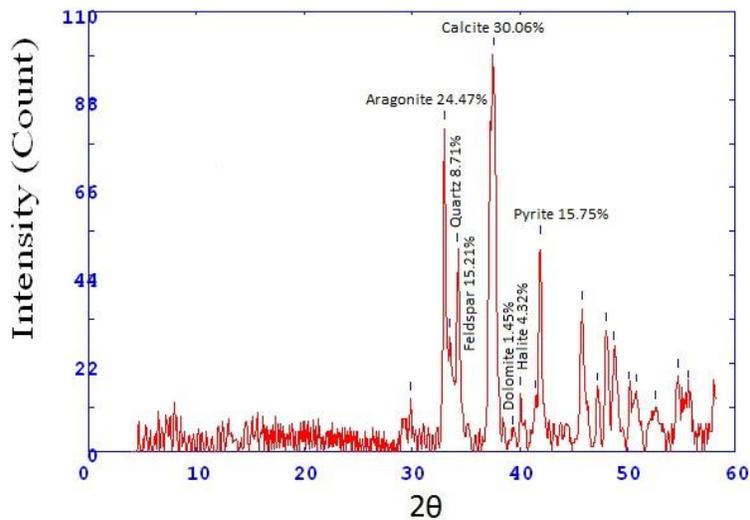
Fig.S9-4 X ray diffractogram of core 6 sample no.4

2Theta	d (A)	Height	Area	FWHM	Identified mineral	WT%
29.108	3.85221	15.7	81	0.2201	-	0
30.352	3.69781	41.5	81	0.2201	-	
32.954	**3.41298**	68.8	134.2	0.226	Aragonite	12.92019
33.59	**3.35016**	194.7	411.6	0.2319	Quartz	36.56338
34.321	**3.28084**	39.7	84	0.4562	feldspar (orthoclase)	7.455399
36.202	**3.1157**	7.3	15.4	0.5684	Albite	1.370892
37.284	**3.02836**	143.6	1363.8	0.6805	Calcite	26.96714
40.085	**2.82456**	41	160.2	0.3105	dolomite	7.699531
41.9	**2.70732**	37.4	116.1	0.3034	Pyrite	7.023474
44.065	2.58048	6.2	19.2	0.3802	-	
45.767	2.48941	48.1	293	0.4569	-	
47.142	2.42075	12.3	75.2	0.3729	Aragonite	
48.022	2.37893	27.5	87.7	0.2888	Aragonite	
48.851	2.34097	20.2	64.3	0.4764	Aragonite	
50.4	2.27353	21.8	183.3	0.664	Pyrite	
Total		352.5				

Table S6-5 X ray diffraction data of core 6 sample no.5
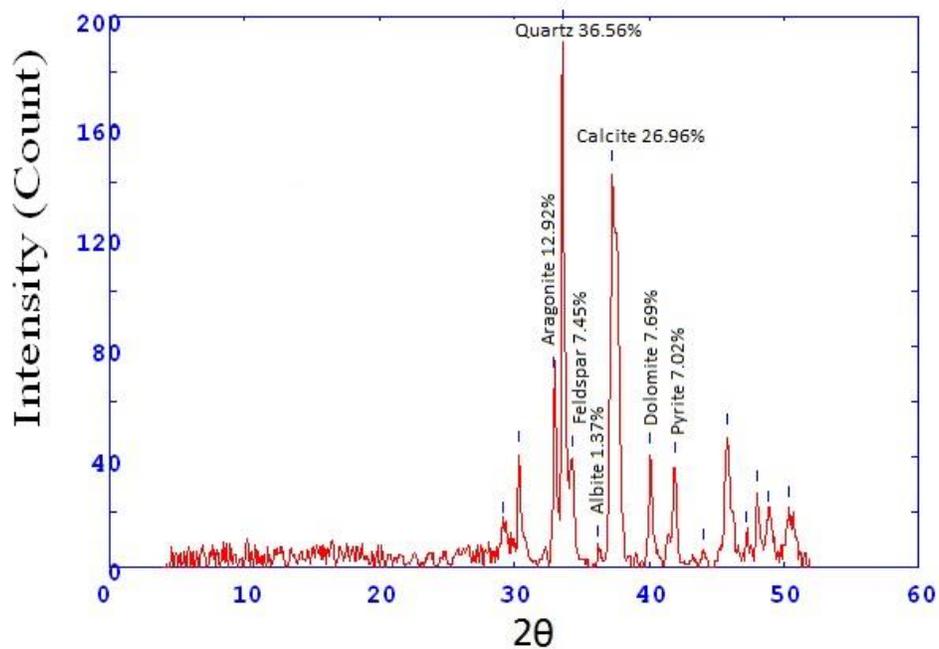
Fig.S9-5 X ray diffractogram of core 6 sample no.5

2Theta	d (A)	Height	Area	FWHM	Identified mineral	WT%
13.083	**8.4971**	28.8	77.7	0.2813	Illite	3.169014
14.609	**7.61383**	21.3	76.1	0.296	Gypsum	2.34375
17.369	6.41117	17.4	89.6	0.4373	-	
23.864	4.68212	13.5	67	0.3772	-	
26.291	4.25642	165.2	458	0.2596	-	
27.655	4.05034	31.1	86.1	0.2552	-	
30.448	**3.68636**	89.9	191.3	0.2508	Aragonite	9.892165
33.633	**3.34597**	329.3	1882.8	0.4046	Quartz	36.2346
34.749	**3.24171**	139.5	797.5	0.3824	feldspar (orthoclase)	15.34991
35.347	**3.18855**	121.9	697.1	0.3712	Albite	13.41329
37.278	**3.02882**	63.4	308.6	0.3601	calcite	6.976232
39.106	**2.89242**	88.8	474.7	0.4111	dolomite	9.771127
40.133	**2.82128**	25.9	138.5	0.8705	halite	2.849912
46.4	2.45727	32	114.2	0.3333	Aragonite, gypsum	
50.219	2.28118	36.6	142	0.3108	Pyrite	
51.244	2.23853	24.9	0	0	Gypsum	
Total		908.8				

Table S6-6 X ray diffraction data of core 6 sample no.6
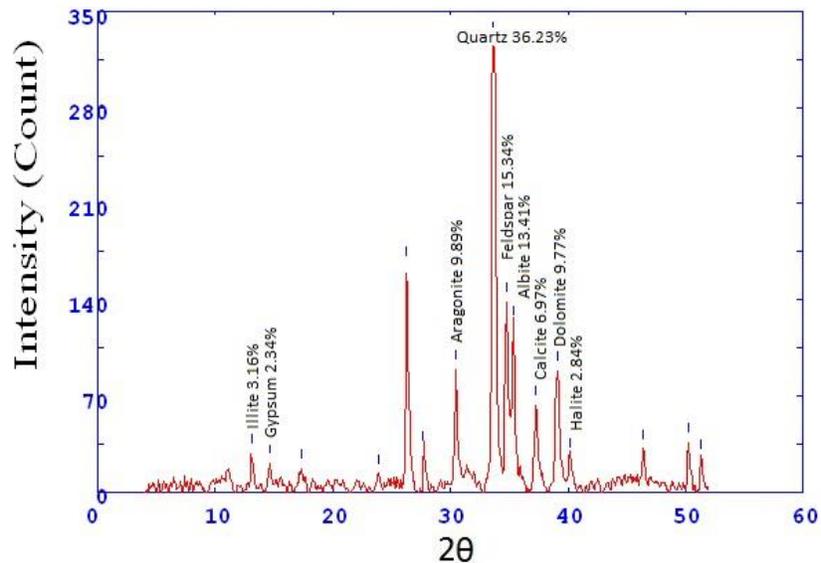
Fig.S9-6 X ray diffractogram of core 6 sample no.6

2Theta	d (A)	Height	Area	FWHM	Identified mineral	WT%
26.275	4.25892	32	96.9	0.2941	-	
29.003	3.8658	14.4	43.6	0.2947	-	0
29.683	3.77913	28.2	84.6	0.2954	-	
30.426	3.68901	13.9	41.9	0.3045	Aragonite	3.020426
33.63	3.34628	147	541.2	0.3136	Quartz	31.94263
34.694	3.24667	34.1	125.7	0.4636	feldspar (orthoclase)	7.409822
35.112	3.20918	26.5	97.6	0.5386	feldspar (Albite)	5.758366
37.265	3.02986	140	1074.2	0.6136	calcite	30.42156
39.072	2.89481	73.8	382.7	0.4123	dolomite	16.03651
39.966	2.83258	13.5	70	0.3169	halite	2.933507
41.913	2.70657	11.4	23.2	0.2215	Pyrite	2.477184
45.833	2.48598	27.8	320.7	0.8956	-	
47.247	2.41566	12.2	140.1	0.7729	Aragonite	
48.837	2.34159	11.3	129.8	0.7116	Aragonite	
50.214	2.28139	29.6	255.5	0.6503	feldspar	
Total		460.2				

Table S6-7 X ray diffraction data of core 6 sample no.7
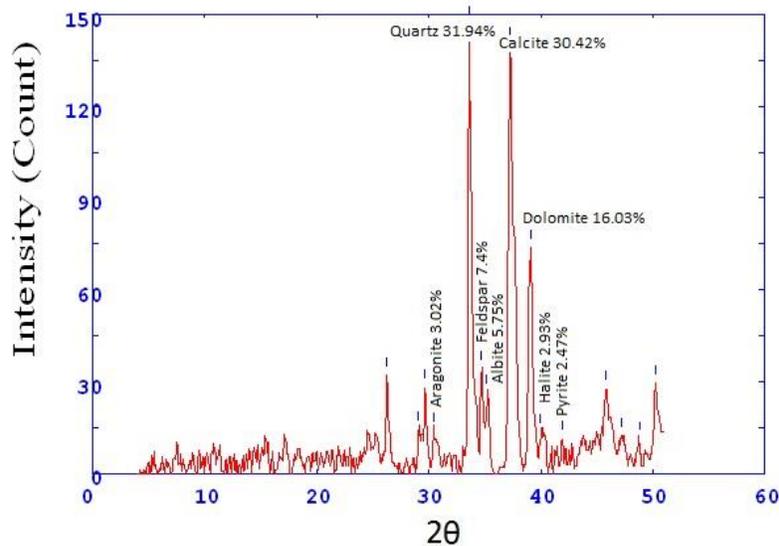
Fig.S9-7 X ray diffractogram of core 6 sample no.7

2Theta	d (A)	Height	Area	FWHM	Identified mineral	WT%
24.891	4.49172	13.9	142.1	0.242	-	0
26.279	4.25843	51.7	142.1	0.242	-	
27.029	**4.1423**	9.5	26.1	0.2925	Goethite	2.071974
27.68	4.04677	8.4	23	0.3051	-	
29.074	3.85659	10.6	29.1	0.3177	-	
30.411	3.69075	24.1	94.3	0.343	-	
33.071	**3.40126**	29.5	115.3	0.2901	Aragonite	6.434024
33.65	**3.34437**	194.9	421.2	0.2373	Quartz	42.50818
34.837	**3.23378**	39.5	85.3	0.3018	feldspar (orthoclase)	8.615049
37.267	**3.02969**	113.4	541.7	0.3663	calcite	24.73282
39.1	**2.89279**	53	266.3	0.3992	dolomite	11.55943
41.996	**2.70143**	18.7	92.2	0.3892	Pyrite	4.078517
45.833	2.48597	25.9	183.8	0.5413	-	
47.385	2.40905	14.5	102.7	0.388	-	
48.137	2.37361	17.5	39.6	0.2346	Pyrite	
48.872	2.34004	13.4	30.3	0.2936	Aragonite	
50.25	2.27988	30	142.2	0.3527	Feldspar	
52.286	2.19697	13.2	73.1	0.4874	Dolomite	
55.017	2.09584	15.1	95.9	0.4776	-	
Total		458.5				

Table S6-8 X ray diffraction data of core 6 sample no.8
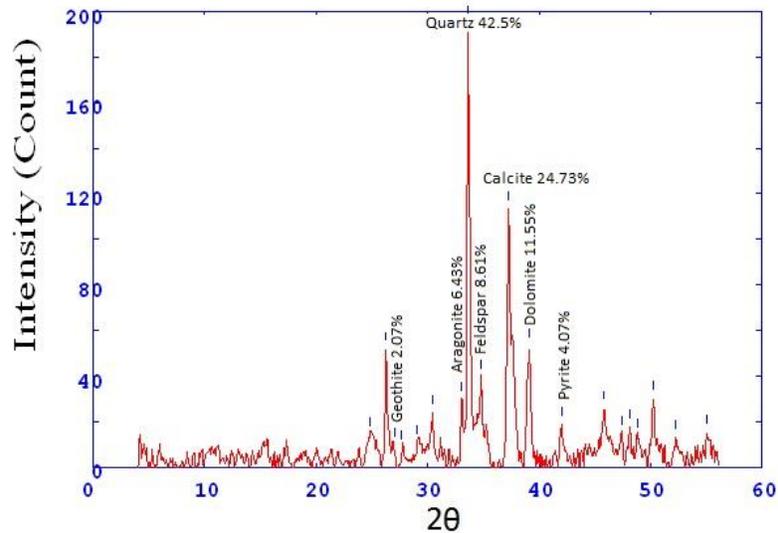
Fig.S9-8 X ray diffractogram of core 6 sample no.8

2Theta	d (A)	Height	Area	FWHM	Identified mineral	WT%
24.559	4.55157	6	112.1	0.3974	-	0
26.334	4.24955	21.7	112.1	0.3974	-	
29.4	3.81471	16.2	102.6	0.4458	-	
31.134	3.60715	10.8	31.9	0.1871	-	
33.062	**3.40212**	75	221.6	0.2165	Aragonite	20.20474
33.685	**3.34095**	106	305.3	0.2459	Quartz	28.55603
34.511	**3.26331**	44.3	127.5	0.4975	feldspar (orthoclase)	11.93427
37.748	**2.99241**	94.1	993	0.7491	Calcite	25.35022
38.956	**2.90306**	9.9	104.8	0.5577	dolomite	2.667026
41.992	**2.70168**	41.9	226.9	0.3664	Pyrite	11.28772
45.886	2.48326	37.7	250.3	0.4643	-	
48.195	2.3709	32.3	196.8	0.4277	Aragonite	
48.909	2.33837	28.4	173	0.6485	feldspar	
50.341	2.27603	26.1	310.1	0.8694	feldspar	
50.842	2.25507	18.8	224.1	1.0566	Pyrite	
52.7	2.18095	9.1	185.8	1.2438	dolomite	
54.817	2.10289	20.1	100.5	0.3489	-	
55.963	2.06319	15.9	79.6	0.4656	-	
Total		371.2				

Table S6-9 X ray diffraction data of core 6 sample no.9
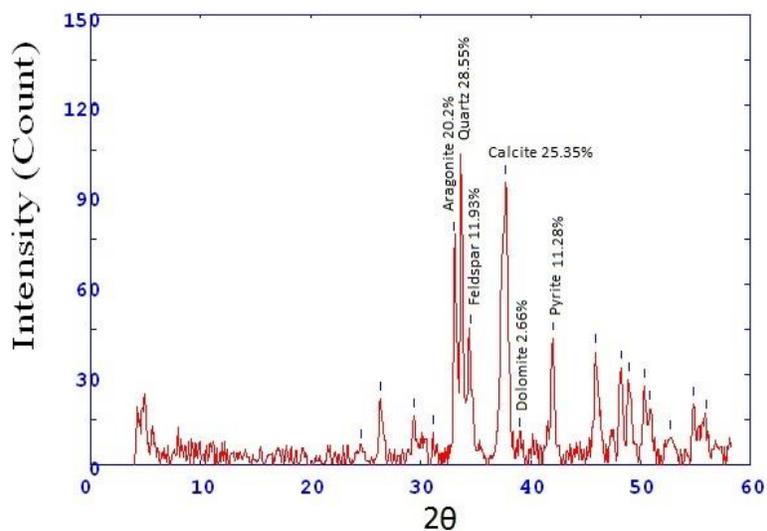
Fig.S9-9 X ray diffractogram of core 6 sample no.9

2Theta	d (A)	Height	Area	FWHM	Identified mineral	WT%
26.275	**4.25894**	16.1	74.2	0.3697	Goethite	4.054394
29.941	3.74735	16.4	61.8	0.3381	-	
33.133	**3.39502**	95	282.5	0.2805	Aragonite	23.92344
33.67	**3.34239**	51.9	154.3	0.4981	Quartz	13.06976
34.373	**3.27606**	47	139.6	0.607	feldspar (orthoclase)	11.83581
37.71	**2.99538**	103.6	1005.2	0.7158	Calcite	26.08915
39.029	**2.89789**	8.9	86.3	0.5725	dolomite	2.241249
40.215	**2.8158**	29.7	167.3	0.4291	halite	7.479224
42.05	**2.69811**	44.9	221.2	0.3484	Pyrite	11.30698
45.913	2.48188	40.2	291.7	0.55	-	
47.374	2.40957	13.5	97.8	0.4694	Aragonite	
48.167	2.37222	35.5	178.8	0.3889	Aragonite	
49.043	2.33238	25.6	129.1	0.5595	feldspar	
50.875	2.25369	17.1	173.9	0.7302	feldspar	
52.614	2.18424	14.2	69.1	0.4222	dolomite	
Total		397.1				

Table S6-10 X ray diffraction data of core 6 sample no.10
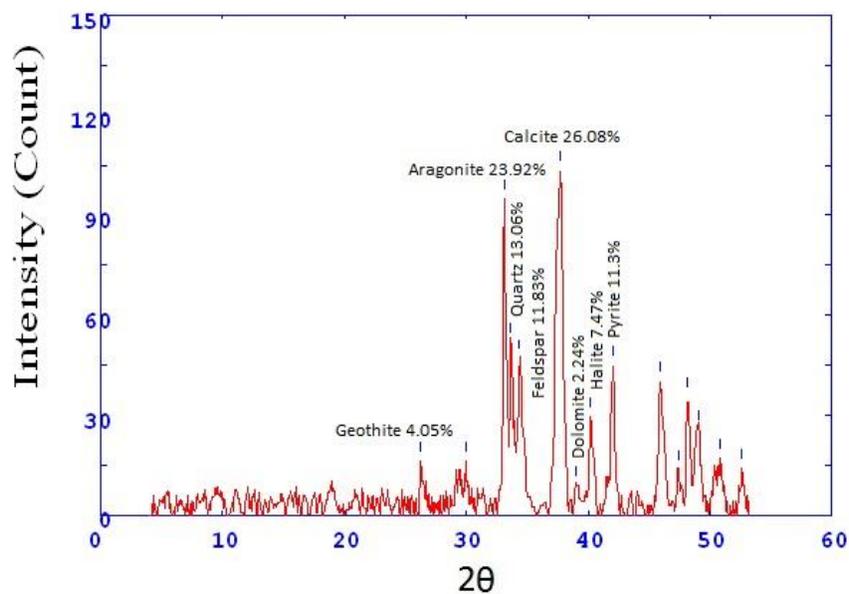
Fig.S9-10 X ray diffractogram of core 6 sample no.10

2Theta	d (A)	Height	Area	FWHM	Identified mineral	WT%
13.112	**8.47866**	73.7	1762.9	0.3861	Illite	9.512132
14.502	**7.66945**	317.4	1762.9	0.3861	Gypsum	40.96541
26.143	4.28013	48.8	294	0.464	Gypsum	
29.396	3.81529	150.4	427.2	0.2441	Gypsum	0
30.305	3.70336	21.3	60.4	0.2477	-	
33.542	**3.35483**	194.7	559	0.2514	quartz	25.12907
34.501	**3.26431**	28.3	81.3	0.2846	feldspar (orthoclase)	3.652555
35.282	**3.19423**	31.8	106.4	0.3179	feldspar (Albite)	4.104285
36.639	3.07974	48.5	162.3	0.3779	gypsum	
37.177	**3.03674**	77.2	454.9	0.4379	calcite	9.963862
39.272	**2.88065**	28.3	166.8	0.3553	dolomite	3.652555
40.044	2.82732	76.4	236.7	0.2727	Feldspar (orthoclase)	
42.192	**2.68945**	23.4	80.1	0.3076	Pyrite	3.020134
45.648	2.49552	18.3	136.3	0.5556	Gypsum	
Total		774.8				

Table S7-1 X ray diffraction data of core 7 sample no.1
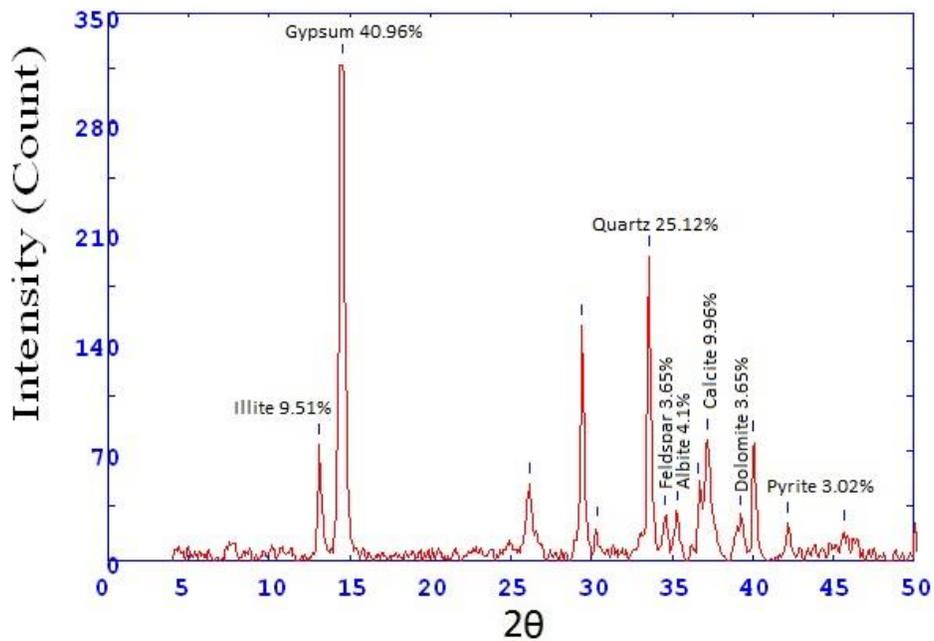
Fig.S10-1 X ray diffractogram of core 7 sample no.1

2Theta	d (A)	Height	Area	FWHM	Identified mineral	WT%
24.849	4.49927	21.8	184.7	0.6198	-	0
26.226	**4.26673**	27.3	138.1	0.4165	Goethite	9.030764
30.233	3.71195	22.5	99.1	0.3589	-	
33.602	**3.34898**	89.1	273.1	0.2922	quartz	29.47403
34.706	**3.24561**	19	58.3	0.3164	feldspar (orthoclase)	6.285147
35.257	**3.19644**	22.7	99.6	0.3406	Albite	7.509097
37.226	**3.03288**	76.4	382.1	0.4324	Calcite	25.27291
39.124	**2.89107**	52.5	269.4	0.4307	Dolomite	17.36685
40.153	**2.81996**	15.3	78.7	0.9224	Halite	5.061197
44.247	2.57041	17.4	325.7	1.4141	quartz	
45.833	2.48598	17.3	280.9	1.1115	-	
47.167	2.41955	16.8	110	0.5568	quartz	
50.233	2.28058	17	110.6	0.4706	Albite	
Total		302.3				

Table S7-2 X ray diffraction data of core 7 sample no.2
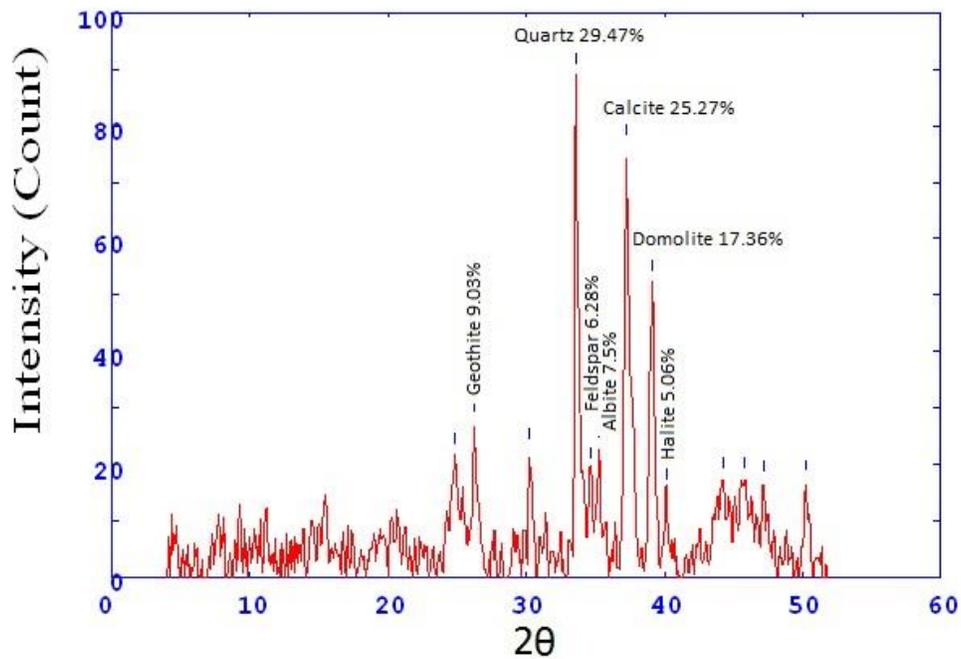
Fig.S10-2 X ray diffractogram of core 7 sample no.2

2Theta	d (A)	Height	Area	FWHM	Identified mineral	WT%
26.211	4.26922	21.2	86.8	0.3373	-	
30.358	3.69709	20.2	112.2	0.466	-	
33.559	**3.35316**	129.6	383	0.2839	quartz	30.38687
34.538	**3.26091**	43.7	129.1	0.2816	feldspar (orthoclase)	10.24619
35.211	**3.20046**	66	205.8	0.2793	Albite	15.47479
37.214	**3.03384**	105.3	423.6	0.3448	calcite	24.68933
39.052	**2.89625**	52.3	377.6	0.5451	dolomite	12.2626
40.155	**2.81984**	12.8	92.8	0.3879	Halite	3.001172
41.942	**2.70479**	16.8	43.7	0.2308	Pyrite	3.939039
45.767	2.4894	19.9	186.1	0.6276	Gypsum	
48.701	2.34777	11.4	97.9	0.4474	feldspar	
50.18	2.28283	23.9	116.2	0.348	Albite	0
52.284	2.19706	14.1	138.5	0.63	Gypsum	
54.055	2.13026	11.6	114.6	0.6233	quartz	
55.033	2.09525	17.7	141.7	0.6166	-	
Total		426.5				

Table S7-3 X ray diffraction data of core 7 sample no.3
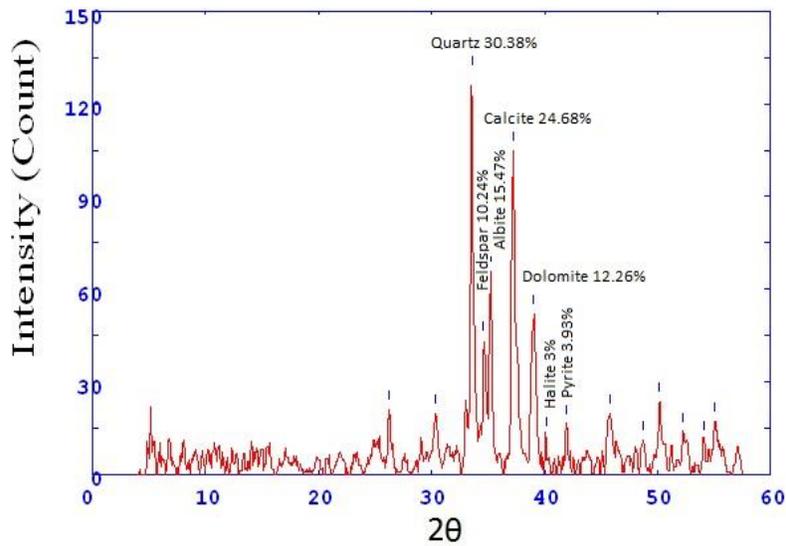
Fig.S10-3 X ray diffractogram of core 7 sample no.3

2Theta	d (A)	Height	Area	FWHM	Identified mineral	WT%
26.19	4.27256	43	100.2	0.2372	-	0
29.066	**3.85759**	18.7	74.9	0.3563	anhydrite	4.066101
30.531	3.67656	13.5	54.1	0.3132	-	
33.012	**3.40712**	22.9	91.4	0.2916	Aragonite	4.979343
33.588	**3.35034**	163.9	483.2	0.27	quartz	35.63818
34.666	**3.24921**	18.2	53.7	0.2884	feldspar (orthoclase)	3.957382
35.217	**3.19992**	16.7	49.1	0.3068	Albite	3.631224
37.228	**3.03275**	152.5	616.2	0.3436	calcite	33.15938
38.934	**2.9047**	35.1	226.1	0.4846	dolomite	7.632094
40.087	**2.82442**	13	83.8	0.4283	Halite	2.826701
41.934	**2.70527**	18.9	92.2	0.372	Magnesite, pyrite	4.109589
44.073	2.58003	10.7	213.9	1.4543	feldspar (orthoclase)	
45.797	2.48785	30.3	173.4	0.4234	Gypsum	
47.989	2.3805	10.9	62.6	0.5535	Pyrite	
48.768	2.34474	11.5	112.4	0.6835	anhydrite	
50.189	2.28246	30.9	164	0.4027	feldspar (orthoclase)	
52.123	2.20336	12	63.6	0.3112	Pyrite	
53.148	2.16389	17.6	39.7	0.2197	-	
55.15	2.09117	25.7	125.4	0.4349	-	
Total		459.9				

Table S7-4 X ray diffraction data of core 7 sample no.4
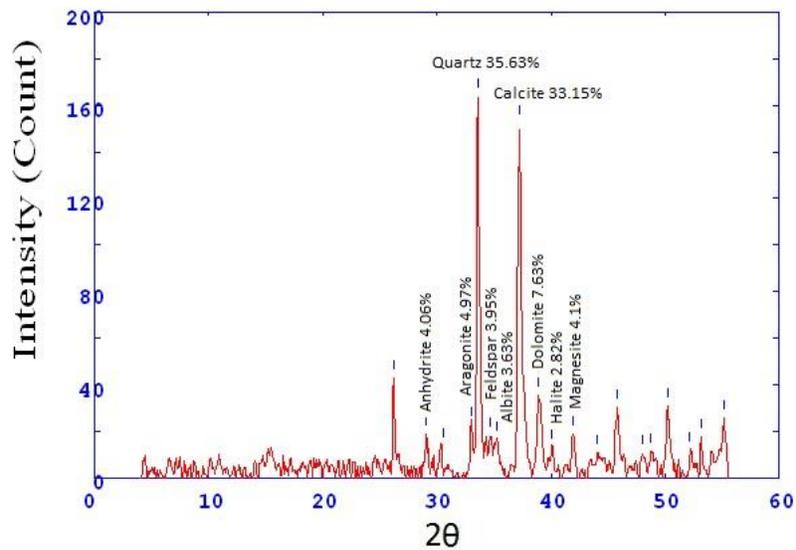
Fig.S10-4 X ray diffractogram of core 7 sample no.4

2Theta	d (A)	Height	Area	FWHM	Identified mineral	WT%
22.3	**5.00587**	7	26.5	0.3264	Gypsum	1.247772
23.5	4.75346	8.3	26.5	0.3264	Gypsum	
26.252	4.26261	13.6	36.2	0.2612	Gypsum	0
29.074	3.85651	18.8	75.9	0.3596	-	
32.87	**3.42148**	47.2	190.8	0.3705	Aragonite	8.413547
33.537	**3.35533**	52.5	215.7	0.3814	quartz	9.358289
34.279	**3.28478**	29.5	121.2	0.4109	feldspar (orthoclase)	5.258467
37.215	**3.03372**	169.5	954.8	0.4405	calcite	30.2139
38.947	**2.90371**	13.4	75.7	0.3464	dolomite	2.388592
40.044	**2.82733**	42.7	125.2	0.2523	Halite	7.611408
41.87	**2.70918**	29.7	114.9	0.3483	Magnesite, pyrite	5.294118
45.733	2.49113	41.4	266	0.466	Aragonite	
47.139	2.4209	12.4	79.5	0.4454	Gypsum	
48.033	2.37842	18.6	100.1	0.4247	Pyrite	
48.812	2.34272	15.1	81.2	0.4447	Gypsum	
50.233	2.28058	29.5	190.8	0.4646	Gypsum	
52.2	2.20035	13.1	64.9	0.3585	Gypsum	
Total		561				

Table S7-5 X ray diffraction data of core 7 sample no.5
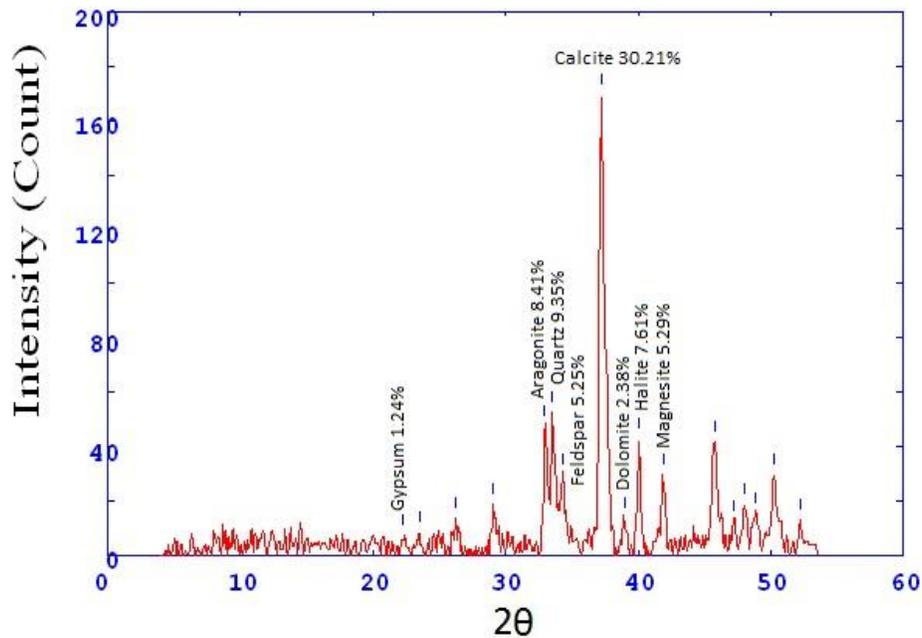
Fig.S10-5 X ray diffractogram of core 7 sample no.5

2Theta	d (A)	Height	Area	FWHM	Identified mineral	WT%
14.494	**7.67379**	35.5	78.4	0.2263	Gypsum	7.011653
26.211	4.26919	44.8	129	0.2502	Gypsum	
29.411	3.81333	20.1	139.2	0.5133	-	0
30.313	3.70237	19.8	137.1	0.3936	-	
32.98	**3.41035**	25.6	176.8	0.3337	Aragonite	5.056291
33.564	**3.35263**	209.8	624.4	0.2738	quartz	41.43788
35.263	**3.19591**	31.8	137.1	0.3543	Albite	6.280861
37.211	**3.03405**	123.7	507.9	0.3458	calcite	24.43215
39.067	**2.89517**	66.7	399	0.4656	Gypsum	13.17401
42.046	**2.69835**	13.2	86.8	0.4398	pyrite	2.60715
45.833	2.48598	23	154.3	0.4812	Gypsum	
46.23	2.4658	19.8	132.8	0.4604	calcite	
47.98	2.3809	8.3	55.9	0.4396	Gypsum	
48.813	2.34268	10.3	68.7	0.398	anhydrite	
50.197	2.28212	36.7	148.7	0.3149	calcite	
Total		506.3				

Table S7-6 X ray diffraction data of core 7 sample no.6
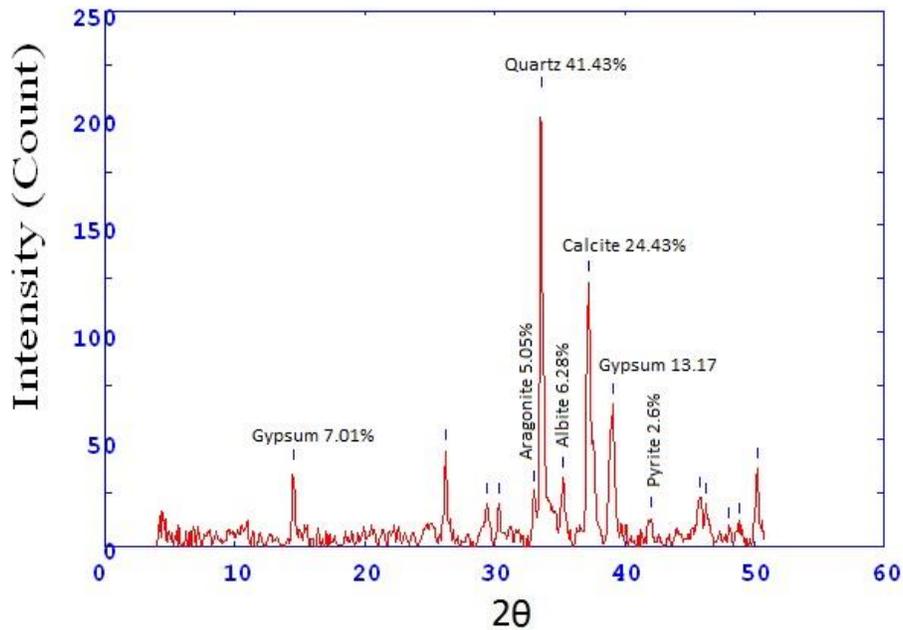
Fig.S10-6 X ray diffractogram of core 7 sample no.6

2Theta	d (A)	Height	Area	FWHM	Identified mineral	WT%
29.354	3.82053	14.2	255.6	0.3246	-	
33.086	**3.39972**	78.2	255.6	0.3246	quartz	35.65891
34.215	3.29073	43.4	141.8	0.5045	-	
37.351	**3.02307**	86.2	823.7	0.6844	calcite	39.30689
39.24	**2.88287**	8.8	83.7	0.5892	dolomite	4.012768
41.465	2.73449	15.3	146.3	0.494	Magnesite, pyrite	
41.933	**2.7053**	46.1	151.6	0.3036	Pyrite	21.02143
43.993	2.58447	6.7	14.5	0.1711	quartz	
45.878	2.4837	36.8	205.5	0.4227	calcite	
47.149	2.42039	14.5	80.9	0.3813	Pyrite	
48.127	2.37407	28.7	122.1	0.3399	-	
48.879	2.33971	22.7	122.1	0.3399	quartz	
Total		219.3				

Table S7-7 X ray diffraction data of core 7 sample no.7
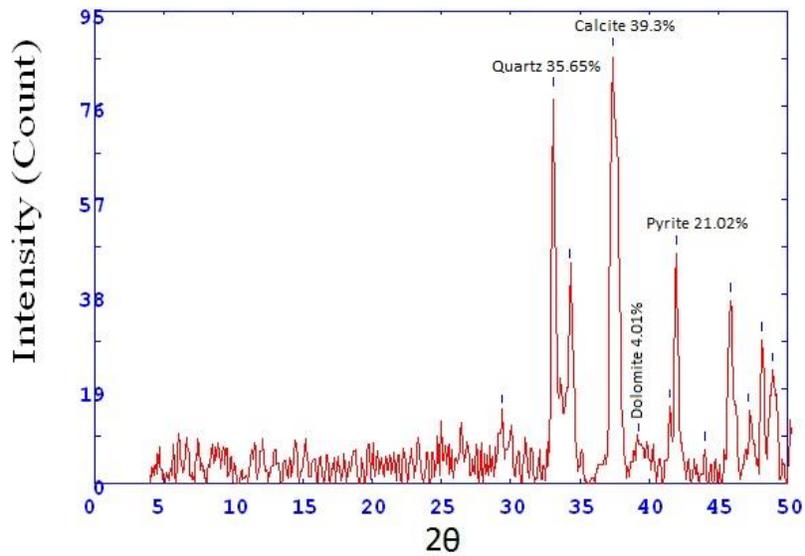
Fig.S10-7 X ray diffractogram of core 7 sample no.7

2Theta	d (A)	Height	Area	FWHM	Identified mineral	WT%
29.167	3.84452	15.5	90.9	0.4459	-	
29.886	3.75409	11.5	67.5	0.3822	-	0
33	**3.40836**	69.5	220.3	0.3185	Aragonite	20.18588
34.176	**3.29437**	44.7	141.7	0.4485	quartz	12.98286
35.166	3.20443	32.3	102.4	0.5135	feldspar	9.381353
37.24	**3.0318**	140.6	951	0.5785	calcite	40.83648
39.992	**2.83086**	17.1	48.6	0.2254	dolomite	4.966599
41.853	**2.71026**	40.1	180.7	0.3353	Pyrite	11.64682
45.7	2.49284	39	224.3	0.4524	Aragonite	
47.211	2.41739	12	68.9	0.376	Pyrite	
48.025	2.3788	31.6	116.7	0.2995	Pyrite	
48.779	2.34423	27	99.9	0.2442	-	
Total		344.3				

Table S7-8 X ray diffraction data of core 7 sample no.8
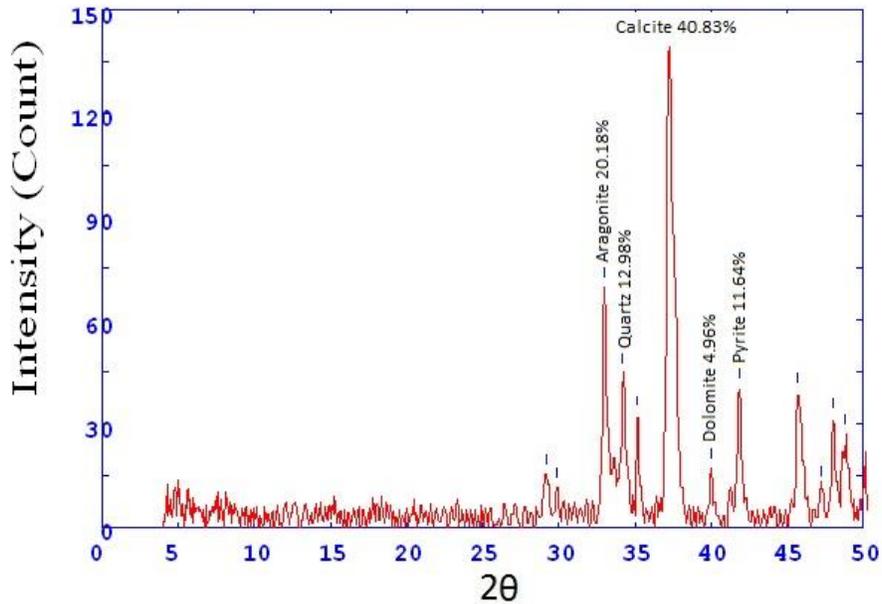
Fig.S10-8 X ray diffractogram of core 7 sample no.8

2Theta	d (A)	Height	Area	FWHM	Identified mineral	WT%
13.117	**8.47535**	84.3	1835.8	0.4044	Illite	14.85462555
14.5	**7.67041**	324.9	1835.8	0.4044	Gypsum	57.25110132
25.98	4.30649	65.1	250.2	0.3347	Gypsum	
26.58	**4.21097**	18.8	72.4	0.293	Geothite	3.31277533
29.386	3.81648	161.1	352.3	0.2513	gypsum	
33.513	**3.35759**	28.3	120.8	0.3605	Quartz	4.986784141
36.678	3.07661	68	217	0.3095	Gypsum	
37.132	**3.04027**	39.8	126.8	0.3925	calcite	7.013215859
39.233	**2.88337**	44.2	273.4	0.4755	dolomite	7.788546256
42.118	**2.69398**	27.2	134.6	0.4495	Pyrite	4.792951542
45.5	2.50321	31.9	178.7	0.4444	Gypsum	
50.167	2.28341	16.6	87.4	0.4167	Quartz	
Total		567.5				

Table S8-1 X ray diffraction data of core 8 sample no.1
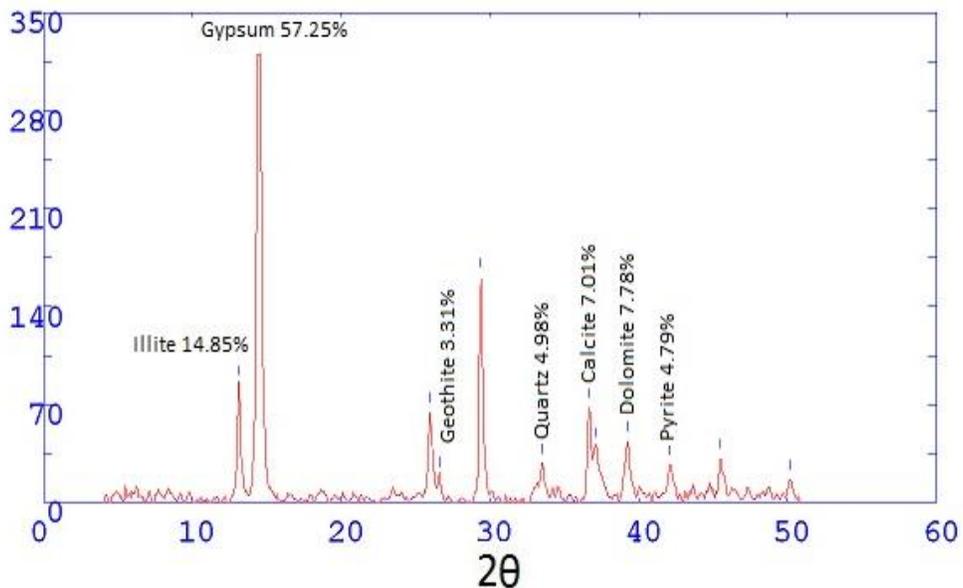
Fig.S11-1 X ray diffractogram of core 8 sample no.1

2Theta	d (A)	Height	Area	FWHM	Identified mineral	WT%
14.441	**7.70171**	11.6	68	0.5052	Gypsum	2.192816635
24.819	4.50464	10	705.3	0.4653	-	
26.074	4.29126	64.5	1883.2	0.4253	Gypsum	
29.087	3.85492	7.5	46.7	0.3822	Gypsum	
30.175	3.71898	37.2	295.9	0.3391	dolomite	
32.936	**3.41473**	26.5	111.1	0.2842	Aragonite	5.009451796
33.439	**3.36488**	285.7	577.9	0.2293	Quartz	54.00756144
34.527	**3.26193**	20.7	55.1	0.2503	feldspar (orthoclase)	3.913043478
35.28	**3.19443**	19.1	734.7	0.2713	feldspar (Albite)	3.610586011
37.205	**3.03457**	101.6	61.5	0.2767	calcite	19.20604915
39.046	**2.89667**	33.1	118.9	0.282	dolomite	6.257088847
39.966	**2.83258**	10	128.1	0.3255	halite	1.890359168
41.975	**2.70273**	20.7	490.7	0.369	Pyrite	3.913043478
44.569	2.55274	15.8	338	0.5075	gypsum	
45.574	2.49939	18.2	119	0.486	calcite	
46.159	2.46937	26.5	59.2	0.4881	Aragonite	
47.917	2.38385	10	118	0.4902	Aragonite	
48.586	2.35295	11.6	146	0.4944	Aragonite	
50.093	2.28656	30.6	123.9	0.2665	calcite	
Total		529				

Table S8-2 X ray diffraction data of core 8 sample no.2
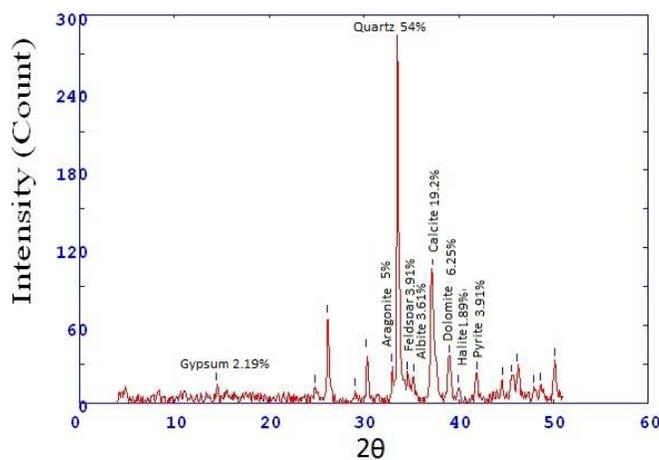
Fig.S11-2 X ray diffractogram of core 8 sample no.2

2Theta	d (A)	Height	Area	FWHM	Identified mineral	WT%
26.214	4.26871	75.3	207.4	0.2619	-	
30.375	3.69505	46.1	167.7	0.2963	-	
32.986	**3.40973**	36.2	131.7	0.3068	Aragonite	5.707978556
33.567	**3.35241**	356.8	1218.4	0.3174	Quartz	56.25985494
34.711	**3.24515**	75.9	259.1	0.3729	feldspar (orthoclase)	11.96783349
37.247	**3.03122**	106.1	520.8	0.4283	calcite	16.72973825
39.084	**2.89395**	37.8	292	0.534	dolomite	5.960264901
41.9	**2.70735**	21.4	115.1	0.4	Pyrite	3.374329864
46.327	2.46093	23	59	0.2442	Aragonite	
48.047	2.37778	18.5	70.6	0.3313	Aragonite	
50.145	2.28435	30.3	122.9	0.3517	feldspar (orthoclase)	
54.1	2.12861	22.2	127.3	0.374	Aragonite	
Total		634.2				

Table S8-3 X ray diffraction data of core 8 sample no.3
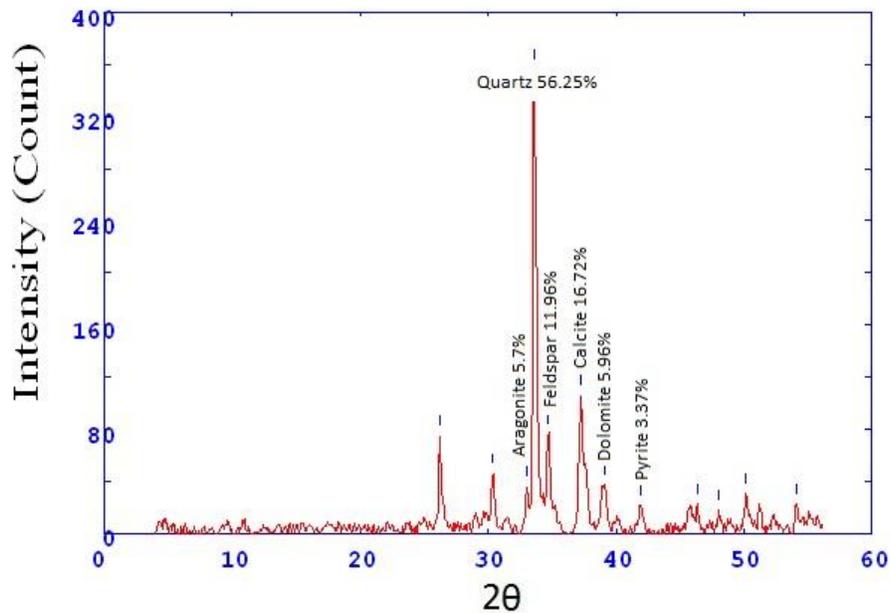
Fig.S11-3 X ray diffractogram of core 8 sample no.3

2Theta	d (A)	Height	Area	FWHM	Identified mineral	WT%
13.125	**8.4702**	313.7	1342.7	0.4503	Illite	28.72447578
14.634	**7.60047**	314.4	2621.8	0.5505	Gypsum	28.78857248
17.307	6.4337	12.6	42.9	0.2941	-	
23.67	4.7199	10.7	36.4	0.2668	-	
26.141	4.28037	67.9	231.1	0.2532	Gypsum	
26.675	**4.19622**	67.9	175.6	0.2395	Geothite	6.217379361
29.437	3.81008	329.6	852.6	0.2489	Gypsum	
33.604	**3.34877**	71	200.7	0.2583	Quartz	6.501236151
34.545	**3.26028**	13.9	39.2	0.2744	feldspar (orthoclase)	1.272777218
36.851	3.06264	71.1	201	0.2824	Gypsum	
37.202	**3.03474**	126.5	382.3	0.2904	calcite	11.58318835
39.347	**2.87539**	115.2	350.3	0.286	dolomite	10.54848457
40.147	**2.82039**	31.9	96.9	0.289	halite	2.920977932
42.272	**2.68459**	37.6	116.7	0.292	Pyrite	3.442908159
44.917	2.53401	41.7	125.4	0.2511	Gypsum	
45.666	2.49458	10.7	32.1	0.2588	Gypsum	
46.387	2.45791	41.5	123.9	0.2665	feldspar (orthoclase)	
Total		1092.1				

Table S8-4 X ray diffraction data of core 8 sample no.4
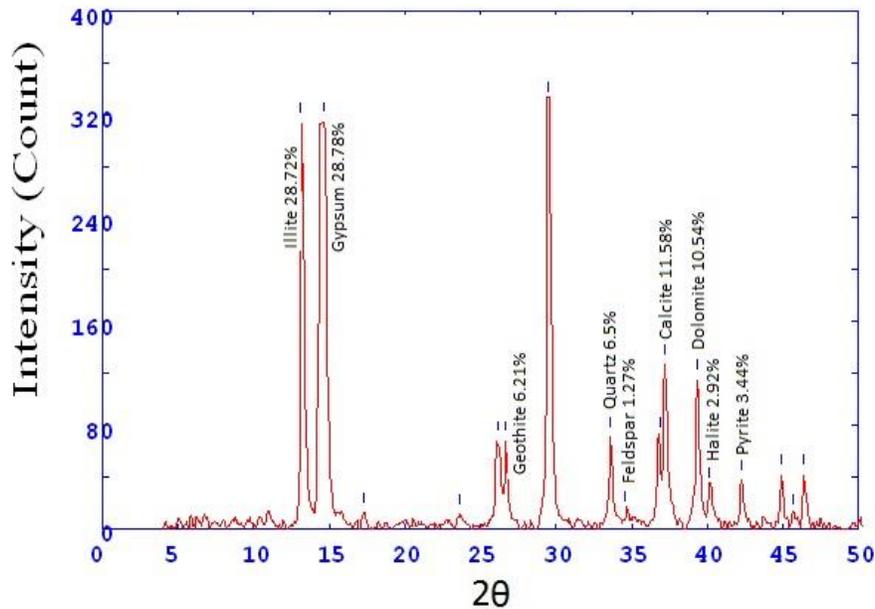
Fig.S11-4 X ray diffractogram of core 8 sample no.4

2Theta	d (A)	Height	Area	FWHM	Identified mineral	WT%
11.214	**9.908**	11.7	68	0.5052	Illite	1.452153407
13.199	8.42294	121.2	705.3	0.4653	Illite	
14.633	**7.60103**	331.4	1883.2	0.4253	Gypsum	41.13193496
17.389	6.40362	8.2	46.7	0.3822	-	
26.197	4.27141	76.1	295.9	0.3391	gypsum	
26.692	**4.19365**	28.6	111.1	0.2842	Geoithite	3.549708328
29.464	3.80659	288.8	577.9	0.2293	gypsum	
30.379	3.6945	27.6	55.1	0.2503	-	
33.611	**3.34811**	256.3	734.7	0.2713	Quartz	31.81084771
34.821	**3.23517**	21.5	61.5	0.2767	feldspar (orthoclase)	2.66848703
35.292	**3.19333**	41.6	118.9	0.282	feldspar (Albite)	170.4918033
36.833	**3.06413**	44.9	128.1	0.3255	calcite	5.572793844
37.241	3.03173	114.4	490.7	0.369	Gypsum	
39.309	**2.87806**	49.1	338	0.5075	Dolomite	6.094079682
42.301	**2.68282**	20.6	119	0.486	Pyrite	2.556782922
43.956	2.58653	10.3	59.2	0.4881	Gypsum	
44.794	2.54056	20.4	118	0.4902	Gypsum	
45.733	2.49112	22	146	0.4944	Gypsum	
50.233	2.28058	24.4	140	0.4323	Quartz	
Total		805.6				

Table S8-5 X ray diffraction data of core 8 sample no.5
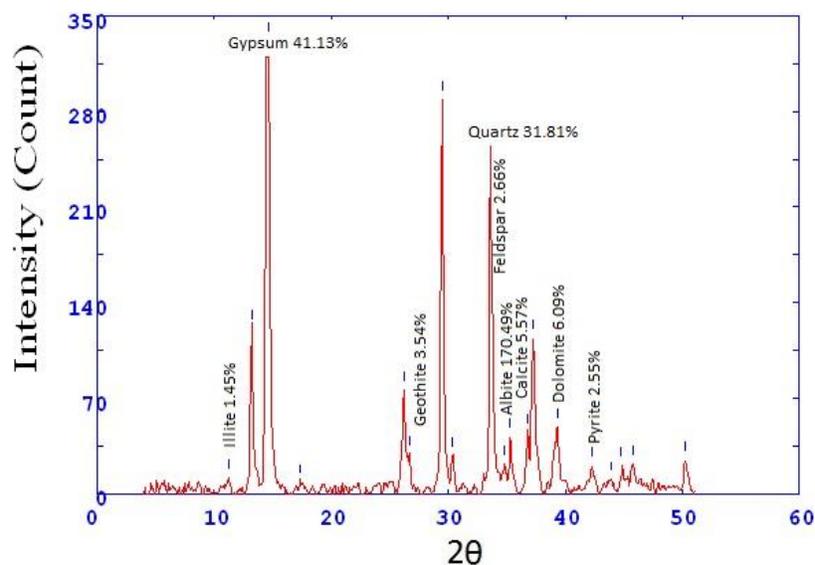
Fig.S11-5 X ray diffractogram of core 8 sample no.5

2Theta	d (A)	Height	Area	FWHM	Identified mineral	WT%
14.419	**7.71334**	11.1	75.4	0.4122	Gypsum	2.149496514
15.481	7.18731	9.8	66.4	0.3705	-	
26.1	4.28703	12.1	76.6	0.3655	Gypsum	
29.035	3.86166	14.3	91	0.2825	-	
30.279	3.70645	22.2	42.9	0.1996	-	
32.814	**3.42716**	56.6	109.3	0.2296	Aragonite	10.96049574
33.507	**3.35825**	184.5	546.1	0.2596	Quartz	35.72811774
34.292	**3.28354**	32.6	96.6	0.4101	-	6.312935709
34.621	**3.25332**	27.5	81.4	0.4854	feldspar (orthoclase)	5.325329202
34.949	**3.22367**	26.9	79.7	0.523	feldspar (Albite)	5.209140201
37.156	**3.03837**	132.2	899.3	0.5606	calcite	25.60030984
38.975	**2.90176**	17.2	117	0.4565	Dolomite	3.330751356
39.632	2.85553	12.6	85.9	0.4044	-	
41.811	**2.71283**	27.8	126.3	0.3523	Pyrite	5.383423703
43.85	2.5925	7.1	35.1	0.3333	gypsum	
45.7	2.49284	31.4	194.5	0.4738	gypsum	
46.203	2.46714	18.9	117.2	0.3613	Aragonite	
47.189	2.41846	8.1	49.9	0.3051	Aragonite	
47.995	2.38019	26	65.8	0.2489	Pyrite	
48.668	2.34926	18.9	0	0	Aragonite	
Total		516.4				

Table S8-6 X ray diffraction data of core 8 sample no.6
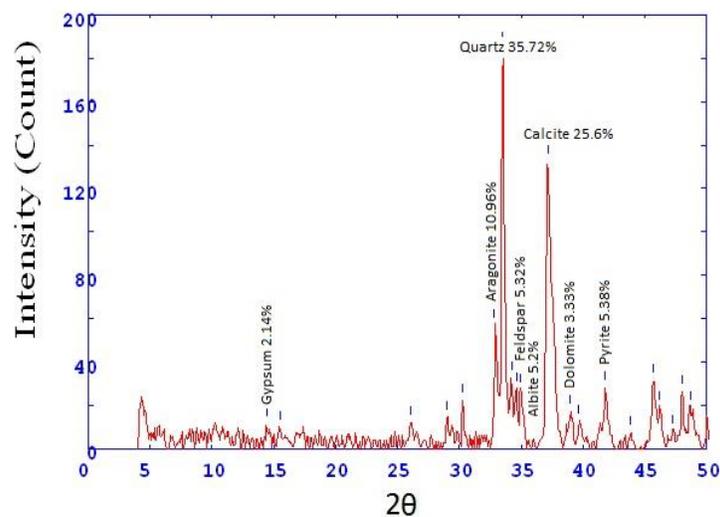
Fig.S11-6 X ray diffractogram of core 8 sample no.6

2Theta	d (A)	Height	Area	FWHM	Identified mineral	WT%
14.275	**7.79104**	10.5	92.4	0.5405	Gypsum	2.975347124
15.601	7.13208	12.2	92.4	0.5405	-	
16.979	6.55699	8.1	61.2	0.4369	-	
26.233	4.26563	11.3	51.1	0.3194	Gypsum	
29.283	3.82962	15.1	101.3	0.5155	gypsum	
33.116	**3.39669**	61.8	248.2	0.2997	Aragonite	17.51204307
33.732	**3.3365**	54.2	217.5	0.48	Quartz	15.35845849
34.43	**3.27084**	36.5	146.7	0.5701	feldspar (orthoclase)	10.34287334
37.328	**3.02491**	126.1	1122	0.6602	calcite	35.73250213
39.141	**2.88989**	15.7	139.5	0.4568	Dolomite	4.448852366
39.926	**2.83531**	8.9	78.8	0.3551	halite	2.521960895
40.275	2.81175	9.3	82.4	0.3042	-	
41.986	**2.70208**	39.2	109.8	0.2533	Pyrite	11.1079626
43.504	2.61213	6.9	19.2	0.355	Quartz	
45.867	2.48427	41	231.4	0.4567	Aragonite	
47.343	2.41107	13.3	74.9	0.4543	Gypsum	
48.148	2.3731	27.2	148.8	0.4519	Aragonite	
49.088	2.33039	25.3	138.6	0.4926	Aragonite	
50.376	2.27453	28.4	176.9	0.5333	gypsum	
50.745	2.25906	19.3	119.9	0.4156	Pyrite	
52.567	2.18608	14.6	51.6	0.2978	feldspar (orthoclase)	
Total		352.9				

Table S8-7 X ray diffraction data of core 8 sample no.7
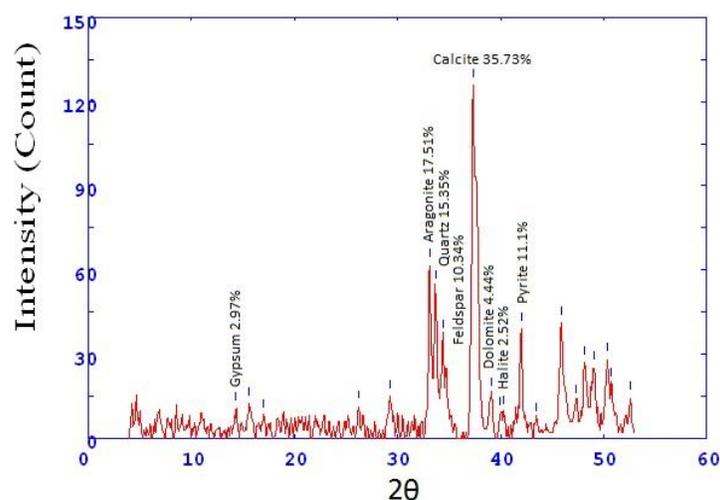
Fig.S11-7 X ray diffractogram of core 8 sample no.7

2Theta	d (A)	Height	Area	FWHM	Identified mineral	WT%
26.291	4.25642	80	11358.7	0	-	
27.547	4.06589	54.2	7696.3	0	-	
29.34	3.82237	62	12396	0	-	
32.979	**3.41045**	111.8	22344.7	0.8627	Aragonite	16.66169896
33.62	**3.34728**	132.5	2822.7	1.7254	Quartz	19.7466468
34.316	**3.28133**	78.8	1679.2	1.3619	feldspar (orthoclase)	11.74366617
37.278	**3.02882**	142.2	2190.7	0.9983	calcite	21.19225037
39.08	**2.89426**	58.7	904.4	0.9983	dolomite	8.748137109
40.073	**2.82533**	62	12428	0.9983	halite	9.239940387
41.891	**2.70789**	85	12624	0.9983	Pyrite	12.66766021
45.858	2.48474	84.1	11516	0.9983	Aragonite	
48.189	2.37119	68.3	9353.5	0.9983	gypsum	
48.98	2.3352	70.4	8161.3	0.9983	feldspar (orthoclase)	
50.027	2.28936	67.4	0	0	feldspar (orthoclase)	
Total		671				

Table S8-8 X ray diffraction data of core 8 sample no.8
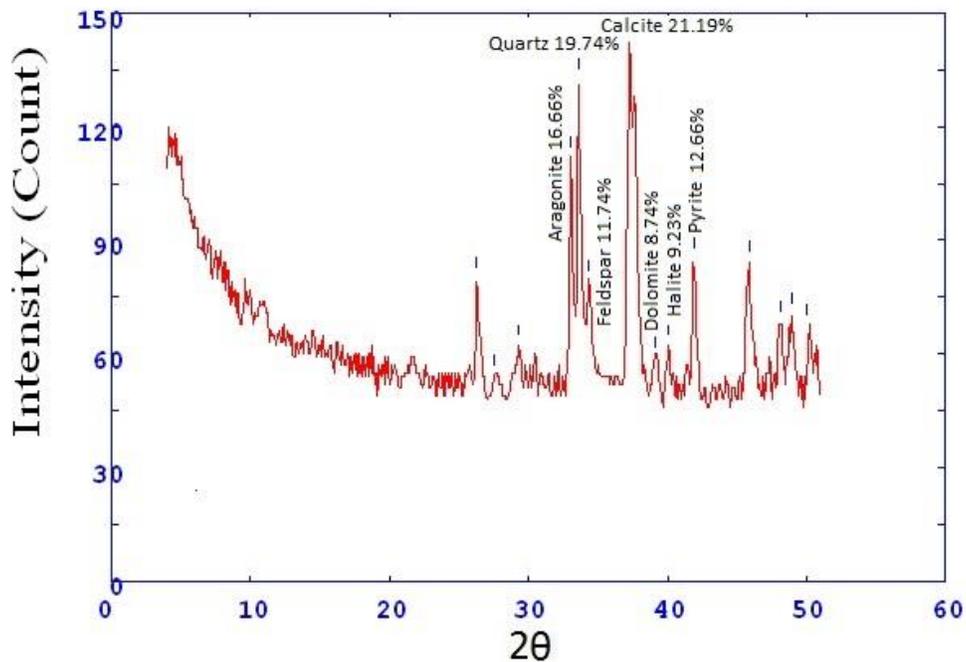
Fig.S11-8 X ray diffractogram of core 8 sample no.8

2Theta	d (A)	Height	Area	FWHM	Identified mineral	WT%
26.234	4.26549	9.5	29	0.2942	-	
29.067	3.85753	11	202.4	1.3297	-	
33.042	**3.40411**	63.9	250.3	0.342	Aragonite	19.5353103
33.686	**3.34089**	54.3	212.4	0.5453	Quartz	16.600428
34.35	**3.27821**	37.5	146.7	0.6469	feldspar (orthoclase)	11.46438398
35.097	**3.21058**	8.4	33	0.6977	feldspar (Albite)	2.568022012
37.255	**3.03059**	101.5	1100.1	0.7485	calcite	31.03026597
37.669	2.9985	87.5	948.1	0.6518	-	
38.996	**2.90019**	15.8	171.7	0.5551	Dolomite	4.830327117
40.075	**2.82521**	8.1	87.7	0.4584	halite	2.47630694
41.887	**2.70817**	37.6	155.8	0.3617	Pyrite	11.49495567
45.783	2.48855	37.1	260	0.5242	-	
47.294	2.4134	8.4	59	0.4413	-	
48.023	2.37889	28.8	118.7	0.3583	Pyrite	
48.954	2.33637	21.7	0	0	feldspar	
50.198	2.28206	18.4	0	0	-	
Total		327.1				

Table S8-9 X ray diffraction data of core 8 sample no.9
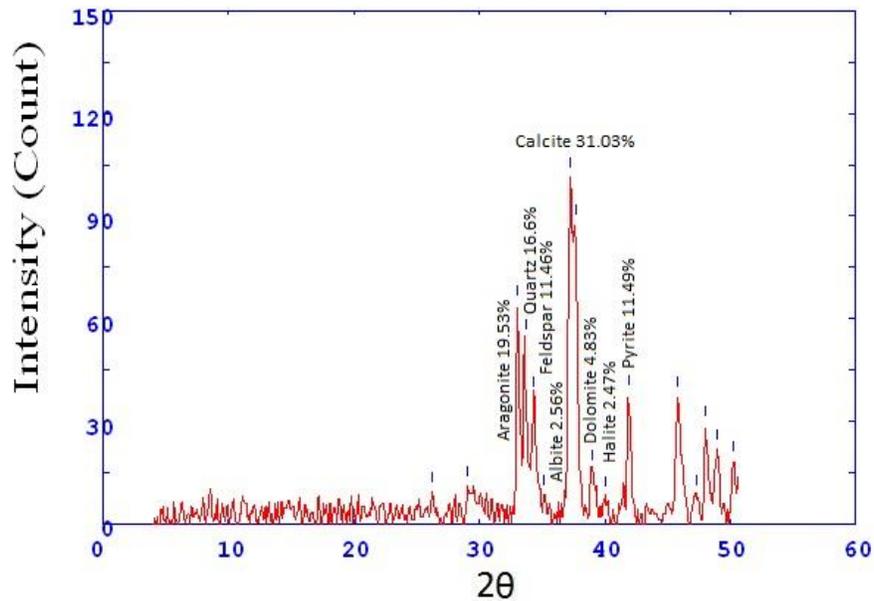
Fig.S11-9 X ray diffractogram of core 8 sample no.9

2Theta	d (A)	Height	Area	FWHM	Identified mineral	WT%
26.167	4.27631	11.5	67.7	0.45	-	0
29.384	3.81679	12.4	163.9	0.9761	-	
33.017	**3.40668**	77.8	247.9	0.2918	Quartz	26.4986376
34.243	**3.28815**	42.7	136.1	0.4985	feldspar (orthoclase)	14.54359673
35.47	**3.17789**	5.3	17	0.6019	feldspar (Albite)	23.24561404
36.369	3.10183	5	15.9	0.6536	-	
37.589	**3.00465**	104	1114.9	0.7053	calcite	35.42234332
39.232	**2.88347**	8	85.4	0.6161	Dolomite	2.72479564
40.033	**2.82806**	16.8	113.5	0.5268	halite	5.722070845
41.9	**2.70733**	39	167.7	0.3471	Pyrite	13.28337875
44.017	2.58315	6.1	9.7	0.1979	-	
45.785	2.48847	41.2	206.2	0.4328	-	
47.247	2.41566	9	44.8	0.4098	-	
48.081	2.3762	27.1	118.8	0.3869	-	
48.883	2.33954	22.8	118.8	0.3869	Pyrite	
Total		293.6				

Table S8-10X ray diffraction data of core 8 sample no.10
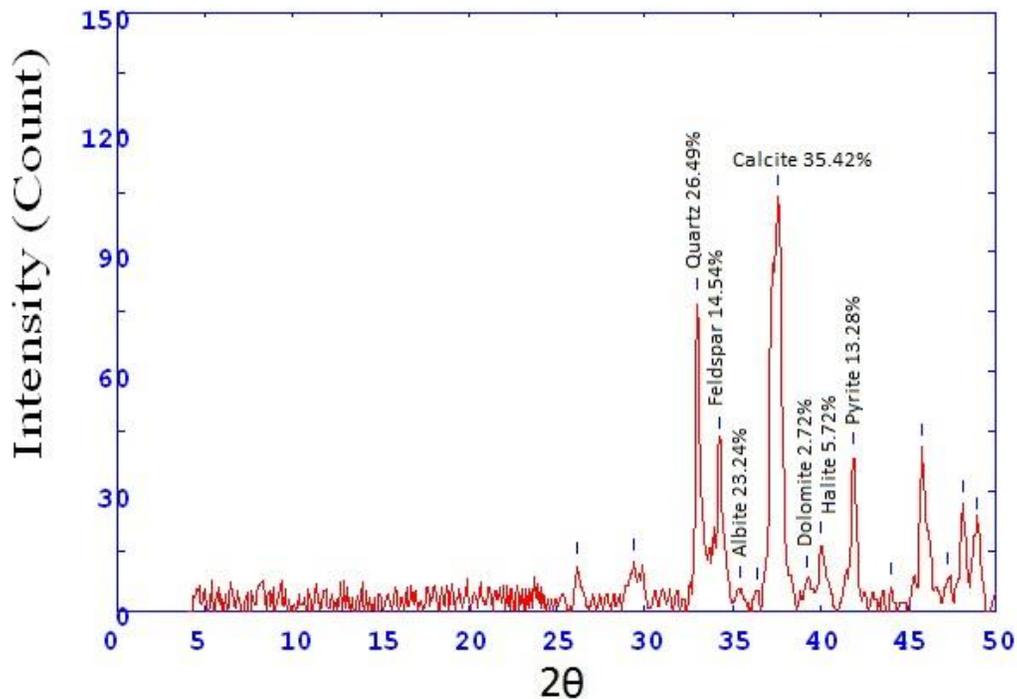
Fig.S11-10 X ray diffractogram of core 8 sample no.10

2Theta	d (A)	Height	Area	FWHM	Identified mineral	WT%
11.058	**10.04719**	19.7	70.4	0.2645	Illlite	5
14.529	**7.65525**	13.8	38.2	0.1372	Gypsum	3.502538
26.22	4.26776	26.1	91.7	0.2111	Gypsum	
27.144	4.12503	22.5	79.2	0.2785	-	
29.141	3.84789	16.4	84.5	0.346	illite	
30.491	3.68126	9.8	50.7	0.3137	Gypsum	
32.782	**3.43042**	44.3	228.6	0.2975	Aragonite	11.24365
33.562	**3.35287**	81.4	252.6	0.2813	Quartz	20.6599
34.191	**3.29299**	26.5	82.3	0.3346	feldspar (orthoclase)	6.725888
34.631	3.25237	69	214.2	0.3879	-	
35.248	**3.19723**	40.7	126.3	0.4411	feldspar (Albite)	10.32995
37.241	**3.03175**	115.4	745.8	0.4944	Calcite	29.28934
38.95	**2.90351**	28.9	165.4	0.4184	Dolomite	7.335025
40.004	2.83001	17.1	98	0.3717	halite	
41.868	**2.70935**	23.3	93	0.325	Pyrite	5.913706
45.719	2.49186	33.2	240.8	0.55	Calcite	
46.434	2.45555	21.8	158.4	0.475	Gypsum	
47.227	2.41664	13.1	95.1	0.4562	Gypsum	
47.932	2.38316	17.1	124.1	0.4375	Pyrite	
48.781	2.34412	21.3	120.2	0.4	gypsum	
50.119	2.28544	24.2	188.8	0.5695	feldspar	
52.3	2.19644	13.2	68.2	0.3	Dolomite	
Total		394				

Table S9-1X ray diffraction data of core 9 sample no.1
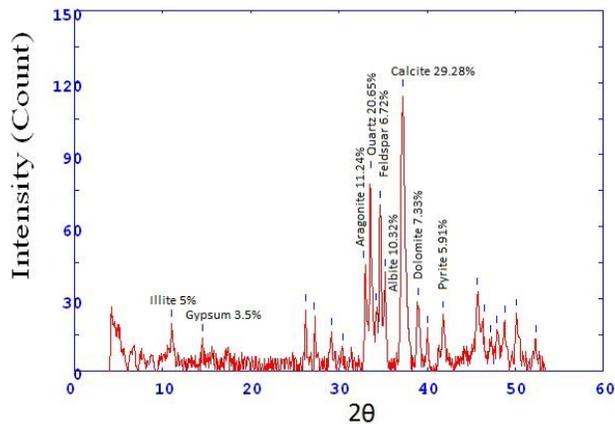
Fig.S12-1 X ray diffractogram of core 9 sample no.1

2Theta	d (A)	Height	Area	FWHM	Identified mineral	WT%
15.402	**7.22381**	13	119.8	0.6363	Gypsum	2.129402
23.733	4.70747	12.9	86.2	0.4821	-	
26.205	4.27016	112.2	325	0.2552	Gypsum	
28.966	3.87064	13.9	60.8	0.2825	-	
30.376	**3.6949**	45.1	219	0.3495	Aragonite	7.387387
33.567	**3.35242**	339.2	1406.8	0.3205	Quartz	55.56102
34.569	**3.25803**	23	95.4	0.3413	feldspar (orthoclase)	3.767404
35.176	**3.20358**	20.9	86.8	0.362	feldspar (Albite)	3.423423
37.202	**3.03475**	80.5	436.3	0.4036	Calcite	13.18591
39.071	**2.89484**	88.8	382.4	0.3469	Dolomite	14.54545
46.272	2.46368	46.5	173.8	0.3152	feldspar (orthoclase)	
48.66	2.34961	13.5	117.5	0.6296	feldspar (orthoclase)	
50.1	2.28625	43.6	199.6	0.3565	feldspar (orthoclase)	
51.121	2.24358	16.8	199.6	0.3565	feldspar (orthoclase)	
Total		610.5				

Table S9-2X ray diffraction data of core 9 sample no.2
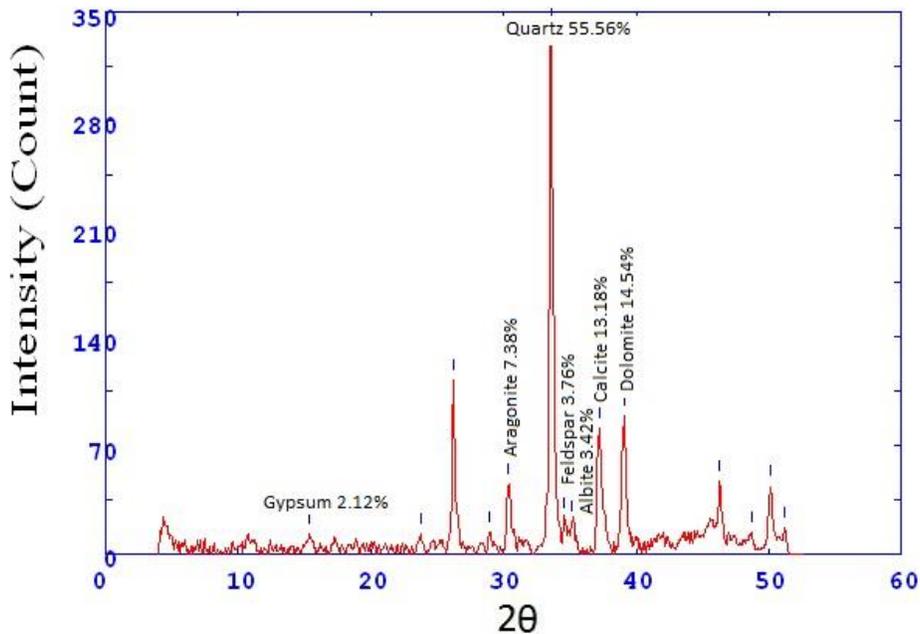
Fig.S12-2 X ray diffractogram of core 9 sample no.2

2Theta	d (A)	Height	Area	FWHM	Identified mineral	WT%
30.434	3.68809	14.2	21.7	0.1935	-	0
32.978	**3.4106**	101.2	155	0.2184	Aragonite	25.33801
33.635	**3.34579**	130.8	286.9	0.2434	Quartz	32.74912
34.402	**3.27336**	59.3	130	0.4794	feldspar (orthoclase)	14.84727
37.73	**2.99385**	48.1	461.6	0.7153	Calcite	12.04306
39.179	**2.88719**	10.1	97	0.5411	Dolomite	2.528793
41.442	2.73592	15.3	147.3	0.454	-	
41.944	**2.70461**	49.9	192.9	0.3669	Pyrite	12.49374
45.8	2.48769	41.6	231.2	0.4759	feldspar (orthoclase)	
47.309	2.4127	17	94.3	0.4063	feldspar (orthoclase)	
48.113	2.37473	41.3	168	0.3368	gypsum	
48.901	2.33874	33.5	136.1	0.2245	gypsum	
50.731	2.25966	12.6	3.3	0.1121	Pyrite	
Total		399.4				

Table S9-3X ray diffraction data of core 9 sample no.3
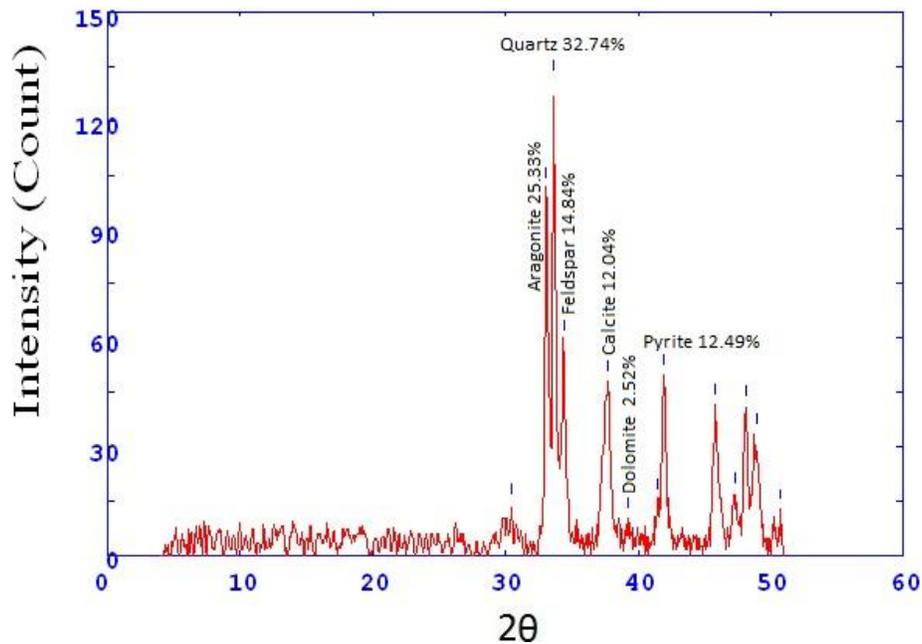
Fig.S12-3 X ray diffractogram of core 9 sample no.3

2Theta	d (A)	Height	Area	FWHM	Identified mineral	WT%
11.053	**10.05114**	18.2	134.2	0.5284	Illite	4.629865
15.595	**7.13484**	17.5	203.4	0.8173	Gypsum	4.451793
22.28	5.01019	7.8	59.8	0.4828	-	
23.863	4.68221	7.5	58	0.4346	-	
24.936	4.4838	19.1	147.3	0.3864	-	
26.288	4.25691	35.4	136.8	0.2901	gypsum	
28.978	3.86902	9.9	38.3	0.3712	-	
30.546	3.67484	12.6	48.8	0.4523	-	
31.473	**3.5692**	13.9	94	0.5064	Aragonite	3.535996
33.651	**3.3443**	108.3	313.3	0.2597	Quartz	27.55024
34.671	**3.24875**	27.7	80	0.3134	feldspar (orthoclase)	7.046553
35.166	**3.20443**	23.9	69.2	0.3402	feldspar (Albite)	6.079878
37.287	**3.02811**	74.7	387.1	0.3671	Calcite	19.0028
39.167	**2.88806**	97.8	488.4	0.3849	Dolomite	24.87917
42.032	**2.69921**	11.1	72.1	0.4696	Pyrite	2.823709
43.927	2.5882	17.5	659.9	2.4667	-	
45.891	2.483	18.1	680.9	1.3996	Aragonite	
46.433	2.4556	21.1	85.4	0.3326	Aragonite	
47.459	2.4055	18.8	75.9	24.9012	Aragonite	
Total		393.1				

Table S9-4X ray diffraction data of core 9 sample no.4
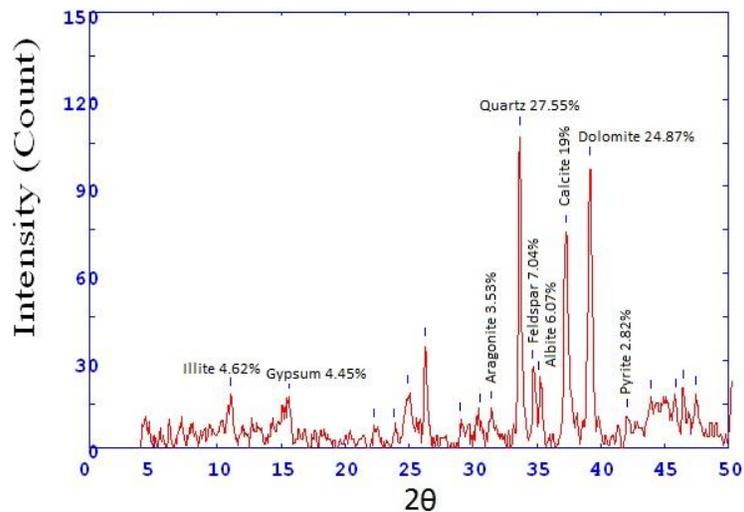
Fig.S12-4 X ray diffractogram of core 9 sample no.4

2Theta	d (A)	Height	Area	FWHM	Identified mineral	WT%
26.189	4.27268	26.9	110.2	0.3512	-	
29.083	3.85544	17	63.2	0.2948	-	
30.367	3.69603	26.1	57	0.2327	-	
32.907	**3.41771**	29.3	63.9	0.2538	Aragonite	6.508219
33.597	**3.34943**	192	565.9	0.2749	Quartz	42.64771
35.259	**3.19621**	22.1	65.2	0.321	feldspar (Albite)	4.908929
37.214	**3.03383**	135.7	551.9	0.3671	Calcite	30.14216
39.117	**2.89157**	34.7	279	0.5248	Dolomite	7.707685
39.965	**2.83271**	16.1	129.3	0.4666	halite	3.576188
41.901	**2.7073**	20.3	98.3	0.4084	Pyrite	4.509107
45.8	2.48769	32.1	133.8	0.3787	-	
46.238	2.46539	19.9	83.1	0.3697	-	
47.284	2.41391	14.4	60	0.3652	Aragonite	
47.981	2.38087	13.8	57.7	0.3641	Aragonite	
48.765	2.34486	14.4	60	0.363	Aragonite	
50.208	2.28164	43	209.1	0.3608	Feldspar	
Total		450.2				

Table S9-5X ray diffraction data of core 9 sample no.5
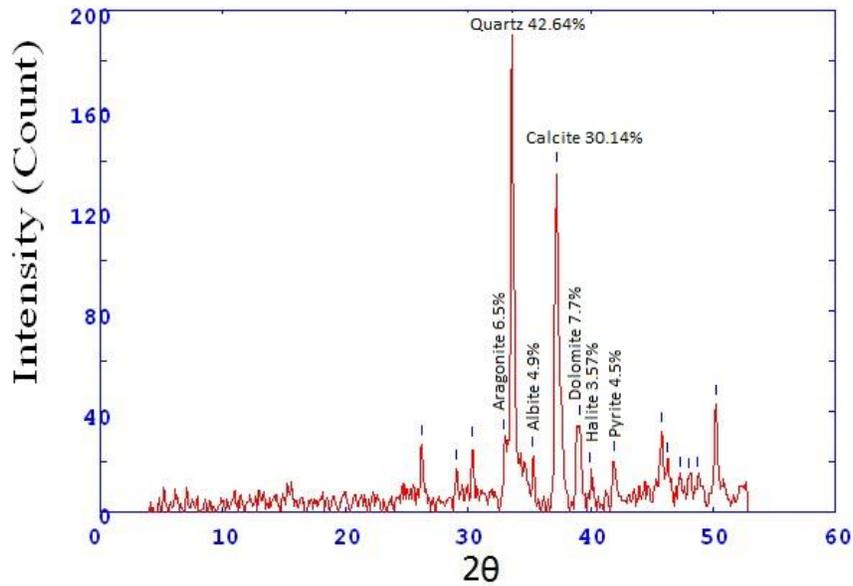
Fig.S12-5 X ray diffractogram of core 9 sample no.5

2Theta	d (A)	Height	Area	FWHM	Identified mineral	WT%
29.167	3.8445	18.9	87.6	0.3487	-	0
29.803	3.76424	11	51	0.3428	-	
32.987	**3.40963**	66.5	268.5	0.337	Aragonite	23.77547
34.259	**3.28667**	36.1	145.6	0.4634	feldspar (orthoclase)	12.90669
37.248	**3.03119**	138.6	1118.4	0.5898	Calcite	49.55309
41.865	**2.70952**	38.5	113.9	0.2779	Pyrite	13.76475
45.742	2.49065	47.1	275.9	0.45	-	
47.294	2.41341	14.1	82.5	0.4383	Aragonite	
48	2.37997	24	128	0.4267	Aragonite	
48.861	2.34051	23.3	128	0.4267	Aragonite	
50.099	2.28629	21.6	128	0.4267	Aragonite	
Total		279.7				

Table S9-6X ray diffraction data of core 9 sample no.6
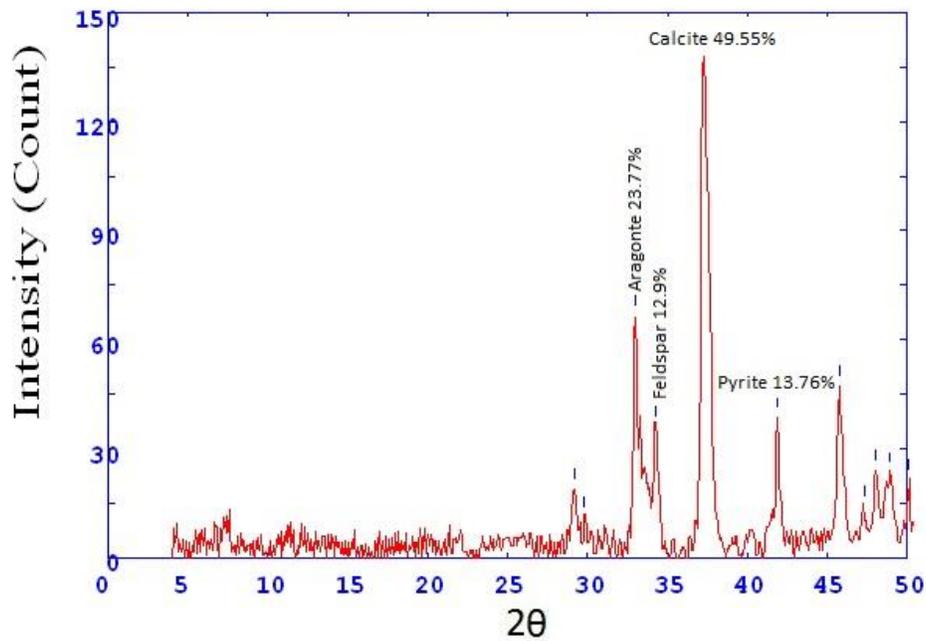
Fig.S12-6 X ray diffractogram of core 9 sample no.6

2Theta	d (A)	Height	Area	FWHM	Identified mineral	WT%
14.584	**7.62642**	55.3	168.6	0.2916	Gypsum	12.28889
26.234	4.26548	23.7	121.8	0.3756	Gypsum	
28.066	3.99216	7.4	56.9	0.4755	-	
29.35	3.82115	12.8	139.4	0.7083	-	
33.029	**3.40545**	81.1	882.8	0.487	Aragonite	18.02222
33.608	**3.34837**	157.7	457	0.2656	Quartz	35.04444
34.232	3.28915	50.6	146.6	0.5187	Quartz	
34.748	**3.24181**	40.1	116.1	0.6453	feldspar (orthoclase)	8.911111
37.261	**3.03012**	53.3	627.4	0.7719	Calcite	11.84444
37.67	2.99843	46.6	548.4	0.7009	-	
39.233	**2.88336**	15.8	144.2	0.6298	Dolomite	3.511111
40.076	2.82514	13	119.3	0.4991	halite	
41.365	2.74077	16.5	151.4	0.4337	-	
41.953	**2.70405**	46.7	225.8	0.3684	Pyrite	10.37778
43.428	2.61645	5	24.4	0.2841	-	
44.267	2.56931	7	10.7	0.1998	-	
45.833	2.48598	40.2	234.5	0.4428	Aragonite	
46.436	2.45546	14.5	84.8	0.4144	-	
47.468	2.4051	13.5	79	0.4003	Aragonite	
48.1	2.37531	36.6	164.6	0.3861	Aragonite	
48.929	2.3375	26.6	119.5	0.6169	Aragonite	
50.767	2.25818	11.2	114	0.8477	Pyrite	
Total		450				

Table S9-7X ray diffraction data of core 9 sample no.7
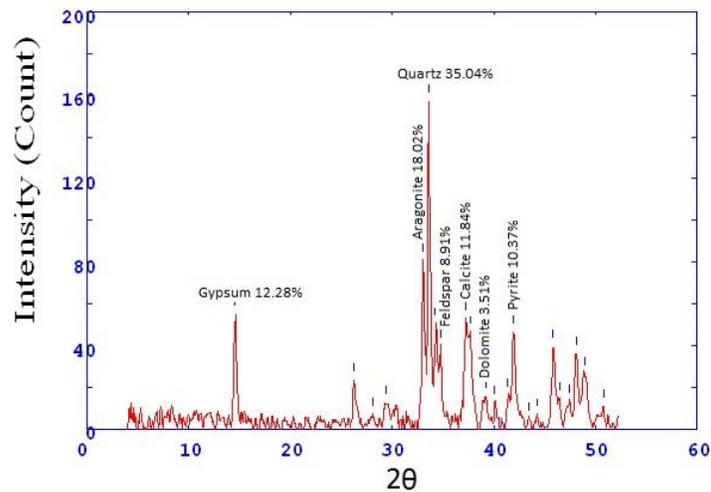
Fig.S12-7 X ray diffractogram of core 9 sample no.7

2Theta	d (A)	Height	Area	FWHM	Identified mineral	WT%
14.61	**7.61338**	17.6	52	0.3002	Gypsum	5.929919
26.367	4.24444	11.3	44.1	0.355	-	
30	3.74012	14.4	52.7	0.3212	-	
31.21	3.59854	10.3	37.6	0.3408	-	
33.147	**3.39367**	87.4	403.1	0.3604	Aragonite	29.44744
34.336	**3.27948**	49	225.8	0.5381	feldspar (orthoclase)	16.50943
37.71	**2.99534**	60.4	625.7	0.7159	Calcite	20.3504
39.272	**2.88065**	9.4	97.6	0.5081	Dolomite	3.167116
40.205	**2.81646**	24.8	82.6	0.3003	halite	8.355795
42	**2.7012**	48.2	188.8	0.3515	Pyrite	16.23989
45.933	2.48086	33.8	200.8	0.4628	Aragonite	
46.429	2.45582	25.7	153.1	0.5298	-	
47.252	2.41545	11.9	70.9	0.5465	Aragonite	
48.074	2.37651	28.8	171.2	0.5632	Aragonite	
48.933	2.33729	31.8	228.6	0.5967	Aragonite	
Total		296.8				

Table S9-8X ray diffraction data of core 9 sample no.8
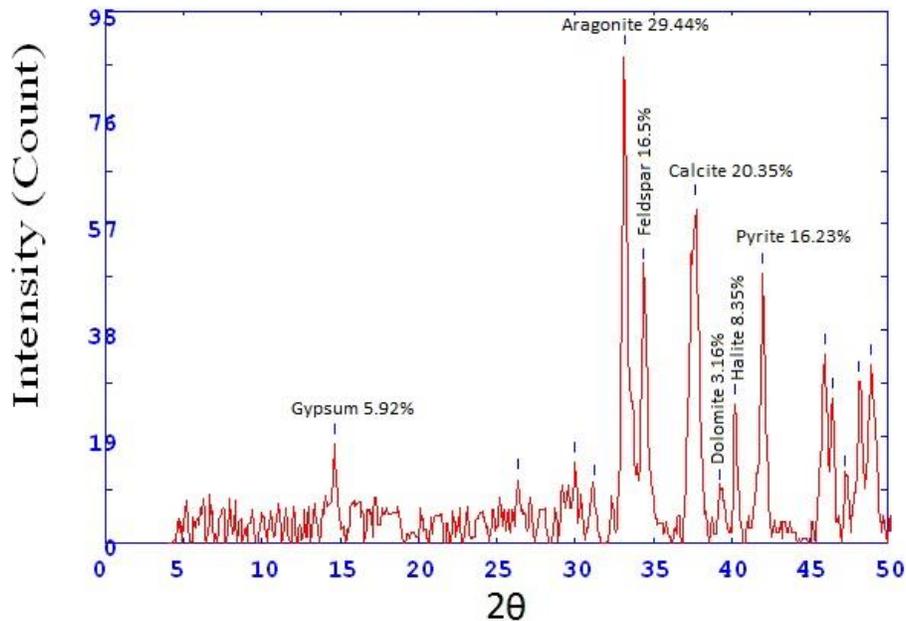
Fig.S12-8 X ray diffractogram of core 9 sample no.8

2Theta	d (A)	Height	Area	FWHM	Identified mineral	WT%
26.234	4.26558	11.4	77.9	0.4278	-	
29.9	3.75241	10.9	263.4	1.8763	-	
33.033	**3.405**	87.5	458.6	0.4214	Aragonite	27.61123
33.592	**3.34993**	53.7	281.6	0.5869	Quartz	16.94541
34.331	**3.27999**	47.2	247.3	0.6697	feldspar (orthoclase)	14.89429
37.633	**3.00123**	59.1	576.2	0.7524	Calcite	18.64942
39.17	**2.88784**	8.5	82.6	0.5478	Dolomite	2.682234
40.154	**2.81986**	12	117.2	0.4455	halite	3.786683
41.385	2.73954	15.3	149.1	0.3944	-	
41.884	**2.7083**	48.9	196.9	0.3432	Pyrite	15.43074
42.779	2.65423	7.4	29.7	0.2994	-	
43.189	2.63021	5.7	23.2	0.2775	-	
44.127	2.57705	8	26.9	0.2556	-	
44.748	2.54307	5.7	19.3	0.393	-	
45.755	2.49003	36.6	273.2	0.5305	Aragonite	
47.209	2.41751	13.1	98	0.4483	Aragonite	
48.056	2.37738	42.1	182.3	0.3661	Aragonite	
48.849	2.34106	29.5	0	0	Aragonite	
Total		316.9				

Table S9-9X ray diffraction data of core 9 sample no.9
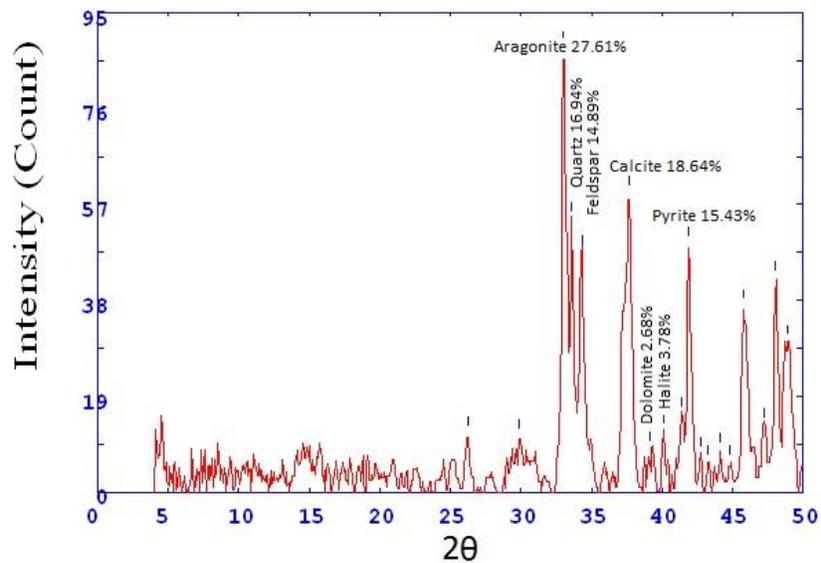
Fig.S12-9 X ray diffractogram of core 9 sample no.9

2Theta	d (A)	Height	Area	FWHM	Identified mineral	WT%
14.538	**7.65074**	67.4	147.2	0.2273	Gypsum	17.95418
29.383	3.81684	17.9	187.2	0.6231	Gypsum	
31.33	3.5851	5.9	73.8	0.5563	-	
33.023	**3.40603**	60.9	248.6	0.3064	Aragonite	16.2227
33.55	**3.35403**	27.8	113.3	0.4844	Quartz	7.405434
34.425	**3.27127**	33	134.7	0.5735	feldspar (orthoclase)	8.790623
37.261	**3.03017**	117.8	1096.6	0.6625	Gypsum	31.37986
39.062	**2.89554**	16.9	157.3	0.5131	Dolomite	4.501865
40.02	**2.82892**	19.9	111.1	0.3637	Halite	5.301012
41.249	2.74817	11.3	63	0.371	-	
41.919	**2.70615**	31.7	170.6	0.3782	Pyrite	8.444326
44.129	2.57694	8.5	69.9	0.5448	-	
45.773	2.48906	42.3	262.4	0.4956	Aragonite	
48.016	2.37922	34.1	107.6	0.2857	Aragonite	
48.773	2.3445	21.4	67.5	0.4283	Aragonite	
50.252	2.27981	26.7	200	0.571	Quartz	
52.233	2.19904	13	101	0.5454	feldspar (orthoclase)	
Total		375.4				

Table S9-10X ray diffraction data of core 9 sample no.10
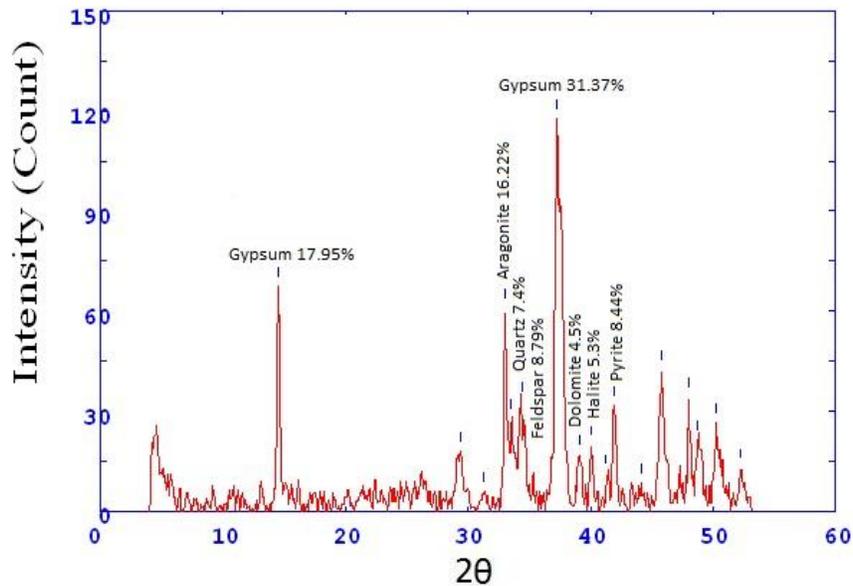
Fig.S12-10 X ray diffractogram of core 9 sample no.10

2Theta	d (A)	Height	Area	FWHM	Identified mineral	WT%
29.133	3.84889	14	40.6	0.2119	-	
33.016	**3.40673**	72.6	233.8	0.3043	Aragonite	21.77564
33.469	**3.36196**	36.3	116.9	0.4946	Quartz	10.88782
34.137	**3.29806**	35.5	114.3	0.5897	feldspar (orthoclase)	10.64787
37.267	**3.0297**	126.7	1273.6	0.6849	Calcite	38.0024
40.112	**2.8227**	20.9	107.9	0.3807	halite	6.268746
41.86	**2.70981**	41.4	169.9	0.3235	Pyrite	12.41752
45.7	2.49285	43.3	227.1	0.4175	Aragonite	
47.212	2.41735	11.7	61.6	0.3753	Aragonite	
47.993	2.38028	28.5	113.4	0.3332	Aragonite	
48.739	2.34603	21	83.4	0.5752	Aragonite	
50.504	2.26917	19.5	236.5	0.8173	Quartz	
52.368	2.19379	14.8	98.6	0.5189	feldspar	
54.466	2.11539	20.6	137.5	0.6595	gypsum	
55.2	2.08942	22	238.9	0.8	-	
Total		333.4				

Table S9-11X ray diffraction data of core 9 sample no.11
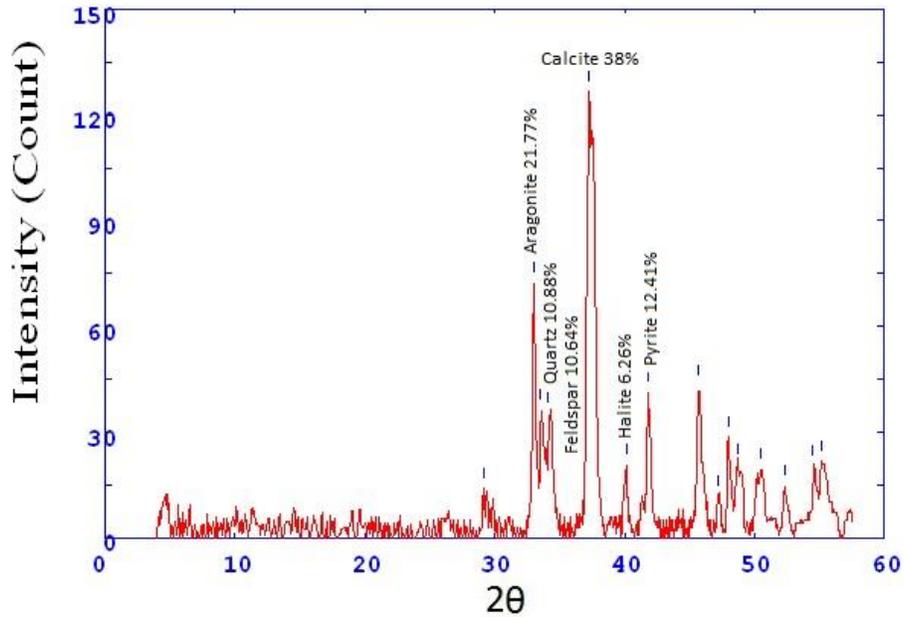
Fig.S12-11 X ray diffractogram of core 9 sample no.11

2Theta	d (A)	Height	Area	FWHM	Identified mineral	WT%
11.078	10.02865	18.7	78	0.3655	Illite	2.265294
14.541	7.64914	73.8	212.9	0.2498	Gypsum	8.940036
17.397	6.40068	9.9	28.6	0.2512	-	
23.879	4.67924	8.8	25.4	0.2516	-	
24.974	4.47704	13.2	38	0.2519	-	
26.247	4.26347	90.1	260.5	0.2526	Gypsum	
29.173	3.84374	15.4	44.4	0.2537	Gypsum	
29.447	3.80877	15.4	44.4	0.2542	-	
30.404	3.69162	81.8	233.2	0.2547	-	
31.273	3.59148	14.3	40.7	0.2976	-	
32.003	3.5116	9.9	28.2	0.319	Aragonite	1.199273
33.567	3.35241	369.7	1580.1	0.3404	Quartz	44.78498
34.559	3.25895	51.4	219.5	0.3874	feldspar (orthoclase)	13.37371
35.198	3.2016	59	252.2	0.4109	feldspar (Albite)	
37.234	3.03226	91.3	558.3	0.4345	calcite	11.05996
39.046	2.89663	98.9	653.9	0.4639	dolomite	11.98062
40.036	2.82783	36.1	238.7	0.5578	halite	4.373107
42.615	2.66401	16.7	144.7	0.6517	Pyrite	2.023016
45.605	2.49776	18.6	161.4	0.496	Gypsum	
46.366	2.45895	24.8	115.7	0.3403	Aragonite	
50.172	2.28317	40.4	181.5	0.3299	Gypsum	
51.265	2.23771	13.2	59.2	0.3793	Gypsum	
54.028	2.13123	16	86.1	0.4288	Gypsum	
		825.5				

Table S10-1 X ray diffraction data of core 10 sample no.1
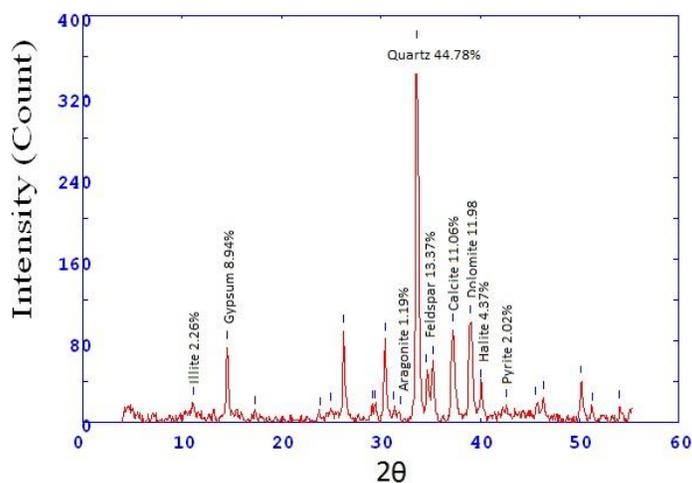
Fig.S13-1 X ray diffractogram of core 10 sample no.1

2Theta	d (A)	Height	Area	FWHM	Identified mineral	WT%
15.329	**7.25803**	16.3	192.2	0.9116	Gypsum	3.03538175
24.89	4.49186	17.9	210.1	0.6001	gypsum	
26.221	4.26753	40.8	120.8	0.2887	Gypsum	
29.017	3.86403	10.7	31.8	0.306	feldspar (orthoclase)	
30.42	3.68972	34.4	126.1	0.3232	-	
31.361	3.58162	13.4	49.2	0.2888	-	
33.624	3.34682	288.5	801.9	0.2544	Quartz	53.72439
34.737	**3.24275**	49.9	138.7	0.4544	feldspar (orthoclase)	9.292364991
35.3	**3.19267**	15.2	42.2	0.5545	feldspar (Albite)	
37.283	**3.02838**	61.5	511.1	0.6545	calcite	11.45251
39.056	**2.89595**	65.4	383.4	0.422	Dolomite	12.17877
40.176	**2.81838**	30.3	177.7	0.3728	halite	5.642458
42.333	**2.68088**	9.9	57.8	0.3482	Pyrite	1.843575
45.109	2.52376	21.6	73.8	0.3236	feldspar (orthoclase)	
50.312	2.27724	18.6	137.1	0.6012	Gypsum	
52.2	2.20035	12	85.1	0.4994	Gypsum	
54.056	2.13021	8.1	57.4	0.4692	-	
55.317	2.08536	12.1	72.9	0.4389	-	
Total		537				

Table S10-2 X ray diffraction data of core 10 sample no.2
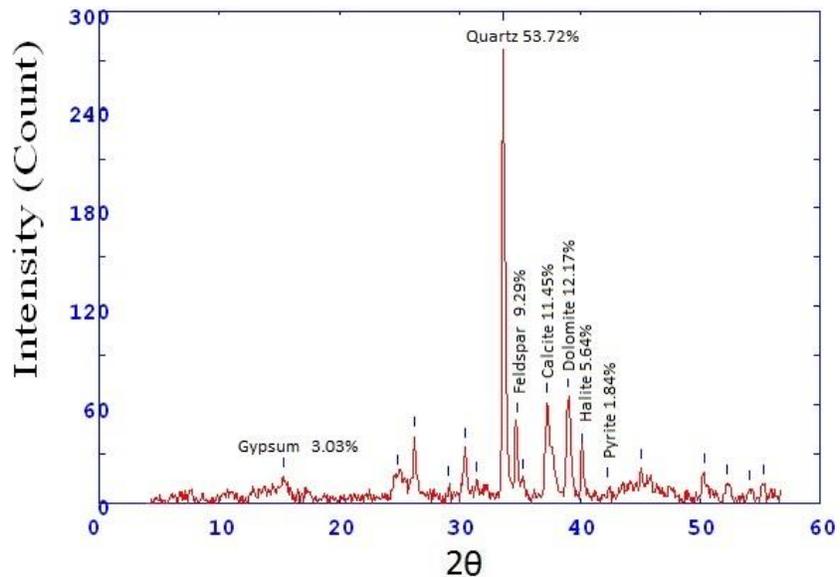
Fig.S13-2 X ray diffractogram of core 10 sample no.2

2Theta	d (A)	Height	Area	FWHM	Identified mineral	WT%
29.478	3.80484	10.4	35	0.3333	-	
31.167	3.60341	7.1	35	0.3333	-	
33.092	**3.39917**	75.6	294.2	0.3123	Aragonite	24.14564
33.643	**3.34503**	28.1	109.2	0.394	Quartz	8.974768
34.323	**3.2807**	43.8	170.2	0.4757	feldspar (orthoclase)	8.156425
37.691	**2.99679**	105.9	822.3	0.6391	dolomite	19.72067
40.125	**2.82181**	18.3	57.6	0.3004	halite	3.407821
41.953	**2.70406**	41.4	204.3	0.3833	Pyrite	7.709497
43.417	2.61706	7.4	36.3	0.38	Gypsum	
44.352	2.56459	7.4	36.3	0.3783	Aragonite	
45.861	2.48455	41	168	0.3767	feldspar (orthoclase)	
46.307	2.46192	21.7	88.9	0.3676	Aragonite	
47.327	2.41181	14	57.5	0.3586	Aragonite	
48.113	2.37469	34.2	145.1	0.3405	Pyrite	
49.027	2.33309	28.7	121.8	0.5452	Aragonite	
50.8	2.2568	20	180.8	0.75	-	
Total		313.1				

Table S10-3 X ray diffraction data of core 10 sample no.3
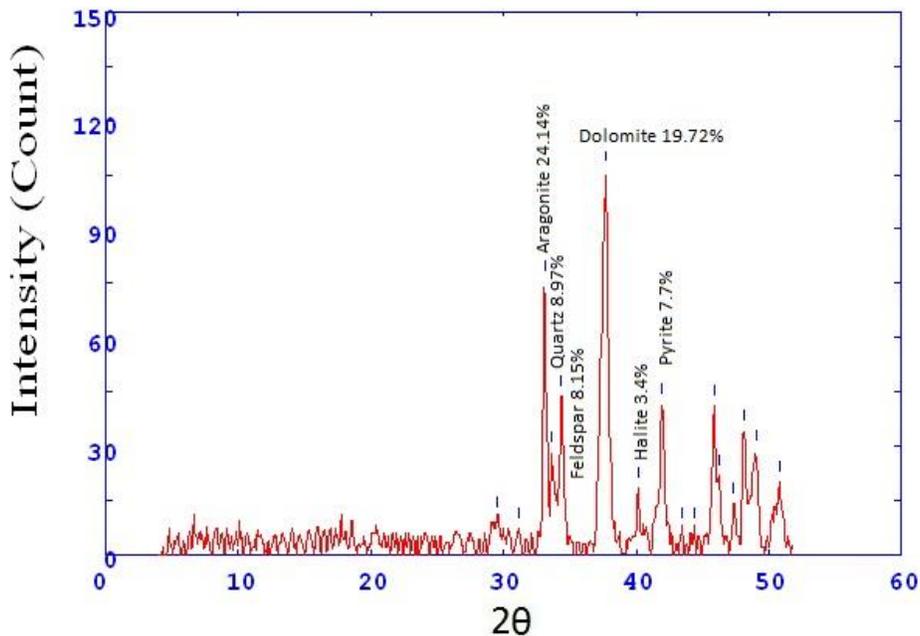
Fig.S13-3 X ray diffractogram of core 10 sample no.3

2Theta	d (A)	Height	Area	FWHM	Identified mineral	WT%
15.458	**7.19766**	11.1	134.3	0.2954	Gypsum	1.973684211
26.146	4.27958	42.8	134.3	0.2954	Gypsum	
28.878	3.88215	11.1	34.9	0.2779	Gypsum	
30.274	3.70706	29.4	78.3	0.2605	-	
31.241	3.595	9.4	25.2	0.259	-	
31.917	3.52086	9.4	25.2	0.2583	-	
32.845	**3.42396**	37.5	100.1	0.2579	Aragonite	6.667852063
33.488	**3.36003**	274.2	768.1	0.2576	Quartz	48.75533428
34.533	**3.26133**	38.4	107.5	0.3209	feldspar (orthoclase)	6.827880512
37.127	**3.04069**	116.2	551.2	0.3842	calcite	20.66145092
39.007	**2.89945**	36.5	178.4	0.4073	Dolomite	6.490042674
39.935	**2.83473**	12.8	62.7	0.3423	halite	2.275960171
41.811	**2.71282**	26.3	90.9	0.2773	Pyrite	4.676386913
45.59	2.49855	21.3	73.9	0.2847	Quartz	
46.295	2.46254	81.4	271.3	0.2921	feldspar (orthoclase)	
47.109	2.42234	12	39.9	0.319	Aragonite	
47.953	2.38216	9.4	31.4	0.3324	Pyrite	
48.713	2.34723	11.1	37.1	0.3391	Gypsum	
50.067	2.28768	21.2	87.6	0.3458	Gypsum	
Total		562				

Table S10-4 X ray diffraction data of core 10 sample no.4
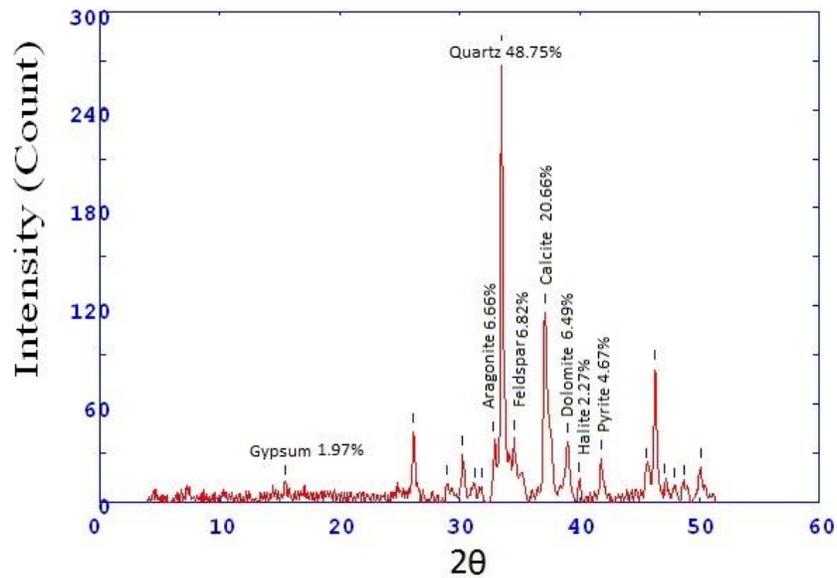
Fig.S13-4 X ray diffractogram of core 10 sample no.4

2Theta	d (A)	Height	Area	FWHM	Identified mineral	WT%
15.619	**7.1242**	10.9	54.8	0.4045	Gypsum	2.42924
26.275	4.25899	56.9	160.3	0.2474	Gypsum	
29.017	3.86397	14.9	42	0.2515	Gypsum	
30.379	3.6945	20.9	48.4	0.2556	dolomite	
31.301	3.58838	4.3	10	0.2575	-	
33.095	**3.39885**	37.8	87.6	0.2595	Aragonite	8.424337
33.624	**3.34688**	171.9	488.2	0.2633	Quartz	38.31068
37.241	**3.03168**	145.7	728.4	0.4444	calcite	32.47158
39.067	**2.89514**	50.4	307.8	0.439	dolomite	11.23245
40.108	**2.82297**	8.6	52.3	0.2873	halite	1.916648
41.902	**2.7072**	23.4	143.3	0.2114	Pyrite	5.215066
42.947	2.64438	32.8	29.2	0.1355	-	
44.023	2.58283	8.6	7.6	0.2922	-	
45.786	2.48843	30.2	162.7	0.4488	Gypsum	
46.469	2.4538	25.6	138	0.4427	Gypsum	
47.366	2.40993	12.3	66.2	0.4397	Aragonite	
48.252	2.36826	13.2	85.6	0.4366	Aragonite	
Total		448.7				

Table S10-5 X ray diffraction data of core 10 sample no.5
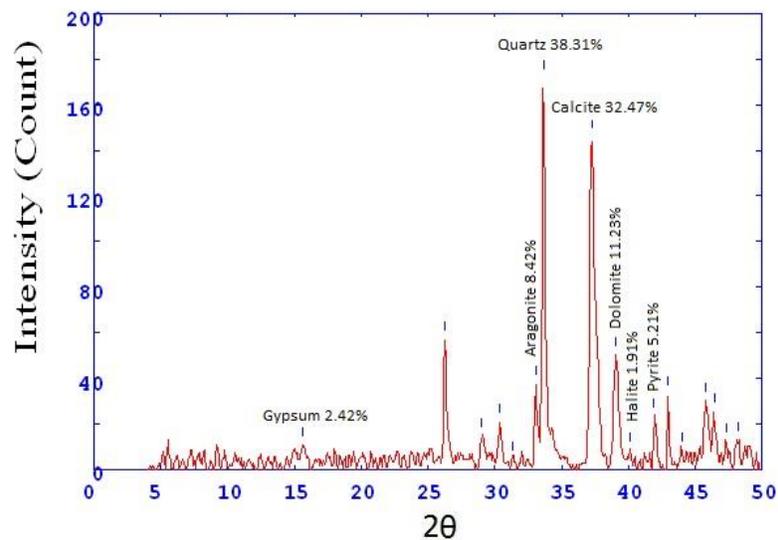
Fig.S13-5 X ray diffractogram of core 10 sample no.5

2Theta	d (A)	Height	Area	FWHM	Identified mineral	WT%
13.44	**8.27245**	92.6	1859.9	0.4128	Illite	9.780313
14.9	**7.46573**	332.9	1859.9	0.4128	Gypsum	35.16054
26.343	4.24818	61.3	370.2	0.4522	Gypsum	
26.888	**4.16359**	25.8	155.7	0.3556	Goethite	2.724968
29.721	3.77448	162.9	355	0.259	Gypsum	
33.276	**3.38084**	21.7	47.2	0.2603	Aragonite	2.291931
33.854	**3.32476**	137.1	389	0.2615	Quartz	14.48035
34.873	**3.23051**	21.7	61.5	0.2837	feldspar (orthoclase)	2.291930714
35.477	**3.17725**	75.8	232.8	0.3059	feldspar (Albite)	
36.89	3.05951	61.8	189.8	0.3559	-	
37.485	**3.0127**	86.2	407.6	0.406	calcite	9.104351
39.496	**2.86495**	60.8	287.2	0.3541	dolomite	6.421631
40.376	**2.80501**	64.2	241.1	0.3023	halite	6.780735
42.424	**2.67539**	28	184	0.5458	Pyrite	2.95733
45.127	2.52279	12.4	81.6	0.5046	-	
46	2.47746	19	116	0.4633	Gypsum	
46.556	2.44948	13.5	82.1	0.4539	Aragonite	
47.481	2.40446	7.3	44.5	0.4492	Aragonite	
48.826	2.34213	11.4	69.6	0.4468	Aragonite	
50.452	2.27132	21.2	115	0.4444	Pyrite	
Total		946.8				

Table S10-6 X ray diffraction data of core 10 sample no.6
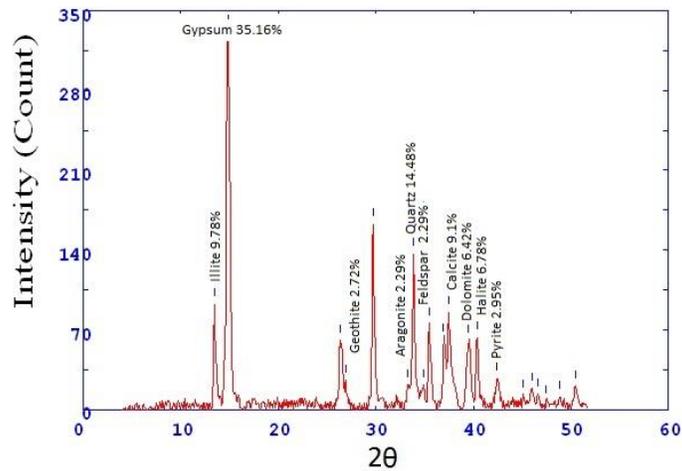
Fig.S13-6 X ray diffractogram of core 10 sample no.6

2Theta	d (A)	Height	Area	FWHM	Identified mineral	WT%
13.245	**8.39388**	166.1	2297.5	0.4949	Illite	15.1981
14.576	**7.63084**	322.2	2297.5	0.4949	Gypsum	29.4812
26.12	4.28388	112.2	566.2	0.3752	Gypsum	
26.649	4.20024	45.8	231.3	0.3342	Gypsum	
29.367	**3.81896**	336.1	1162.3	0.2931	Aragonite	30.75304
33.54	**3.355**	22	167.7	0.6167	Quartz	2.012993
35.586	**3.16786**	6.5	49.3	0.4847	Feldspar (Albite)	0.594748
36.7	**3.07482**	107.4	455.2	0.3527	Calcite	9.827066
39.285	**2.87974**	59.4	217.6	0.3023	dolomite	5.435081
40.054	**2.82666**	25.6	93.8	0.3381	halite	2.342392
42.227	**2.68735**	47.6	211	0.374	Pyrite	4.355385
43.628	2.60502	11.8	52.2	0.3747	-	
44.817	2.53935	22	114	0.3754	-	
45.416	2.50762	15	77.5	0.35	-	
47.389	2.40883	18.8	78	0.3245	Feldspar (Albite)	
51.667	2.22147	19.9	119.6	0.4425	Gypsum	
55.233	2.08825	25.3	256	0.7151	calcite	
58.084	1.99407	25.9	142.6	0.4116	Feldspar (orthoclase)	
61.214	1.90126	61.7	379.2	0.4244	-	
65.95	1.77856	21.2	175.7	0.6341	-	
Total		1092.9				

Table S10-7 X ray diffraction data of core 10 sample no.7
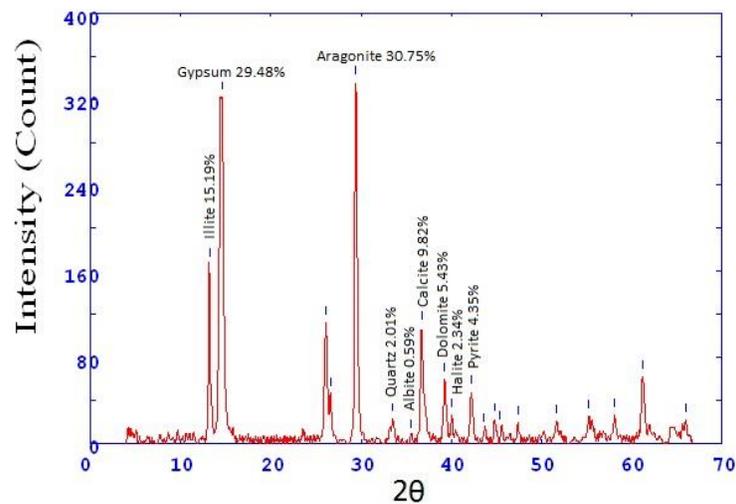
Fig.S13-7 X ray diffractogram of core 10 sample no.7

2Theta	d (A)	Height	Area	FWHM	Identified mineral	WT%
13.133	8.46496	165	2297.5	0.4949	Illite	20.72604
14.576	7.63084	322.2	2297.5	0.4949	Gypsum	40.4723
23.558	4.74198	14.3	58.2	0.2891	-	
26.12	4.28388	112.2	566.2	0.3752	Gypsum	
26.649	4.20024	46.9	236.7	0.3342	Goethite	5.89122
29.367	3.81896	336.1	1162.3	0.2931	Gypsum	
33.54	3.355	22	167.7	0.6167	Quartz	2.763472
36.7	3.07482	107.4	455.2	0.3527	Calcite	13.49077
39.285	2.87974	59.4	217.6	0.3023	dolomite	7.461374
40.054	2.82666	25.6	93.8	0.3381	halite	3.215676
42.227	2.68735	47.6	211	0.374	Pyrite	5.979148
43.74	2.5987	16	71.1	0.3747	Gypsum	
44.817	2.53935	22	114	0.3754	-	
45.751	2.49023	18.2	94.1	0.35	Gypsum	
47.389	2.40883	18.8	78	0.3245	-	
51.667	2.22147	19.9	119.6	0.4425	Gypsum	
55.233	2.08825	25.3	256	0.7151	Gypsum	
58.084	1.99407	25.9	142.6	0.4116	-	
61.214	1.90126	61.7	379.2	0.4244	-	
65.95	1.77856	21.2	175.7	0.6341	-	
Total		796.1				

Table S10-8 X ray diffraction data of core 10 sample no.8
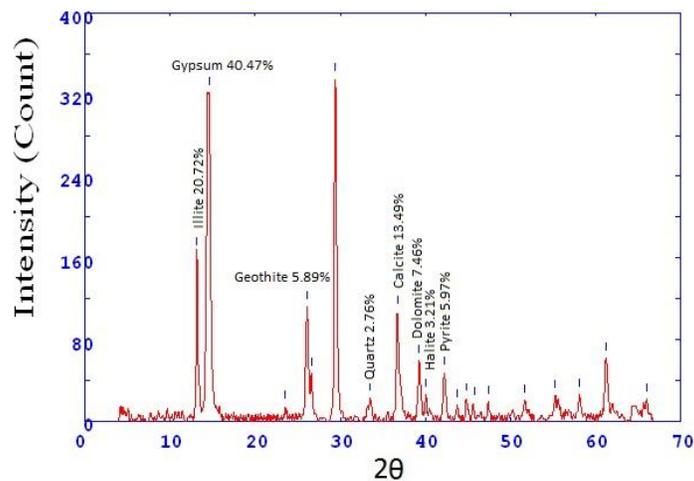
Fig.S13-8 X ray diffractogram of core 10 sample no.8

2Theta	d (A)	Height	Area	FWHM	Identified mineral	WT%
26.145	4.27986	17.5	42.6	0.2766	Goethite	4.995718
29.266	3.83178	16.2	107.1	0.5342	-	
32.967	3.41169	73.3	290.5	0.3406	Aragonite	20.92492
33.547	3.35431	51.7	204.8	0.5615	Quartz	0.147588
34.257	3.28678	49.4	195.6	0.672	feldspar (orthoclase)	14.1022
37.573	3.00589	92.1	1041.5	0.7824	calcite	26.29175
38.963	2.90255	19.8	223.7	0.5718	Dolomite	5.652298
40.207	2.81635	8.2	92.3	0.4664	halite	2.340851
41.272	2.74669	11.6	131.7	0.4138	-	
41.851	2.71036	38.3	170.1	0.3611	Pyrite	10.93349
45.747	2.49043	34.2	262.6	0.58	Quartz	
47.133	2.4212	12.8	98.3	0.4744	Aragonite	
48.033	2.37841	30.6	154.5	0.3688	Pyrite	
48.82	2.3424	23.5	118.8	0.6386	Gypsum	
50.152	2.28406	16.6	83.7	0.7734	Gypsum	
50.67	2.26222	19	234.4	0.9083	-	
52.65	2.18287	11.2	90.3	0.5666	calcite	
Total		350.3				

Table S10-9 X ray diffraction data of core 10 sample no.9
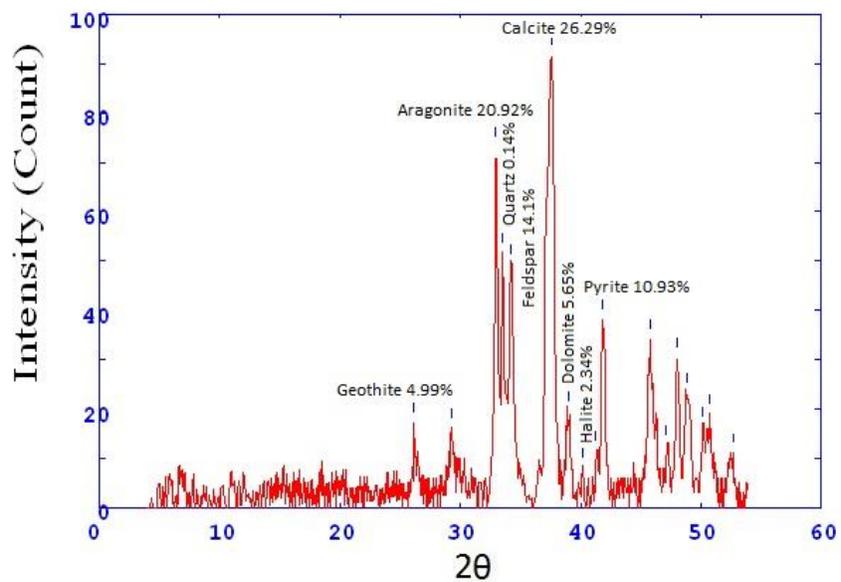
Fig.S13-9 X ray diffractogram of core 10 sample no.9

2Theta	d (A)	Height	Area	FWHM	Identified mineral	WT%
26.334	4.24966	14.8	55.2	0.3062	Goethite	4.766506
29.5	3.8021	14.4	82.4	0.4775	-	
30.065	3.73223	11.1	63.4	0.3829	-	
33.127	3.39568	79.8	246.6	0.2882	Aragonite	25.70048
34.413	3.27241	47.9	148	0.4741	Quartz	15.42673
37.767	2.99101	113.4	1019.1	0.6599	calcite	36.52174
40.236	2.81435	11.1	99.7	0.5267	dolomite	3.574879
42.016	2.70022	43.5	205.5	0.3934	Pyrite	14.00966
45.933	2.48086	40	281.3	0.5578	Quartz	
47.455	2.4057	17.9	125.7	0.5089	Aragonite	
48.233	2.36914	32.2	198.7	0.46	Gypsum	
48.931	2.33737	26.8	198.7	0.46	Aragonite	
Total		310.5				

Table S10-10 X ray diffraction data of core 10 sample no.10
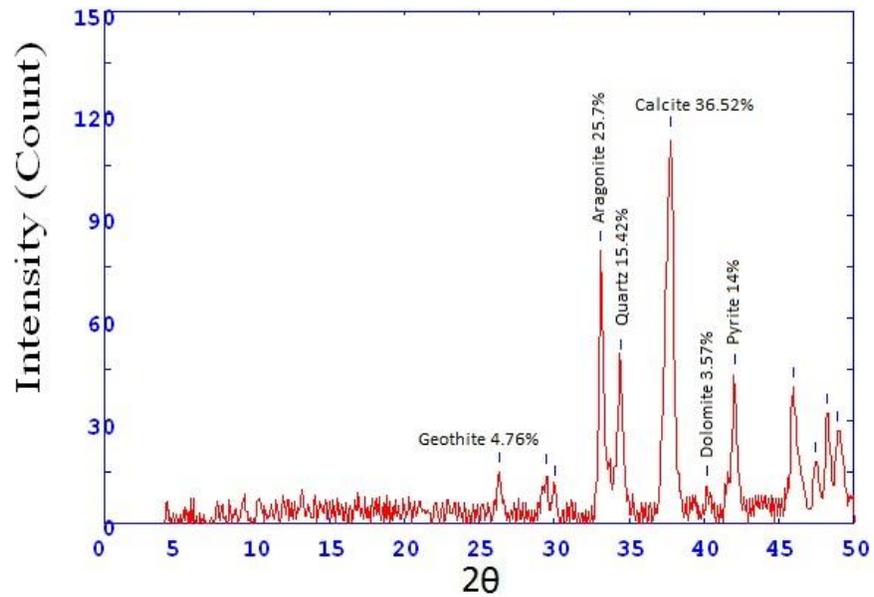
Fig.S13-10 X ray diffractogram of core 10 sample no.10

2Theta	d (A)	Height	Area	FWHM	Identified mineral	WT%
13.085	8.49562	27.5	771.1	0.2181	Illite	4.838142
14.479	7.68149	311.2	771.1	0.2181	gypsum	54.75018
26.025	4.29921	37.7	199.4	0.3953	gypsum	
29.39	3.81604	72.3	157.3	0.2621	gypsum	
32.854	3.42306	25.5	55.6	0.2432	aragonite	
33.534	3.3556	116.9	227.8	0.2243	quartz	20.5665
34.331	3.27999	19.7	38.3	0.2924	feldspar (orthoclase)	3.465869
36.545	3.0874	38.3	74.6	0.3605	gypsum	
37.193	3.03546	39	239.7	0.4968	calcite	6.861365
39.088	2.89366	12.8	78.8	0.3953	dolomite	2.251935
40.017	2.82916	23.7	87.6	0.2938	halite	4.169599
42.168	2.69091	17.6	161.3	0.6133	pyrite	3.096411
43.682	2.602	6.9	63.7	0.59	feldspar (orthoclase)	
45.767	2.48941	14.1	111.3	0.5667	aragonite	
47.947	2.38244	12.8	101	0.4655	gypsum	
48.733	2.34629	25	120	0.3643	aragonite	
Total		568.4				

Table S11-1X ray diffraction data of core 11sample no.1
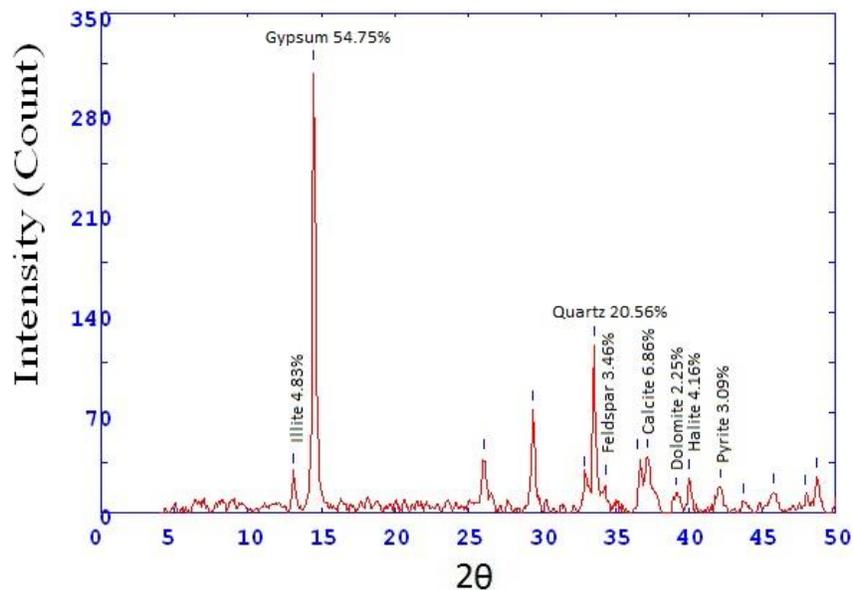
Fig.S14-1 X ray diffractogram of core 11 sample no.1

2Theta	d (A)	Height	Area	FWHM	Identified mineral	WT%
11.431	9.72024	33.2	496.1	0.9852	Illite	7.628676
13.025	8.53509	145	2166.7	0.7899	Illite	
14.567	7.63558	159.5	1492.7	0.5946	gypsum	36.64982
25.992	4.3045	46	174.4	0.3146	gypsum	
26.716	4.18996	26.8	101.5	0.3458	geothite	
29.367	3.81897	171.5	923.7	0.377	gypsum	
33.525	3.35643	59.6	173.8	0.2681	quartz	13.69485
34.433	3.27055	8.1	23.5	0.2858	feldspar (orthoclase)	1.861213
36.686	3.07595	66.6	206.4	0.3036	calcite	15.30331
39.259	2.88158	25.9	105.7	0.3451	dolomite	5.951287
42.149	2.69208	37.4	141.3	0.3329	pyrite	8.59375
44.808	2.53982	18.1	50.7	0.2667	Quartz	4.159007
Total		435.2				

Table S11-2X ray diffraction data of core 11sample no.2
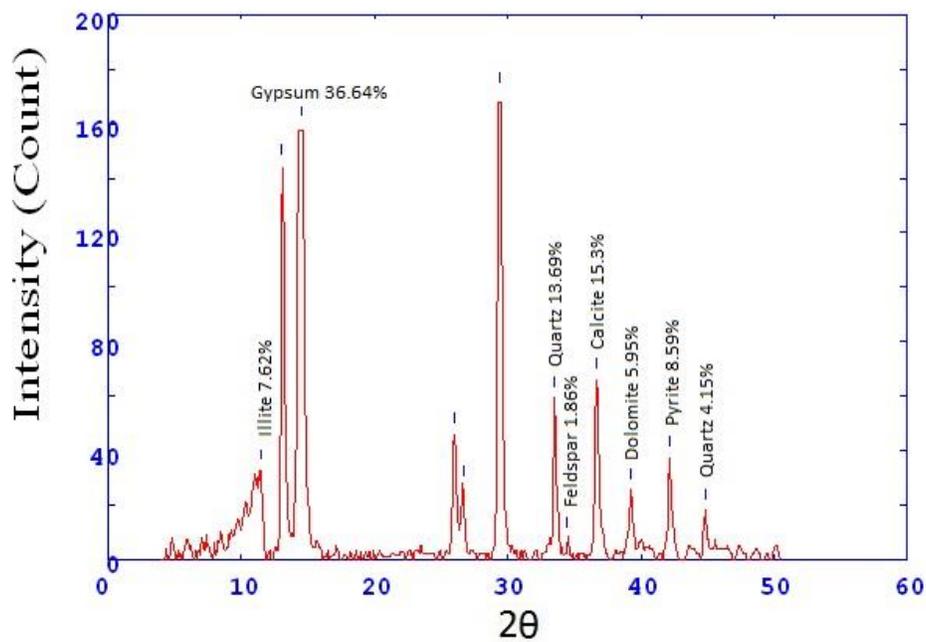
Fig.S14-2 X ray diffractogram of core 11 sample no.2

2Theta	d (A)	Height	Area	FWHM	Identified mineral	WT%
13.078	8.50026	258.4	2934.4	0.5637	Illite	33.25611
14.634	7.60093	322.3	2934.4	0.5637	gypsum	41.48005
15.765	7.05871	15.5	140.9	0.5067	gypsum	0
23.6	4.73375	13.5	74.6	0.4497	gypsum	
26.093	4.28811	117.9	599.8	0.3863	gypsum	
26.683	4.19496	49.6	252.1	0.3521	geothite	
29.5	3.80206	357.3	1249.3	0.3179	gypsum	
30.41	3.69092	30.9	107.9	0.2749	gypsum	
31.19	3.60084	26.5	92.5	0.2534	-	
33.553	3.35371	53	137.3	0.2319	quartz	6.821107
36.733	3.07214	77.7	241.6	0.2968	calcite	10
39.301	2.87863	25.7	147.7	0.456	dolomite	3.307593
40.115	2.8225	7.8	44.7	0.3746	halite	1.003861
42.189	2.68964	32.1	97.3	0.2933	pyrite	4.131274
43.668	2.60276	5.6	16.9	0.1467	gypsum	
44.708	2.54522	8.9	0	0	calcite	
50.081	2.28707	6.7	0	0	gypsum	
51.641	2.22252	10	0	0	-	
Total		777				

Table S11-3X ray diffraction data of core 11sample no.3
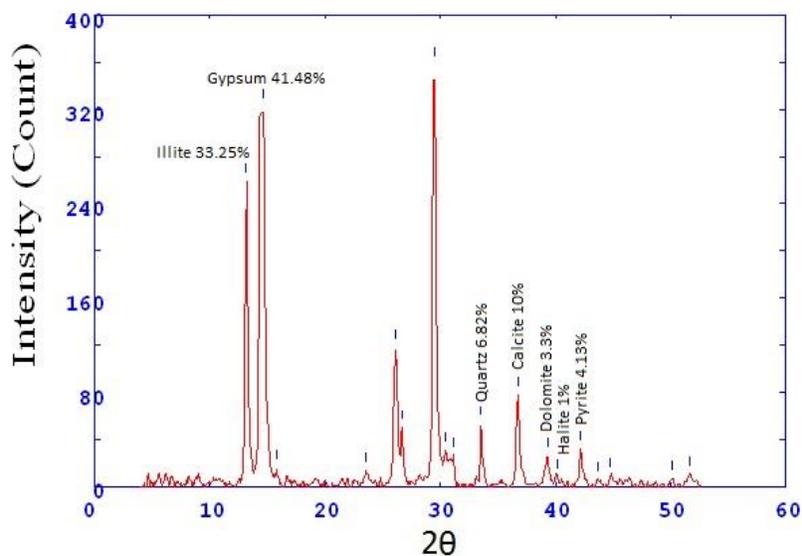
Fig.S14-3 X ray diffractogram of core 11 sample no.3

2Theta	d (A)	Height	Area	FWHM	Identified mineral	WT%
13.15	8.45396	160.8	85.2	0.3255	Illite	17.24212
14.521	7.65931	316.2	85.2	0.3255	gypsum	33.90521
15.978	6.96482	16.1	4.3	0.3255	-	
23.699	4.71427	17.1	85.2	0.3255	-	
26.135	4.28143	143.9	458.1	0.3115	Gypsum	
26.692	4.19364	43.7	139.3	0.2908	Goethite	0
29.515	3.80019	337.2	1044.5	0.2702	gypsum	
33.677	3.34179	115.6	334.5	0.242	Quartz	12.39545
35.434	3.18097	29.9	86.5	0.2725	feldspar (Albite)	3.20609
36.838	3.0637	184.6	724.3	0.303	calcite	19.79412395
39.398	2.87178	54.8	439.1	0.5693	dolomite	5.876045
40.234	2.81454	20.3	162.8	0.4656	halite	2.17671
42.31	2.68233	50.4	241.7	0.3619	pyrite	5.404246
43.833	2.59343	8.6	41.2	0.3344	Gypsum	
44.948	2.53235	21.2	91.6	0.3069	gypsum	
50.264	2.27929	22	80.2	0.2841	gypsum	
51.8	2.21615	24	84.9	0.3139	gypsum	
Total		932.6				

Table S11-4 X ray diffraction data of core 11sample no.4
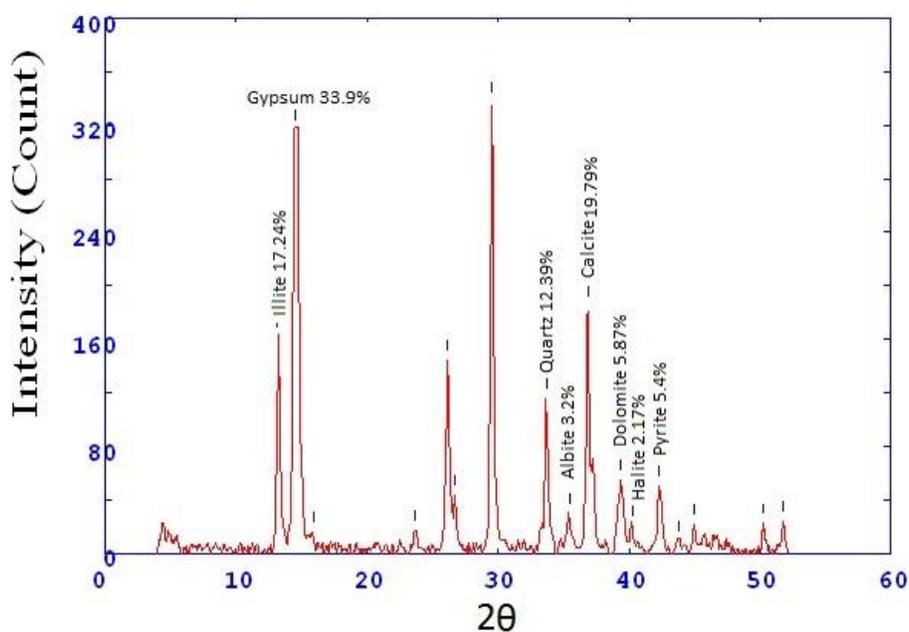
Fig.S14-4 X ray diffractogram of core 11 sample no.4

2Theta	d (A)	Height	Area	FWHM	Identified mineral	WT%
13.046	8.5212	230.9	2673.3	0.5535	Illite	27.12004
14.516	7.66217	317.4	3675.5	0.3844	Gypsum	37.27977
15.741	7.06918	17.2	199	0.2998	-	
23.594	4.73486	20.3	38	0.2152	-	
26.043	4.29618	200.3	581.8	0.2689	gypsum	
26.603	4.20735	63.1	183.3	0.2939	Goethite	
29.434	3.81042	347.1	1220.3	0.319	gypsum	0
33.149	3.39345	17.4	39.1	0.2182	Quartz	2.043693
36.692	3.0755	159.7	633.1	0.3195	calcite	18.75734085
39.223	2.88408	53.2	230.7	0.3593	Dolomite	6.248532
40.569	2.79223	11.8	51.3	0.3515	gypsum	
42.126	2.69348	72.8	320.4	0.3437	Pyrite	8.550623
43.591	2.60714	7.6	33.3	0.3206	gypsum	
44.75	2.54296	27.4	95.5	0.2975	gypsum	
45.388	2.50907	12.9	45.1	0.1488	-	
46.368	2.45887	11.8	0	0	gypsum	
Total		851.4				

Table S11-5X ray diffraction data of core 11sample no.5
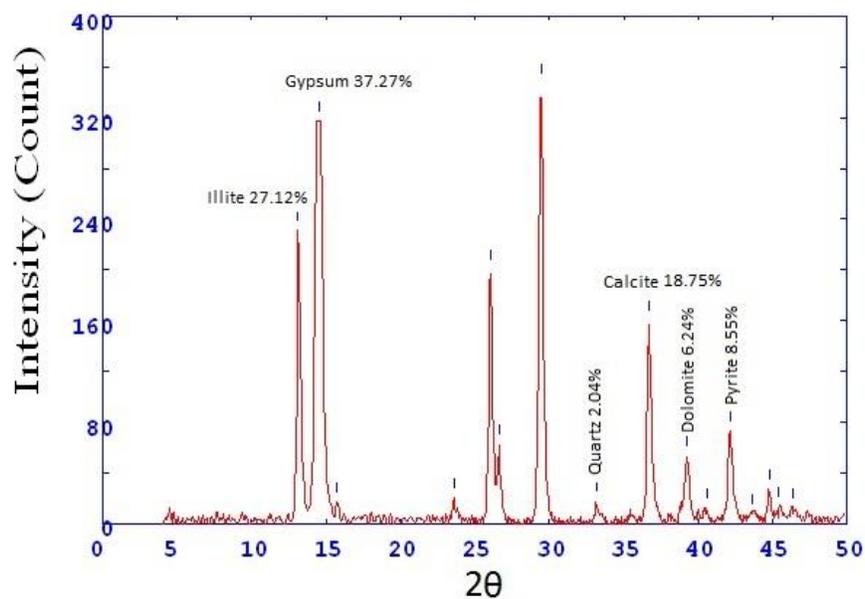
Fig.S14-5 X ray diffractogram of core 11 sample no.5

2Theta	d (A)	Height	Area	FWHM	Identified mineral	WT%
14.568	7.63516	21.9	69.2	0.2894	gypsum	5.968929
26.273	4.25925	14	96	0.5222	gypsum	0
29.873	3.75563	13.9	48.4	0.2814	gypsum	
33.018	3.40653	102.9	399.2	0.3424	aragonite	28.04579
33.566	3.35251	66.6	258.6	0.5313	quartz	18.15209
34.272	3.2854	59.2	229.8	0.6258	orthoclase (feldspar)	16.13519
37.54	3.00842	38.8	150.7	0.4192	calcite	10.57509
39.218	2.88444	8.4	32.7	0.3159	dolomite	2.289452
40.056	2.82654	17.1	39.1	0.2126	halite	0.770384
41.338	2.74252	15.2	34.8	0.2843	-	
41.888	2.70807	52	216.7	0.356	pyrite	14.172799
43.192	2.63004	6.5	27	0.5535	-	
43.94	2.58744	6.5	55.9	0.7509	-	
45.752	2.49017	36.8	212	0.434	gypsum	
47.079	2.42382	18.5	106.2	0.4225	pyrite	
48.052	2.37753	39.6	206.7	0.411	pyrite	
48.757	2.34524	36.2	189	0.5132	gypsum	
50.7	2.26095	6.8	57.9	0.6153	-	
52.433	2.19125	12.6	112.6	0.568	gypsum	
Total		366.9				

Table S11-6X ray diffraction data of core 11sample no.6
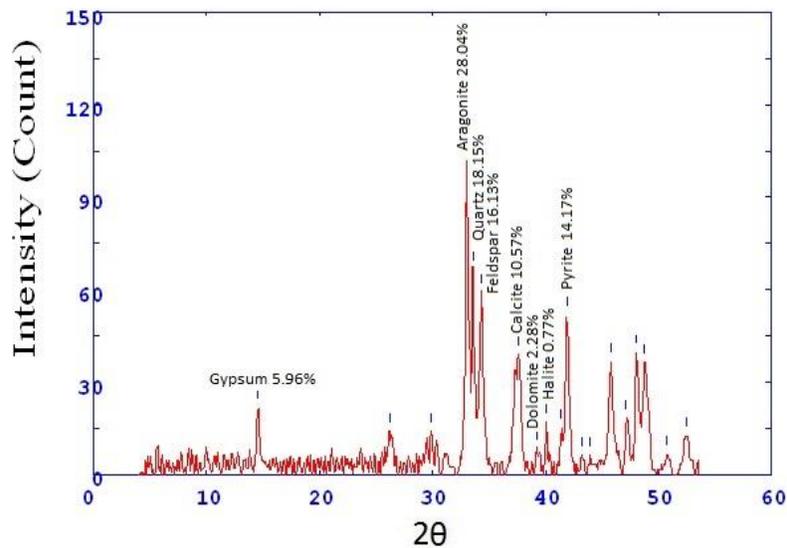
Fig.S14-6 X ray diffractogram of core 11 sample no.6

2Theta	d (A)	Height	Area	FWHM	Identified mineral	WT%
11.154	9.96052	13.3	34.8	0.281	Illite	3.066635923
13.156	8.44991	163.1	428.7	0.3976	Illite	
14.64	7.59788	322.1	2402.1	0.5142	gypsum	74.26792714
23.684	4.71709	9.7	72.2	0.4608	-	
26.081	4.29008	103.9	535.1	0.4074	gypsum	
26.654	4.19956	35.3	181.6	0.3319	Goethite	0
29.479	3.8047	337.3	966.5	0.2563	gypsum	
33.595	3.34968	83.5	314.1	0.2918	quartz	19.25293982
35.472	3.1777	11.8	44.4	0.298	feldspar (Albite)	2.720774729
36.786	3.06789	119.3	454.8	0.3041	-	
38.081	2.96722	7.5	28.8	0.4539	calcite	1.729305972
39.318	2.87737	48.7	376.4	0.6036	dolomite	11.22896011
40.061	2.82618	25.7	198.3	0.4921	halite	5.92575513
42.256	2.68556	44.8	226.1	0.3806	pyrite	10.32972101
43.66	2.60322	11.8	59.5	0.3713	-	
44.83	2.53867	19.3	97.2	0.3621	-	
45.675	2.49415	24.1	101.4	0.3436	gypsum	
50.154	2.28397	18.4	68.3	0.3392	feldspar (Albite)	
51.768	2.21742	22.7	120.6	0.4082	-	
54.089	2.12901	16.2	94.8	0.5283	-	
Total		433.7				

Table S11-7X ray diffraction data of core 11sample no.7
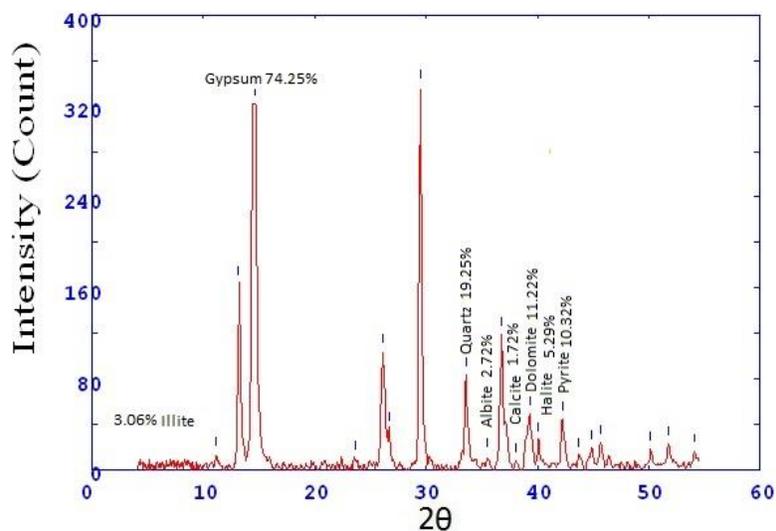
Fig.S14-7 X ray diffractogram of core 11 sample no.7

2Theta	d (A)	Height	Area	FWHM	Identified mineral	WT%
13.194	8.42603	75.4	1795.1	0.3764	Illite	8.070213
14.51	7.66524	323.2	7690.2	0.38	gypsum	34.59274
23.724	4.70933	8.3	198.5	0.3818	-	
26.242	4.26418	71.4	338.3	0.3836	gypsum	0
27.673	4.04778	5.2	24.8	0.3181	-	
29.478	3.80485	136.8	396.4	0.2526	gypsum	
30.387	3.69357	24.9	72	0.2516	-	
33.102	3.39812	33.1	95.9	0.2511	aragonite	3.542759
33.619	3.34734	327.7	925.7	0.2506	quartz	35.07439
35.329	3.19008	35.6	200.3	0.3887	feldspar (Albite)	
36.804	3.06644	39.3	221.4	0.4389	feldspar (Albite)	4.206358
37.246	3.03128	57.9	350.9	0.489	calcite	6.197153
39.151	2.88919	29.1	296.5	0.6689	dolomite	3.114631
40.095	2.8239	25.9	264.2	0.6163	halite	2.772129
41.967	2.70324	22.7	202.1	0.5636	pyrite	2.429626
45.767	2.48941	19.4	145.8	0.53	feldspar (Albite)	
48.1	2.37531	14.5	54.8	0.2686	feldspar (Albite)	
Total		934.3				

Table S11-8X ray diffraction data of core 11sample no.8
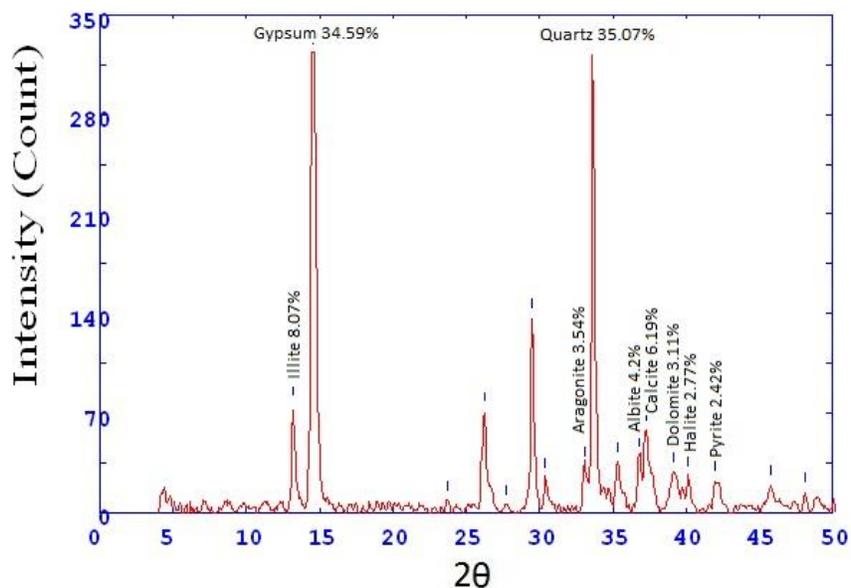
Fig.S14-8 X ray diffractogram of core 11 sample no.8

2Theta	d (A)	Height	Area	FWHM	Identified mineral	WT%
26.162	4.27704	57.1	155.2	0.2525	-	0
29	3.8662	17	52	0.2888	-	
30.362	3.69663	27.2	96	0.2949	feldspar	
32.87	3.42147	45.4	160.6	0.2799	aragonite	7.706671
33.567	3.35241	264.5	753.7	0.265	quartz	44.899
34.575	3.25751	65.3	186.2	0.415	feldspar (orthoclase)	11.08471
35.238	3.1981	35.9	102.2	0.49	feldspar (albite)	6.094042
37.21	3.03418	88.1	658.1	0.5651	calcite	14.95502
39.043	2.89686	39.8	206.7	0.4117	dolomite	6.756069
40.069	2.82562	14.4	74.8	0.3346	halite	2.444407
41.872	2.70909	35.7	101.7	0.2575	pyrite	6.060092
45.748	2.49039	27	132	0.4045	aragonite	
47.269	2.41463	10.4	51	0.379	aragonite	
47.932	2.38316	12.8	62.7	0.3534	feldspar (Albite)	
48.879	2.33973	13.6	66.6	0.3279	feldspar (Albite)	
50.11	2.28585	37.4	120	0.3023	feldspar (Albite)	
52.333	2.19514	12	48	0.3222	feldspar (Albite)	
54.067	2.12982	12	38.7	0.3	aragonite	
Total		589.1				

Table S11-9X ray diffraction data of core 11sample no.9
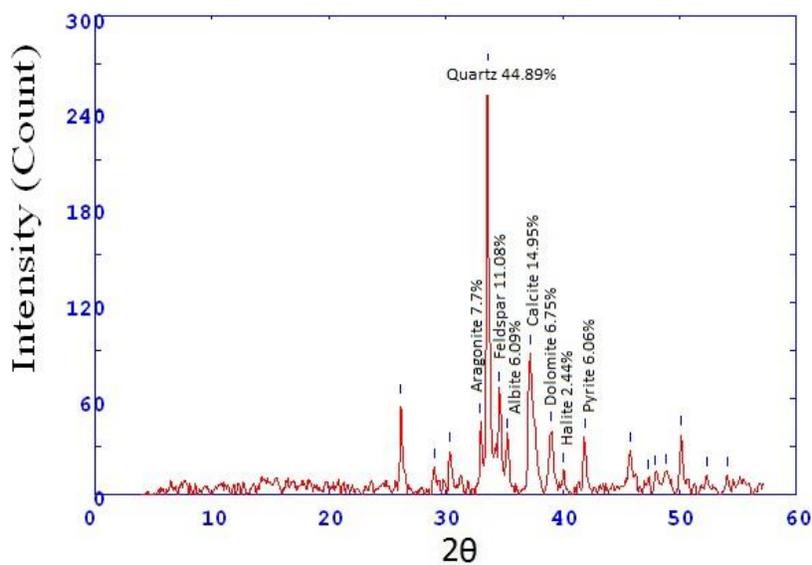
Fig.S14-9 X ray diffractogram of core 11 sample no.9

2Theta	d (A)	Height	Area	FWHM	Identified mineral	WT%
14.569	7.63443	15.3	40.3	0.2568	gypsum	2.32311
15.407	7.22146	11.7	30.8	0.2559	-	
17.058	6.52712	25.3	66.2	0.2549	-	0
22.473	4.96771	8	53.1	0.4604	-	
26.16	4.27743	84.7	249.3	0.2594	gypsum	
29.085	3.85519	13.1	38.5	0.2549	-	
30.32	3.7016	23.8	49.9	0.2505	-	
31.429	3.57404	9.7	20.3	0.2517	-	
32.895	3.41893	35.1	73.5	0.2522	Aragonite	5.329487
33.549	3.35414	218.4	605	0.2528	quartz	33.16125
34.653	3.25035	72.8	201.6	0.3132	feldspar (orthoclase)	11.05375038
35.24	3.19796	37.1	102.8	0.3434	feldspar , Albite	5.633161
37.177	3.03676	103.7	497.7	0.3736	calcite	15.74552
38.953	2.90333	79.2	396.6	0.3926	feldspar (orthoclase)	
40.027	2.82849	62.5	312.9	0.3362	halite	9.489827
41.862	2.7097	29	109.6	0.2797	pyrite	4.40328
45.693	2.49319	23.4	88.3	0.2806	gypsum	
46.308	2.46186	41.9	134.2	0.2814	feldspar (orthoclase)	
48.084	2.37607	13.9	59.6	0.3432	pyrite	
48.624	2.35124	12.4	53.3	0.3252	gypsum	
50.167	2.2834	38.1	147.5	0.3071	calcite	
52.271	2.19758	20.2	85.8	0.4221	gypsum	
55.1	2.09292	13.4	120	0.6429	calcite	
57.905	1.99968	19.3	173.2	0.5592	feldspar (orthoclase)	
58.467	1.98216	23.9	145.2	0.4755	feldspar (orthoclase)	
Total		658.6				

Table S11-10X ray diffraction data of core 11sample no.10
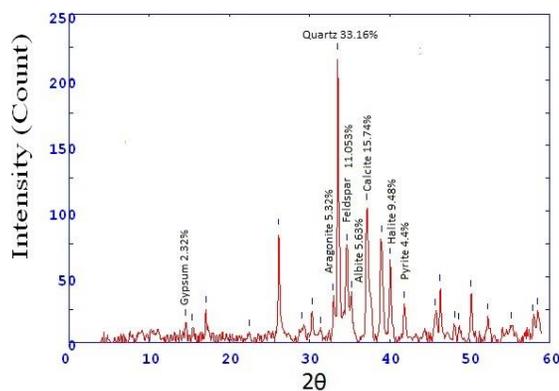
Fig.S14-10 X ray diffractogram of core 11 sample no.10

2Theta	d (A)	Height	Area	FWHM	Identified mineral	WT%
6.57	16.89327	17.1	96	0.4417	Montmorillonite	3.085528
15.768	7.05719	10.3	57.5	0.5417	gypsum	1.8585348
23.664	4.72114	14	22.6	0.1632	-	
25.122	4.45102	11.9	19.2	0.205	-	0
26.161	4.27723	85.9	172.9	0.2467	gypsum	
29.054	3.85916	14.4	28.9	0.2544	calcite	
30.316	3.70204	23.5	68.1	0.2621	-	
32.986	3.40978	22	63.8	0.2519	Aragonite	3.9696860
33.542	3.35481	265.6	727.6	0.2417	quartz	47.924936
35.17	3.2041	24.5	67.1	0.3417	feldspar (Albite)	4.4207867
37.167	3.03756	98.2	482.6	0.4418	calcite	17.719234
39.01	2.89921	62.6	248.4	0.3787	dolomite	11.295561
39.975	2.83198	28.7	114	0.4163	halite	5.1786358
41.835	2.71137	25.2	135.5	0.4538	pyrite	4.5470949
45.71	2.49235	28.4	146.6	0.416	gypsum	
48.101	2.37529	16.1	83	0.4093	pyrite	
48.887	2.33937	16.1	83	0.4026	gypsum	
50.11	2.28585	31.2	149.1	0.3892	calcite	
52.25	2.19839	16.8	69.8	0.3453	gypsum	
Total		554.2				

Table S11-11X ray diffraction data of core 11sample no.11
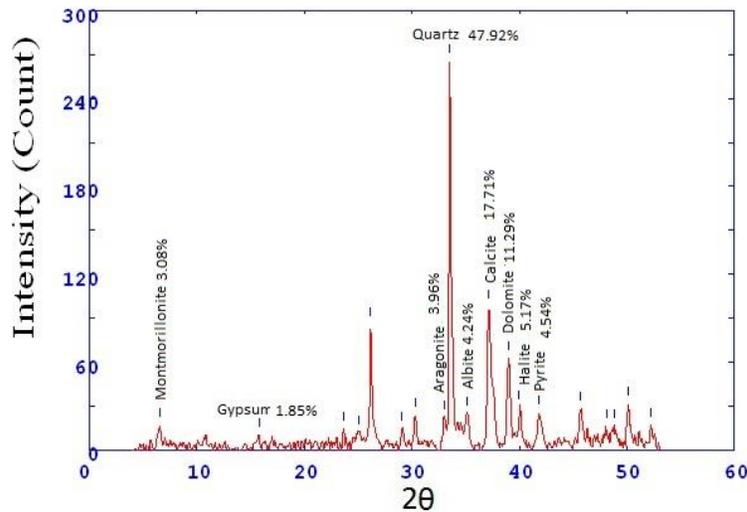
Fig.S14-11 X ray diffractogram of core 11 sample no.11

2Theta	d (A)	Height	Area	FWHM	Identified mineral	WT%
26.225	4.26691	74.8	157.4	0.259	-	
29.169	3.84427	9.1	19.2	0.2647	calcite	0
30.4	3.69211	29.2	84.8	0.2704	-	
31.241	3.5951	9.1	26.5	0.2668	-	
32.981	3.41029	23.2	67.4	0.2633	Aragonite	3.754653
33.611	3.34812	318.1	906.5	0.2561	Quartz	51.48082
34.638	3.25178	42.4	120.7	0.3253	feldspar (orthoclase)	6.861952
35.301	3.19261	11.2	31.8	0.36	feldspar (Albite)	1.812591
37.233	3.03231	109.1	544.6	0.3946	calcite	17.65658
39.101	2.89275	66.8	450	0.4976	Dolomite	10.81081
40.106	2.8231	23.2	156.5	0.4179	halite	3.754653
41.9	2.70737	23.9	99.4	0.3382	pyrite	3.86794
44.166	2.57484	6.1	25.5	0.3266	-	
45.741	2.49074	19.2	79.9	0.315	calcite	
46.35	2.45977	28.8	101	0.2918	-	
47.398	2.40842	8.1	28.5	0.3062	-	
48.061	2.37713	7.1	25	0.3134	pyrite	
48.889	2.33926	5.1	17.9	0.317	gypsum	
50.248	2.27995	30.9	137.8	0.3206	gypsum	
Total		617.9				

Table S11-12X ray diffraction data of core 11sample no.12
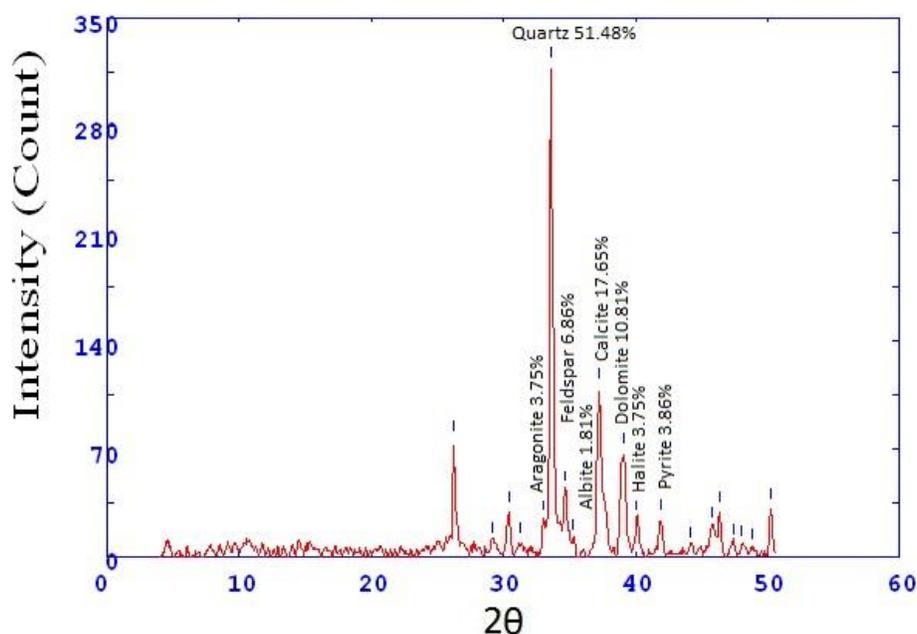
Fig.S14-12 X ray diffractogram of core 11 sample no.12

2Theta	d (A)	Height	Area	FWHM	Identified mineral	WT%
12.975	8.50772	40.1	1397	0.3309	Illite	6.78625825
14.434	7.67568	326.8	1397	0.3309	Gypsum	55.30546624
25.953	4.31094	63.8	328.6	0.412	Gypsum	
29.344	3.82189	80.3	242.9	0.2732	gypsum	
32.85	3.42345	34.9	105.7	0.2686	-	
33.472	3.33165	71.8	207.9	0.264	Quartz	12.15095617
34.307	3.28221	17.5	50.7	0.5412	feldspar	2.961584024
35.42	3.18217	9.3	26.9	0.6799	feldspar(Albite)	1.573870367
36.678	3.07663	66	727.3	0.8185	Gypsum	
37.134	3.03016	62.6	689.7	0.6471	Calcite	10.59400914
39.221	2.88423	27	159.7	0.4758	dolomite	4.569301066
39.789	2.84467	18.5	109.5	0.5747	dolomite	
42.085	2.69597	35.8	339.1	0.6736	pyrite	6.058554747
Total		590.9				

Table S12-1 X ray diffraction data of core 12 sample no.1
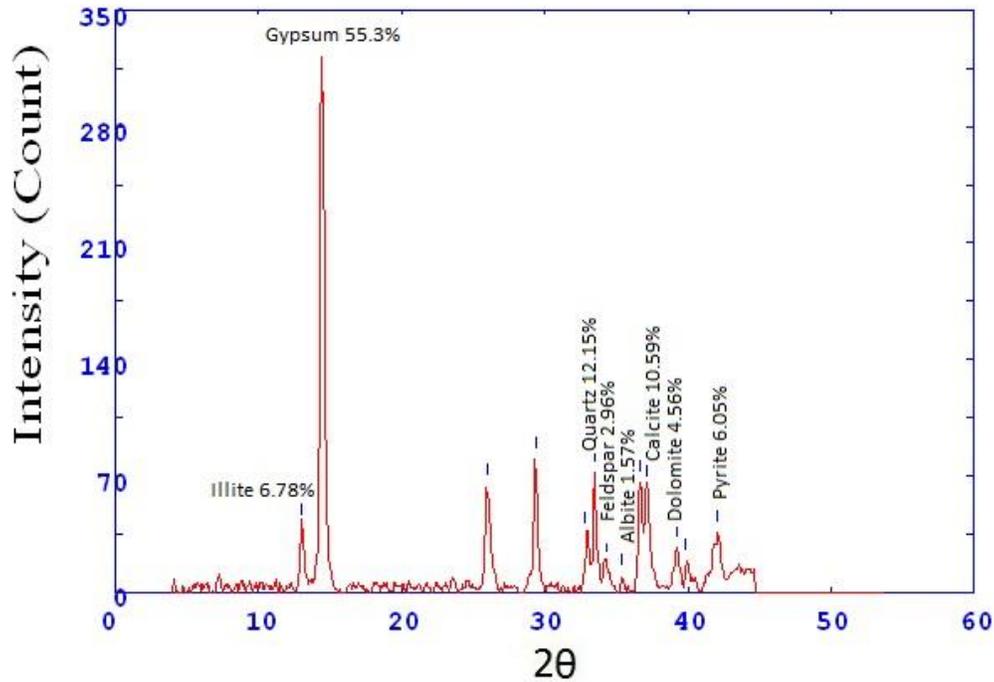
Fig.S15-1 X ray diffractogram of core 12 sample no.1

2Theta	d (A)	Height	Area	FWHM	Identified mineral	WT%
13.249	8.39123	41.4	1689.8	0.3565	Illite	6.461682535
14.633	7.601	331.7	1689.8	0.3565	Gypsum	51.77149992
26.156	4.278	75.1	304	0.3578	Gypsum	
29.53	3.79827	91.1	270.9	0.2799	Gypsum	
33.104	3.39795	75	359.2	0.3984	Aragonite	11.70594662
33.645	3.3448	50.7	242.9	0.3812	Quartz	7.913219916
34.48	3.26622	41.4	198.4	0.3726	feldspar	6.461682535
36.826	3.06465	66	264.3	0.364	Gypsum	
37.354	3.02288	35.2	140.9	0.3218	Calcite	5.493990947
39.414	2.87071	26.9	79.3	0.2796	dolomite	4.198532855
41.993	2.70163	38.4	294.6	0.6176	Pyrite	2.107070392
43.751	2.59808	13.5	103.6	0.5926	Quartz	
45.866	2.48429	33.3	262.5	0.5675	Aragonite	
48.108	2.37493	20.7	163.6	0.5059	Aragonite	
48.862	2.3405	26.4	140.4	0.4444	Aragonite	
51.724	2.21918	11.4	60.8	0.4041	Gypsum	
52.451	2.19058	13.5	75.2	0.3638	Gypsum	
54.733	2.10584	19.9	113.8	0.4712	Aragonite	
Total		640.7				

Table S12-2 X ray diffraction data of core 12 sample no.2
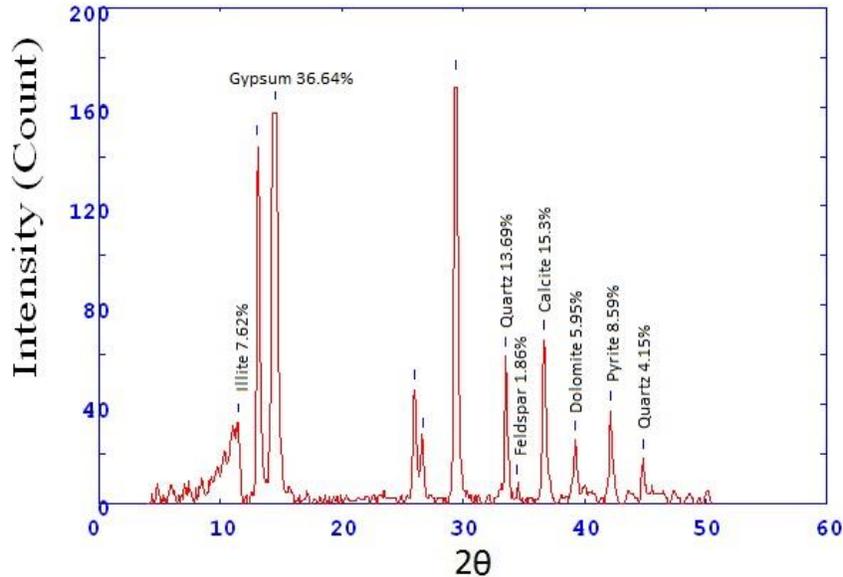
Fig.S15-2 X ray diffractogram of core 12 sample no.2

2Theta	d (A)	Height	Area	FWHM	Identified mineral	WT%
13.22	8.40944	32.3	1019.3	0.28	Illite	4.594594595
14.598	7.61946	326.4	1019.3	0.28	Gypsum	46.42958748
23.634	4.72692	13.1	53.5	0.3608	-	
26.146	4.27965	62.6	248.4	0.3395	Gypsum	
29.513	3.8004	55	205.6	0.2971	Gypsum	
33.045	3.40387	78	291.8	0.2839	Aragonite	11.09530583
33.699	3.33965	117.7	336.1	0.2707	Quartz	16.74253201
34.389	3.27462	44.8	127.8	0.2983	feldspar (orthoclase)	6.372688478
36.829	3.06445	58	234	0.3259	Gypsum	
37.329	3.02484	27.1	109.3	0.3217	Calcite	3.854907539
39.394	2.8721	29.8	92.1	0.3175	dolomite	4.238975818
41.958	2.70379	46.9	311.4	0.5299	pyrite	6.67140825
42.369	2.67874	33.3	221.4	0.5348	Gypsum	
45.767	2.48941	30	194	0.5397	Quartz ,Aragonite	
48.142	2.37338	29.8	167.6	0.4552	Aragonite	
48.837	2.34162	26.1	0	0	anhydrite	
Total		703				

Table S12-3 X ray diffraction data of core 12 sample no.3
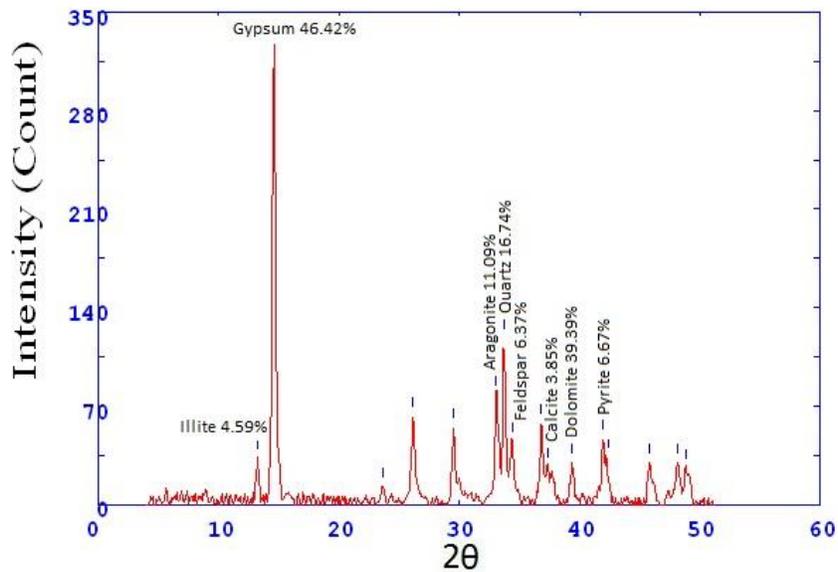
Fig.S15-3 X ray diffractogram of core 12 sample no.3

2Theta	d (A)	Height	Area	FWHM	Identified mineral	WT%
12.973	8.56908	16.3	37.6	0.273	Illite	2.788708298
15.662	7.14458	10.9	37.6	0.273	Gypsum	1.864841745
26.213	4.26888	68.2	182	0.2559	Gypsum	
27.72	4.04102	39	76.1	0.2294	-	
30.387	3.69362	36.7	113.5	0.2593	dolomite	
31.379	3.57967	12	37.1	0.2708	feldspar	
32.976	3.41079	26	80.5	0.2765	Aragonite	
33.603	3.34886	339.4	1126.7	0.2823	Quartz	58.0667237
34.572	3.25774	34.7	115	0.2814	feldspar (orthoclase)	5.936698033
35.329	3.19014	12	39.7	0.281	feldspar (Albite)	
37.212	3.03397	83.9	244.8	0.2806	calcite	14.35414885
39.086	2.89381	59.8	297.9	0.3958	dolomite	10.23096664
40.119	2.82222	17.4	86.5	0.3375	halite	2.976903336
41.88	2.70858	22.1	71.7	0.2791	pyrite	3.78100941
43.986	2.58491	9.8	31.8	0.344	feldspar (orthoclase)	
45.7	2.49284	20	104	0.4088	Quartz	
47.179	2.41894	9.8	51	0.296	Aragonite	
48.026	2.37876	12.7	20	0.1832	pyrite	
50.157	2.28382	31.4	98.6	0.2687	Quartz	
Total		584.5				

Table S12-4 X ray diffraction data of core 12 sample no.4
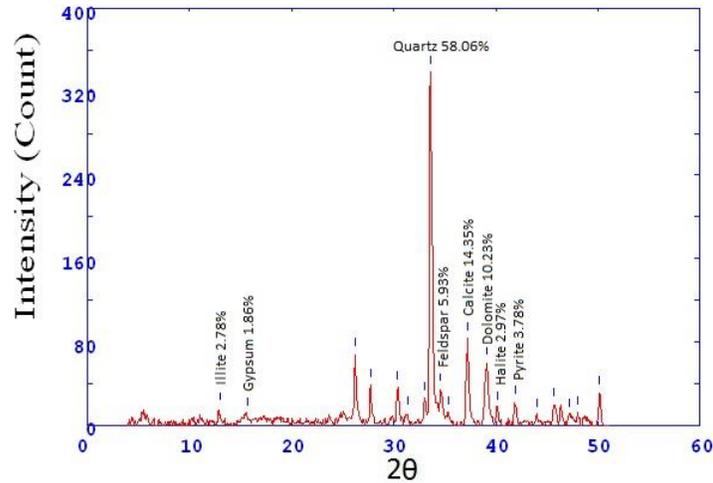
Fig.S15-4 X ray diffractogram of core 12 sample no.4

2Theta	d (A)	Height	Area	FWHM	Identified mineral	WT%
13.223	8.40755	77.2	1993	0.4373	Illite	10.49055578
14.7	7.56674	348.8	1993	0.4373	gypsum	47.39774426
23.675	4.71894	11.9	30	0.291	-	
26.158	4.27775	87.4	358.4	0.3694	gypsum	
26.746	4.18531	19.4	79.4	0.3169	Geothite	2.636227748
29.534	3.79782	163.3	473.3	0.2645	gypsum	
33.08	3.40036	51.5	149.2	0.2733	anhydrite	
33.681	3.34138	56.7	160.1	0.2821	Quartz	7.704851203
34.363	3.27694	25.8	72.8	0.3164	feldspar (orthoclase)	3.505911129
35.476	3.17732	8.7	24.4	0.3336	feldspar (Albite)	
36.869	3.06122	102.4	401.8	0.3507	calcite	13.91493409
37.445	3.01581	47.2	185.3	0.3975	Calcite	
39.4	2.87163	36.6	212.7	0.4442	feldspar (orthoclase)	4.973501834
40.269	2.81216	15.1	87.7	0.5333	halite	2.051909227
42.262	2.68521	39	306.7	0.6223	pyrite	5.299633102
43.778	2.59654	5.4	42.8	0.5143	gypsum	
45.867	2.48427	27	140	0.4063	anhydrite	
47.373	2.40962	6.5	33.8	0.3732	Gypsum	
48.138	2.37354	20	84	0.34	pyrite	
48.914	2.33817	10.8	45.3	0.3467	gypsum	
51.8	2.21615	14	60	0.3533	gypsum	
Total		735.9				

Table S12-5 X ray diffraction data of core 12 sample no.5
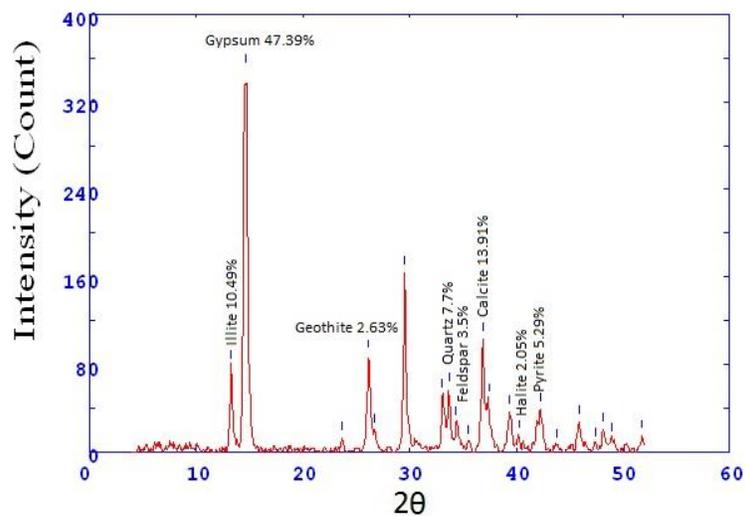
Fig.S15-5 X ray diffractogram of core 12 sample no.5

2Theta	d (A)	Height	Area	FWHM	Identified mineral	WT%
14.572	7.63263	49.6	96.1	0.2098	Gypsum	9.53479431
26.211	4.26917	40.2	113.7	0.257	gypsum	0
28.471	3.9365	5.3	15.1	0.3687	-	
29.216	3.83826	11.2	31.7	0.4245	gypsum	
29.766	3.76882	20	127.1	0.4804	Gypsum	
30.374	3.69514	16	101.3	0.3646	dolomite	
33.022	3.40615	89.2	566.3	0.3068	Aragonite	17.14725106
33.582	3.35088	168.8	361.8	0.2489	Quartz	32.44905805
34.263	3.28627	46.2	99	0.4042	feldspar (orthoclase)	8.881199539
35.173	3.20382	4.8	10.3	0.4819	feldspar (Albite)	
37.151	3.03878	34.8	243.1	0.5596	calcite	6.689734717
39.062	2.89553	37.7	263.6	0.4389	dolomite	7.247212611
40.086	2.82448	40	157.2	0.3181	halite	7.247212611
41.9	2.70735	53.9	177.3	0.3157	pyrite	10.36139946
43.613	2.60592	5.9	19.4	0.3504	-	
45.796	2.48788	37	160	0.3852	gypsum	
46.26	2.46428	16.5	71.3	0.3651	Aragonite	
47.336	2.4114	18.6	80.5	0.3451	Aragonite	
48.033	2.37841	37	145.3	0.3049	pyrite	
48.825	2.34215	25	0	0	gypsum	
Total		520.2				

Table S12-6 X ray diffraction data of core 12 sample no.6
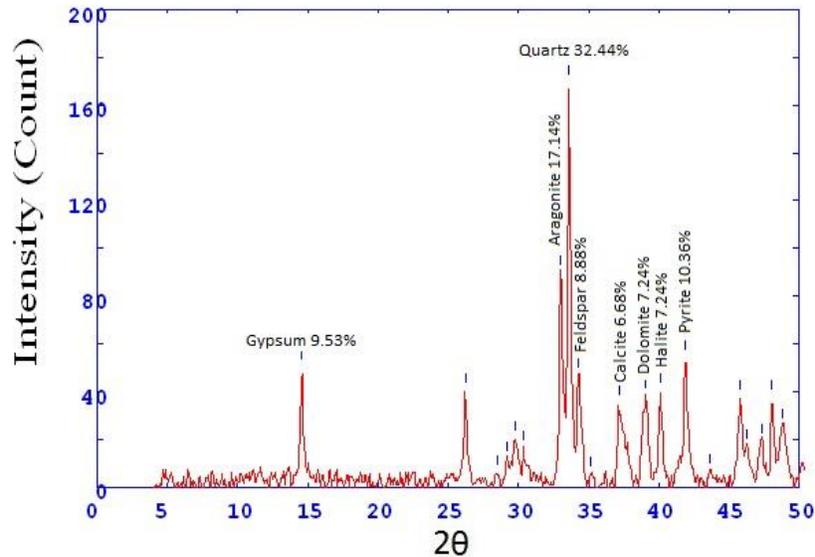
Fig.S15-6 X ray diffractogram of core 12 sample no.6

2Theta	d (A)	Height	Area	FWHM	Identified mineral	WT%
26.233	4.26562	36.5	108	0.2689	-	0
30.393	3.69288	37	104.8	0.2492	dolomite	
33.014	3.40694	57.4	162.8	0.2472	Aragonite	
33.6	3.34922	346.3	1019.9	0.2453	Quartz	62.75824574
34.364	3.27686	27.7	81.4	0.5125	feldspar (orthoclase)	5.019934759
35.293	3.19329	11.1	32.7	0.6462	feldspar (Albite)	2.011598405
37.269	3.02949	68.5	759.2	0.7798	calcite	12.41391809
39.006	2.89948	27.7	306.7	0.5521	dolomite	5.019934759
40.188	2.8176	15.5	172.2	0.4382	halite	2.808988764
41.93	2.70551	55	207.8	0.3243	pyrite	9.967379485
45.793	2.48803	34.7	257.6	0.5446	-	
47.278	2.41419	15.5	115.2	0.4879	Aragonite	
48.05	2.37764	24.7	136.1	0.4313	pyrite	
48.797	2.34341	21	115.8	0.2156	Aragonite	
50.316	2.27706	15.5	0	0	-	
Total		551.8				

Table S12-7 X ray diffraction data of core 12 sample no.7
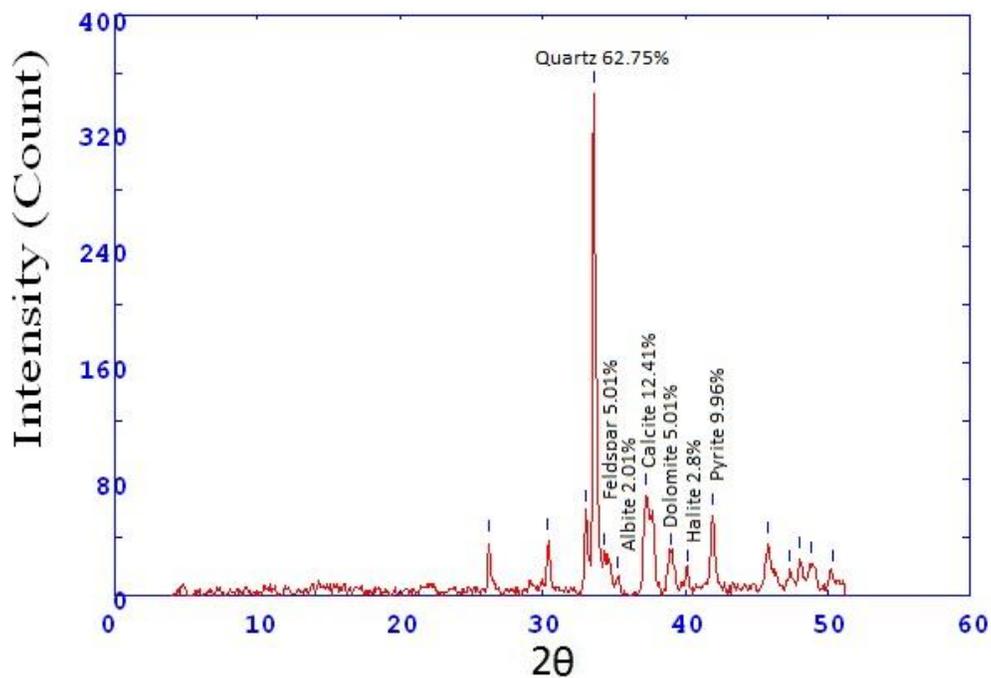
Fig.S15-7 X ray diffractogram of core 12 sample no.7

2Theta	d (A)	Height	Area	FWHM	Identified mineral	WT%
23.767	4.70096	15.4	30.7	0.189	-	
26.236	4.26528	95.3	205.3	0.2405	-	
29.135	3.84865	10.5	22.6	0.2464	-	
30.4	3.69209	78.9	219.2	0.2523	dolomite	
32.892	3.41921	36.5	101.4	0.2985	Aragonite	5.916680175
33.567	3.35241	347	1471.6	0.3447	Quartz	56.24898687
34.689	3.24714	38.5	163.5	0.3662	feldspar(orthoclase)	6.240881828
35.261	3.19612	31.3	132.6	0.377	feldspar (Albite)	5.073755876
37.242	3.0316	94.5	424.6	0.3878	calcite	15.31852812
39.11	2.89208	21.7	128.1	0.4701	dolomite	3.51758794
40.079	2.82494	17.8	104.7	0.3671	halite	2.885394716
41.913	2.70657	29.6	89.4	0.2641	pyrite	4.798184471
45.633	2.49631	24	72.5	0.3654	Aragonite	
46.333	2.46061	28	142.3	0.4667	Aragonite	
48.852	2.34092	16.2	126.7	0.5917	gypsum	
Total		616.9				

Table S12-8 X ray diffraction data of core 12 sample no.8
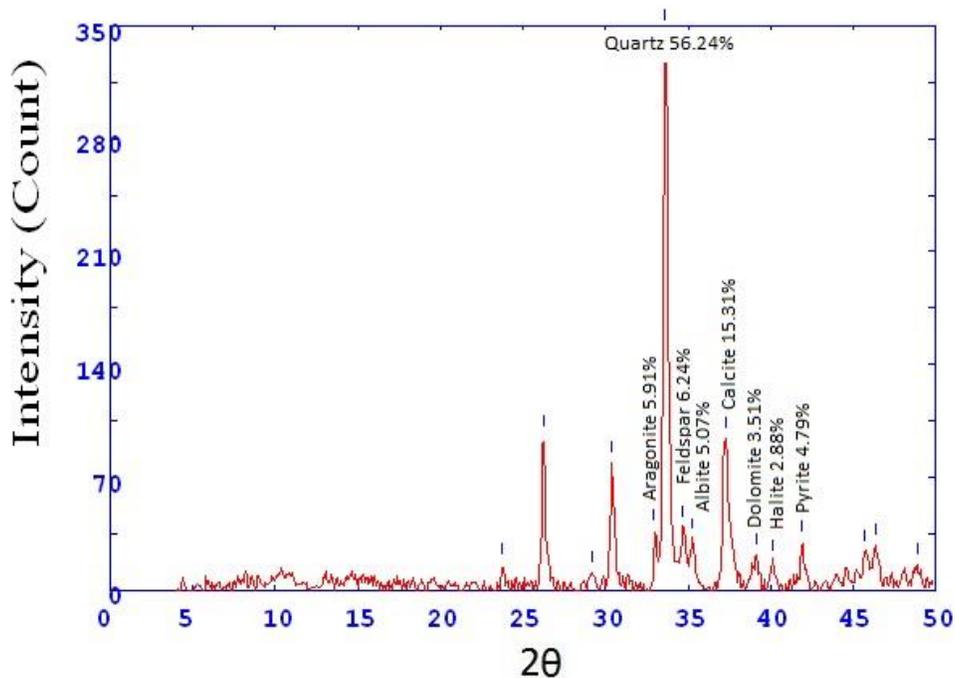
Fig.S15-8 X ray diffractogram of core 12 sample no.8

2Theta	d (A)	Height	Area	FWHM	Identified mineral	WT%
26.273	4.25936	124.3	335.1	0.2414	-	
29.103	3.85288	9	24.2	0.2596	-	
30.433	3.68813	32.2	103.4	0.2778	dolomite	
31.328	3.58537	7	22.5	0.2766	-	
33.089	3.39942	33.7	108.2	0.2753	Aragonite	
33.64	3.34533	318.5	947	0.2728	Quartz	39.01273885
34.758	3.24088	119.9	356.4	0.3201	feldspar(orthoclase)	14.68642822
35.314	3.19142	24.8	73.8	0.3438	feldspar	3.037726605
37.271	3.02933	122.4	615.8	0.3674	calcite	14.99265066
39.034	2.89748	28.3	196.2	0.4591	dolomite	3.466438021
40.228	2.81493	13	89.6	0.4009	halite	1.592356688
41.954	2.70403	29.5	130.4	0.3427	pyrite	3.613424792
45.698	2.49295	23.8	105.5	0.3124	Aragonite	
46.399	2.45731	26.4	105.7	0.2821	dolomite	
47.367	2.40992	10	40	0.3052	-	
48.108	2.37493	11	43.9	0.3167	pyrite	
48.85	2.34103	12	47.9	0.3224	gypsum	
50.267	2.27914	34.9	157.9	0.3282	pyrite	
51.261	2.23788	11	49.6	0.3824	pyrite	
52.373	2.19359	10	45.2	0.4094	gypsum	
54.166	2.1262	27.2	181.4	0.4365	Aragonite	
Total		816.4				

Table S12-9 X ray diffraction data of core 12 sample no.9
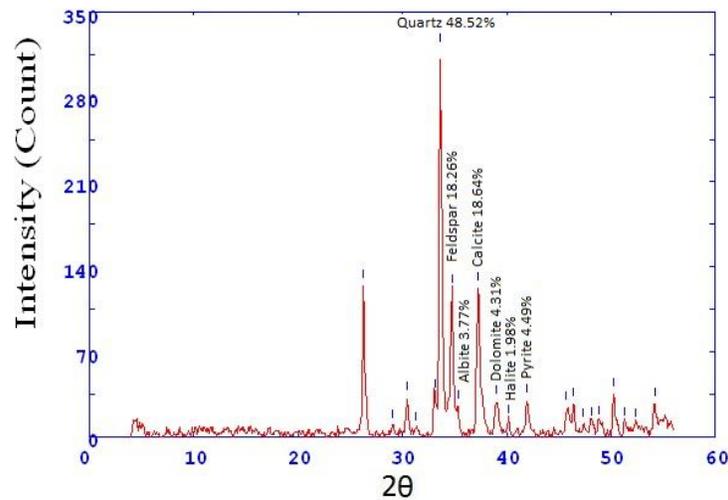
Fig.S15-9 X ray diffractogram of core 12 sample no.9

2Theta	d (A)	Height	Area	FWHM	Identified mineral	WT%
23.8	4.69453	13.1	21.7	0.2221	-	
26.252	4.26269	111.7	252.5	0.2582	gypsum	0
30.426	3.689	45.3	137.8	0.2576	dolomite	
33.029	3.40546	30.9	94	0.2794	Aragonite	4.556850022
33.633	3.34596	359.2	1390.3	0.3011	Quartz	52.97153812
34.743	3.24225	37.5	145	0.3237	feldspar (orthoclase)	5.530157794
35.333	3.18975	91	369.5	0.3464	feldspar (Albite)	13.41984958
37.259	3.03033	68.5	360.7	0.3821	calcite	10.1017549
39.034	2.89751	37.2	238.1	0.471	dolomite	5.485916531
40.066	2.82585	14.4	92	0.4066	halite	2.123580593
41.951	2.70423	22.8	104.2	0.3422	pyrite	3.362335939
45.749	2.49029	16.6	75.9	0.308	Aragonite	3.362335939
46.381	2.45822	48.3	151.6	0.2738	Aragonite	
47.193	2.41828	8.9	27.9	0.2837	gypsum	
48.005	2.37974	10	31.3	0.2887	gypsum	
50.176	2.283	34.8	134.2	0.2937	Aragonite	
51.253	2.23819	6.7	25.8	0.2965	pyrite	
54.109	2.12826	28.4	94.5	0.2993	Aragonite	
Total		678.1				

Table S12-10 X ray diffraction data of core 12 sample no.10
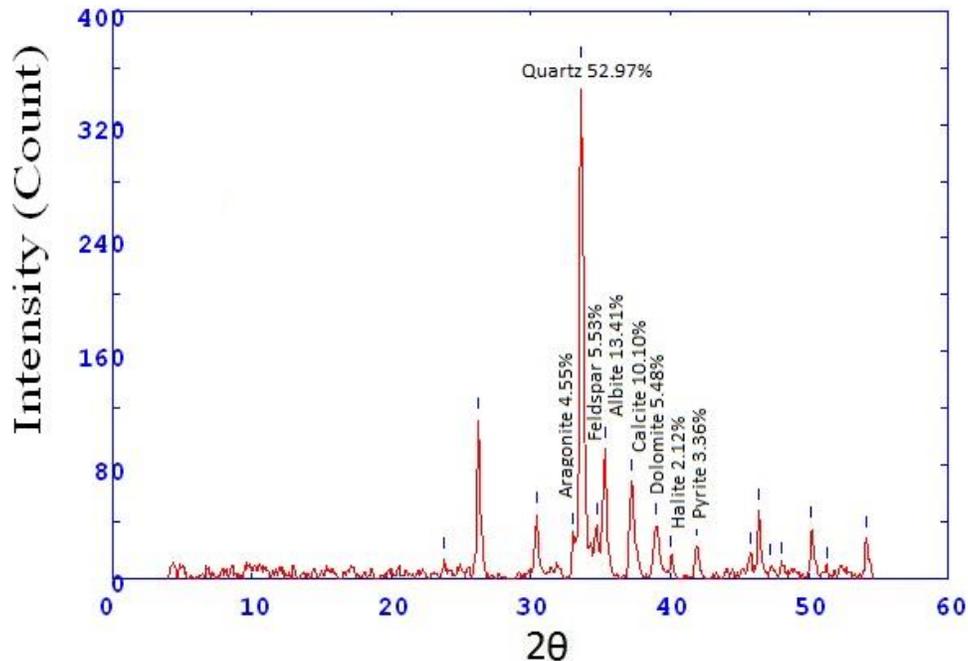
Fig.S15-10 X ray diffractogram of core 12 sample no.10

2Theta	d (A)	Height	Area	FWHM	Identified mineral	WT%
13.099	8.48713	92.9	1562.9	0.3663	Illite	13.18852924
14.504	7.66869	324.1	1562.9	0.3663	Gypsum	46.01078932
25.992	4.26456	39.4	147.3	0.3496	gypsum	
29.378	3.81753	78.9	170.4	0.2584	gypsum	
32.814	3.42716	47.5	102.6	0.2562	aragonite	11.20102215
33.548	3.34424	89.7	258	0.2539	Quartz	12.73424191
34.21	3.29119	24.8	71.4	0.3554	feldspar (orthoclase)	3.52072686
36.592	3.08356	34.1	98.1	0.4061	gypsum	
37.198	3.03507	62.3	307.4	0.4569	calcite	4.840999432
39.25	2.88219	20.7	224.3	0.78	dolomite	2.93867121
39.878	2.83859	12.5	135.1	0.7039	Halite	1.774559909
41.875	2.70886	29.9	251.9	0.6278	pyrite	4.244747303
45.687	2.49353	28.5	121.3	0.3778	gypsum	
47.107	2.42244	14.5	61.9	0.3944	Aragonite	
48.075	2.37647	20.1	94	0.4111	Aragonite	
48.75	2.34554	15.5	0	0	Aragonite	
Total		704.5				

Table S12-11 X ray diffraction data of core 12 sample no.11
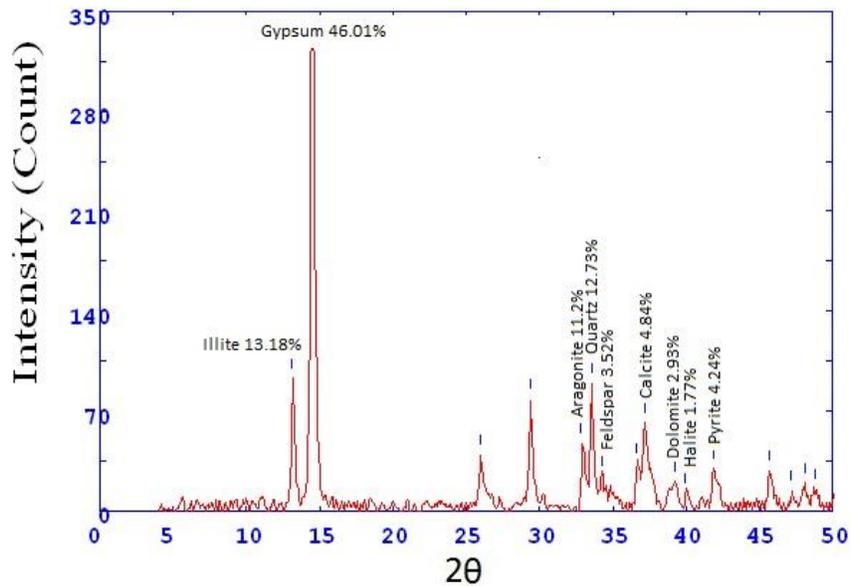
Fig.S15-11 X ray diffractogram of core 12 sample no.11

2Theta	d (A)	Height	Area	FWHM	Identified mineral	WT%
13.115	8.47674	56.2	1615	0.376	Illite	8.27565896
14.567	7.63559	347.8	1615	0.376	gypsum	51.21484317
24.922	4.48631	7.6	35.5	0.3659	-	
26.025	4.29922	68.6	280.9	0.3558	gypsum	
29.42	3.8122	120.6	337.9	0.2577	gypsum	
32.937	3.41472	58.4	163.6	0.2587	aragonite	8.59961714
33.587	3.35048	71.4	200.9	0.2597	Quartz	10.51391548
34.229	3.2894	32.5	91.5	0.2879	feldspar (orthoclase	4.78574584
36.752	3.07062	82.9	254.8	0.3161	gypsum	
37.16	3.03812	45.4	139.7	0.3377	calcite	6.685318804
39.291	2.87933	33.5	142.1	0.3592	dolomite	4.932999558
41.913	2.70654	33.9	332.4	0.6817	pyrite	4.991901046
45.767	2.48941	30.4	177.6	0.4676	gypsum	
47.243	2.41587	8.7	51	0.4096	aragonite	
48.024	2.37886	22.9	100.9	0.3517	aragonite	
48.794	2.34355	19.5	0	0	Aragonite	
51.724	2.21917	8.7	0	0	pyrite	
Total		679.1				

Table S12-12 X ray diffraction data of core 12 sample no.12
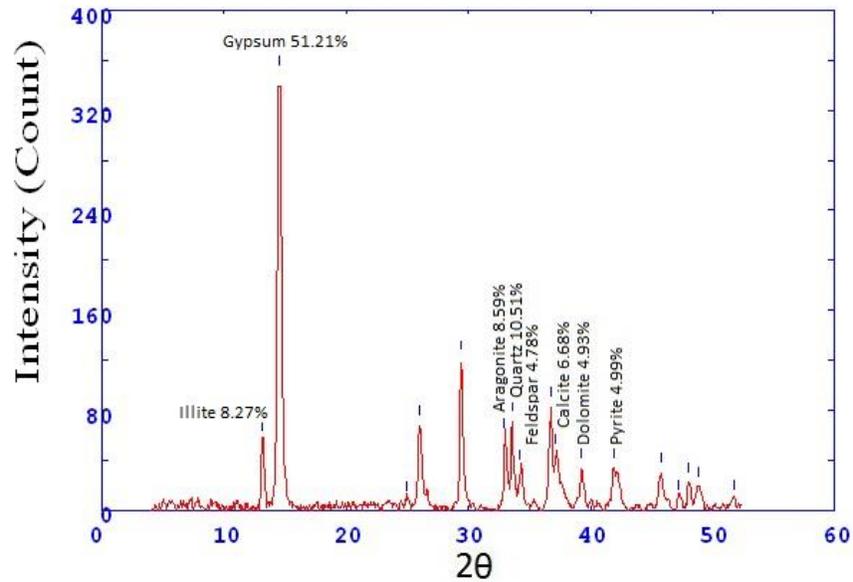
Fig.S15-12 X ray diffractogram of core 12 sample no.12

2Theta	d (A)	Height	Area	FWHM	Identified mineral	WT%
13.078	8.50054	7.4	167	0.2466	Illite	0.980781975
14.516	7.66224	78.7	167	0.2466	gypsum	10.43074884
15.352	7.24701	10.8	22.9	0.2456	-	
24.976	4.47667	9.4	20.1	0.2451	-	
26.196	4.27166	48.8	99.4	0.2446	gypsum	
29.088	3.85475	14.1	28.8	0.2321	-	
29.438	3.80992	14.1	28.8	0.2258	-	
30.316	3.70203	17.8	36	0.2195	-	
32.15	3.49596	14.8	30	0.2366	anhydrite	1.96156395
32.938	3.41462	28.2	57.2	0.2452	Aragonite	3.737574553
33.543	3.35475	211.7	597.2	0.2537	quartz	28.05831677
34.25	3.28748	20.2	56.9	0.239	feldspar (orthoclase)	2.677269715
35.268	3.19543	168.1	341.5	0.2244	feldspar (Albite)	22.2796554
37.197	3.03514	124	577.2	0.344	calcite	16.43472498
38.99	2.90066	53.6	382.3	0.5219	dolomite	7.104042412
39.937	2.83461	20.2	144.1	0.4376	halite	2.677269715
41.249	2.74817	7.4	53.1	0.3954		
41.846	2.71067	27.6	111.9	0.3533	pyrite	3.65805169
45.767	2.48941	26.5	139.6	0.4239	Aragonite	
46.411	2.45673	16.2	85	0.3322		
47.286	2.41381	7.4	39.1	0.2864	Aragonite	
47.995	2.38019	15.9	34.1	0.2406	Aragonite	
48.773	2.3445	8.8	18.8	0.2913	Aragonite	
Total		754.3				

Table S12-13 X ray diffraction data of core 12 sample no.13
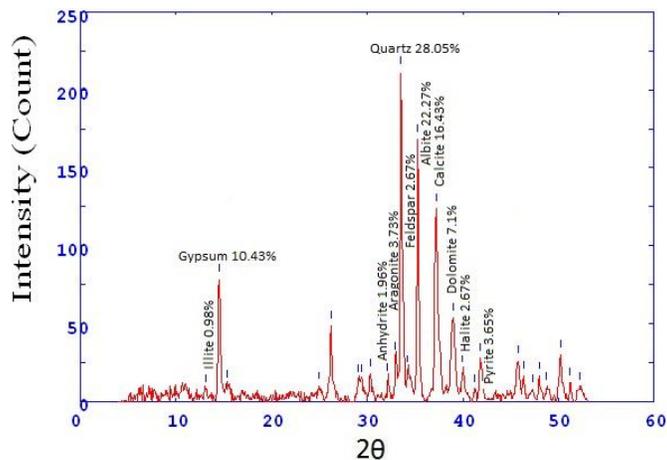
Fig.S15-13 X ray diffractogram of core 12 sample no.13

2Theta	d (A)	Height	Area	FWHM	Identified mineral	WT%
15.202	7.31808	10.6	126.1	0.9042	gypsum	2.703391992
17.34	6.42162	8.1	24.9	0.2794	-	
19.545	5.70319	6.7	22.4	0.3362	-	
22.4	4.9837	6.4	21.8	0.2377	-	
25.083	4.45783	5	17	0.2315	-	
26.261	4.26125	35	70.6	0.2254	gypsum	8.926294313
29.193	3.84117	21.9	111.1	0.4063	-	
33.064	3.4019	49.7	252	0.3292	Aragonite	
33.67	3.34243	120.6	339.5	0.2521	quartz	30.75745983
34.394	3.27409	32.8	92.2	0.3939	feldspar (orthoclase)	8.365212956
37.304	3.02679	174.6	1102	0.5358	calcite	44.52945677
39.271	2.88068	14.2	89.8	0.4252	dolomite	3.621525121
40.158	2.81961	10.9	69.1	0.3698	Halite	2.779903086
41.968	2.70318	28.4	91.2	0.3145	pyrite	7.243050242
45.81	2.48719	44.6	214	0.4	anhydrite ,gypsum	
48.1	2.37532	19.7	91.1	0.3626	pyrite	
48.848	2.3411	15.9	73.4	0.4224	feldspar	
50.233	2.28058	34.9	191.9	0.4822	-	
52.5	2.18866	9.5	85.6	0.6277	gypsum	
Total		392.1				

Table S12-14 X ray diffraction data of core 12 sample no.14
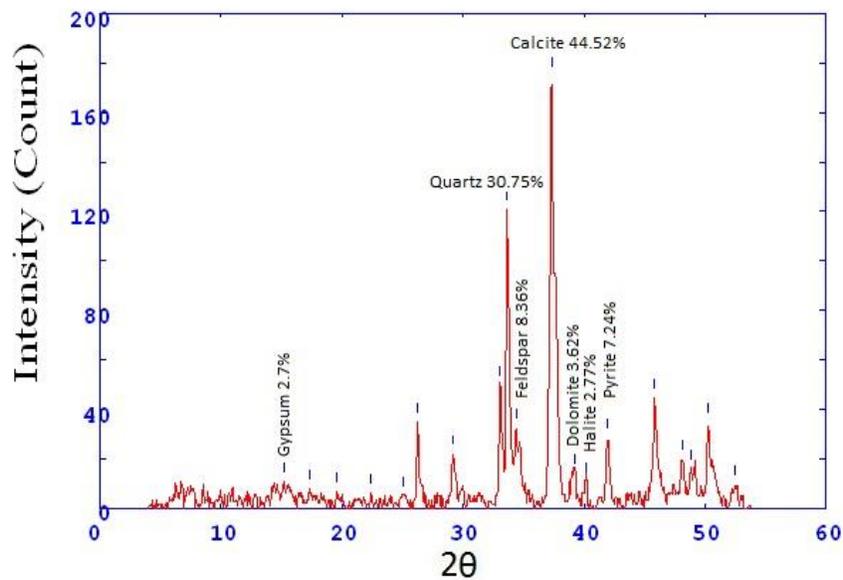
Fig.S15-14 X ray diffractogram of core 12 sample no.14

2Theta	d (A)	Height	Area	FWHM	Identified mineral	WT%
29.25	3.83387	12.1	58.5	0.4441	-	
32.967	3.41169	68.3	261.1	0.3236	Aragonite	13.36333399
33.533	3.35572	19.3	73.6	0.3487	Quartz	3.776169047
34.259	3.28661	40.8	184.3	0.3738	feldspar (orthoclase)	56.56427314
37.557	3.0371	289.1	897.2	0.7315	calcite	56.56427314
39.934	2.83477	9	37.5	0.334	dolomite	1.760907846
41.844	2.71082	39.9	160.2	0.3362	pyrite	7.80669145
45.7	2.49285	34.4	185.4	0.464	dolomite	6.7305811
47.203	2.41778	10.3	55.6	0.4143	anhydrite, gypsum	2.015261201
47.953	2.38214	23.8	107.5	0.3647	anhydrite	
48.85	2.34101	24	215.3	0.5968	pyrite	
50.734	2.25954	15.7	117.5	0.5868	Quartz	
52.533	2.18736	10.3	90.5	0.6469	Aragonite	
54.578	2.11138	19.8	97.1	0.3789	Aragonite	
55.644	2.07405	19.8	96.5	0.4105	gypsum	
56.638	2.0406	7.5	96.5	0.4105	dolomite	
Total		511.1				

Table S12-15 X ray diffraction data of core 12 sample no.15
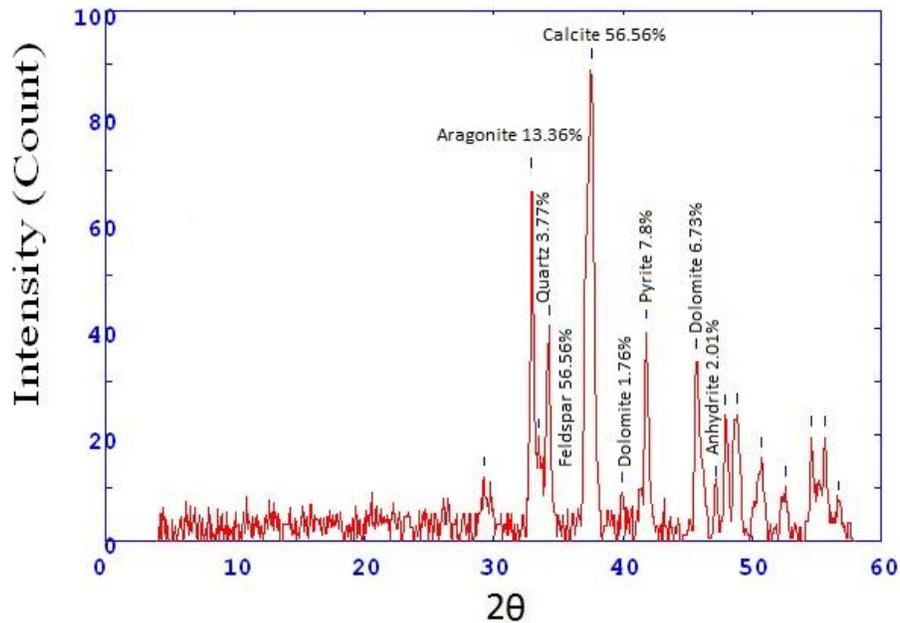
Fig.S15-15 X ray diffractogram of core 12 sample no.15

2Theta	d (A)	Height	Area	FWHM	Identified mineral	WT%
29.46	3.8072	12.1	165.4	0.9856	-	
33.038	3.40448	79.2	321.7	0.334	anhydrite	13.67454068
33.609	3.34832	52.1	211.7	0.4703	Quartz	13.67454068
34.332	3.27989	48.8	198	0.5384	feldspar (orthoclase)	12.80839895
37.652	3.01981	106.8	815.4	0.6066	calcite	28.03149606
39.21	2.88503	6.8	51.9	0.4611	dolomite	1.784776903
40.113	2.82264	11.9	90.7	0.3883	halite	3.12335958
41.916	2.70639	44.9	171.6	0.3155	magnesite, pyrite	11.7847769
45.785	2.48844	39.1	216.8	0.4512	Gypsum ,anhydrite	
47.34	2.41119	14.2	78.9	0.2768	gypsum	
48.063	2.37704	30.5	168.8	0.1896	pyrite	8.005249344
48.966	2.33582	25.1	138.9	0.146	anhydrite	
50.773	2.25792	16.9	93.9	0.1242	-	
52.309	2.1961	11.9	65.8	0.1133	calcite	
Total		381				

Table S12-16X ray diffraction data of core 12 sample no.16
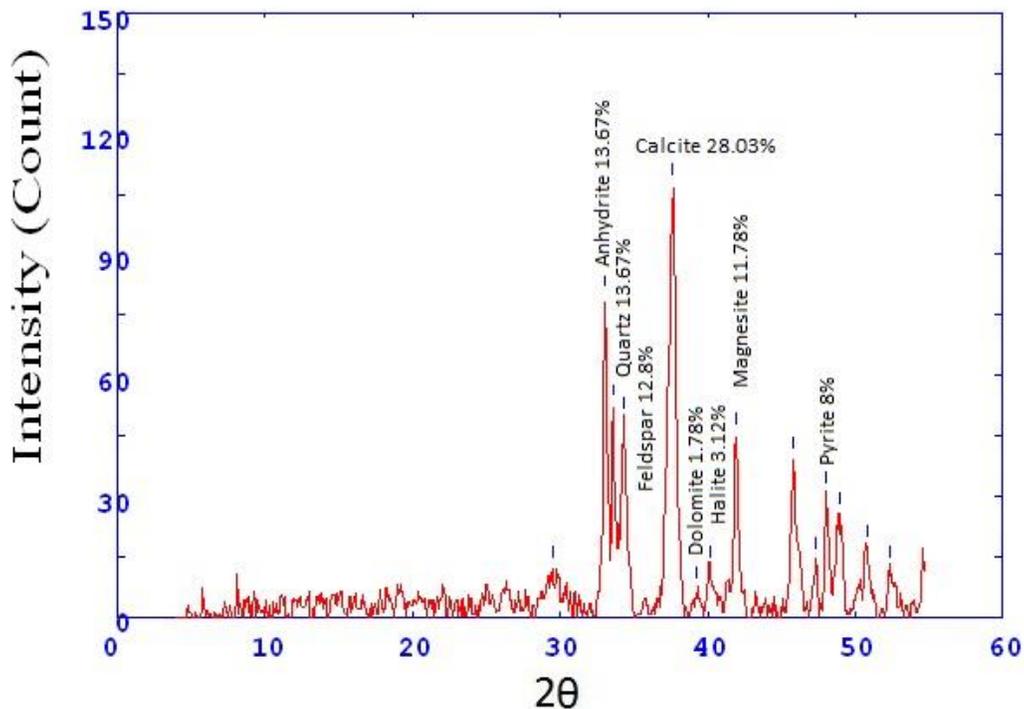
Fig.S15-16 X ray diffractogram of core 12 sample no.16

Grain size cores analysis

Size	WT%	cumulative WT%
0	1.516	1.516
0.321928	3.475	4.991
0.736965	4.14	9.131
1.736966	7.775	16.906
2.736966	7.971	24.877
3.736966	38.403	63.28
5.64385619	36.72	100
Mean size	**sorting**	
6.33377	8.839632	

Table S13-1 Grain size analysis of core 1 sample 1
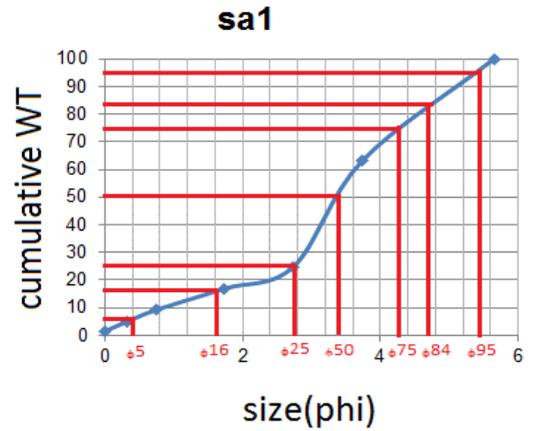
Fig.S16-1 cumulative weight with grain size in Phi unit of core 1 sample no. 1

size	WT %	Cumulative WT %
0	1.117	1.117
0.321928	3.238	4.355
0.736965	5.785	10.14
1.736966	18.671	28.811
2.736966	24.524	53.335
3.736966	22.838	76.173
5.64385619	23.827	100
Mean size	**sorting**	
5.09153	8.493642	

Table S13-2 Grain size analysis of core 1 sample 2
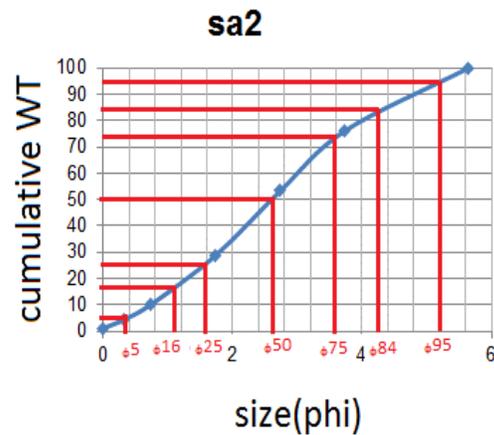
Fig.S16-2 cumulative weight with grain size in Phi unit of core 1 sample no. 2

size	WT %	cumulative WT %
0	1.651	1.651
0.321928	2.915	4.566
0.736965	3.799	8.365
1.736966	14.429	22.794
2.736966	22.992	45.786
3.736966	27.14	72.926
5.64385619	27.074	100
Mean size	**sorting**	
6.580573	9.066486	
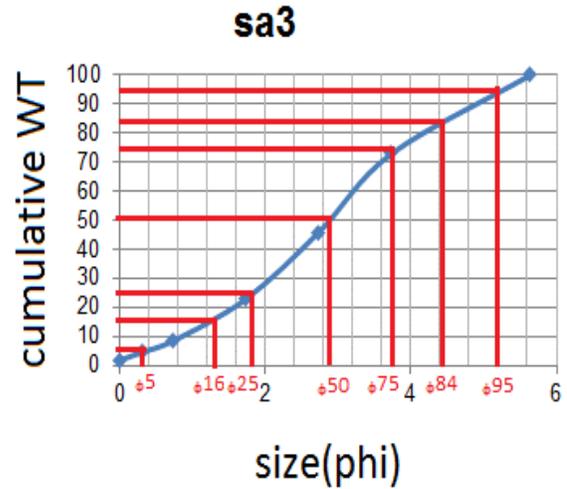
Table S13-3 Grain size analysis of core 1 sample 3

Fig.S16-3 cumulative weight with grain size in Phi unit of core 1 sample no. 3

size	WT %	cumulative WT %
0	6.945	6.945
0.321928	2.65	9.595
0.736965	3.057	12.652
1.736966	11.249	23.901
2.736966	19.759	43.66
3.736966	29.754	73.414
5.64385619	26.586	100
Mean size	**sorting**	
5.4685	8.619654	
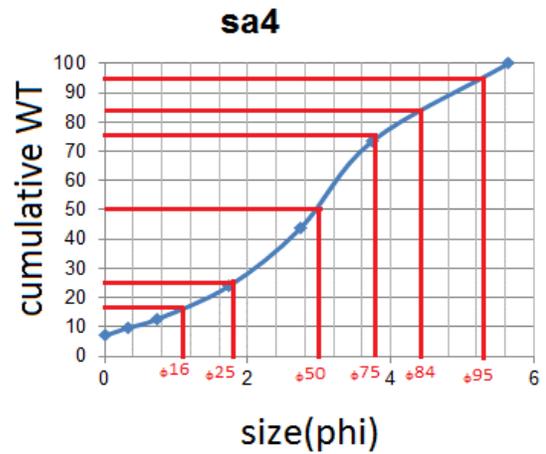
Table S13-4Grain size analysis of core 1 sample 4

Fig.S16-4 cumulative weight with grain size in Phi unit of core 1 sample no. 4

size	WT %	cumulativeWT %
0	2.98	2.98
0.321928	2.787	5.767
0.736965	3.64	9.407
1.736966	12.878	22.285
2.736966	22.384	44.669
3.736966	34.527	79.196
5.64385619	20.804	100
Mean size	**sorting**	
5.506978	7.819768	

Table S13-5Grain size analysis of core 1 sample 5
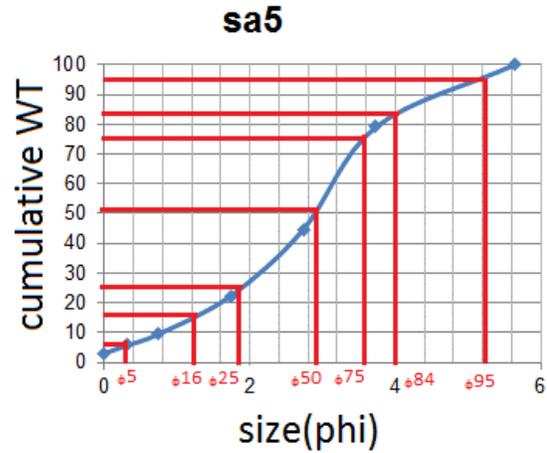
Fig.S16-5 cumulative weight with grain size in Phi unit of core 1 sample no. 5

size	WT%	Cumulative WT%
0	10.958	10.958
0.321928	4.267	15.225
0.736965	5.723	20.948
1.736966	15.118	36.066
2.736966	20.065	56.131
3.736966	25.736	81.867
5.64385619	18.133	100
Mean size	sorting	
4.13475	8.08206	
Mean size	**sorting**	
4.13475	8.08206	

Table S13-6Grain size analysis of core 1 sample 6

Fig.S16-6 cumulative weight with grain size in Phi unit of core 1 sample no. 6

size	WT %	cumulative WT %
0	20.949	20.949
0.321928	5.501	26.45
0.736965	6.341	32.791
1.736966	14.324	47.115
2.736966	21.165	68.28
3.736966	19.862	88.142
5.64385619	11.858	100
Mean size	**sorting**	
2.881786	7.495146	

Table S13-7Grain size analysis of core 1 sample 7
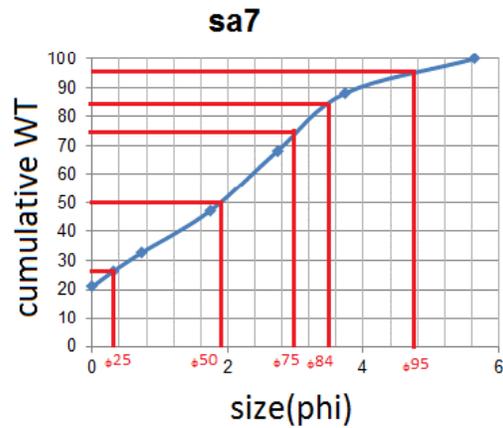
Fig.S16-7 cumulative weight with grain size in Phi unit of core 1 sample no. 7

size	WT %	cumulative WT%
0	20.349	20.349
0.321928	4.215	24.564
0.736965	5.857	30.421
1.736966	15.859	46.28
2.736966	24.085	70.365
3.736966	17.573	87.938
5.64385619	12.062	100
Mean size	**sorting**	
2.818043	7.57713	

Table S13-8Grain size analysis of core 1 sample 8
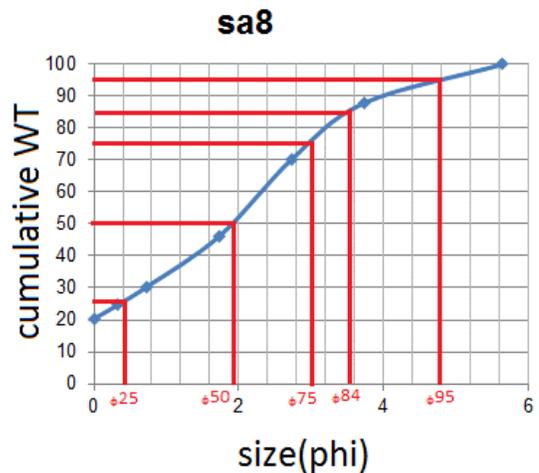
Fig.S16-8 cumulative weight with grain size in Phi unit of core 1 sample no. 8

size	WT %	cumulative WT %
0	13.83	13.83
0.321928	5.279	19.109
0.736965	6.085	25.194
1.736966	15.091	40.285
2.736966	22.453	62.738
3.736966	20.412	83.15
5.64385619	16.85	100
Mean size	**sorting**	
3.5758	8.098216	
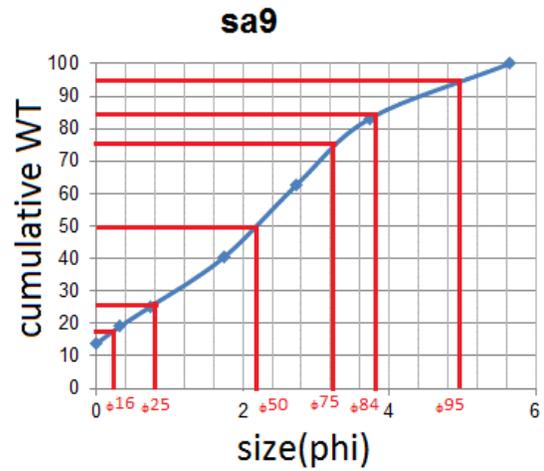
Table S13-9Grain size analysis of core 1 sample 9	Fig.S16-9 cumulative weight with grain size in Phi unit of core 1 sample no. 9

size	WT %	cumulative WT %
0	10.231	10.231
0.321928	5.149	15.38
0.736965	6.662	22.042
1.736966	20.046	42.088
2.736966	28.617	70.705
3.736966	19.805	90.51
5.64385619	9.49	100
Mean size	**sorting**	
3.482771	7.050196	
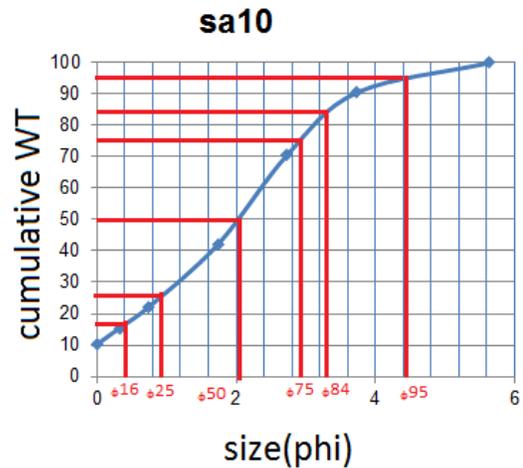
Table S13-10Grain size analysis of core 1 sample 10	Fig.S16-10 cumulative weight with grain size in Phi unit of core 1 sample no. 10

size	WT%	cumulative WT%
0	4.981	4.981
0.321928	4.598	9.579
0.736965	5.122	14.701
1.736966	11.992	26.693
2.736966	15.448	42.141
3.736966	25.44	67.581
5.64385619	32.419	100
Mean size	**sorting**	
5.255839	9.14149	

Table S14-1 Grain size analysis of core2 sample 1
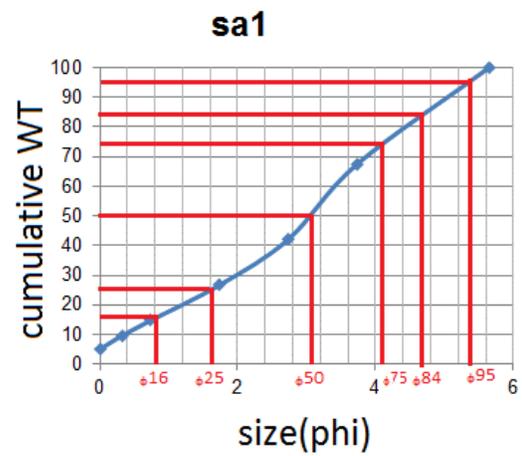
Fig.S17-1 cumulative weight with grain size in Phi unit of core 2 sample no. 1

size	WT %	cumulative WT %
0	17.241	17.241
0.321928	9.81	27.051
0.736965	9.511	36.562
1.736966	16.492	53.054
2.736966	21.986	75.04
3.736966	14.879	89.919
5.64385619	10.081	100
Mean size	**sorting**	
2.610193	7.160603	

Table S14-2 Grain size analysis of core2 sample 2

Fig.S17-2 cumulative weight with grain size in Phi unit of core 2 sample no. 2

size	WT %	cumulative WT %
0	7.754	7.754
0.321928	5.239	12.993
0.736965	7.807	20.8
1.736966	17.744	38.544
2.736966	31.624	70.168
3.736966	20.145	90.313
5.64385619	9.687	100
Mean size	**sorting**	
3.714673	7.026248	

Table S14-3Grain size analysis of core2 sample 3
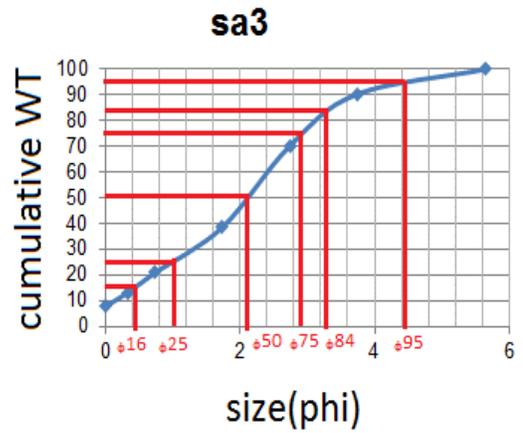
Fig.S17-3 cumulative weight with grain size in Phi unit of core 2 sample no. 3

size	WT %	cumulative WT %
0	9.07	9.07
0.321928	4.529	13.599
0.736965	5.905	19.504
1.736966	12.857	32.361
2.736966	33.027	65.388
3.736966	27.835	93.223
5.64385619	6.777	100
Mean size	**sorting**	
3.919714	6.748145	

Table S14-4Grain size analysis of core2 sample 4
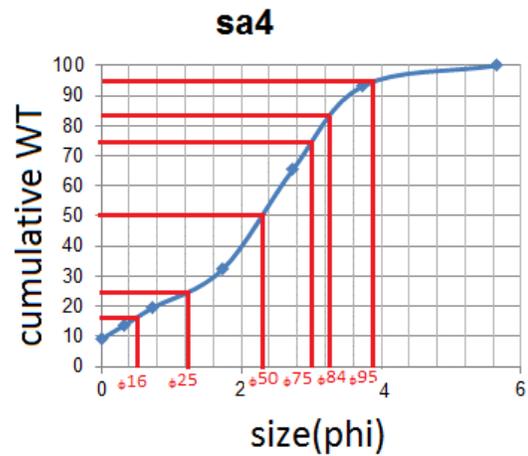
Fig.S17-4 cumulative weight with grain size in Phi unit of core 2 sample no. 4

size	WT%	cumulative WT %
0	16.614	16.614
0.321928	5.16	21.774
0.736965	4.92	26.694
1.736966	11.802	38.496
2.736966	29.354	67.85
3.736966	30.29	98.14
5.64385619	1.86	100
Mean size	**sorting**	
3.23065	6.599271	

Table S14-5Grain size analysis of core2 sample 5
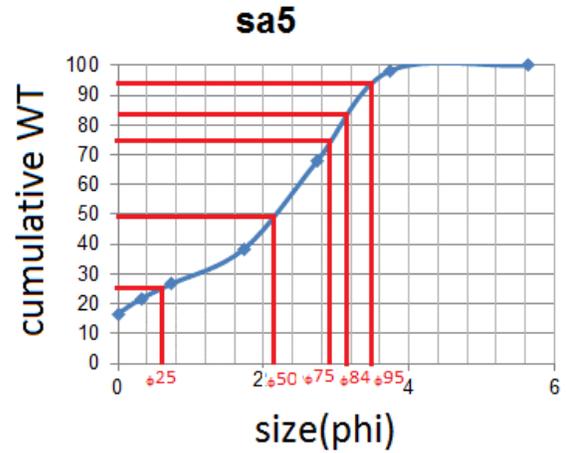
Fig.S17-5 cumulative weight with grain size in Phi unit of core 2 sample no. 5

size	WT %	cumulative WT %
0	11.766	11.766
0.321928	3.518	15.284
0.736965	4.545	19.829
1.736966	10.982	30.811
2.736966	29.922	60.733
3.736966	37.695	98.428
5.64385619	1.572	100
Mean size	**sorting**	
3.973583	6.66662	

Table S14-6Grain size analysis of core2 sample 6
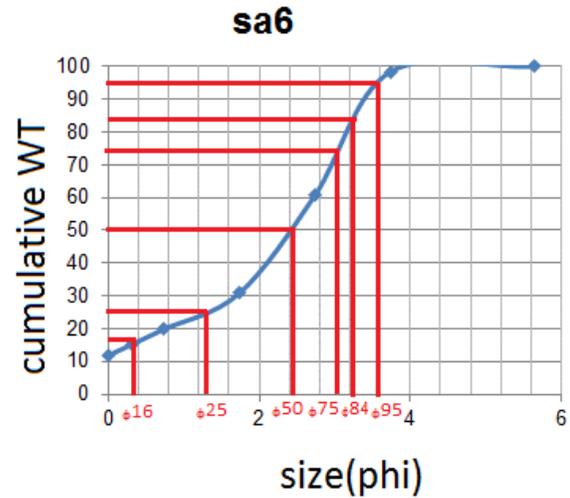
Fig.S17-6 cumulative weight with grain size in Phi unit of core 2 sample no. 6

size	WT%	cumulative WT%
0	12.636	12.636
0.321928	3.975	16.611
0.736965	4.307	20.918
1.736966	7.429	28.347
2.736966	6.665	35.012
3.736966	34.028	69.04
5.64385619	30.96	100
Mean size	**sorting**	
3.0551	7.308591	

Table S15-1Grain size analysis of core3 sample 1
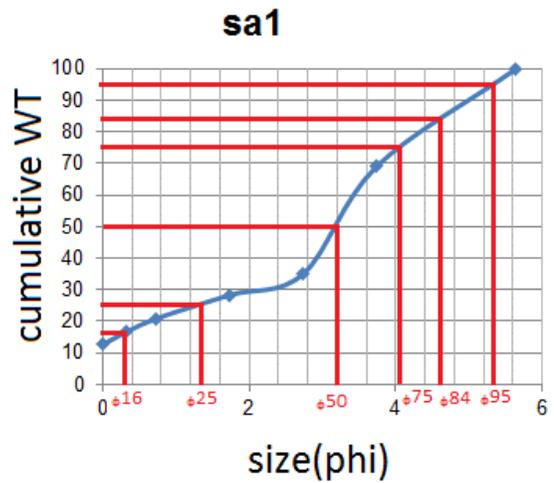
Fig.S18-1 cumulative weight with grain size in Phi unit of core 3 sample no. 1

size	WT %	Cumulative WT %
0	14.221	14.221
0.321928	5.407	19.628
0.736965	7.675	27.303
1.736966	18.575	45.878
2.736966	19.461	65.339
3.736966	18.054	83.393
5.64385619	16.607	100
Mean size	**sorting**	
2.603333	6.83197	

Table S15-2Grain size analysis of core3 sample 2

Fig.S18-2 cumulative weight with grain size in Phi unit of core 3 sample no. 2

size	WT%	cumulative WT %
0	9.713	9.713
0.321928	3.923	13.636
0.736965	5.654	19.29
1.736966	16.091	35.381
2.736966	19.215	54.596
3.736966	26.055	80.651
5.64385619	19.349	100
Mean size	**sorting**	
2.411333	6.962644	
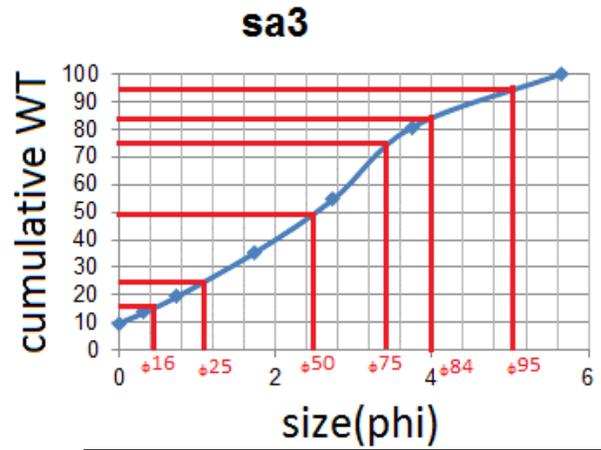
Table S15-3Grain size analysis of core3 sample 3

Fig.S18-3 cumulative weight with grain size in Phi unit of core 3 sample no. 3

size	WT%	cumulative WT %
0	10.846	10.846
0.321928	3.598	14.444
0.736965	4.656	19.1
1.736966	12.749	31.849
2.736966	19.323	51.172
3.736966	30.2	81.372
5.64385619	18.628	100
Mean size	**sorting**	
2.26	8.868258	
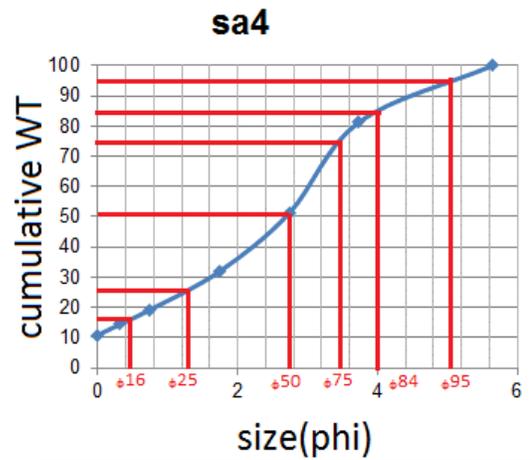
Table S15-4Grain size analysis of core3 sample 4

Fig.S18-4 cumulative weight with grain size in Phi unit of core 3 sample no. 4

size	WT%	cumulative WT %
0	12.297	12.297
0.321928	3.562	15.859
0.736965	5.31	21.169
1.736966	14.819	35.988
2.736966	41.575	77.563
3.736966	20.632	98.195
5.64385619	1.805	100
Mean size	**sorting**	
1.133333	5.394	

sa5

Table S15-5Grain size analysis of core3 sample 5
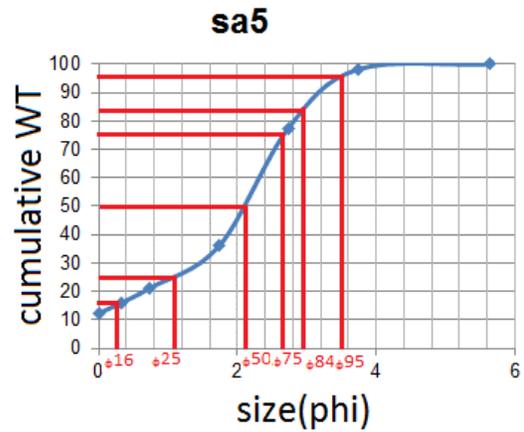
Fig.S18-5 cumulative weight with grain size in Phi unit of core 3 sample no. 5

size	WT%	Cumulative WT %
0	7.58	7.58
0.321928	3.659	11.239
0.736965	5.588	16.827
1.736966	14.779	31.606
2.736966	26.043	57.649
3.736966	24.062	81.711
5.64385619	18.289	100
Mean size	**sorting**	
3.826667	4.614773	

sa6

Table S15-6Grain size analysis of core3 sample 6
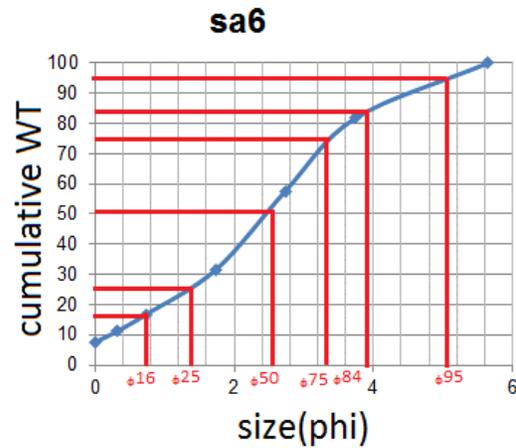
Fig.S18-6 cumulative weight with grain size in Phi unit of core 3 sample no. 6

size	WT %	cumulative WT %
0	13.825	13.825
0.321928	5.019	18.844
0.736965	6.616	25.46
1.736966	15.425	40.885
2.736966	26.575	67.46
3.736966	20.563	88.023
5.64385619	11.977	100
Mean size	**sorting**	
2.168	6.854667	

Table S15-7Grain size analysis of core3 sample 7
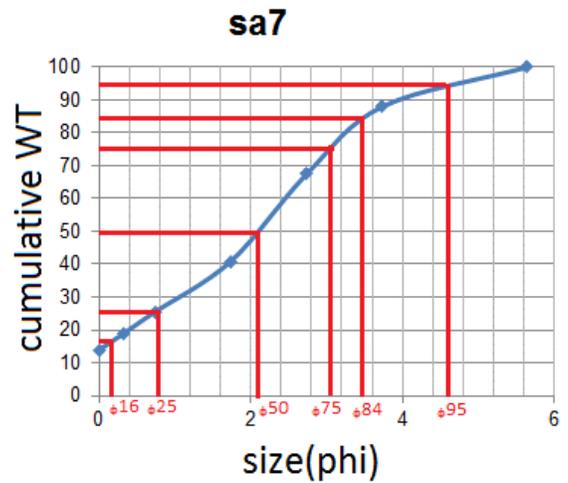
Fig.S18-7 cumulative weight with grain size in Phi unit of core 3 sample no. 7

size	WT %	cumulative WT%
0	10.434	10.434
0.321928	3.548	13.982
0.736965	4.49	18.472
1.736966	10.457	28.929
2.736966	31.902	60.831
3.736966	34.684	95.515
5.64385619	4.485	100
Mean size	**sorting**	
4.503333	8.117197	

Table S15-8Grain size analysis of core3 sample 8
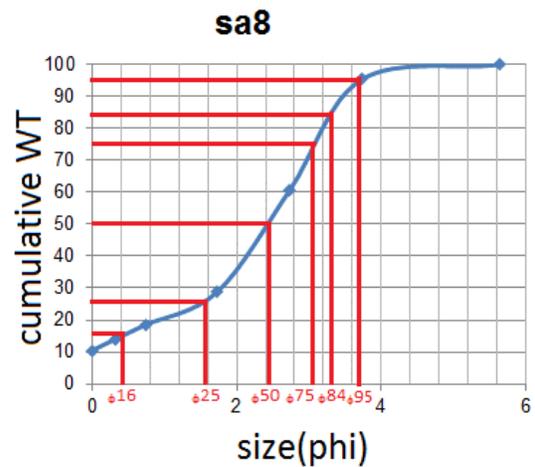
Fig.S18-8 cumulative weight with grain size in Phi unit of core 3 sample no. 8

size	WT%	cumulative WT %
0	17.504	17.504
0.321928	5.288	22.792
0.736965	5.944	28.736
1.736966	12.566	41.302
2.736966	28.547	69.849
3.736966	26.365	96.214
5.64385619	3.7866	100.0006
Mean size	**sorting**	
5.521667	8.403295	
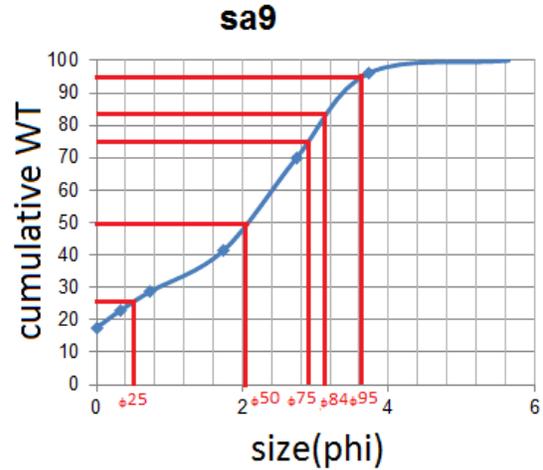
Table S15-9Grain size analysis of core3 sample 9	Fig.S18-9 cumulative weight with grain size in Phi unit of core 3 sample no. 9

size	WT%	cumulative WT%
0	20.868	20.868
0.321928	5.971	26.839
0.736965	7.033	33.872
1.736966	14.446	48.318
2.736966	19.609	67.927
3.736966	15.972	83.899
5.64385619	16.101	100
Mean size	**sorting**	
2.61	8.152424	
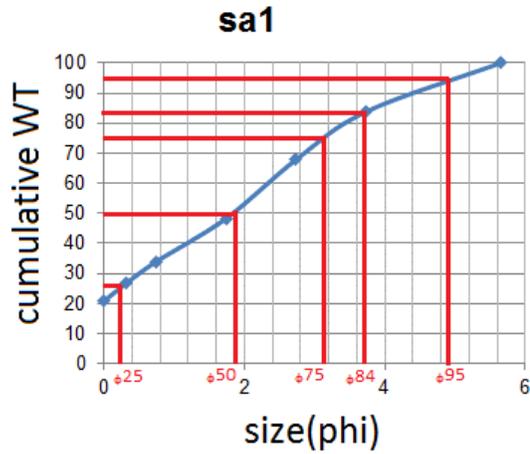
Table S16-1Grain size analysis of core4sample 1	Fig.S19-1 cumulative weight with grain size in Phi unit of core 4 sample no. 1

size	WT %	cumulative WT %
0	10.467	10.467
0.321928	4.664	15.131
0.736965	7.441	22.572
1.736966	18.776	41.348
2.736966	27.045	68.393
3.736966	19.205	87.598
5.64385619	12.402	100
Mean size	**sorting**	
3.612333	7.475674	

Table S16-2Grain size analysis of core4sample 2
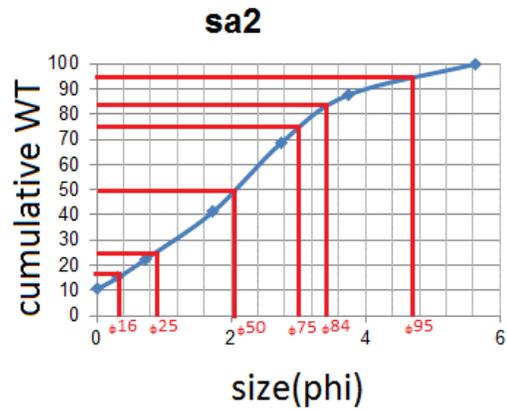
Fig.S19-2 cumulative weight with grain size in Phi unit of core 4 sample no. 2

size	WT %	cumulative WT %
0	4.267	4.267
0.321928	2.509	6.776
0.736965	4.977	11.753
1.736966	17.793	29.546
2.736966	41.518	71.064
3.736966	22.173	93.237
5.64385619	6.763	100
Mean size	**sorting**	
4.417333	6.411205	

Table S16-3Grain size analysis of core4sample 3
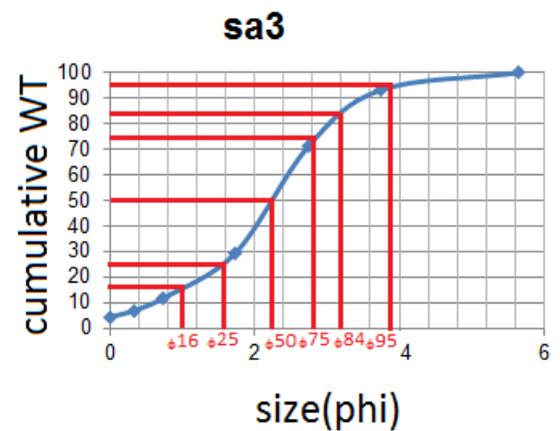
Fig.S19-3 cumulative weight with grain size in Phi unit of core 4 sample no. 3

size	WT%	cumulative WT %
0	1.974	1.974
0.321928	1.521	3.495
0.736965	2.94	6.435
1.736966	13.239	19.674
2.736966	44.122	63.796
3.736966	29.995	93.791
5.64385619	6.209	100
Mean size	**sorting**	
5.139333	6.347348	

Table S16-4Grain size analysis of core4sample 4
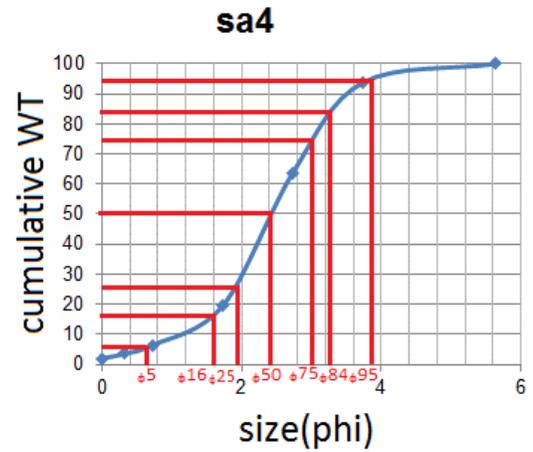
Fig.S19-4 cumulative weight with grain size in Phi unit of core 4 sample no. 4

size	WT %	cumulative WT %
0	1.492	1.492
0.321928	0.996	2.488
0.736965	2.348	4.836
1.736966	19.587	24.423
2.736966	54.548	78.971
3.736966	18.903	97.874
5.64385619	2.126	100
Mean size	**sorting**	
4.651133	5.529535	

Table S16-5Grain size analysis of core4sample 5
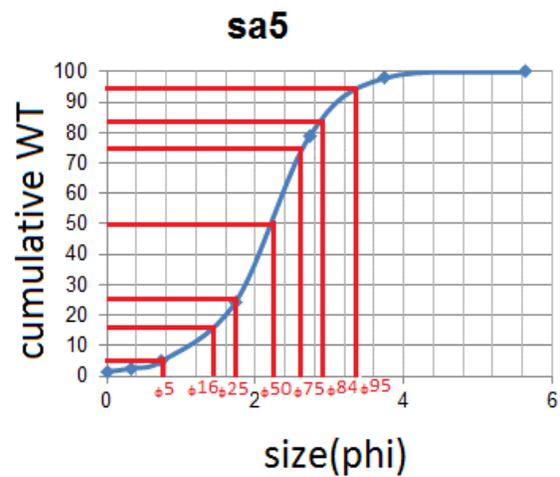
Fig.S19-5 cumulative weight with grain size in Phi unit of core 4 sample no. 5

size	WT %	cumulative WT %
0	1.98	1.98
0.321928	1.176	3.156
0.736965	2.204	5.36
1.736966	14.286	19.646
2.736966	49.199	68.845
3.736966	29.081	97.926
5.64385619	2.074	100
Mean size	**sorting**	
5.05732	5.918961	

Table S₁6-6Grain size analysis of core4sample 6
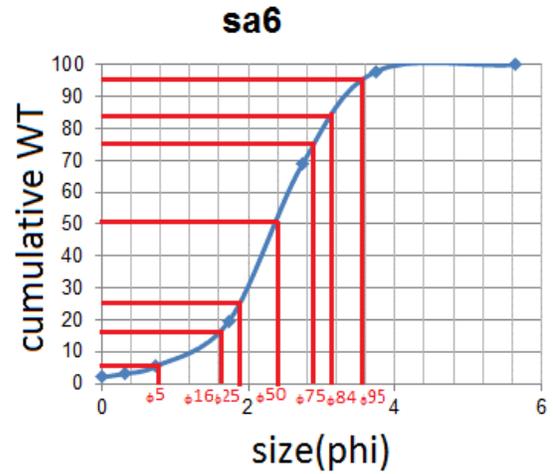
Fig.S19-6 cumulative weight with grain size in Phi unit of core 4 sample no. 6

size	WT %	cumulative WT %
0	5.032	5.032
0.321928	2.25	7.282
0.736965	4.296	11.578
1.736966	17.577	29.155
2.736966	43.282	72.437
3.736966	22.791	95.228
5.64385619	4.772	100
Mean size	**sorting**	
4.3663	6.256008	

Table S₁6-7Grain size analysis of core4sample 7
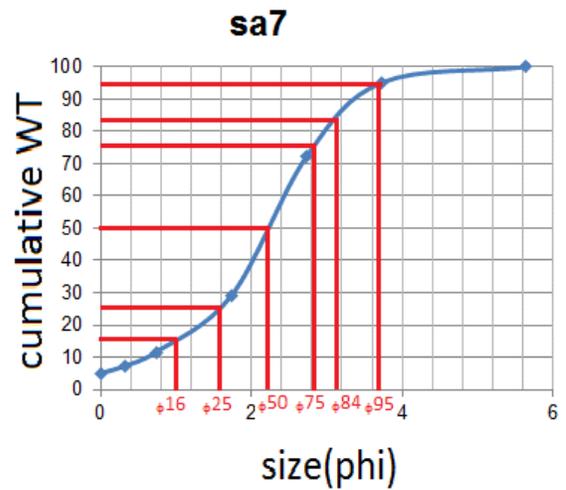
Fig.S19-7 cumulative weight with grain size in Phi unit of core 4 sample no. 7

size	WT %	cumulative WT %
0	3.749	3.749
0.321928	1.338	5.087
0.736965	2.404	7.491
1.736966	12.335	19.826
2.736966	43.912	63.738
3.736966	34.301	98.039
5.64385619	1.961	100
Mean size	**sorting**	
5.112867	6.173006	
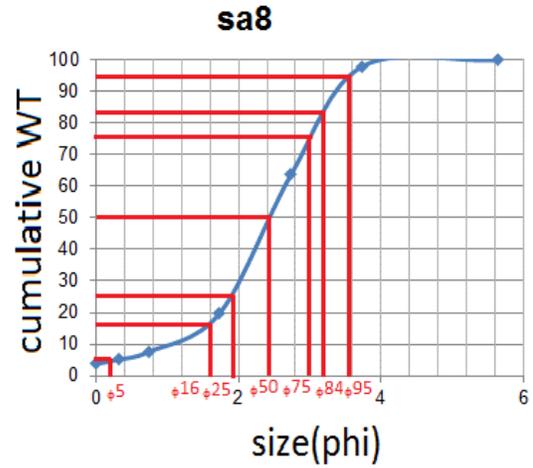
Table S₁6-8Grain size analysis of core4sample 8

Fig.S19-8 cumulative weight with grain size in Phi unit of core 4 sample no. 8

size	WT%	cumulative WT %
0	28.101	28.101
0.321928	5.886	33.987
0.736965	7.673	41.66
1.736966	17.664	59.324
2.736966	18.281	77.605
3.736966	15.24	92.845
5.64385619	7.155	100
Mean size	**sorting**	
1.95299	6.695535	
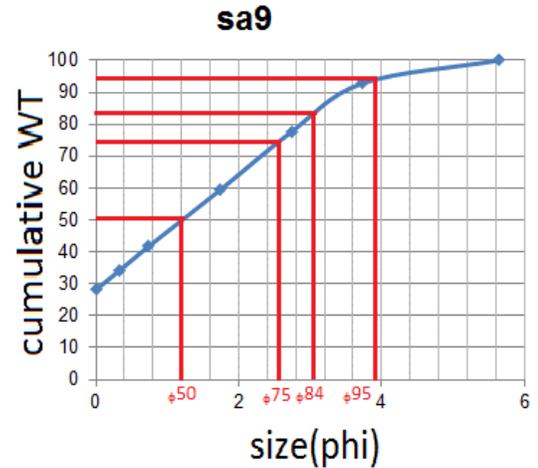
Table S₁6-9Grain size analysis of core4sample 9

Fig.S19-9 cumulative weight with grain size in Phi unit of core 4 sample no. 9

size	WT%	cumulative WT%
0	17.86	17.86
0.321928	5.667	23.527
0.736965	7.56	31.087
1.736966	17.098	48.185
2.736966	21.178	69.363
3.736966	20.526	89.889
5.64385619	10.111	100
Mean size	**sorting**	
2.74735	7.207403	
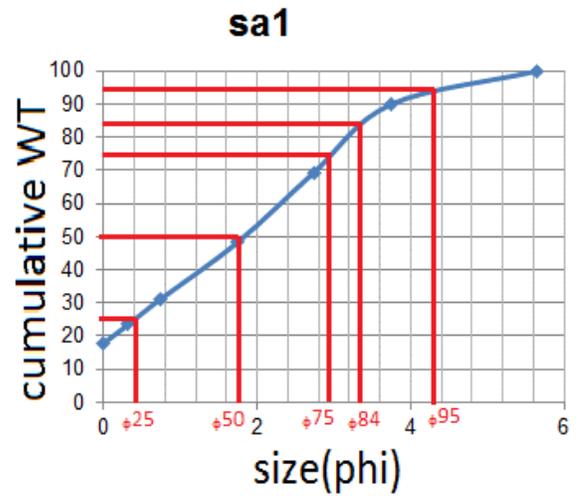
Table S17-1 Grain size analysis of core5sample1

Fig.S20-1 cumulative weight with grain size in Phi unit of core 5sample no. 1

size	WT %	cumulative WT %
0	14.668	14.668
0.321928	6.026	20.694
0.736965	8.783	29.477
1.736966	18.397	47.874
2.736966	19.26	67.134
3.736966	14.08	81.214
5.64385619	18.786	100
Mean size	**sorting**	
3.194333	8.320795	

Table S17-2 Grain size analysis of core5 sample 2

Fig.S20-2 cumulative weight with grain size in Phi unit of core 5sample no.2

size	WT %	cumulative WT %
0	9.063	9.063
0.321928	5.166	14.229
0.736965	7.214	21.443
1.736966	16.778	38.221
2.736966	39.002	77.223
3.736966	19.362	96.585
5.64385619	3.415	100
Mean size	**sorting**	
3.444333	6.181198	

Table S17-3 Grain size analysis of core 5 sample 3
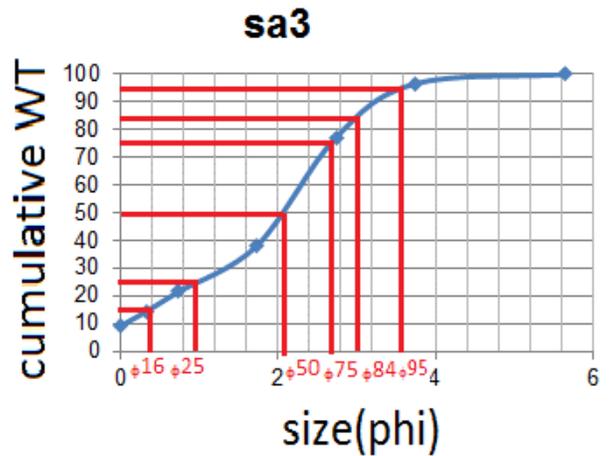
Fig.S20-3 cumulative weight with grain size in Phi unit of core 5sample no.3

size	WT %	cumulative WT %
0	8.832	8.832
0.321928	5.005	13.837
0.736965	8.729	22.566
1.736966	23.847	46.413
2.736966	39.947	86.36
3.736966	11.968	98.328
5.64385619	1.672	100
Mean size	**sorting**	
3.143667	5.499894	

Table S17-4Grain size analysis of core5 sample 4

Fig.S20-4 cumulative weight with grain size in Phi unit of core 5sample no.4

size	WT%	cumulative WT%
0	12.08	12.08
0.321928	5.501	17.581
0.736965	7.653	25.234
1.736966	20.936	46.17
2.736966	33.546	79.716
3.736966	15.336	95.052
5.64385619	4.948	100
Mean size	**sorting**	
2.9542	6.301268	

Table S18-1 Grain size analysis of core6 sample 1
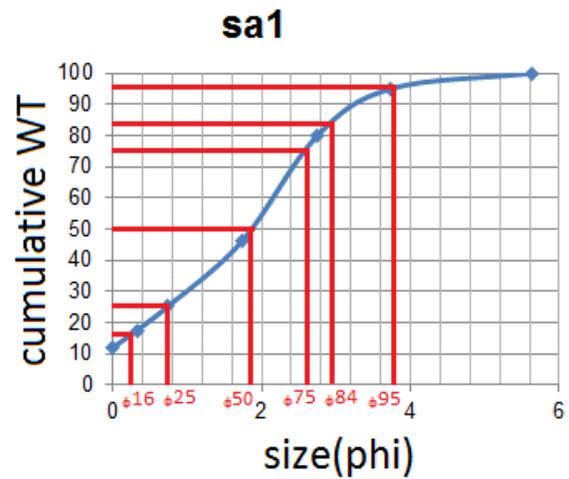
Fig.S21-1 cumulative weight with grain size in Phi unit of core 6sample no.1

size	WT %	cumulative WT %
0	6.629	6.629
0.321928	5.523	12.152
0.736965	10.884	23.036
1.736966	30.902	53.938
2.736966	30.55	84.488
3.736966	11.7	96.188
5.64385619	3.812	100
Mean size	**sorting**	
3.016567	5.800123	

Table S18-2 Grain size analysis of core6 sample 2
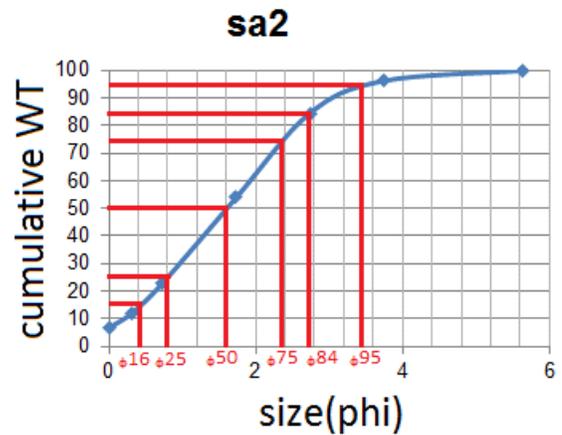
Fig.S21-2 cumulative weight with grain size in Phi unit of core 6sample no.2

size	WT %	cumulative WT %
0	5.373	5.373
0.321928	2.471	7.844
0.736965	4.715	12.559
1.736966	18.741	31.3
2.736966	42.834	74.134
3.736966	23.531	97.665
5.64385619	2.335	100
Mean size	**sorting**	
4.230667	6.066864	

Table S18-3 Grain size analysis of core6 sample 3
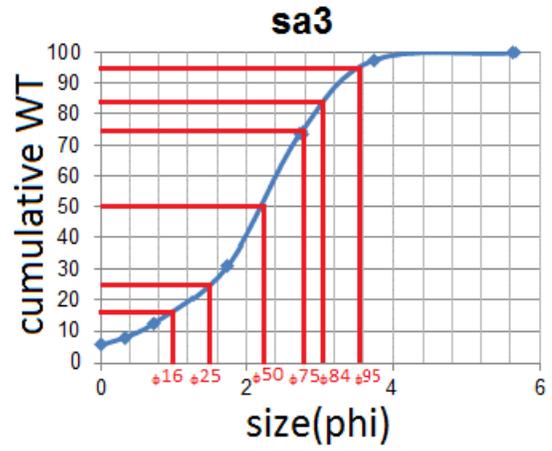
Fig.S21-3 cumulative weight with grain size in Phi unit of core 6sample no.3

size	WT %	cumulative WT %
0	7.461	7.461
0.321928	4.024	11.485
0.736965	5.243	16.728
1.736966	12.751	29.479
2.736966	34.17	63.649
3.736966	33.099	96.748
5.64385619	3.252	100
Mean size	**sorting**	
4.14435	6.565728	

Table S18-4 Grain size analysis of core6 sample 4
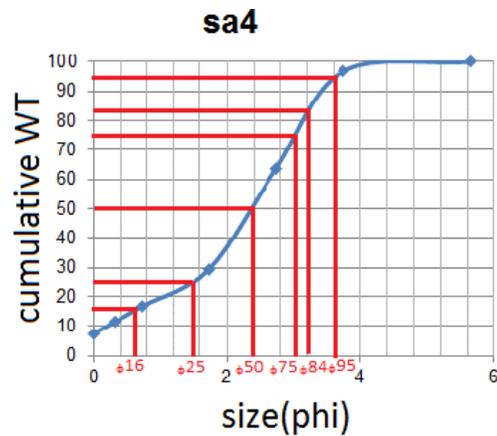
Fig.S21-4 cumulative weight with grain size in Phi unit of core 6sample no.4

size	WT %	Cumulative WT %
0	21.232	21.232
0.321928	3.486	24.718
0.736965	4.22	28.938
1.736966	13.023	41.961
2.736966	39.06	81.021
3.736966	16.889	97.91
5.64385619	2.09	100
Mean size	**sorting**	
2.792303	6.09195	
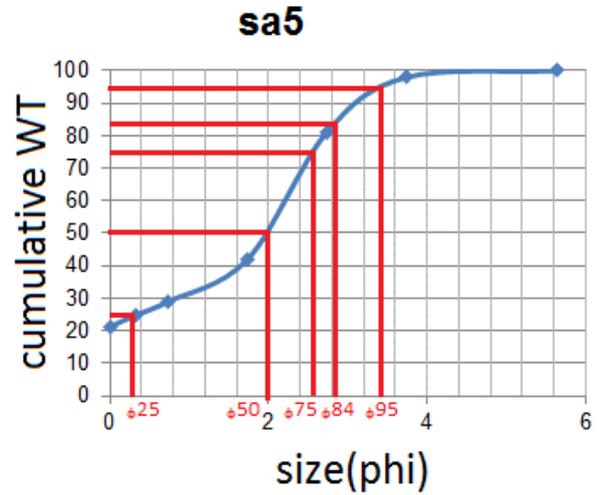
Table S18-5 Grain size analysis of core6 sample 5

Fig.S21-5 cumulative weight with grain size in Phi unit of core 6sample no.5

size	WT %	cumulative WT %
0	5.714	5.714
0.321928	1.877	7.591
0.736965	3.492	11.083
1.736966	8.056	19.139
2.736966	7.149	26.288
3.736966	50.041	76.329
5.64385619	23.571	99.9
Mean size	**sorting**	
5.77684	7.746483	
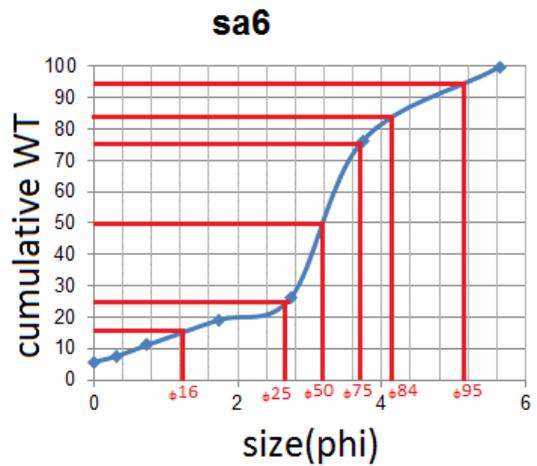
Table S18-6 Grain size analysis of core6 sample 6

Fig.S21-6 cumulative weight with grain size in Phi unit of core 6sample no.6

size	WT %	cumulative WT %
0	6.71	6.71
0.321928	4.838	11.548
0.736965	7.451	18.999
1.736966	18.138	37.137
2.736966	19.345	56.482
3.736966	20.685	77.167
5.64385619	22.833	100
Mean size	**sorting**	
4.407733	8.591306	

Table S18-7Grain size analysis of core6 sample 7
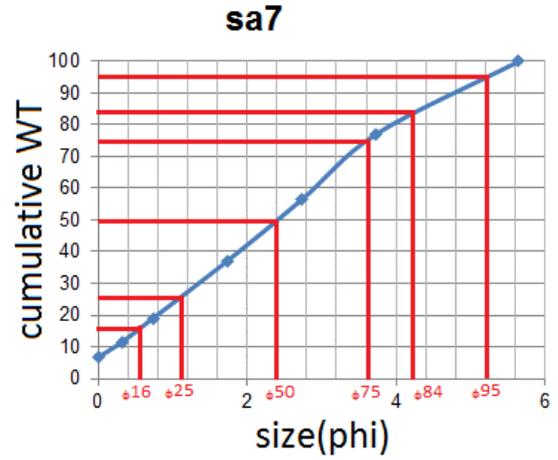
Fig.S21-7 cumulative weight with grain size in Phi unit of core 6sample no.7

size	WT %	cumulative WT %
0	12.974	12.974
0.321928	3.688	16.662
0.736965	5.139	21.801
1.736966	13.819	35.62
2.736966	19.25	54.87
3.736966	23.246	78.116
5.64385619	21.884	100
Mean size	**sorting**	
4.124667	8.556376	

Table S18-8 Grain size analysis of core6 sample 8
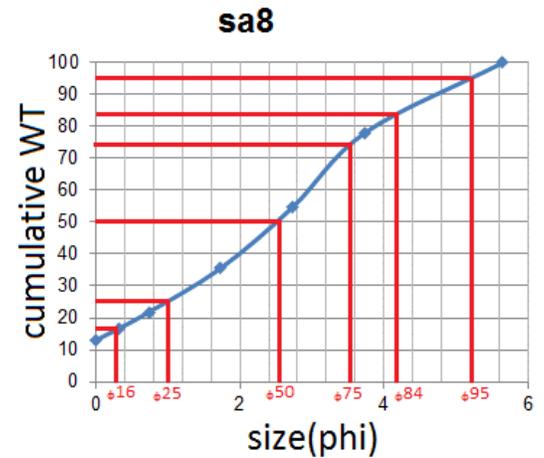
Fig.S21-8 cumulative weight with grain size in Phi unit of core 6sample no.8

size	WT %	cumulative WT %
0	20.926	20.926
0.321928	5.227	26.153
0.736965	9.033	35.186
1.736966	23.875	59.061
2.736966	25.999	85.06
3.736966	10.568	95.628
5.64385619	4.372	100
Mean size	**sorting**	
2.126867	6.011352	

Table S18-9 Grain size analysis of core6 sample 9
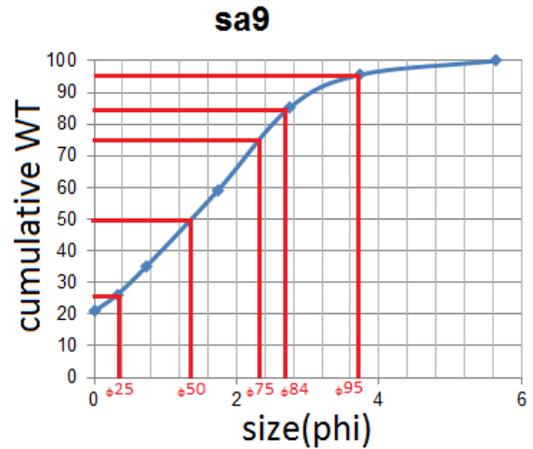
Fig.S21-8 cumulative weight with grain size in Phi unit of core 6sample no.8

size	WT %	cumulative WT %
0	8.888	8.888
0.321928	5.284	14.172
0.736965	7.095	21.267
1.736966	18.871	40.138
2.736966	34.261	74.399
3.736966	22.765	97.164
5.64385619	2.836	100
Mean size	**sorting**	
2.158133	5.641148	

Table S18-10 Grain size analysis of core6 sample 10
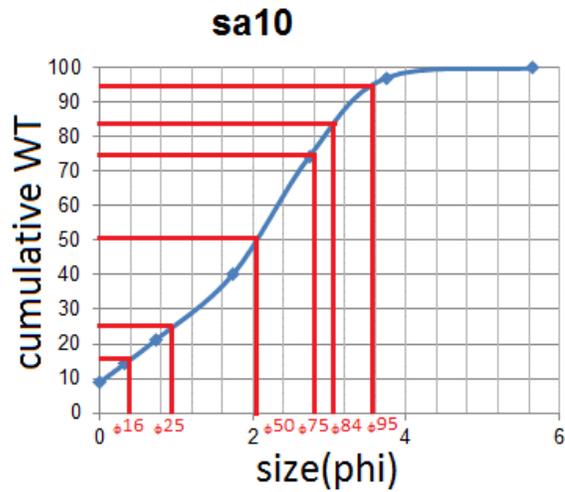
Fig.S21-10cumulative weight with grain size in Phi unit of core 6sample no.10

size	WT%	cumulative WT%
0	19.705	19.705
0.321928	4.66	24.365
0.736965	5.441	29.806
1.736966	12.106	41.912
2.736966	12.109	54.021
3.736966	22.004	76.025
5.64385619	23.975	100
Mean size	**sorting**	
3.559667	8.908765	
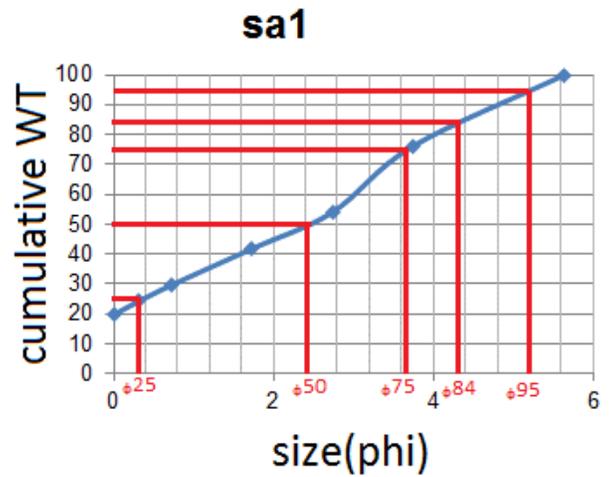
Table S19-1 Grain size analysis of core7 sample 1

Fig.S22-1cumulative weight with grain size in Phi unit of core 7 sample no.1

size	WT %	cumulative WT %
0	1.479	1.479
0.321928	1.991	3.47
0.736965	3.739	7.209
1.736966	18.045	25.254
2.736966	24.221	49.475
3.736966	26.999	76.474
5.64385619	23.526	100
Mean size	**sorting**	
5.427333	8.258818	
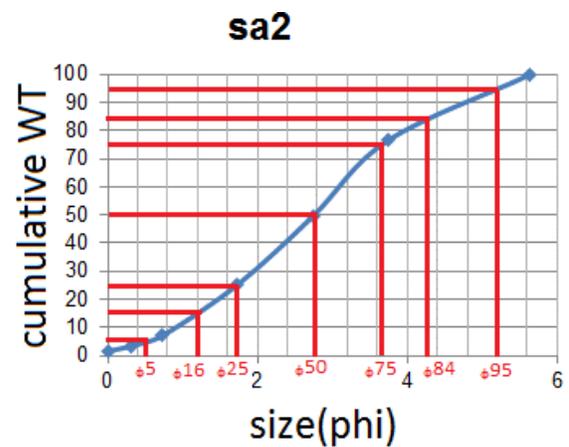
Table S19-2 Grain size analysis of core7 sample 2

Fig.S22-2cumulative weight with grain size in Phi unit of core 7 sample no.2

size	WT %	cumulative WT %
0	7.745	7.745
0.321928	4.267	12.012
0.736965	6.528	18.54
1.736966	14.631	33.171
2.736966	16.548	49.719
3.736966	31.631	81.35
5.64385619	18.65	100
Mean size	**sorting**	
4.609333	7.874689	
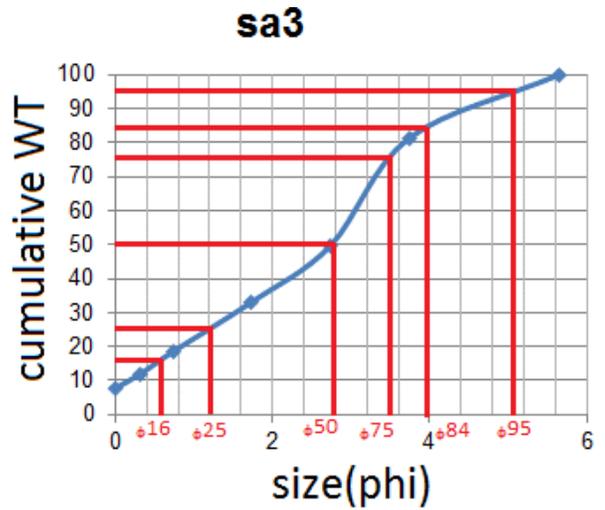
Table S19-3 Grain size analysis of core 7 sample 3

Fig.S22-3cumulative weight with grain size in Phi unit of core 7 sample no.3

size	WT %	cumulative WT %
0	5.017	5.017
0.321928	5.279	10.296
0.736965	9.404	19.7
1.736966	20.586	40.286
2.736966	22.231	62.517
3.736966	21.633	84.15
5.64385619	15.85	100
Mean size	**sorting**	
4.035333	7.772455	
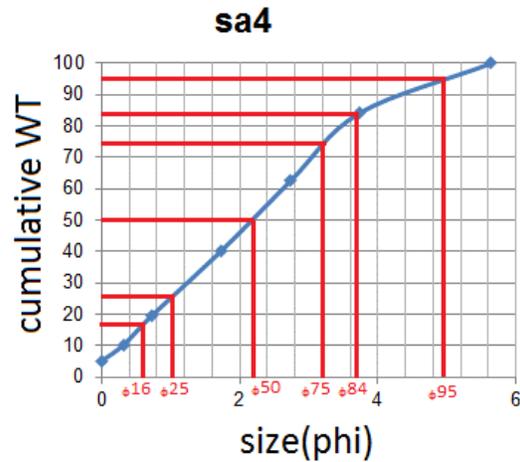
Table S19-4 Grain size analysis of core7 sample 4

Fig.S22-4cumulative weight with grain size in Phi unit of core 7 sample no.4

size	WT %	cumulative WT %
0	16.421	16.421
0.321928	6.253	22.674
0.736965	6.933	29.607
1.736966	14.186	43.793
2.736966	25.079	68.872
3.736966	20.125	88.997
5.64385619	11.003	100
Mean size	**sorting**	
3.146333	7.327932	
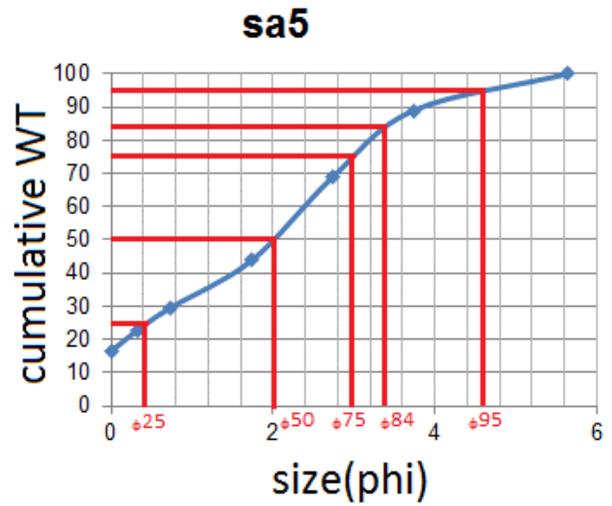
Table S19-5 Grain size analysis of core7 sample 5	Fig.S22-5cumulative weight with grain size in Phi unit of core 7 sample no.5

size	WT %	cumulative WT %
0	17.089	17.089
0.321928	4.37	21.459
0.736965	5.675	27.134
1.736966	14.06	41.194
2.736966	19.277	60.471
3.736966	21.661	82.132
5.64385619	17.868	100
Mean size	**sorting**	
3.145	7.283932	
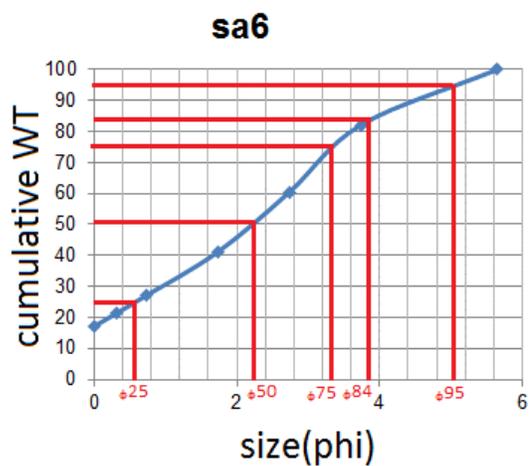
Table S19-6 Grain size analysis of core7 sample 6	Fig.S22-6cumulative weight with grain size in Phi unit of core 7 sample no.6

size	WT %	cumulative WT %
0	2.677	2.677
0.321928	2.189	4.866
0.736965	4.133	8.999
1.736966	12.959	21.958
2.736966	35.526	57.484
3.736966	38.678	96.162
5.64385619	3.838	100
Mean size	**sorting**	
5.089	6.445371	
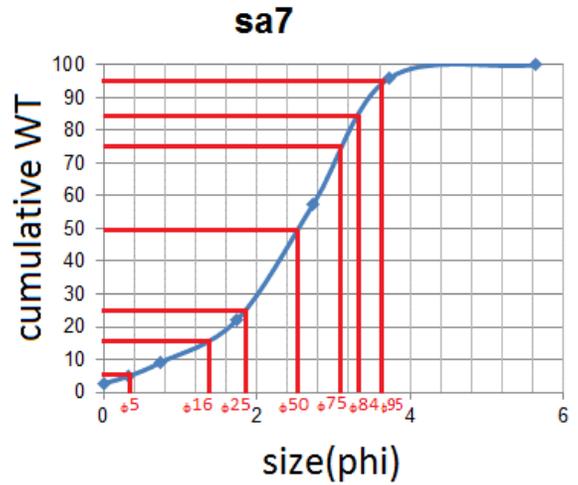
Table S19-7 Grain size analysis of core7 sample 7

Fig.S22-7cumulative weight with grain size in Phi unit of core 7 sample no.7

size	WT %	Cumulative WT %
0	3.342	3.342
0.321928	2.276	5.618
0.736965	4.229	9.847
1.736966	16.873	26.72
2.736966	45.967	72.687
3.736966	25.797	98.484
5.64385619	1.516	100
Mean size	**sorting**	
4.566333	5.950106	
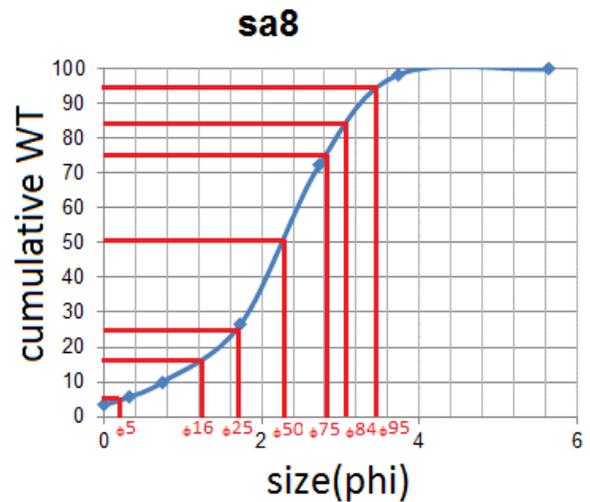
Table S19-8 Grain size analysis of core7 sample 8

Fig.S22-8cumulative weight with grain size in Phi unit of core 7 sample no.8

size	WT %	Cumulative WT %
0	20.675	20.675
0.321928	5.094	25.769
0.736965	5.709	31.478
1.736966	13.476	44.954
2.736966	17.944	62.898
3.736966	20.785	83.683
5.64385619	16.317	100
Mean size	**sorting**	
2.936667	8.100682	

Table S20-1 Grain size analysis of core8 sample 1
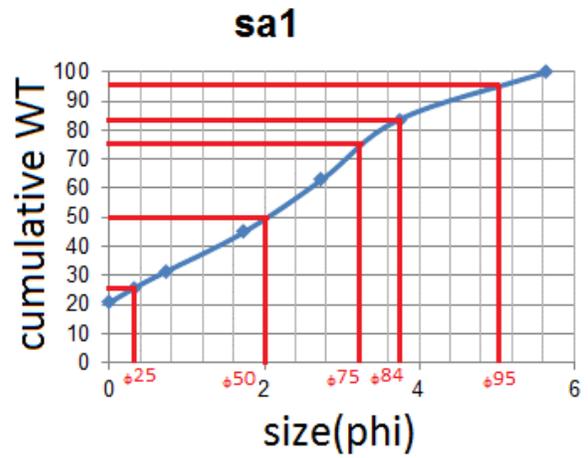
Fig.S23-1 cumulative weight with grain size in Phi unit of core 8 sample no.1

size	WT %	cumulative WT %
0	11.854	11.854
0.321928	5.719	17.573
0.736965	7.968	25.541
1.736966	17.606	43.147
2.736966	19.204	62.351
3.736966	25.493	87.844
5.64385619	12.156	100
Mean size	**sorting**	
3.563333	7.391894	

Table S20-2 Grain size analysis of core8 sample 2
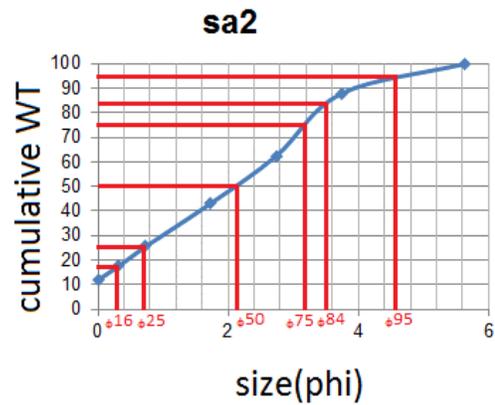
Fig.S23-2 cumulative weight with grain size in Phi unit of core 8 sample no.2

size	WT %	cumulative WT %
0	12.99	12.99
0.321928	5.506	18.496
0.736965	7.494	25.99
1.736966	16.485	42.475
2.736966	20.307	62.782
3.736966	23.481	86.263
5.64385619	13.737	100
Mean size	**sorting**	
3.54	7.601212	

Table S20-3 Grain size analysis of core8 sample 3
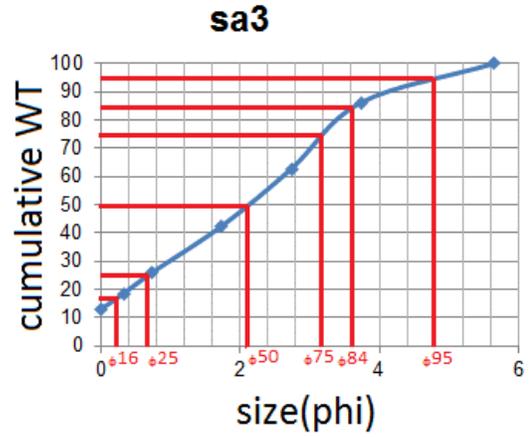
Fig.S23-3 cumulative weight with grain size in Phi unit of core 8 sample no.3

size	WT %	cumulative WT %
0	5.575	5.575
0.321928	5.022	10.597
0.736965	10.469	21.066
1.736966	28.401	49.467
2.736966	20.078	69.545
3.736966	15.339	84.884
5.64385619	15.116	100
Mean size	**sorting**	
3.53	7.738227	

Table S20-4 Grain size analysis of core8 sample 4
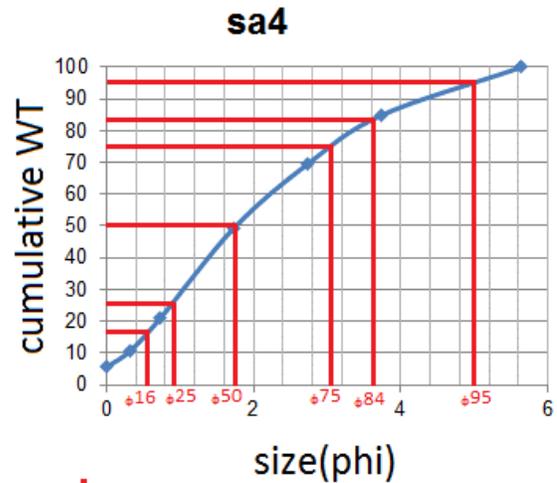
Fig.S23-4 cumulative weight with grain size in Phi unit of core 8 sample no.4

size	WT %	cumulative WT %
0	7.791	7.791
0.321928	2.314	10.105
0.736965	3.58	13.685
1.736966	13.61	27.295
2.736966	40.906	68.201
3.736966	22.597	90.798
5.64385619	9.202	100
Mean size	**sorting**	
4.473	6.872477	
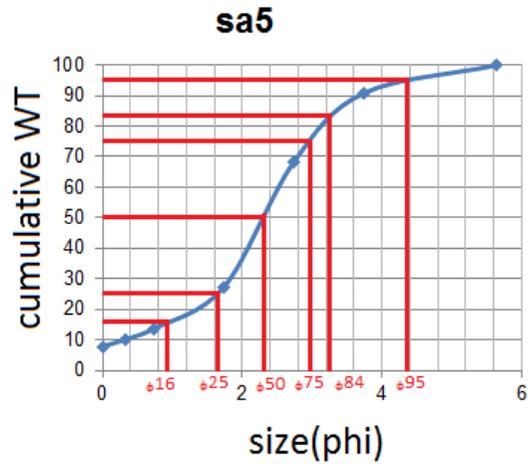
Table S20-5 Grain size analysis of core8 sample 5

Fig.S23-5 cumulative weight with grain size in Phi unit of core 8 sample no.5

size	WT %	cumulative WT %
0	2.102	2.102
0.321928	1.637	3.739
0.736965	3.341	7.08
1.736966	14.67	21.75
2.736966	41.881	63.631
3.736966	27.373	91.004
5.64385619	8.996	100
Mean size	**sorting**	
5.066	6.644068	
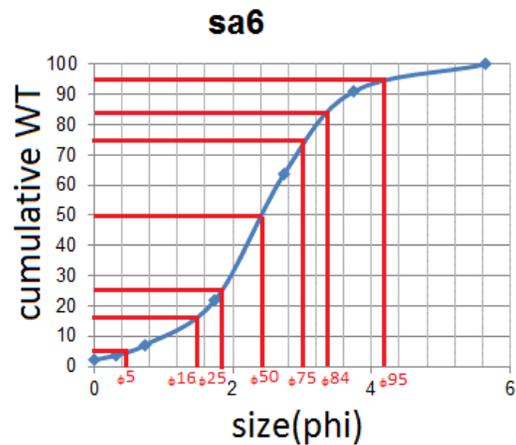
Table S20-6 Grain size analysis of core8 sample 6

Fig.S23-6 cumulative weight with grain size in Phi unit of core 8 sample no.6

size	WT %	cumulative WT %
0	2.811	2.811
0.321928	2.381	5.192
0.736965	4.761	9.953
1.736966	18.791	28.744
2.736966	36.495	65.239
3.736966	24.988	90.227
5.64385619	9.773	100
Mean size	**sorting**	
4.643333	6.827212	

Table S20-7 Grain size analysis of core8 sample 7
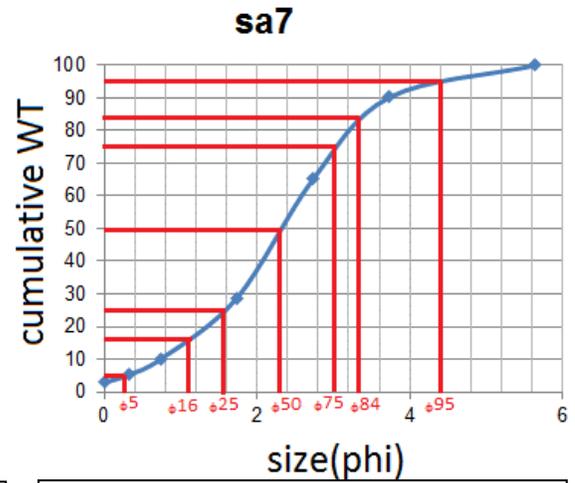
Fig.S23-7 cumulative weight with grain size in Phi unit of core 8 sample no.7

size	WT %	cumulative WT %
0	4.576	4.576
0.321928	4.191	8.767
0.736965	7.763	16.53
1.736966	24.216	40.746
2.736966	30.117	70.863
3.736966	19.961	90.824
5.64385619	9.176	100
Mean size	**sorting**	
3.853667	6.859189	

Table S20-8 Grain size analysis of core8 sample 8
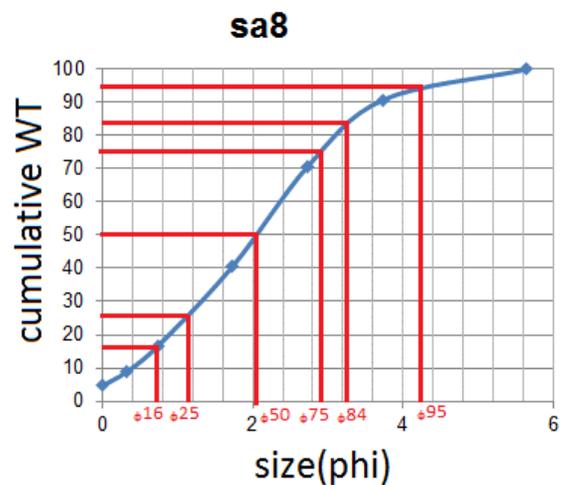
Fig.S23-8 cumulative weight with grain size in Phi unit of core 8 sample no.8

size	WT %	cumulative WT %
0	5.259	5.259
0.321928	4.712	9.971
0.736965	8.533	18.504
1.736966	23.677	42.181
2.736966	31.706	73.887
3.736966	18.695	92.582
5.64385619	7.418	100
Mean size	**sorting**	
3.786667	6.868432	

Table S20-9 Grain size analysis of core8 sample 9
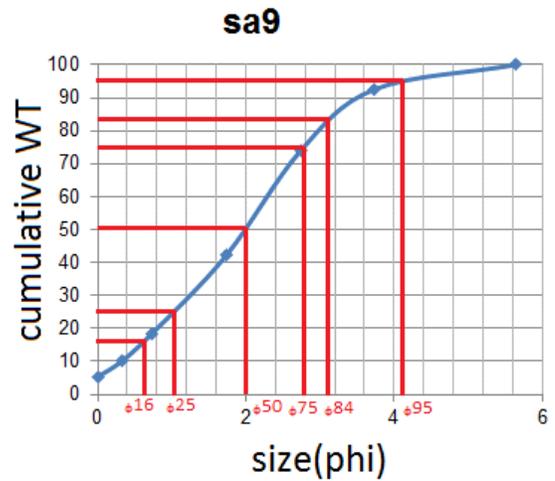
Fig.S23-9 cumulative weight with grain size in Phi unit of core 8 sample no.9

size	WT %	cumulative WT %
0	47.888	47.888
0.321928	15.571	63.459
0.736965	10.567	74.026
1.736966	12.851	86.877
2.736966	8.662	95.539
3.736966	4.116	99.655
5.64385619	0.615	100.27
Mean size	**sorting**	
0.343667	3.553182	

Table S20-10 Grain size analysis of core8 sample 10
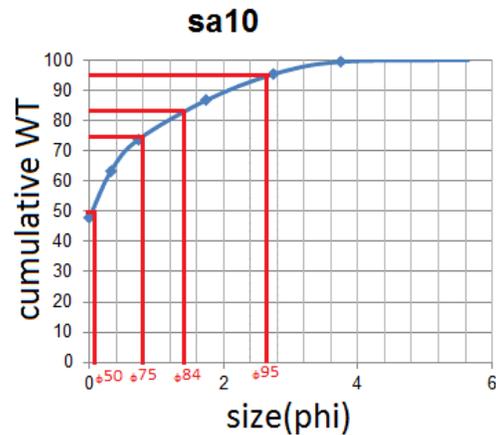
Fig.S23-10 cumulative weight with grain size in Phi unit of core 8 sample no.10

size	WT %	cumulative WT %
0	30	30
0.321928	3.948	33.948
0.736965	6	39.948
1.736966	1.616	41.564
2.736966	17.006	58.57
3.736966	17.14	75.71
5.64385619	24.29	100
Mean size	**sorting**	
3.281333	9.046121	

Table S21-1 Grain size analysis of core 9 sample 1
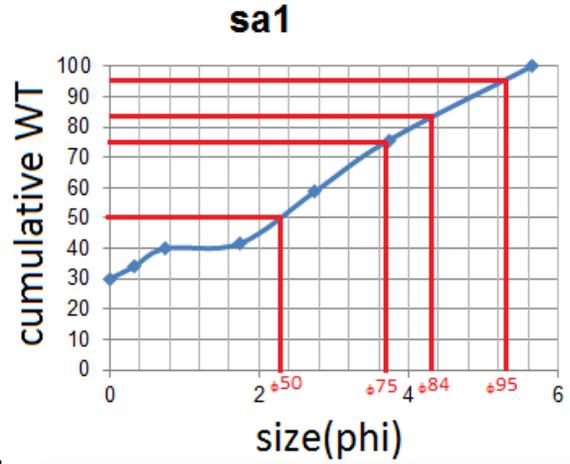
Fig.S24-1 cumulative weight with grain size in Phi unit of core 9 sample no.1

size	WT %	cumulative WT %
0	2.866	2.866
0.321928	1.744	4.61
0.736965	2.286	6.896
1.736966	7.879	14.775
2.736966	8.924	23.699
3.736966	36.107	59.806
5.64385619	40.194	100
Mean size	**sorting**	
7.052333	8.930379	

Table S21-2 Grain size analysis of core 9 sample 2

Fig.S24-2 cumulative weight with grain size in Phi unit of core 9 sample no.2

size	WT %	Cumulative WT %
0	1.922	1.922
0.321928	0.988	2.91
0.736965	2.487	5.397
1.736966	22.663	28.06
2.736966	62.407	90.467
3.736966	7.156	97.623
5.64385619	2.377	100
Mean size	**sorting**	
4.39	4.889439	

Table S21-3 Grain size analysis of core 9 sample 3
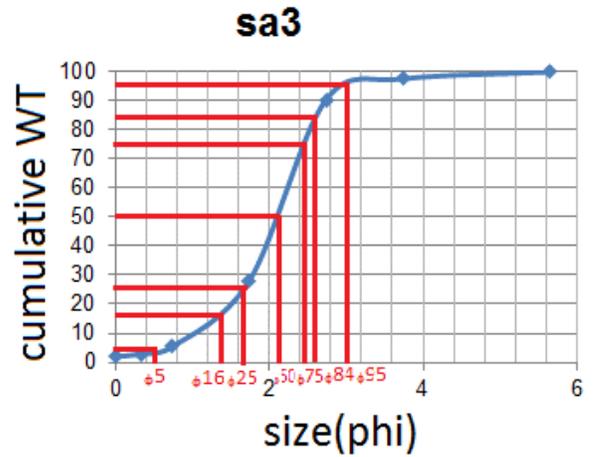
Fig.S24-3 cumulative weight with grain size in Phi unit of core 9 sample no.3

size	WT %	cumulative WT %
0	13.306	13.306
0.321928	7.608	20.914
0.736965	9.232	30.146
1.736966	17.168	47.314
2.736966	13.067	60.381
3.736966	25.112	85.493
5.64385619	14.507	100
Mean size	**sorting**	
3.279	7.672144	

Table S21-4 Grain size analysis of core 9 sample 4
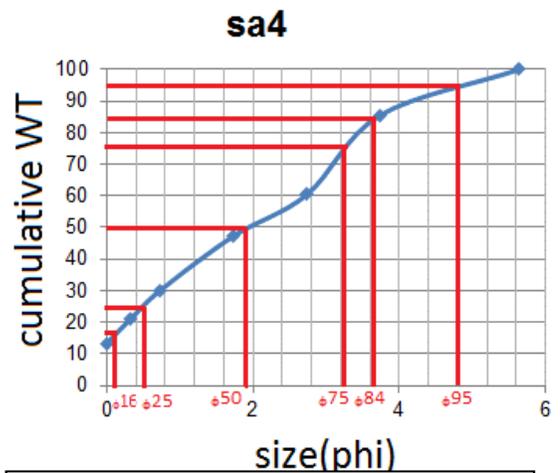
Fig.S24-4 cumulative weight with grain size in Phi unit of core 9 sample no.4

size	WT %	cumulative WT %
0	5.608	5.608
0.321928	3.922	9.53
0.736965	5.718	15.248
1.736966	18.1	33.348
2.736966	28.262	61.61
3.736966	21.006	82.616
5.64385619	17.384	100
Mean size	**sorting**	
4.378333	8.00303	
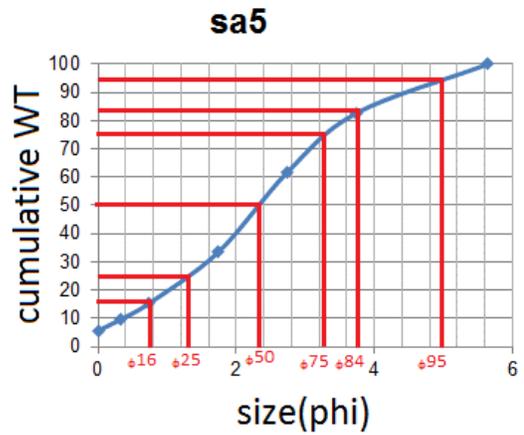
Table S21-5 Grain size analysis of core 9 sample 5

Fig.S24-5 cumulative weight with grain size in Phi unit of core 9 sample no.5

size	WT %	cumulative WT %
0	3.909	3.909
0.321928	2.029	5.938
0.736965	3.91	9.848
1.736966	17.192	27.04
2.736966	46.686	73.726
3.736966	24.519	98.245
5.64385619	1.755	100
Mean size	**sorting**	
4.378333	7.94303	
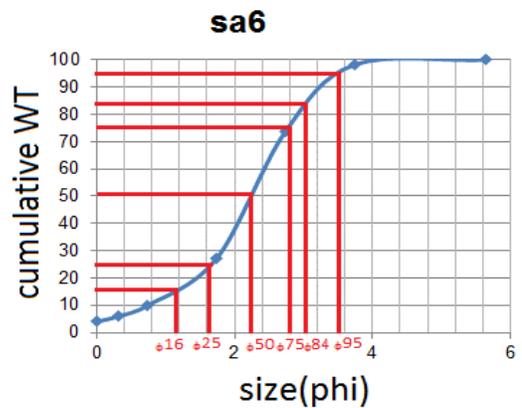
Table S21-6 Grain size analysis of core 9 sample 6

Fig.S24-6 cumulative weight with grain size in Phi unit of core 9 sample no.6

size	WT %	cumulative WT %
0	1.839	1.839
0.321928	1.448	3.287
0.736965	2.941	6.228
1.736966	18.49	24.718
2.736966	52.466	77.184
3.736966	13.853	91.037
5.64385619	8.963	100
Mean size	**sorting**	
4.645667	5.921045	

Table S21-7 Grain size analysis of core 9 sample 7
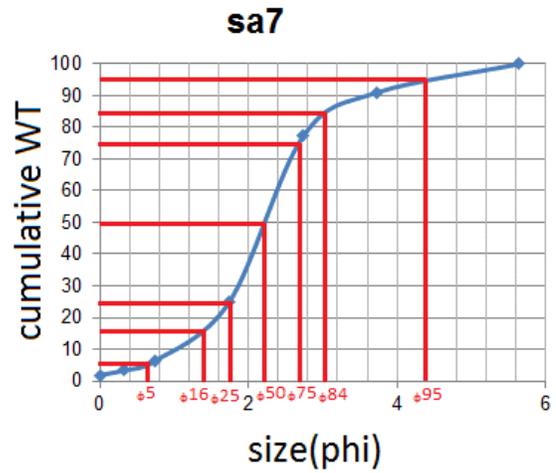
Fig.S24-7 cumulative weight with grain size in Phi unit of core 9 sample no.7

size	WT %	cumulative WT %
0	0.434	0.434
0.321928	0.639	1.073
0.736965	2.108	3.181
1.736966	22.012	25.193
2.736966	67.129	92.322
3.736966	4.206	96.528
5.64385619	3.472	100
Mean size	**sorting**	
4.746667	6.8925	

Table S21-8 Grain size analysis of core 9 sample 8
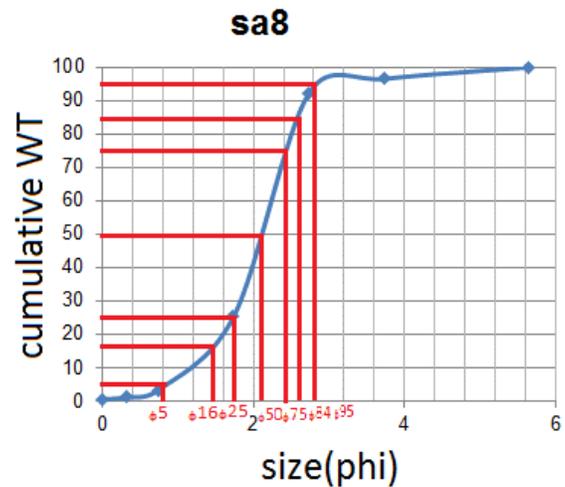
Fig.S24-8 cumulative weight with grain size in Phi unit of core 9 sample no.8

size	WT %	cumulative WT %
0	1.408	1.408
0.321928	1.524	2.932
0.736965	3.903	6.835
1.736966	30.593	37.428
2.736966	56.744	94.172
3.736966	3.622	97.794
5.64385619	2.206	100
Mean size	**sorting**	
3.97	4.647561	
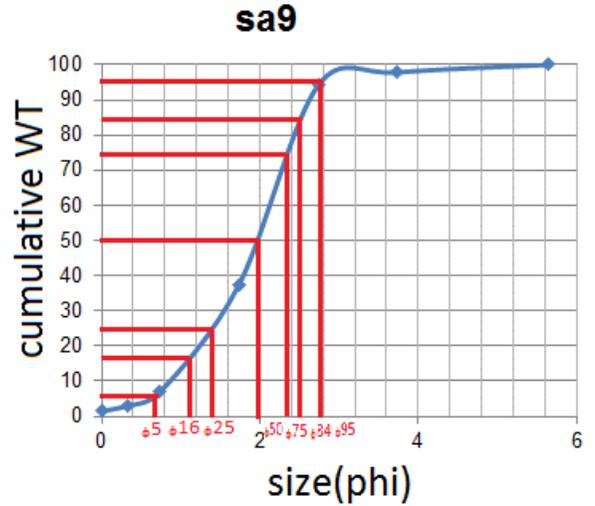
Table S21-9 Grain size analysis of core 9 sample 9

Fig.S24-9 cumulative weight with grain size in Phi unit of core 9 sample no.9

size	WT %	cumulative WT %
0	3.509	3.509
0.321928	1.295	4.804
0.736965	2.69	7.494
1.736966	17.405	24.899
2.736966	47.067	71.966
3.736966	22.487	94.453
5.64385619	5.547	100
Mean size	**sorting**	
4.756	6.198659	
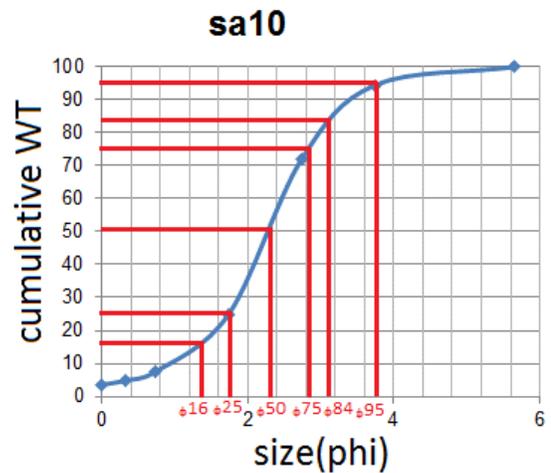
Table S21-10 Grain size analysis of core 9 sample 10

Fig.S24-10 cumulative weight with grain size in Phi unit of core 9 sample no.10

size	WT %	cumulative WT %
0	3.315	3.315
0.321928	2.344	5.659
0.736965	4.935	10.594
1.736966	16.751	27.345
2.736966	44.147	71.492
3.736966	24.123	95.615
5.64385619	4.385	100
Mean size	**sorting**	
4.538533	6.145212	

Table S21-11 Grain size analysis of core 9 sample 11
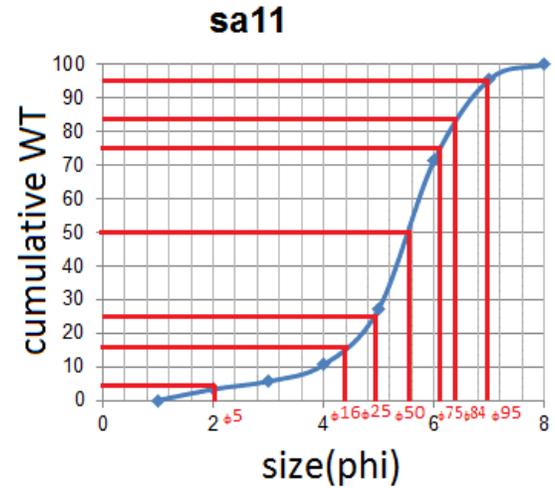
Fig.S24-11 cumulative weight with grain size in Phi unit of core 9 sample no.11

size	WT %	cumulative WT %
0	6.218	6.218
0.321928	4.247	10.465
0.736965	5.447	15.912
1.736966	10.081	25.993
2.736966	6.807	32.8
3.736966	31.491	64.291
5.64385619	35.709	100
Mean size	**sorting**	
5.437333	9.155152	

Table S22-1 Grain size analysis of core 10 sample 1
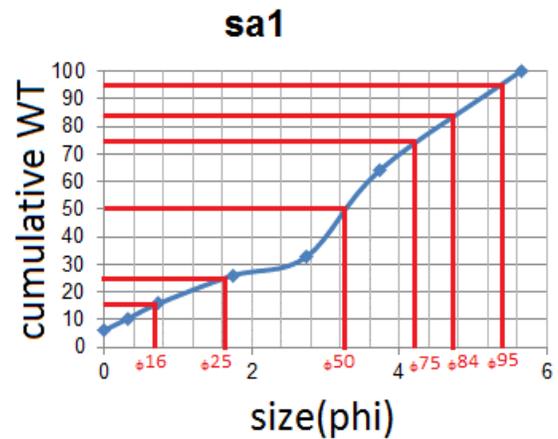
Fig.S25-1 cumulative weight with grain size in Phi unit of core 10 sample no.1

size	WT %	cumulative WT %
0	11.452	11.452
0.321928	5.568	17.02
0.736965	7.146	24.166
1.736966	15.77	39.936
2.736966	15.462	55.398
3.736966	26.091	81.489
5.64385619	18.511	100
Mean size	**sorting**	
1290.38	8.093182	

Table S22-2 Grain size analysis of core 10 sample 2
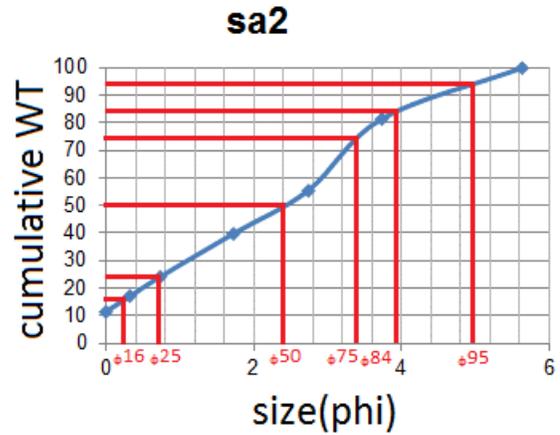
Fig.S25-2 cumulative weight with grain size in Phi unit of core 10 sample no.2

size	WT %	cumulative WT %
0	10.549	10.549
0.321928	4.603	15.152
0.736965	6.955	22.107
1.736966	14.546	36.653
2.736966	17.9	54.553
3.736966	23.196	77.749
5.64385619	22.251	100
Mean size	**sorting**	
4.99	7.655432	

Table S22-3 Grain size analysis of core 10 sample 3
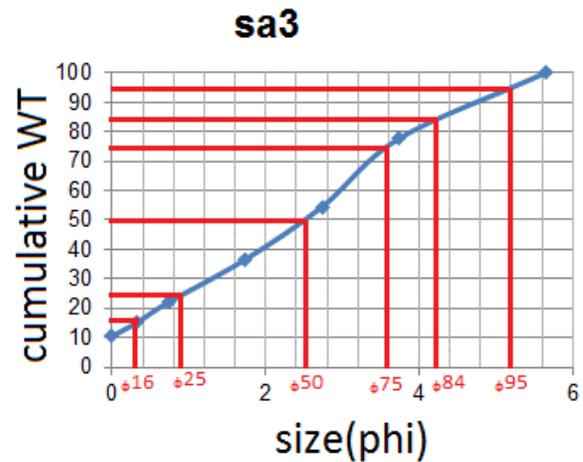
Fig.S25-3 cumulative weight with grain size in Phi unit of core 10 sample no.3

size	WT %	cumulative WT %
0	13.758	13.758
0.321928	4.032	17.79
0.736965	5.453	23.243
1.736966	14.843	38.086
2.736966	19.629	57.715
3.736966	21.844	79.559
5.64385619	20.441	100
Mean size	**sorting**	
3.501667	7.650432	

Table S22-4 Grain size analysis of core 10 sample 4
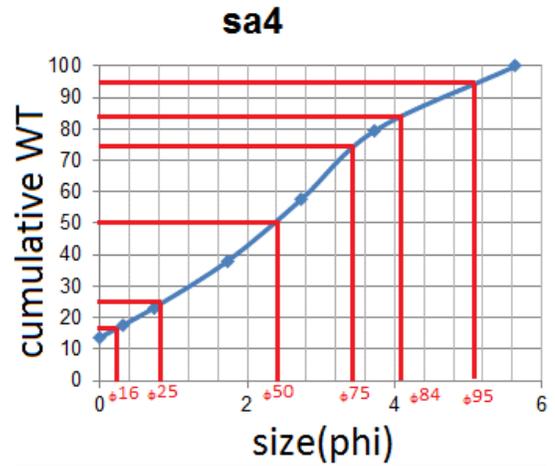
Fig.S25-4 cumulative weight with grain size in Phi unit of core 10 sample no.4

size	WT %	cumulative WT %
0	10.065	10.065
0.321928	5.696	15.761
0.736965	9.239	25
1.736966	19.811	44.811
2.736966	20.169	64.98
3.736966	20.92	85.9
5.64385619	14.1	100
Mean size	**sorting**	
3.571333	7.642705	

Table S22-5 Grain size analysis of core 10 sample 5
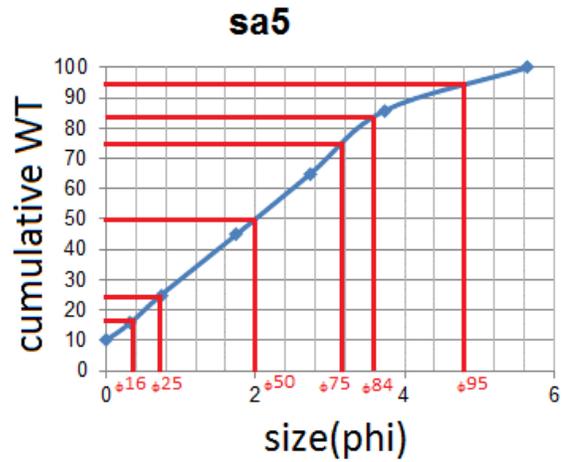
Fig.S25-5 cumulative weight with grain size in Phi unit of core 10 sample no.5

size	WT %	cumulative WT %
0	22.967	22.967
0.321928	6.79	29.757
0.736965	8.252	38.009
1.736966	14.72	52.729
2.736966	11.574	64.303
3.736966	19.403	83.706
5.64385619	16.294	100
Mean size	**sorting**	
2.558	8.056432	
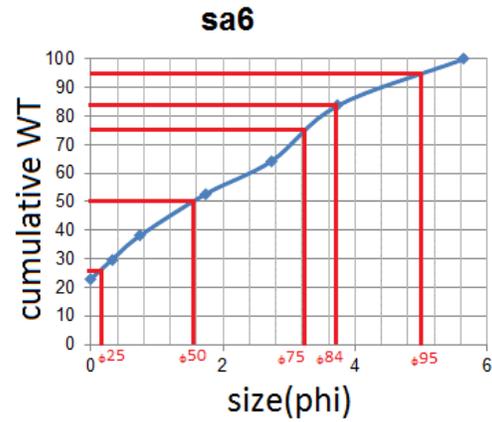
Table S22-6 Grain size analysis of core 10 sample 6

Fig.S25-6 cumulative weight with grain size in Phi unit of core 10 sample no.6

size	WT %	cumulative WT %
0	22.427	22.427
0.321928	11.185	33.612
0.736965	13.982	47.594
1.736966	23.76	71.354
2.736966	12.991	84.345
3.736966	10.598	94.943
5.64385619	5.057	100
Mean size	**sorting**	
1.598333	5.682985	
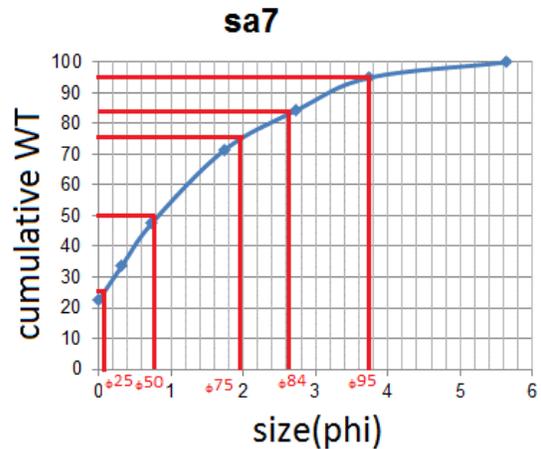
Table S22-7 Grain size analysis of core 10 sample 7

Fig.S25-7 cumulative weight with grain size in Phi unit of core 10 sample no.7

size	WT %	cumulative WT %
0	5.061	5.061
0.321928	4.958	10.019
0.736965	8.251	18.27
1.736966	21.226	39.496
2.736966	36.676	76.172
3.736966	19.194	95.366
5.64385619	4.634	100
Mean size	**sorting**	
3.072667	6.393205	

Table S22-8 Grain size analysis of core 10 sample 8
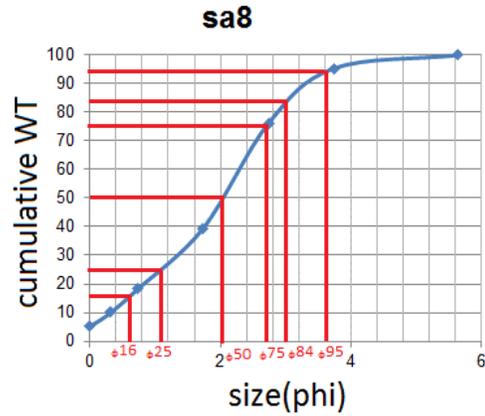
Fig.S25-8 cumulative weight with grain size in Phi unit of core 10 sample no.8

size	WT %	cumulative WT %
0	5.049	5.049
0.321928	3.466	8.515
0.736965	6.746	15.261
1.736966	19.703	34.964
2.736966	34.84	69.804
3.736966	22.215	92.019
5.64385619	7.981	100
Mean size	**sorting**	
4.067333	6.683636	

Table S22-9 Grain size analysis of core 10 sample 9
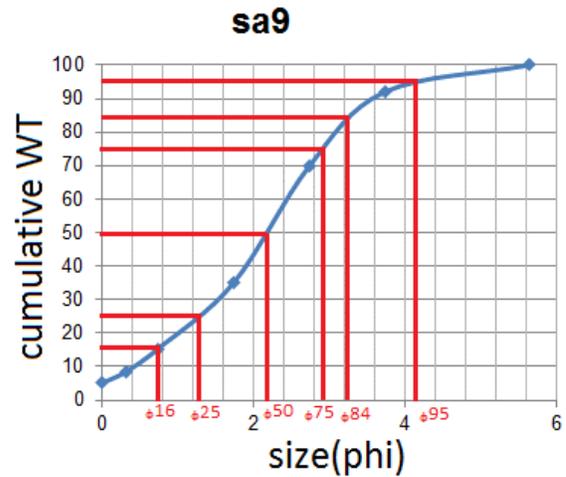
Fig.S25-9 cumulative weight with grain size in Phi unit of core 10 sample no.9

size	WT %	cumulative WT %
0	5.379	5.379
0.321928	3.316	8.695
0.736965	5.837	14.532
1.736966	21.458	35.99
2.736966	39.146	75.136
3.736966	23.372	98.508
5.64385619	1.492	100
Mean size	**sorting**	
3.975667	6.014902	
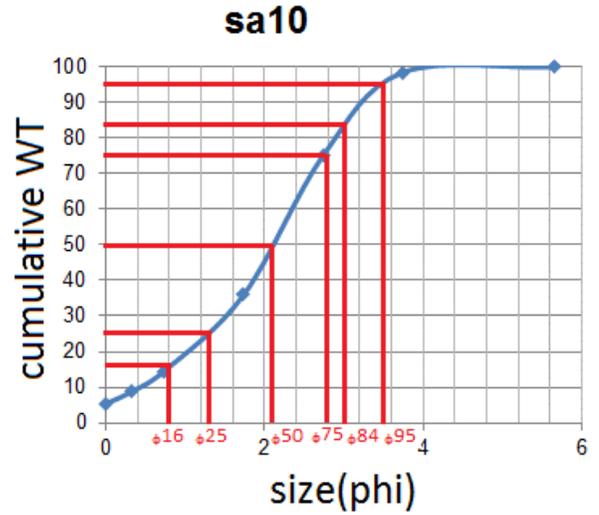
Table S22-10 Grain size analysis of core 10 sample 10

Fig.S25-10 cumulative weight with grain size in Phi unit of core 10 sample no.10

size	WT%	cumulative WT%
0	11.988	11.988
0.321928	4.821	16.809
0.736965	7.175	23.984
1.736966	23.451	47.435
2.736966	26.101	73.536
3.736966	15.357	88.893
5.64385619	11.107	100
Mean size	**sorting**	
3.0551	7.308591	
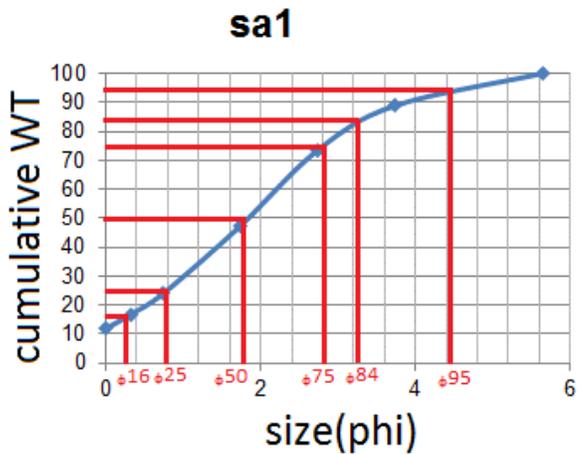
Table S23-1 Grain size analysis of core 11 sample 1

Fig.S26-1 cumulative weight with grain size in Phi unit of core 11 sample no.1

size	WT %	cumulative WT %
0	10.002	10.002
0.321928	6.29	16.292
0.736965	11.833	28.125
1.736966	32.391	60.516
2.736966	23.359	83.875
3.736966	7.461	91.336
5.64385619	8.664	100
Mean size	**sorting**	
2.603333	6.83197	
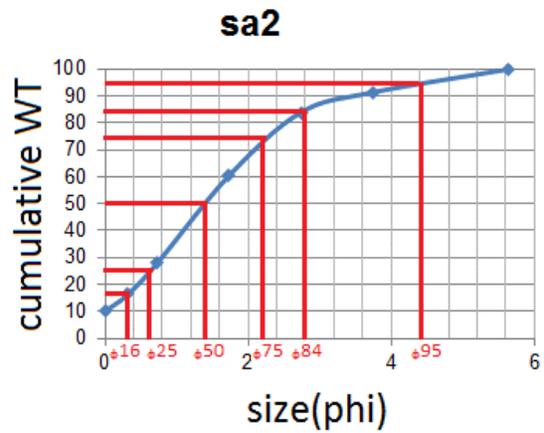
Table S23-2 Grain size analysis of core 11 sample 2

Fig.S26-2 cumulative weight with grain size in Phi unit of core 11 sample no.2

size	WT %	cumulative WT %
0	10.086	10.086
0.321928	9.937	20.023
0.736965	15.85	35.873
1.736966	30.433	66.306
2.736966	12.631	78.937
3.736966	9.7	88.637
5.64385619	11.363	100
Mean size	**sorting**	
2.411333	6.962644	
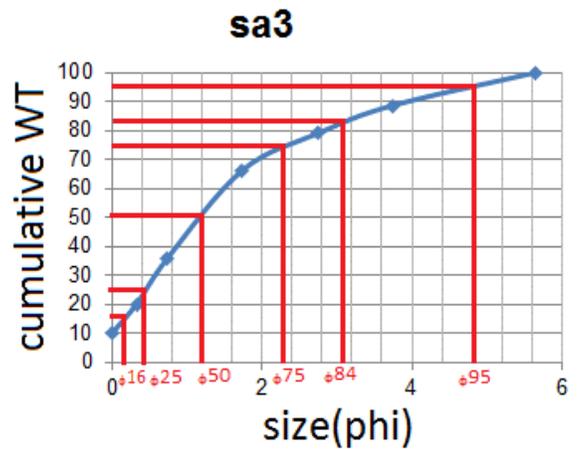
Table S23-3 Grain size analysis of core 11 sample 3

Fig.S26-3 cumulative weight with grain size in Phi unit of core 11 sample no.3

size	WT %	cumulative WT %
0	21.078	21.078
0.321928	7.295	28.373
0.736965	10.255	38.628
1.736966	21.391	60.019
2.736966	12.408	72.427
3.736966	9.7	82.127
5.64385619	11.363	93.49
Mean size	**sorting**	
2.26	8.868258	

Table S23-4 Grain size analysis of core 11 sample 4
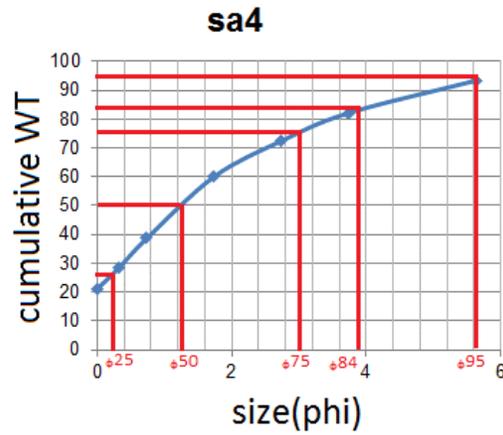
Fig.S26-4 cumulative weight with grain size in Phi unit of core 11 sample no.4

size	WT %	cumulative WT %
0	40.677	40.677
0.321928	8.696	49.373
0.736965	10.204	59.577
1.736966	17.489	77.066
2.736966	10.146	87.212
3.736966	7.402	94.614
5.64385619	5.386	100
Mean size	**sorting**	
1.133333	5.394	

Table S23-5 Grain size analysis of core 11 sample 5
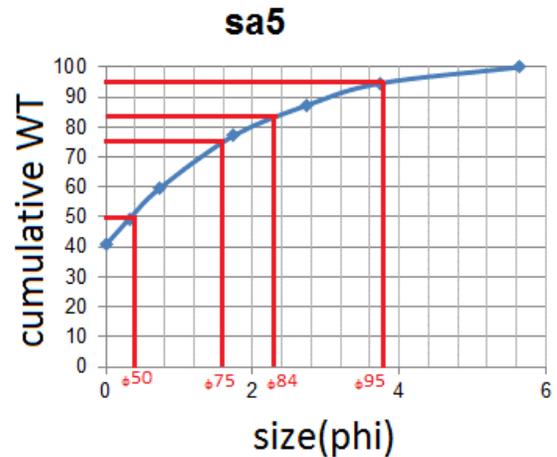
Fig.S26-5 cumulative weight with grain size in Phi unit of core 11 sample no.5

size	WT %	cumulative WT %
0	0.848	0.848
0.321928	1.313	2.161
0.736965	4.696	6.857
1.736966	34.518	41.375
2.736966	54.704	96.079
3.736966	2.3	98.379
5.64385619	1.621	100
Mean size	**sorting**	
3.826667	4.614773	

Table S23-6 Grain size analysis of core 11 sample 6
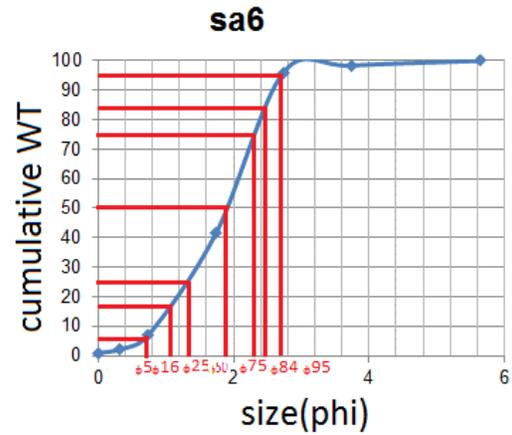
Fig.S26-6 cumulative weight with grain size in Phi unit of core 11 sample no.6

size	WT %	cumulative WT %
0	13.269	13.269
0.321928	10.165	23.434
0.736965	14.999	38.433
1.736966	28.467	66.9
2.736966	14.591	81.491
3.736966	8.007	89.498
5.64385619	10.502	100
Mean size	**sorting**	
2.168	6.854667	

Table S23-7 Grain size analysis of core 11 sample 7
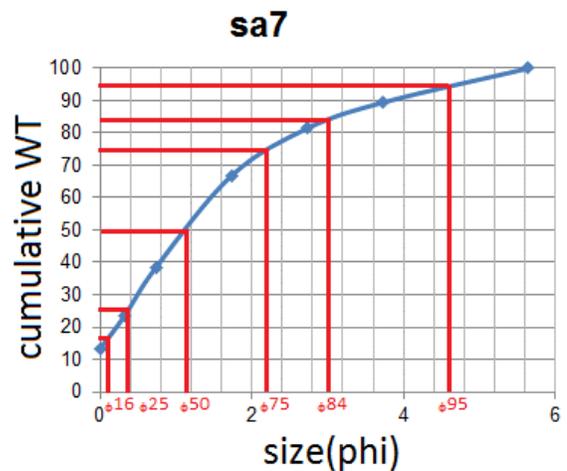
Fig.S26-7 cumulative weight with grain size in Phi unit of core 11 sample no.7

size	WT %	cumulative WT %
0	7.155	7.155
0.321928	3.783	10.938
0.736965	6.379	17.317
1.736966	17.027	34.344
2.736966	19.941	54.285
3.736966	26.131	80.416
5.64385619	19.584	100
Mean size	**sorting**	
4.503333	8.117197	

Table S23-8 Grain size analysis of core 11 sample 8
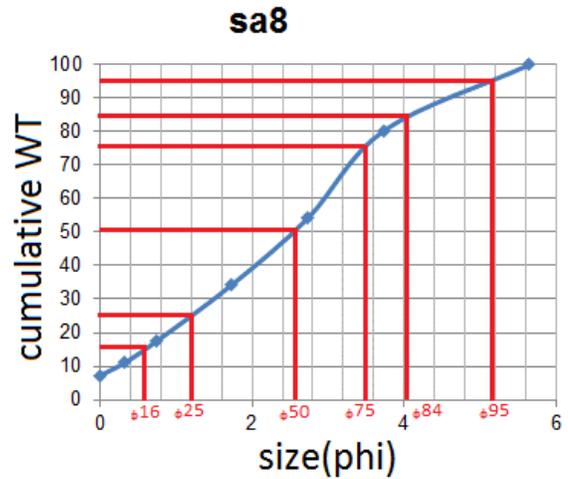
Fig.S26-8 cumulative weight with grain size in Phi unit of core 11 sample no.8

size	WT %	Cumulative WT %
0	4.078	4.078
0.321928	2.223	6.301
0.736965	3.898	10.199
1.736966	13.951	24.15
2.736966	19.363	43.513
3.736966	30.763	74.276
5.64385619	25.724	100
Mean size	**sorting**	
5.521667	8.403295	

Table S23-9 Grain size analysis of core 11 sample 9
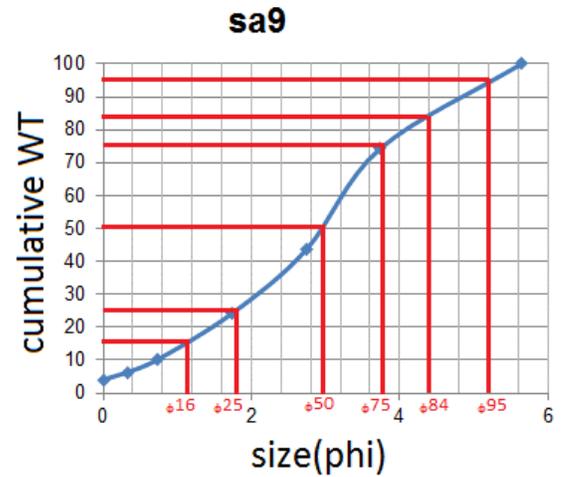
Fig.S26-9 cumulative weight with grain size in Phi unit of core 11 sample no.9

size	WT %	cumulative WT %
0	7.479	7.479
0.321928	3.866	11.345
0.736965	6.738	18.083
1.736966	16.711	34.794
2.736966	19.754	54.548
3.736966	30.446	84.994
5.64385619	15.006	100
Mean size	**sorting**	
4.395333	7.523212	

sa10

Table S23-10 Grain size analysis of core 11 sample 10
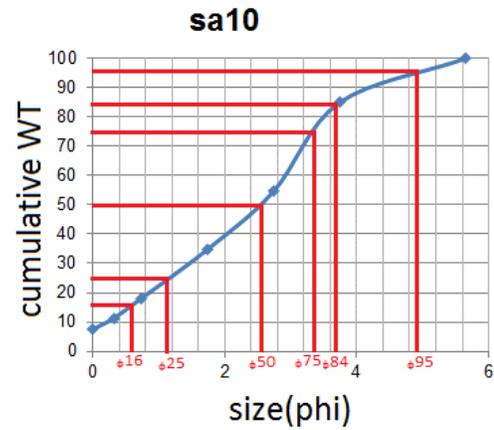
Fig.S26-10 cumulative weight with grain size in Phi unit of core 11 sample no.10

size	WT %	cumulative WT %
0	13.374	13.374
0.321928	4.919	18.293
0.736965	6.201	24.494
1.736966	14.968	39.462
2.736966	18.022	57.484
3.736966	25.313	82.797
5.64385619	17.203	100
Mean size	**sorting**	
3.802	7.975182	

sa11

Table S23-11 Grain size analysis of core 11 sample 11
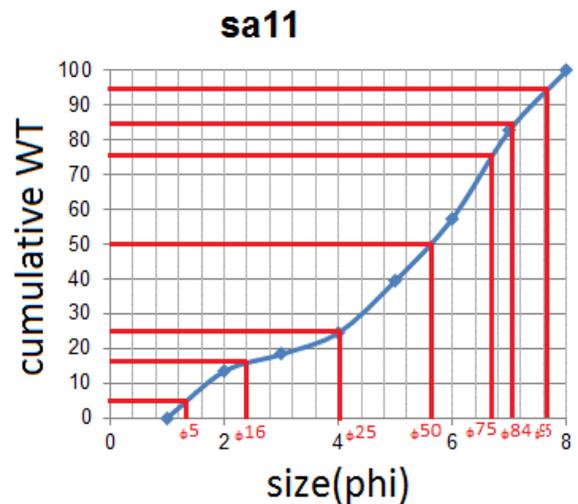
Fig.S26-11 cumulative weight with grain size in Phi unit of core 11 sample no.11

size	WT %	cumulative WT %
0	10.711	10.711
0.321928	3.694	14.405
0.736965	5.85	20.255
1.736966	14.821	35.076
2.736966	18.712	53.788
3.736966	29.811	83.599
5.64385619	16.401	100
Mean size	**sorting**	
4.276667	7.708561	

Table S23-12 Grain size analysis of core 11 sample 12
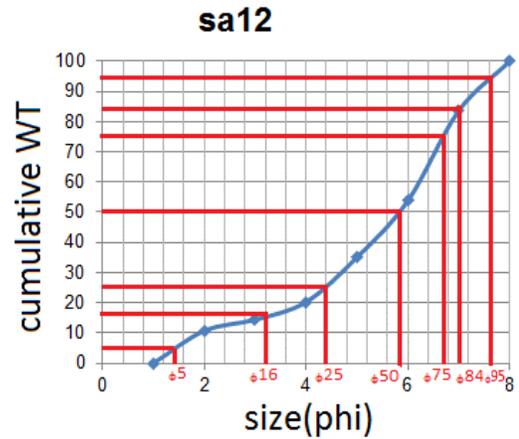
Fig.S26-12 cumulative weight with grain size in Phi unit of core 11 sample no.12

size	WT %	cumulative WT%
0	9.854	9.854
0.321928	5.75	15.604
0.736965	8.798	24.402
1.736966	20.983	45.385
2.736966	27.509	72.894
3.736966	14.455	87.349
5.64385619	12.651	100
Mean size	**sorting**	
3.075333	7.631083	

Table S24-1 Grain size analysis of core 12 sample 1
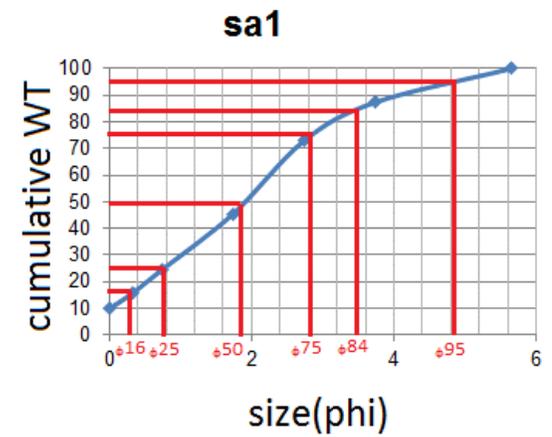
Fig.S27-1 cumulative weight with grain size in Phi unit of core 12 sample no.1

size	WT %	cumulative WT %
0	4.632	4.632
0.321928	4.193	8.825
0.736965	9.161	17.986
1.736966	43.668	61.654
2.736966	28.44	90.094
3.736966	7.465	97.559
5.64385619	2.441	100
Mean size	**sorting**	
2.826667	5.420303	

Table S24-2 Grain size analysis of core 12 sample 2
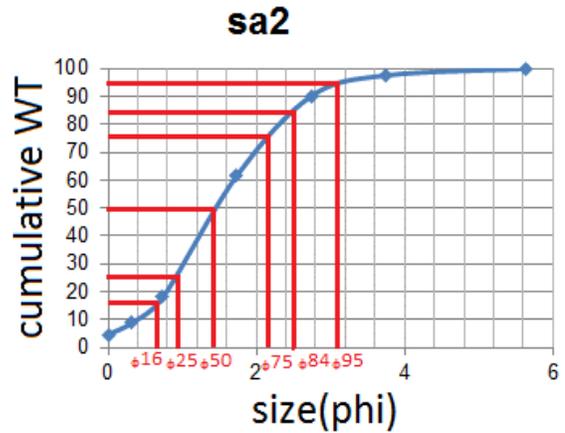
Fig.S27-2 cumulative weight with grain size in Phi unit of core 12 sample no.2

size	WT %	cumulative WT %
0	8.819	8.819
0.321928	3.271	12.09
0.736965	5.559	17.649
1.736966	25.105	42.754
2.736966	50.012	92.766
3.736966	4.888	97.654
5.64385619	2.346	100
Mean size	**sorting**	
3.339667	5.02425	

Table S24-3 Grain size analysis of core 12 sample 3
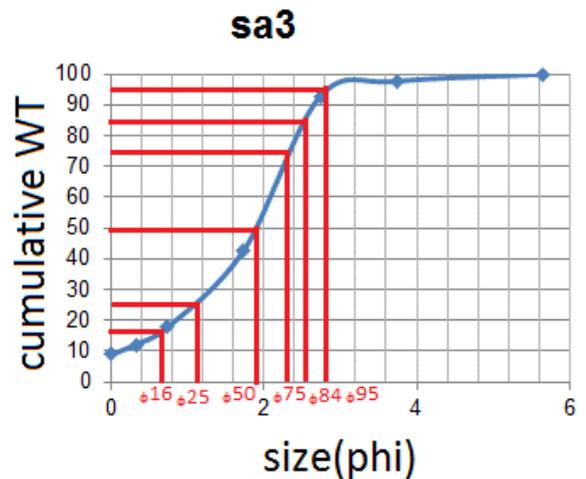
Fig.S27-3 cumulative weight with grain size in Phi unit of core 12 sample no.3

size	WT %	cumulative WT %
0	2.539	2.539
0.321928	3.144	5.683
0.736965	5.949	11.632
1.736966	15.052	26.684
2.736966	10.793	37.477
3.736966	22.711	60.188
5.64385619	39.812	100
Mean size	**sorting**	
5.936667	9.46303	

Table S24-4 Grain size analysis of core 12 sample 4
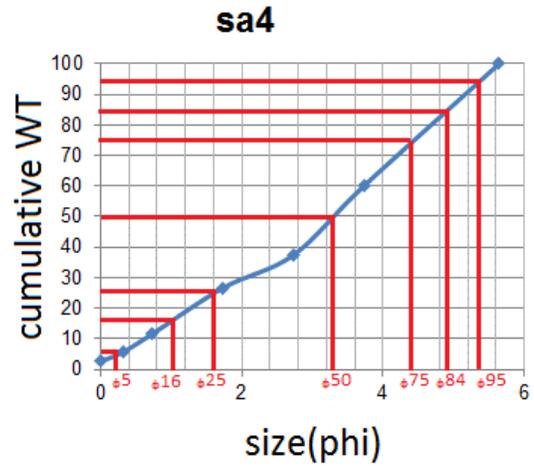
Fig.S27-4 cumulative weight with grain size in Phi unit of core 12 sample no.4

size	WT %	cumulative WT %
0	4.68	4.68
0.321928	6.167	10.847
0.736965	11.747	22.594
1.736966	32.955	55.549
2.736966	35.854	91.403
3.736966	5.662	97.065
5.64385619	2.935	100
Mean size	**sorting**	
3.553333	4.313409	

Table S24-5 Grain size analysis of core 12 sample 5
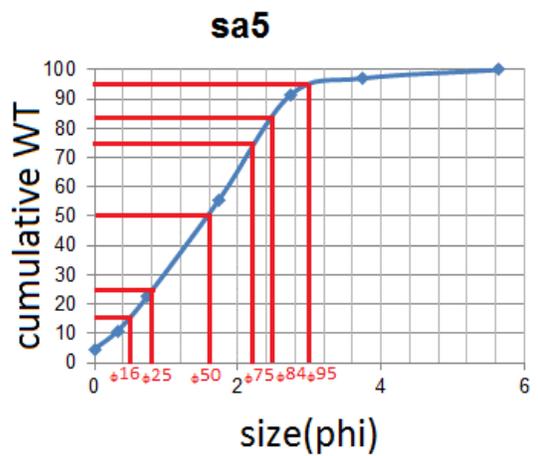
Fig.S27-5 cumulative weight with grain size in Phi unit of core 12 sample no.5

size	WT %	cumulative WT %
0	11.792	11.792
0.321928	4.069	15.861
0.736965	5.672	21.533
1.736966	14.261	35.794
2.736966	31.853	67.647
3.736966	18.887	86.534
5.64385619	13.466	100
Mean size	**sorting**	
3.71	7.66803	

Fig.S27-6 cumulative weight with grain size in Phi unit of core 12 sample no.6

Table S24-6 Grain size analysis of core 12 sample 6
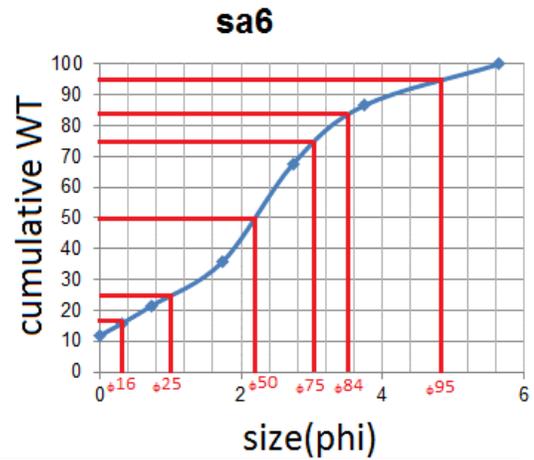
size	WT %	cumulative WT %
0	15.062	15.062
0.321928	5.53	20.592
0.736965	7.774	28.366
1.736966	21.463	49.829
2.736966	18.533	68.362
3.736966	20.752	89.114
5.64385619	10.886	100
Mean size	**sorting**	
2.964333	7.324447	

Fig.S27-7 cumulative weight with grain size in Phi unit of core 12 sample no.7

Table S24-7 Grain size analysis of core 12 sample 7

size	WT %	cumulative WT %
0	2.008	2.008
0.321928	2.098	4.106
0.736965	4.8	8.906
1.736966	15.069	23.975
2.736966	22.651	46.626
3.736966	37.649	84.275
5.64385619	15.725	100
Mean size	**sorting**	
5.293333	7.278864	

Table S24-8 Grain size analysis of core 12 sample 8
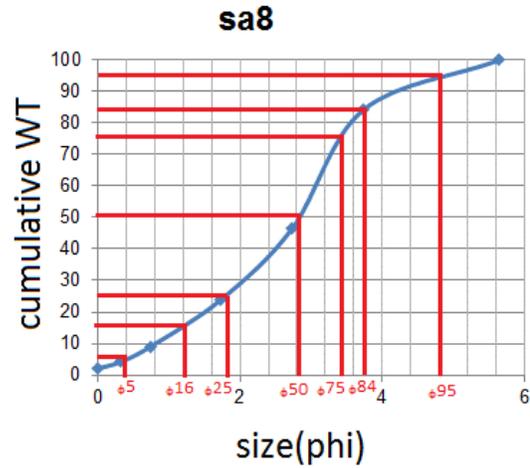
Fig.S27-8 cumulative weight with grain size in Phi unit of core 12 sample no.8

size	WT %	cumulative WT %
0	0.623	0.623
0.321928	0.674	1.297
0.736965	2.252	3.549
1.736966	13.422	16.971
2.736966	20.545	37.516
3.736966	46.18	83.696
5.64385619	16.304	100
Mean size	**sorting**	
5.926667	7.091667	

Table S24-9 Grain size analysis of core 12 sample 9
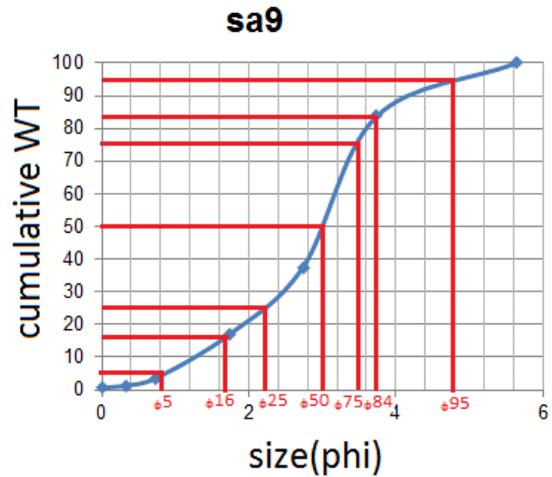
Fig.S27-9 cumulative weight with grain size in Phi unit of core 12 sample no.9

size	WT %	cumulative WT %
0	1.645	1.645
0.321928	1.656	3.301
0.736965	2.486	5.787
1.736966	5.867	11.654
2.736966	9.46	21.114
3.736966	65.026	86.14
5.64385619	13.86	100
Mean size	**sorting**	
7.02	6.731061	

Table S24-10 Grain size analysis of core 12 sample 10
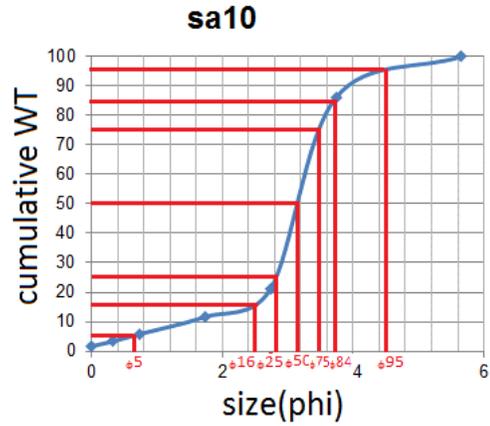
Fig.S27-10 cumulative weight with grain size in Phi unit of core 12 sample no.10

size	WT %	cumulative WT %
0	18.281	18.281
0.321928	6.467	24.748
0.736965	9.038	33.786
1.736966	20.24	54.026
2.736966	19.068	73.094
3.736966	14.157	87.251
5.64385619	12.749	100
Mean size	**sorting**	
2.56	7.622273	

Table S24-11 Grain size analysis of core 12 sample 11
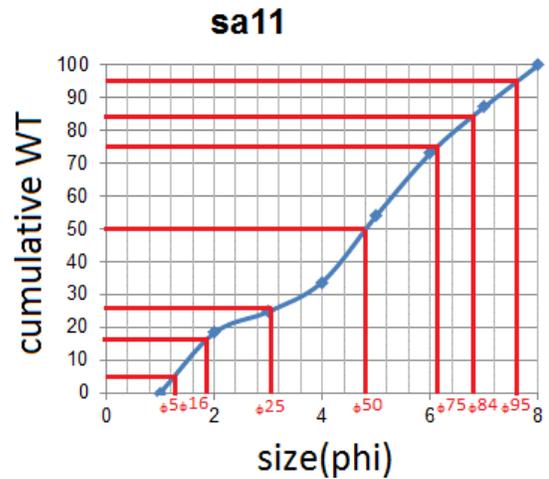
Fig.S27-11 cumulative weight with grain size in Phi unit of core 12 sample no.11

size	WT %	cumulative WT %
0	12.174	12.174
0.321928	6.325	18.499
0.736965	9.701	28.2
1.736966	27.948	56.148
2.736966	35.438	91.586
3.736966	4.988	96.574
5.64385619	3.426	100
Mean size	**sorting**	
2.57	5.132727	

Table S24-12 Grain size analysis of core 12 sample 12
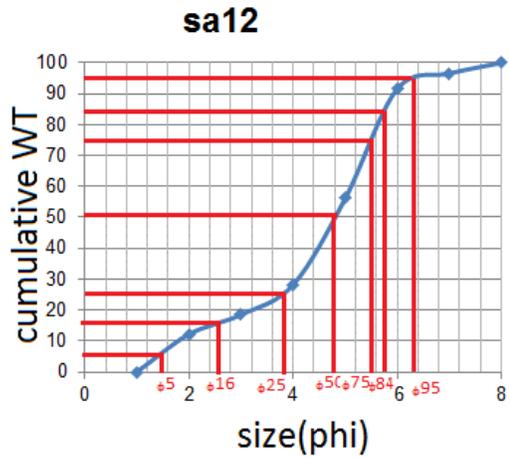
Fig.S27-12 cumulative weight with grain size in Phi unit of core 12 sample no.12

size	WT %	cumulative WT %
0	12.735	12.735
0.321928	4.881	17.616
0.736965	6.162	23.778
1.736966	14.451	38.229
2.736966	22.015	60.244
3.736966	29.012	89.256
5.64385619	10.744	100
Mean size	**sorting**	
3.713333	7.26053	

Table S24-13 Grain size analysis of core 12 sample 13
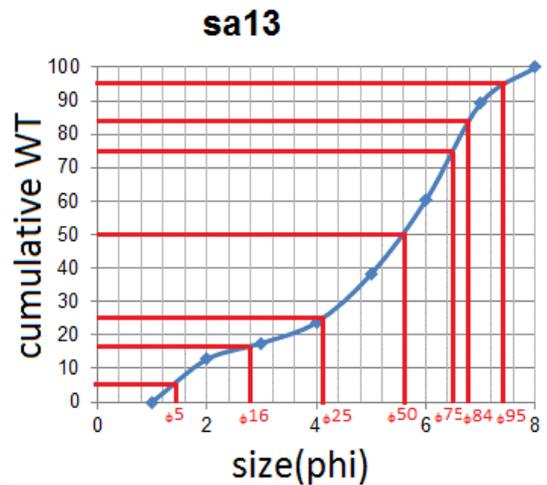
Fig.S27-13 cumulative weight with grain size in Phi unit of core 12 sample no.13

size	WT %	cumulative WT %
0	2.5	2.5
0.321928	2.196	4.696
0.736965	4.124	8.82
1.736966	16.57	25.39
2.736966	35.652	61.042
3.736966	25.582	86.624
5.64385619	13.376	100
Mean size	**sorting**	
4.916667	7.232955	
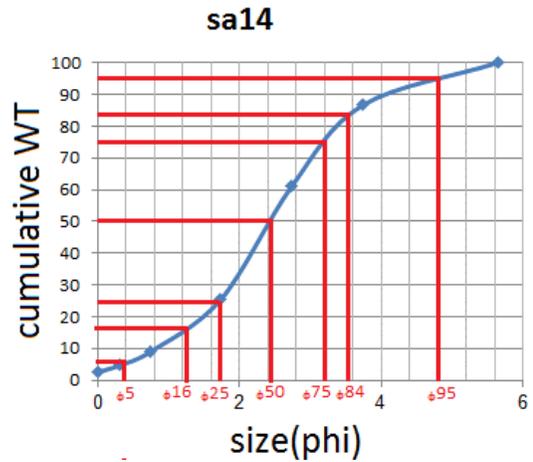
Table S24-14 Grain size analysis of core 12 sample 14

Fig.S27-14 cumulative weight with grain size in Phi unit of core 12 sample no.14

size	WT %	cumulative WT %
0	6.321	6.321
0.321928	3.465	9.786
0.736965	5.701	15.487
1.736966	15.566	31.053
2.736966	35.536	66.589
3.736966	29.898	96.487
5.64385619	3.513	100
Mean size	**sorting**	
4.136667	6.443788	
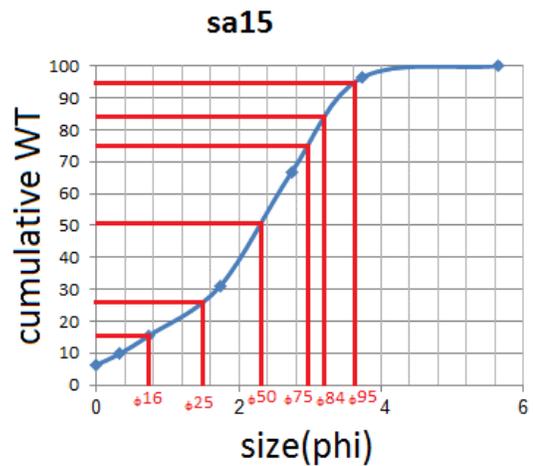
Table S24-15 Grain size analysis of core 12 sample 15

Fig.S27-15 cumulative weight with grain size in Phi unit of core 12 sample no.15

size	WT %	cumulative WT %
0	4.265	4.265
0.321928	2.435	6.7
0.736965	5.084	11.784
1.736966	15.797	27.581
2.736966	37.109	64.69
3.736966	32.643	97.333
5.64385619	2.667	100
Mean size	**sorting**	
4.543333	6.332348	

Table S24-16 Grain size analysis of core 12 sample 16
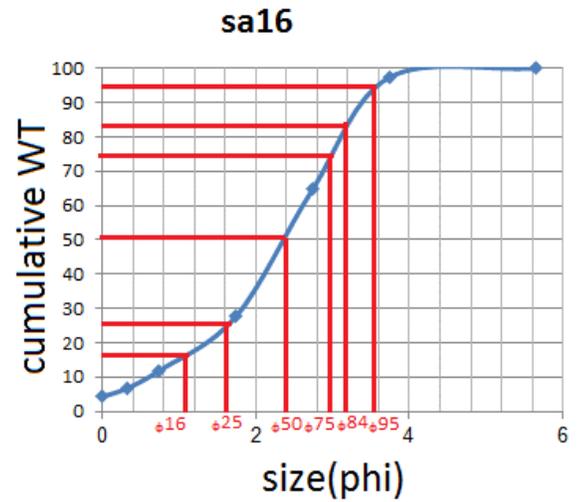
Fig.S27-16 cumulative weight with grain size in Phi unit of core 12 sample no.16